

Sonne -Berichte

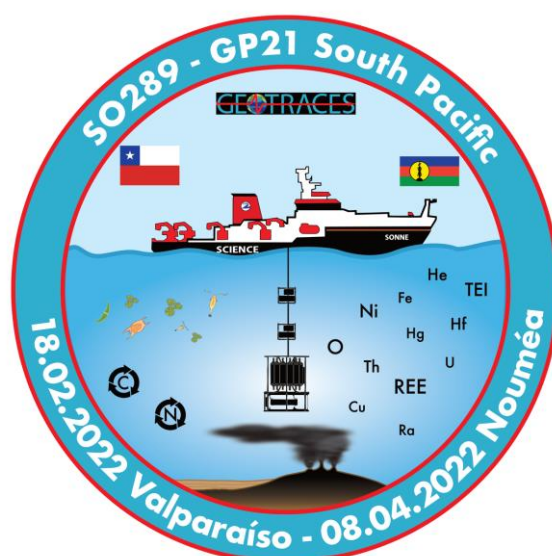
South Pacific GEOTRACES

Cruise No. SO289

18.02.2022-08.04.2022

Valparaiso (Chile) – Noumea (New Caledonia)

GEOTRACES GP21



Authors: Prof. Dr. Eric Achterberg, Dr. Zvi Steiner and Dr. Christopher Galley

Chief Scientist: Prof. Dr. Eric Achterberg
GEOMAR Helmholtz Centre for Ocean Research Kiel

2022

Table of Contents

1	Cruise Summary	4
1.1	Summary in English	4
1.2	Zusammenfassung	4
2	Participants	5
2.1	Principal Investigators	5
2.2	Scientific Party	5
2.3	Participating Institutions	6
3	Research Program	7
3.1	Description of the Work Area	7
3.2	Aims of the Cruise.....	7
3.2	Agenda of the Cruise.....	8
4	Narrative of the Cruise	9
5	Preliminary Results	11
5.1	Stainless-steel CTD surveying	11
5.2	Underwater Vision Profiler	12
5.3	Multibeam data collection and processing	15
5.4	Dissolved inorganic carbon and total alkalinity sampling	16
5.5	Acoustic Doppler Current Profiler data collection.....	17
5.6	Sulfur isotope sampling.....	17
5.7	The control of surface ocean microbial communities by (micro) nutrient supply, phytoplankton abundance, community composition and photophysiology.....	18
5.8	Assessment of marine aggregates-associated bacterial and archaeal life and diversity of extracellular vesicles in marine waters	22
5.9	Full depth water collection with trace metal clean CTD/Rosette.....	24
5.10	On-deck sampling for He and DOC	25
5.11	Oxygen	26
5.12	Particulate and dissolved siderophores	26
5.13	Sampling and analysis of dissolved Al	26
5.14	N ₂ O-CH ₄ -CO and Nitrate-isotopes	27
5.15	Radiogenic Isotopes (neodymium, hafnium) and Rare Earth Elements	28
5.16	Stable Silicon isotopes and Barium isotopes.....	29
5.17	Transient Tracers in the South Pacific Ocean: ¹²⁹ I and ²³⁶ U	30
5.18	Mercury collection and analysis from the South Pacific.....	31
5.19	Investigation of trace-metals, HFSE, Cr and V redox speciation and organic Fe, and Cu ligands in different size fractions.....	34
5.20	Major elements	38
5.21	Nutrient distribution	39
5.22	Sampling and analysis of Ammonium	40
5.23	Suspended particles and radiogenic tracers.....	40
5.24	Radium 226, 228 isotopes	41
5.25	²³⁴ Th, ²³⁰ Th and ²³⁸ U	42
5.26	Sampling for Pa/Th and Ac	43
5.27	Aerosol sampling using high volume collector.....	43
5.28	Assessing plastic pollution along the South Pacific.....	44
7	Station List MXX/Y	44
7.1	Overall Station List	44
8	Data and Sample Storage and Availability	48
9	Acknowledgements	50
10	References	50

11	Abbreviations	55
12	Appendices	58
12.1	SS-CTD	58
12.2	UVP data	86
12.3	Phytoplankton experiments	88
12.4	Samples collected for assessment of marine aggregates-associated bacterial and diversity of extracellular vesicles	91
12.5	In-situ pump deployments and samples for natural level radiogenic elements....	92
12.6	Jacobs University cleaning and sampling procedures	102
12.7	Oxygen, siderophores and microplastic samples	103
12.8	Sulfur isotopes and carbonate chemistry samples	112
12.9	Sampling tables Ra, REE, tow-fish, ISP	124

1 Cruise Summary

1.1 Summary in English

Research cruise SO289 with FS Sonne was sailed in austral autumn of 2022 in the South Pacific Ocean (SPO) from Valparaiso (Chile) to Noumea (New Caledonia), with a focus on trace element biogeochemistry and chemical oceanography but also including physical and biological oceanographic components. The research topic of the cruise was to determine in detail the distributions, sources and sinks of trace elements and their isotopes (TEIs) in the water column along a zonal section in one of the least studied ocean regions on earth. Our aim was to investigate the biogeochemical cycling of TEIs, and their interactions with surface ocean productivity and the carbon and nitrogen cycles (incl. N₂ fixation) given that some TEIs act as micronutrients. The findings will have global significance for understanding the chemical environment in which ecosystems operate. The supply pathways of TEIs to the SPO from ocean boundaries including the atmosphere (Australian dust), continents (mainly Maipo River), sediments (on continental shelves/slopes), and ocean crust (hydrothermalism) were investigated. The TEI transport within water masses was determined with a focus on the southward flow of hydrothermally derived TEIs towards the Southern Ocean but also the deep inflow of Southern Ocean waters in the western SPO. The TEI transport assessment along the cruise track (Figs. 1.1, 1.2) will allow a more reliable use of some TEIs as paleo-circulation proxies. The cruise will officially be part of the international GEOTRACES program.

1.2 Zusammenfassung

Die Forschungsfahrt SO289 mit FS Sonne wurde im australischen Herbst 2022 im Südpazifik (SPO) von Valparaiso (Chile) nach Noumea (Neukaledonien) durchgeführt, wobei der Schwerpunkt auf der Biogeochemie von Spurenelementen und der chemischen Ozeanographie lag, aber auch physikalische und biologische ozeanographische Komponenten einbezogen wurden. Das Forschungsthema der Ausfahrt ist die detaillierte Erfassung der Verteilung und der Quellen und Senken von Spurenelementen und deren Isotopen (TEIs) in der Wassersäule entlang eines zonalen Schnitts in einem der am wenigsten untersuchten Gebiete der Erde. Unser Ziel war, die biogeochemischen Zyklen der TEIs, deren Wechselwirkungen mit der Bioproduktivität des Oberflächenwassers und den Stickstoff- und Kohlenstoffkreisläufen zu untersuchen. Die Ergebnisse werden von globaler Bedeutung für das Verständnis der geochemischen Umweltbedingungen für marine Ökosysteme sein. Die Eintragspfade der TEIs in den SPO von den Ozeanrändern, also der Atmosphäre (australischer Staub), den Kontinenten (hauptsächlich dem Maipo Fluss), den Sedimenten der Kontinentanhänge und die ozeanische Kruste (Hydrothermalismus) wurden untersucht. Der TEI-Transport innerhalb von Wassermassen wurde bestimmt, wobei der Schwerpunkt auf dem südwärts gerichteten Fluss von hydrothermal abgeleiteten TEIs in Richtung Südpolarmeer lag, aber auch auf dem tiefen Einstrom von Südpolarmeerwasser in den westlichen SPO. Die Bewertung des TEI-Transports entlang der Fahrtroute (Abb. 1.1, 1.2) wird eine zuverlässigere Verwendung einiger TEIs als Proxies für die Paläozirkulation ermöglichen. Die Fahrt wird offiziell Teil des internationalen GEOTRACES-Programms sein.

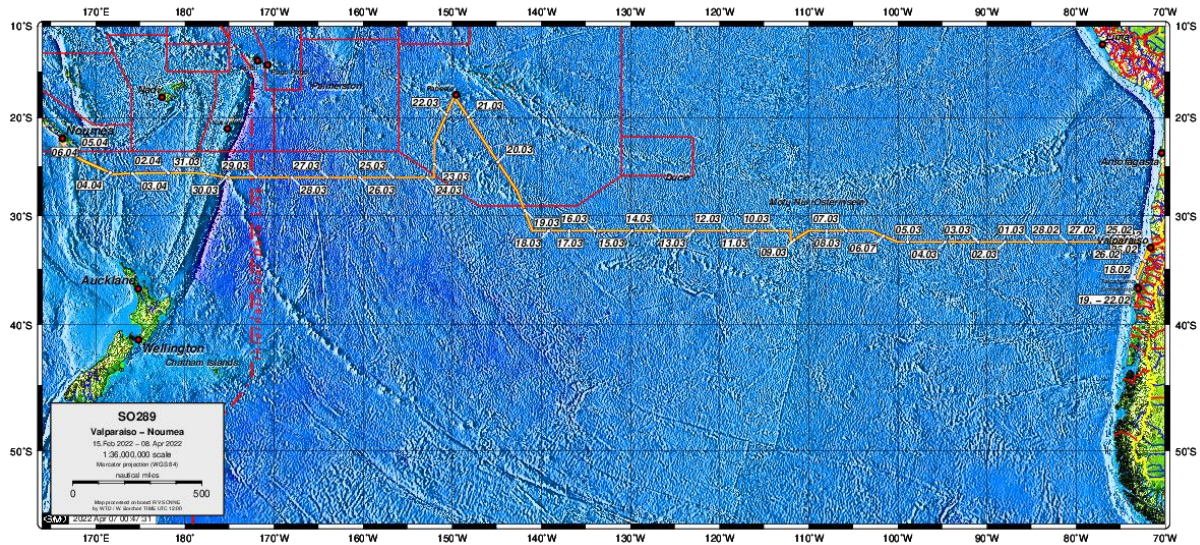


Fig. 1.1 Cruise track (yellow line) and stations locations of RV SONNE cruise SO289

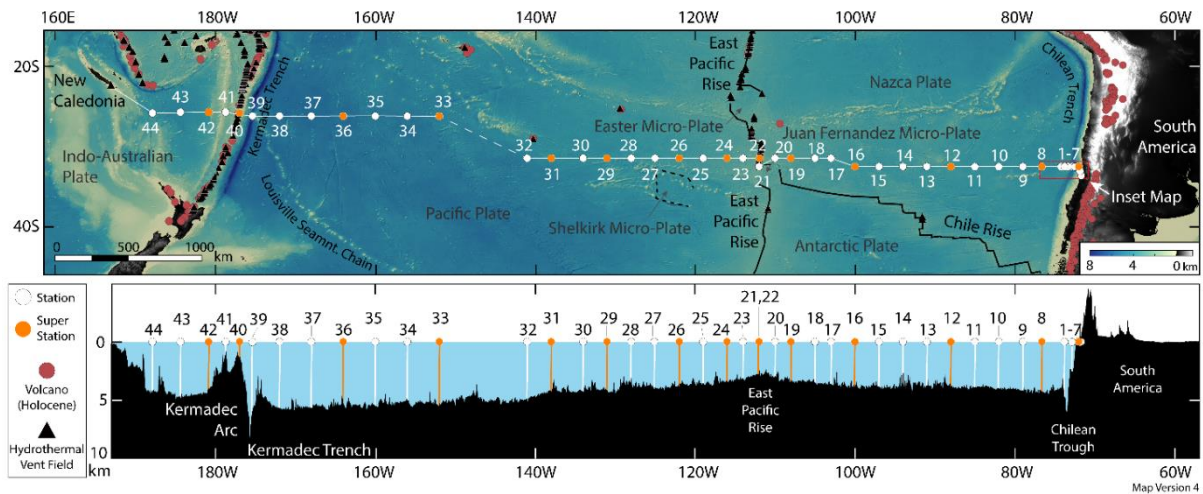


Fig. 1.2 Cruise track (white line) for SO289 with standard stations as white dots and superstations as orange dots. Brown dots are volcanoes and black triangle hydrothermal vent fields. Bottom: stations positioned on bathymetry map. Figure by Chris Galley.

2 Participants

2.1 Principal Investigators

Name	Institution
Achterberg, Eric P., Prof. Dr.	GEOMAR
Frank, Martin, Prof. Dr.	GEOMAR
Koschinsky, Andrea, Prof. Dr.	Jacobs University, Bremen

2.2 Scientific Party

Name	Discipline	Institution
Achterberg, Eric, Prof. Dr.	Mar. Biogeochem/ Chief Scientist	GEOMAR
Frank, Martin, Prof. Dr.	Paleo Oceanography/Co-Chief Sci.	GEOMAR
Blum, Lea	Marine Biogeochemistry	GEOMAR
Mutzberg, Andre	Marine Biogeochemistry	GEOMAR

Schott, Thorsten	Paleo Oceanography	GEOMAR
Zhang, Zhouling, Dr.	Marine Geochemistry	GEOMAR
Fröhberg, Nico	Marine Biogeochemistry	Jacobs Uni
Pedre, Ignacio	Marine Biogeochemistry	Jacobs Uni
Steiner, Zvi, Dr.	Marine Biogeochemistry	GEOMAR
Li, Guanlin	Marine Geochemistry	GEOMAR
Gosnell, Kati, Dr.	Marine Biogeochemistry	GEOMAR
Jasinski, Dominik	Marine Biogeochemistry	GEOMAR
Fadeev, Eduard, Dr.	Marine Biogeochemistry	Uni Vienna
Vieira, Lucia, Dr.	Marine Biogeochemistry	GEOMAR
Wen, Zouzhu, Dr.	Biological Oceanography	GEOMAR
Yuan, Zhongwei	Marine Biogeochemistry	GEOMAR
Liu, Te	Marine Biogeochemistry	GEOMAR
Kleindienst, Alina	Marine Biogeochemistry	Pau
Galley, Chris, Dr.	Geophysical Oceanography	Ottawa Uni
Xu, Antao	Paleo Oceanography	GEOMAR
Evers, Florian	Paleo Oceanography	GEOMAR
Tammen, Juliane	Marine Biogeochemistry	GEOMAR
Battermann, Paul	Marine Geology	GEOMAR
Browning, Thomas, Dr.	Marine Biogeochemistry	GEOMAR
Von Keitz, Tabea	Marine Biogeochemistry	GEOMAR
Köhler, Dennis	Marine Geochemistry	AWI
O'Sullivan, Edel, Dr.	Marine Biogeochemistry	GEOMAR
Pöhle, Sandra, Dr.	Marine Biogeochemistry	Jacobs Uni
Moriarty, Sarah	Marine Geochemistry	Memorial Uni
Hamisch, Stephan	Marine Biogeochemistry	GEOMAR
Liu, Haoran	Marine Biogeochemistry	GEOMAR
Gürses, Can	Marine Biogeochemistry	GEOMAR
Amenabar, Maria	Biological Oceanography	Observer Chile

2.3 Participating Institutions

GEOMAR	Helmholtz-Zentrum für Ozeanforschung Kiel
Jacobs	Jacobs University Bremen
Memorial	Memorial University, Canada
Ottawa	University of Ottawa, Canada
Vienna	University of Vienna, Austria
Pau	University of Pau, France
AWI	Alfred Wegener Institute Bremerhaven

3 Research Program

3.1 Description of the Work Area

Hydrography- The dominant feature of the South Pacific Ocean (SPO) is the wind-forced anticyclonic subtropical gyre, which has South America as its eastern boundary, and Australia as its western boundary. The SPO gyre is inextricably linked to the South Atlantic and South Indian Ocean gyres via the Southern Ocean circulation and also via the Indonesian Through Flow. The SPO subtropical gyre includes the eastward flowing South Pacific Current (SPC) in the south, a broad northward flowing Peru Chile Current (PCC) in the eastern part, a westward flowing South Equatorial Current (SEC) in the north, and a southward flowing East Australian Current (EAC) along its western boundary. The cruise track allowed sampling of the current systems along the eastern and western boundaries, whilst sailing through the northern regions of the SPC and sampling the subtropical gyre.

A major topographic feature of the SPO is the East Pacific Rise, a fast spreading ridge that separates the deep waters of the southeast from the rest of the Pacific, with some communication of deep waters across the ridge through fracture zones. The western side of the EPR in the SPO features a deep trench (>6000 m) and allows a northerly flow of Southern Ocean waters as part of a Deep Western Boundary Current (DWBC).

The deep-water circulation in our study region is dominated by major water masses (Antarctic Intermediate Waters, Lower Circumpolar Deep Water, Upper Circumpolar Deep Water, and Pacific Deep Water).

3.2 Aims of the Cruise

The main scientific aim of cruise SO289 is to determine the distributions of trace elements and their isotopes (TEIs), quantify their sources from the four major ocean boundaries (rivers, atmosphere, exchange with sediments, ocean crust), and determine their biogeochemical cycling and relationships to large scale ocean circulation along a cruise track in the SPO.

We have the following major goals that we want to achieve for the cruise:

Objective 1. Determine the distribution, as well as the physical and chemical speciation of TEIs, including micronutrients, non-biologically essential elements and a range of isotope systems in high resolution full-depth profiles.

Objective 2. Quantify the fluxes of these TEIs and micronutrients to the ocean from the four ocean boundaries: atmosphere, continent, ocean crust and sediments and assess the role of physical and chemical speciation of TEIs for their fluxes from the different sources.

Objective 3. Assess, using chemical tracers and physical oceanography, the mixing and advection of these TEIs away from their sources into the ocean interior, and upwards into the surface ocean.

Objective 4. Explore the relationship between macro- and micro-nutrient concentrations and fluxes, ocean productivity, nutrient utilization and limitation, diazotrophy, and the nitrogen and carbon cycles.

3.3 Agenda of the Cruise

The cruise was conducted along a zonal section from Chile to New Caledonia, which is an ideal section to assess the cycling of micronutrients in general, and in the SPO in particular. The section features important hydrothermal inputs to deep waters and pronounced contrasts in surface ocean productivity. The cruise connected with the GEOTRACES section cruise GP13, which sampled for TEIs between Australia and 150°W, but lacks REEs and Nd/Hf isotopes as water-mass tracers for the region between ca. 150°W to 180°W.

The major questions that we addressed on the are: 1. The S Pacific gyre is ultra-oligotrophic with low concentrations of nitrate and the micronutrient Fe, and low to medium phosphate concentrations. What are the proximally limiting or co-limiting (micro)nutrients for surface water microbiological processes in this region? How are micronutrients and nitrate supplied to support surface ocean productivity in the SPO?

2. Intermediate and deep-water masses in the SPO upwell to the south and north to supply micronutrients to the Fe-starved Pacific sector of the Southern Ocean, and the productive Equatorial PO. The Fe/N ratios in these waters are very likely below those required by phytoplankton communities in surface waters, but in terms of the total Fe supply to the surface ocean, these waters play a fundamental role in setting surface productivity. Which processes control the concentration and distribution of micronutrients in intermediate and deep waters in the SPO, and therefore ultimately the supply of micronutrients to the remote surface waters?

3. The sources, sinks, and internal cycling of TEIs, including micronutrients, in the SPO are poorly understood despite its importance for the global cycling of nutrients and carbon. Which processes control the fluxes, supplies and cycling of TEIs?

4. Hydrothermal vents along the East Pacific Rise (EPR) provide large deep-water Fe inputs. What are the stabilisation mechanisms of vent derived Fe, and what is the length scale of the Fe plume?

5. The flow of the hydrothermal tracer ^3He suggests potentially substantial transport of hydrothermally derived TEIs to the Southern Ocean. Does this transport mechanism form an important supply route of Fe, and other TEIs such as Zn, to the Fe limited Southern Ocean?

6. The Maipo river is an important Chilean river flowing into the Pacific Ocean. What are the TEI inputs of this river reaching the open ocean and how are they distributed by ocean circulation?

7. Are the Chilean shelf and slope system important sources of Fe and other elements to the SPO?

8. How does large scale ocean circulation affect the TEI distributions in water masses in the deep SPO? Is the advection of water masses from the Southern Ocean reflected in their TEI distributions, which would allow more reliable application of certain TEIs (Nd/Hf isotopes, REEs) as paleo circulation tracers recorded in sediments?

The SPO is strongly understudied due to its remoteness. Nevertheless, it is a critical ocean basin for understanding the cycling of TEIs. The SPO is dominated by a large ultra-oligotrophic gyre. Large regions of the subtropical waters of the SPO are considered a net CO₂ sink,

operating primarily through the solubility pump, but only very few data are available to confirm this. The anthropogenic carbon in the SPO occurs predominantly in surface and intermediate waters of the equatorward flowing Antarctic Intermediate Water (AAIW). There is active exchange of TEIs (including micronutrients, such as Fe, Co) in this region at the ocean boundaries, such as with the atmosphere (Australian dust plume), ocean crust (hydrothermal vent systems on the EPR), continent via rivers (e.g. Maipo River) and the shelf/slope system with its oxygen minimum zone (OMZ) related to eastern boundary upwelling, and deep-sea sediments. The SPO subtropical gyre has extremely low surface water micronutrient (e.g. Fe (0.1 nM) and nitrate levels, but low to relatively elevated phosphate. The nitrate depletion provides a favourable habitat for N₂ fixers (diazotrophs). Diazotrophs have a higher demand for Fe than other microbial groups due to the high Fe content of the N₂ fixing enzyme (nitrogenase), however sources of Fe to diazotrophs in the SPO are not well constrained. The low Fe and nitrate concentrations in the gyre provide challenging growth conditions for phytoplankton, but experimental data to show limitation by N, P, Fe or other micronutrients are lacking.

4 Narrative of the Cruise

February 14-16, 2021- Scientists and technicians travelled from their home laboratories to Chile (Valparaiso) to join RV Sonne. A group of GEOMAR scientists and technicians had travelled already on February 14 to arrive earlier in Valparaiso to set to unload containers and set up the equipment for the cruise. Unfortunately, the port of Valparaiso was not able to handle containers for the Sonne. The Agent in Chile then managed to get us a berth in Talcahuano, a port 2 days sailing south from Valparaiso. All the cruise participants of SO289 were transferred by Pilot boat from the quayside to the vessel in the Bay of Valparaiso on the morning of February 17. We arrived in Talcahuano on February 19, and commenced with the off-loading of containers of the previous two cruises, before we loaded the 6 containers for SO289 plus the supply containers for the cruise. The GEOMAR trace metal clean winch container with a new cable guiding deck block was installed, as were our clean container for filtration. The CTD sensors, UVP and other instruments were installed. The cruise participants installed their laboratories. We sailed in the evening of February 21 with moderate wave conditions in the coastal waters off Chile. The wind and waves were still a little demanding for some of the cruise participants, but all got over their sea-sickness within the first few days of the cruise.

February 23, 2022- The cruise started sampling surface waters from our trace metal clean tow fish for trace elements and biological variables at the first station in the outflow of the Maipo river. This sampling activity using the tow fish continued until we reached New Caledonia, but was halted for a few hours prior to reaching the international waters outside the Chilean EEZ (February 28). In addition, we halted the sampling from the tow fish whilst in the EEZ of French Polynesia (March 18 to 23) and New Caledonia (after April 4). The surface waters were sampled for nitrogen fixation, nutrients and trace elements to establish the rates of nitrogen fixation, types of diazotrophs present (using *nifH* gene analysis), and the chemical environment of the diazotrophs. Nutrients and trace elements were sampled typically every 3 hours when steaming, and also upon arrival or departure at stations. The tow fish was deployed throughout the cruise and only taken out of the water for inspection once or twice.

The ship's ADCP and TSG were functioning whilst the vessel was in international waters.

In addition, we sampled for aerosols. The aerosol collector was placed on the top deck of the Sonne and filters changed every 48 or 72 h.

We have been deploying 2 different CTDs (titanium GEOMAR CTD, stainless steel Sonne CTD) and also a set of 11 in-situ pumps. The titanium GEOMAR CTD is operated by a dedicated winch system with a Kevlar cable, thereby preventing contamination of the samples during the sample collection. The deployments of the CTDs have been successful. The deployment of the in-situ pumps was also very successful and greatly contributed to the success of the cruise.

At each station we sampled the full water column with the titanium GEOMAR CTD for contamination prone variables (GEO-CTD), and using the stainless steel Sonne CTD for less contamination prone variables, including isotopes like Nd (SS-CTD). An additional titanium CTD (BIO-CTD) was deployed daily to about 250 m depth for collection of samples for biological variables. Biological rate experiments of nitrification and di-nitrogen fixation were conducted using the water from the titanium CTD (and also tow fish). Phytoplankton resource limitation experiments were conducted in the ship-board laboratory and also in incubation tanks on the aft deck.

We sampled a total of 44 stations on SO289, and 14 were so-called superstations. At the superstations, we deployed an additional SS-CTD for the collection of additional waters for isotope measurements. In addition, at the superstations we deployed up to 11 in-situ pumps on the stainless-steel wire of the SS-CTD. The pumps and SS-CTD deployment occurred simultaneously. This operation saved us 4-5 hours at each superstation, thereby making up for lost time for the delayed departure in Chile. The stainless-steel wire of the Sonne was clean and released few particles. The freshwater rinsing system of the cable facilitated a clean CTD wire.

The in-situ pumps were used to collect particles for geochemical and biological investigations. Particulate Th isotopes (Th 234) obtained from the filters of the in-situ pumps were measured on-board. In addition, a Mn cartridge was placed on a number of the in-situ pumps, which allowed for the collection of long-lived Ra samples. We also sampled the Niskins from the SS-CTD for helium isotopes which we will use as a tracer of the hydrothermal fluid inputs to the ocean. Helium is a conservative tracer and allows us to follow the plume and determine the fluxes of elements.

The first station on February 23 (2022) was conducted in the bay right in front of the outflow of the Maipo river. The problems with the ports in Chile had ultimately resulted in a 5-day delay of our cruise programme. The GEOMAR titanium (Ti) CTD with OTE Niskin bottles worked well, as did the stainless steel (SS) CTD from the Sonne. The first station is always important as challenges with the CTD systems can be identified and rectified. However, all went smooth, and the shallow station was completed within a few hours.

The first 4 stations were conducted in waters with depths of less than 2500 m, and therefore took only a few hours to complete. Also, the distance between the stations was short with only a few hours steaming between stations. Therefore, the ship had to wait on occasions at a station prior to the start of sampling activities, as the samples from the previous station had not yet been processed. We reached our intended latitude of 32°30 S at station 5, with the intention to follow this until New Zealand waters. Following station 7, the depths were about 4000 m, and

steaming distances about 12-15 h, which allowed good time for sample handling and also sleep between stations.

Our last station in the EEZ of Chile was on February 28 (Station 10), and the next station (Station 11) was in international waters. All further stations were sampled in international waters, as we shelved our plan to work in the EEZ of New Zealand. Station distances were 2 or 3 degrees (longitude) in the region between the Chilean EEZ and the East Pacific Rise. The stations in the region of the East Pacific Rise were occupied at shorter distances (down to 1 degree) and we also moved 1 degree north to 31°25'S at station 17 in order to sample the hydrothermal plume, and we sampled a hydrothermal system right above the East Pacific Rise at 111°59'W, 31°25'S (Station 22).

Sailing west from the East Pacific Rise, we turned to sampling stations at a 3- or 4-degree distance along 31°25'S. Station occupation continued until station 32 (March 18), following which we sailed to Tahiti for a medical evacuation of a crew member. We returned to international waters to the south of French Polynesia on March 23, and occupied Station 33. The diversion to Tahiti took about 5 days, and we decided to follow a cruise track that was even more northerly (26°10'S) in order to save steaming time on our way to New Caledonia; station spacing was 4 degrees. The chosen track allowed us to avoid the EEZ of New Zealand as there were some challenges in obtaining the additionally required permissions to sample in the New Zealand EEZ (the official Diplomatic Clearance had been obtained in time, but not yet the permissions from the Environment Ministry). The transect allowed us to sample in the international waters between the EEZs of New Zealand and Tonga. The narrow gap between these EEZs allowed us to sample the Kermadec-Tonga Trench (Station 39) and also an underwater volcanic system on the ridge (Station 40). The last 4 stations of cruise SO289 were conducted in the South Fiji Basin, which is impacted by hydrothermal inputs in addition to a range of inputs from continental run-off and sediments. The last station (Station 44) was occupied in the early morning of April 4. Following this station, we start packing up and loading our containers. A threat of a tropical cyclone forced us to pack swiftly and allow us to unload the container in the port of Noumea on April 8, before flying home on April 9.

The weather in the study area has been kind and we have not lost any station time as a result of poor weather.

5 Preliminary Results

5.1 Stainless-steel CTD surveying

(C. Galley, T. Schott)

The Sonne's stainless-steel rosette (SS-CTD) was deployed in addition to Geomar's clean Ti-CTD to survey the water column. The SS-CTD was equipped with a *Sea-Bird Scientific* SBE 911Plus Conductivity, Temperature, and Depth (CTD) device, 24 Niskin bottles, and an *Underwater Vision Profiler 5 DEEP* device (UVP). The SBE 911Plus device measured seawater temperature, conductivity, dissolved oxygen, fluorescence, turbidity, and pressure at a 24Hz sampling rate. However, to construct the transect's interpolated plots (Fig. 5.1) the data was processed to remove spikes, and then a moving mean smoothing was applied, binning the data to 10 m segments. The data was processed and plotted using the program MATLAB, and the raw data was converted into an ASCII-format using *Sea-Bird Scientific's*

SBEDataProcessing program. The preliminary oxygen and salinity profiles were used during the cruise to identify water masses for sampling purposes (Fig. 5.1). See Appendix CTD for all the station profiles' turbidity, oxygen, salinity, fluorescence, and bottle depth data. The SS-CTD was not used at station 21.

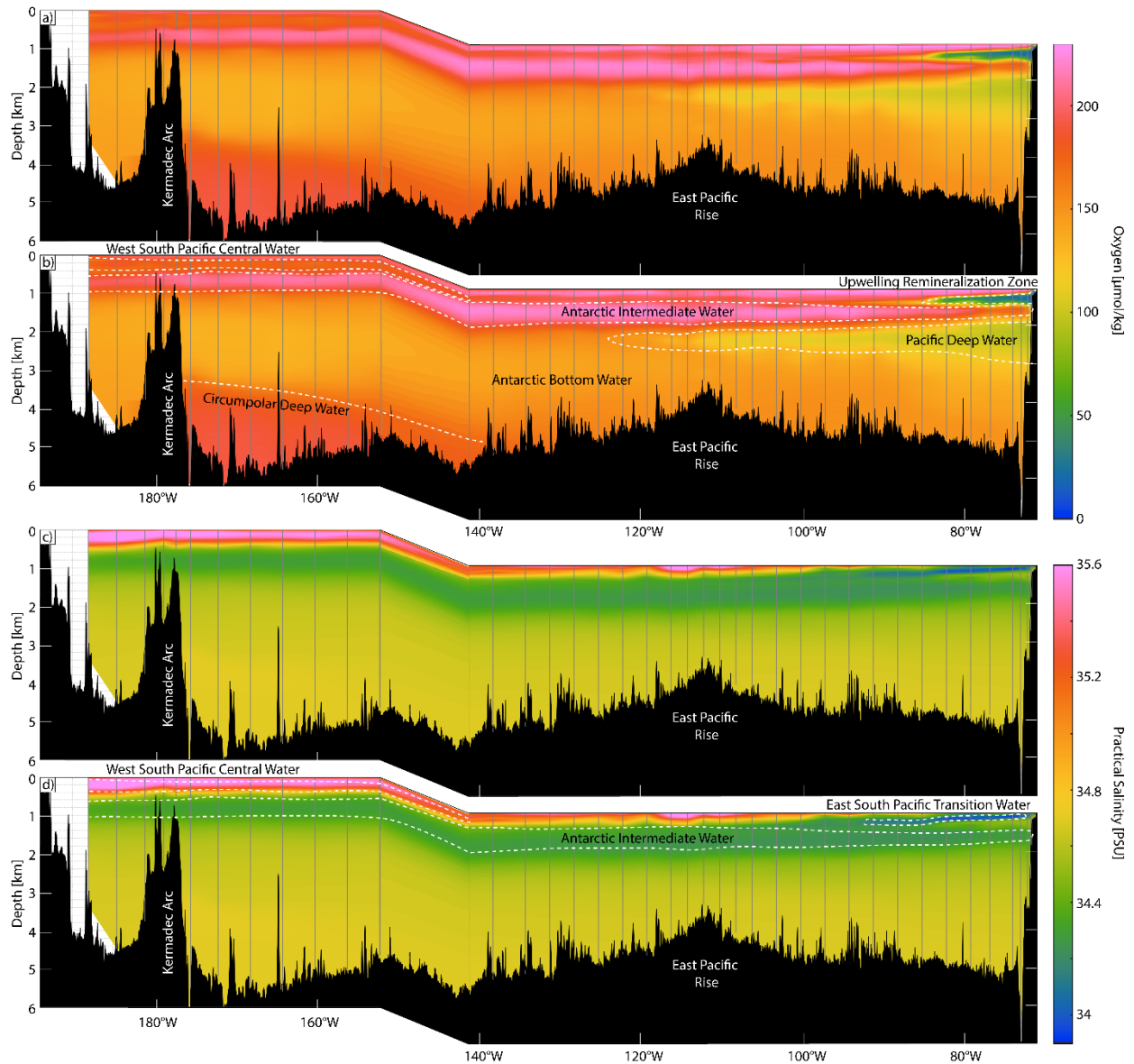


Fig. 5.1 The oxygen (a,b) and practical salinity (c,d) survey profiles, made with preliminary data collected from the SS-CTD. Plots b and d have interpreted water masses outlined and labeled.

5.2 Underwater Vision Profiler

(C. Galley, T. Schott)

A *Hydroptic* Underwater Vision Profiler (UVP) 5 DEEP (CNRS patent) was attached to our SS-CTD rosette, which collected data during the vertical downcasts. The UVP is a high-resolution camera system that shines a thin beam of light horizontally between its two lamps, and then takes rapid pictures (6-11 images per second) of the illuminated volume of water (Fig. 5.2). Based off the reflectance of the light beam within that volume of water the camera can

measure the density of macroscopic particles and zooplankton $> 100 \mu\text{m}$ in size (Picheral et al., 2010).

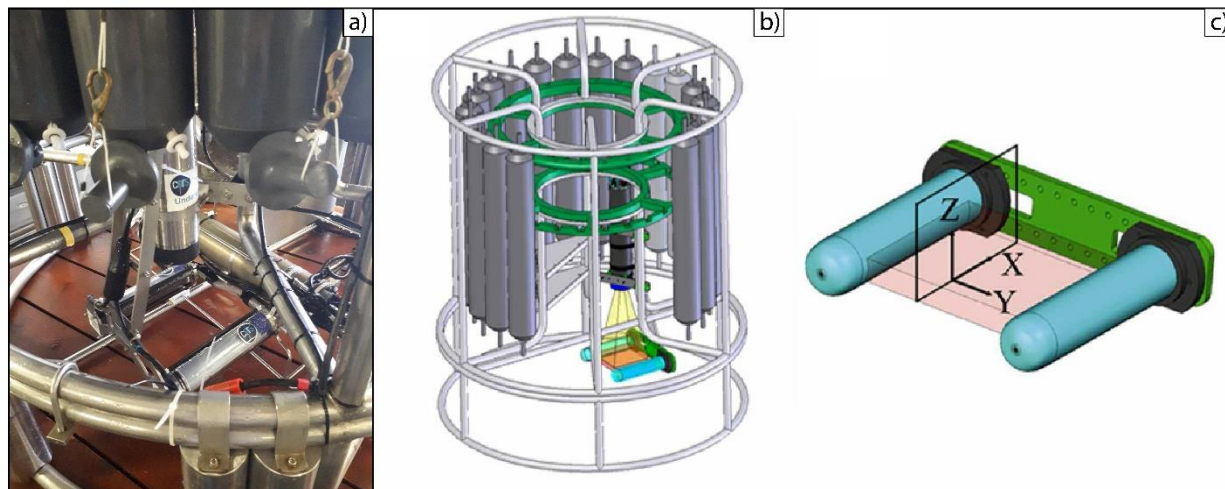


Fig. 5.2 The UVP system in use during the SO289 cruise. a) shows the UVP installed within our stainless-steel CTD frame, below the bottles; b) a diagram of the CTD frame, showing the area viewed by the UVP camera; c) a zoomed in view of the UVP lamps that illuminate a volume of seawater between them to measure particulate density and some water properties such as density (modified from Picheral et al., 2010; Photo: Chris Galley [a]).

Data processing and preliminary plotting was performed on board with *ZooProcess* (Gorsky et al., 2010) and MATLAB, producing six particle density bins (<125 , 125-250, 250-500, 500-1000, 1000-2000, and $>2000 \mu\text{m}$, see Appendix UVP) measured at an average depth interval of 2 m but binned to 10 m intervals during the processing. An example plot of the cruise profile is shown in Fig. 5.3, showing the distribution of particles $<125 \mu\text{m}$ in size. From Fig. 5.3, high particle densities are shown to appear in the top 250 m of the profile (within the epipelagic zone), and near the Chilean coast and Kermadec Arc. Two additional prominent features are the EPR hydrothermal plume and the Monowai cone vent field. High temperature hydrothermal venting occurs along the EPR, producing a plume of precipitating metals spanning the six of the UVP's particle size bins. This contrasts with the venting sampled at the Monowai volcanic cone, which is shallower and contains a mixture of volcanic degassing and hydrothermal venting (Leybourne et al., 2012) (Fig. 5.4). As the Monowai cone's station sampled directly above the vent location, the density of particles in the vent fluid were much higher than that at the EPR station where we sampled near an inferred vent site but were not sure of its exact location. However, the venting at the EPR station contained a higher relative concentration of larger particles. UVP data were collected at Stations 7-44, excluding Station 36.

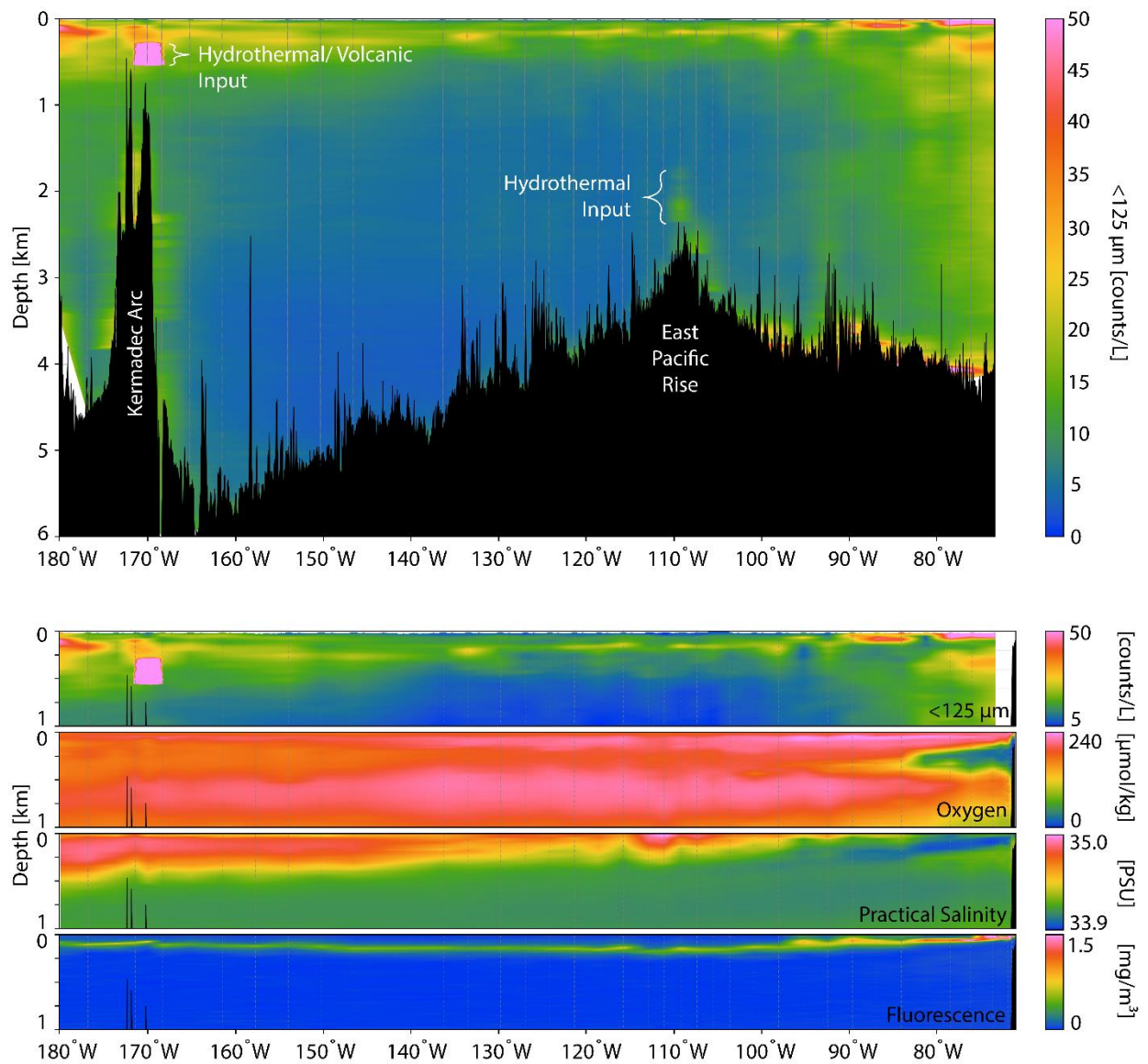


Fig. 5.3 The top plot displays the processed particle density data, for particles <math>< 125 \mu\text{m}</math> in size. The bottom plot shows the top 1km of the profile compared against the preliminary oxygen, salinity, and fluorescence data.

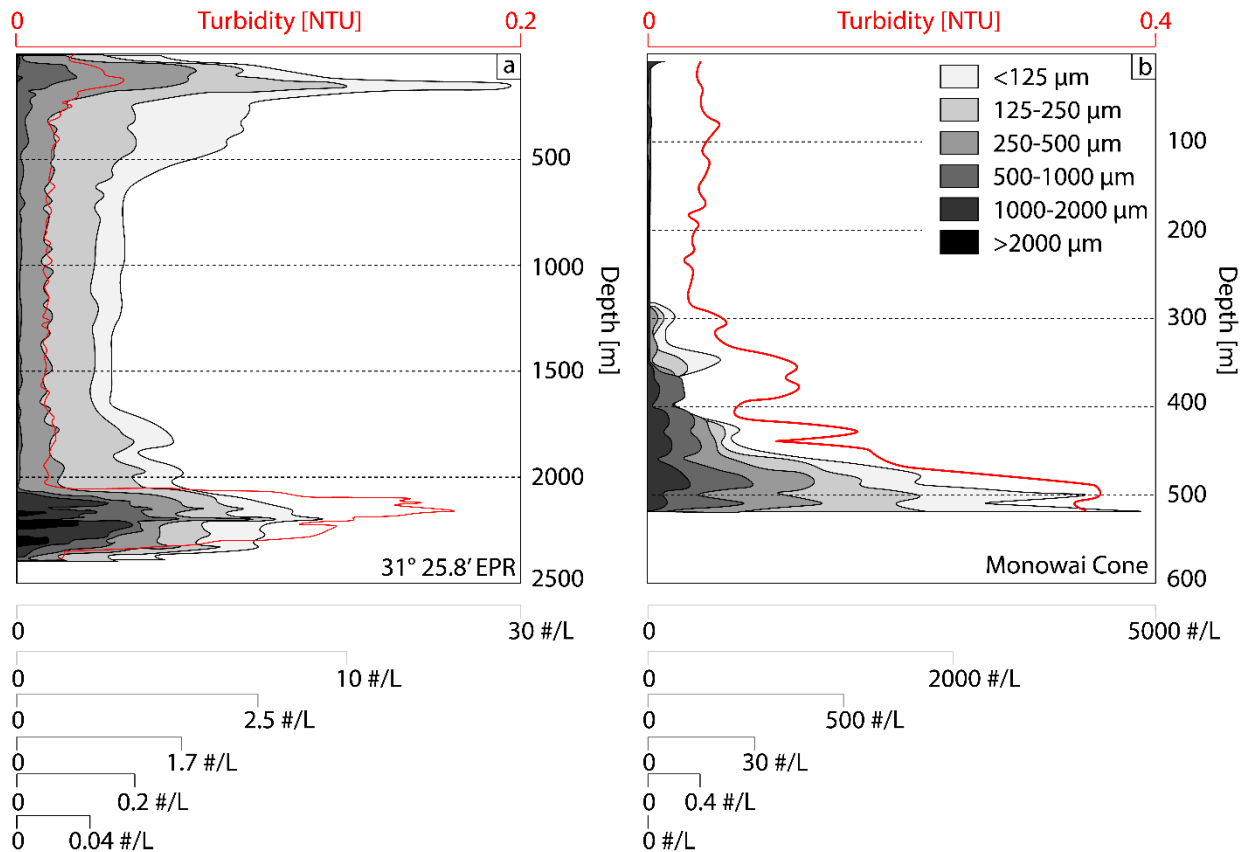


Fig. 5.4 Two turbidity and UVP plots, a) from the EPR station and b) from the Monowai volcanic cone station.

5.3 Multibeam data collection and processing

(C. Galley)

The RV Sonne was equipped with a *Simrad* EM-122 multibeam sonar system from *Kongsberg*, which continuously collected data while the ship was sailing. EM122 data collection was paused while on station, as the ship was stationary. Preliminary processing of the EM122 data was done with the open-source software *MB-System* (Caress & Chayes, 2017). The cleaned data was gridded and interpolated to 25 m resolution mesh with the open-source software *GMT* (Wessel et al., 2019), and was plotted using the open-source program *QGIS* (QGIS Development Team, 2022). Approximately 145,000 km² of high-resolution bathymetry data was collected during the SO289 cruise (Fig. 5.5).

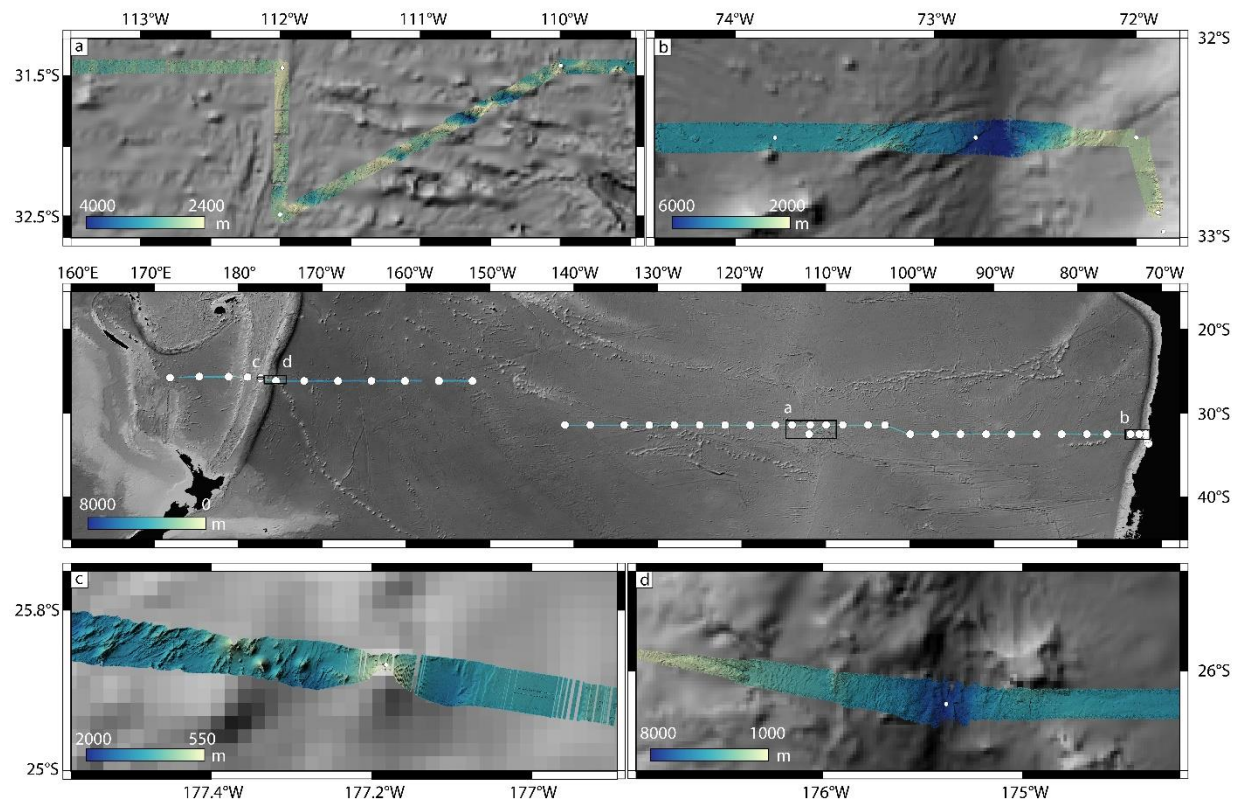


Fig. 5.5 The multibeam data collected during the SO289 cruise, coloured, plotted against grey-scale GEBCO bathymetry data (GEBCO Compilation Group, 2021). Four example sections of the transect have been zoomed in on: a) the EPR spreading center; b) the Chilean Through subduction zone; c) the hydrothermally active Monowai volcanic cone; and d) the Kermadec Trench subduction zone. The cruise's stations are marked by white circles, and depths are in meters below sea-level.

5.4 Dissolved inorganic carbon and total alkalinity sampling

(C. Galley, P. Battermann)

Dissolved inorganic carbon (DIC) water samples were collected from the SS-CTD at every station, except 21. From these samples the total inorganic carbon and total alkalinity can be measured from a number through the water column, across the transect of the SPO. As the amount of carbon dioxide (CO_2) gas dissolved in the samples is a component of the DIC, it was important to collect the samples such that they are free of any air bubbles within the bottle. They were then poisoned with mercuric chloride (HgCl_2) to ensure no organic processes would produce any more CO_2 gas before the samples could be analyzed on land. This data is collected regularly across Earth's oceans to provide information on the amount of anthropogenic carbon being added to the system. For stations 1 to 32 DIC samples were collected at 3 to 6 depths, with every depth being sampled during the last twelve stations that made up the North-West segment of the SO289 transect. 250 mL borosilicate bottles were primarily used to store the DIC samples, however to test an alternate method duplicates were also collected in 150 mL plastic bottle and 25 mL glass vial pairs.

5.5 Acoustic Doppler Current Profiler data collection

(C. Galley)

The RV Sonne was equipped with an acoustic doppler current profiler (ADCP) system, which, as with the EM122 data, was collected continuously when the ship was sailing. ADCP systems acoustically measure the lateral direction and magnitude of ocean current vectors up to 1600 m below the vessel. By releasing an acoustic signal of a known frequency, the ADCP system can infer depth by the arrival time of the signal and the current vector by its frequency shift. All data processing will take place after the cruise.

5.6 Sulfur isotope sampling

(S. Moriarty, C. Galley)

A total of 162 samples were collected for S isotope analysis. The S isotope analyses conducted on the samples will specifically be used to better constrain the average seawater sulfate S isotope value ($\delta^{34}\text{S}$ and D^{33}S), as well as to investigate potential water body-associated isotopic variances in the water column.

Sampling for S isotope analyses involved the collection of ~20 mL of seawater from the stainless steel CTD. Samples were stored in 20 mL plastic vials at room temperature for the duration of the cruise. Samples were collected from specific water masses at each station based primarily on oxygen and salinity CTD profiles, in order to test if water masses can be further delineated & traced using their respective multiple S isotope ($\delta^{34}\text{S}$ and D^{33}S) seawater SO_4 signatures. Generally, ~4 samples were collected from main water bodies per cast: 1 from a shallow depth (<200 mbsl), 1 from an intermediate depth (~800-1000 mbsl), 1 from below the pycnocline (>2000 mbsl, with particular interest in PDW), and 1 bottom water sample generally collected at the maximum depth of the cast. Additional S isotope samples were also collected from water bodies of particular interest. This included the OMZ off the coast of Chile, as well as the oxygenated LCDW in the West Pacific, because S isotope variances may be correlated to deviations in oxygen concentration in the water column (e.g., Li et al., 2010). Samples for S isotope analyses were not collected at every station due to sampling constraints, limitations with respect to post-cruise analytical procedures.

Additional samples (>4) were also collected from particular sites associated with increased S influx, specifically the hydrothermal vent sites at the EPR (Stations 19 to 24; n=29) and Kermadec-Tonga Arc (Station 40; n=12) in order to investigate potential mixing and fractionation processes occurring during hydrothermal fluid discharge and eventual equilibration with the ambient seawater. Higher resolution sampling profiles were collected in the South Fiji Sea (stations 43 & 44; n=18) due to a general lack of published seawater SO_4 S isotope data in that region.

These S isotope analyses will provide critical insight into global seawater sulfate cycling on modern timescales, and specifically test the idea that global ocean sulfate is homogenous with respect to S isotope compositions. These analyses may also help to provide important context to more high priority GEOTRACES investigations, as water column S isotope inhomogeneities (or lack thereof) may be related to the ecological biogeochemical environment from which they were collected. Post-cruise analyses will be completed by Sarah Moriarty at Memorial

University of Newfoundland, following methodology described in Ono et al. (2012) and sources therein.

5.7 The control of surface ocean microbial communities by (micro) nutrient supply phytoplankton abundance, community composition and photophysiology

(Z. Yuan, H. Liu, J. Tammen, Z. Wen, J. LaRoche, T. Browning)

Samples were collected to characterise phytoplankton biomass, community structure throughout the cruise transect. As phytoplankton are the primary driver of nutrient and carbon cycling in surface waters, and nutrient and carbon export to deeper waters, these measurements will also be valuable for interpreting chemical data collected on the cruise. Samples were collected at 42 stations (Station numbers 1-3, 5-21, 23-44) at either 3 depths (Station 1) or 6 depths (all remaining stations) on a dedicated cast throughout the upper water column (surface to a maximum of 225 m depth) using the Ti trace-metal-clean CTD. Depths of sampling were selected after consultation of the beam transmission trace on the CTD (no fluorescence sensor was available on the Ti-CTD unit). Samples for inorganic and organic nutrients and dissolved trace elements were also sampled at these six depths from the same CTD cast.

Chlorophyll-a concentrations: Water was collected in 10 L opaque carboys and processed immediately after collection. 100-200 mL samples were filtered onto Fisher MF300 glass fibre filter pads and extracted for 12-24 hours in 10 mL 90% acetone in a $-20\text{ }^{\circ}\text{C}$ freezer in the dark before measurement on a Turner Designs trilogy fluorometer following the method of Welschmeyer (1994).

Analytical flow cytometry: Water was collected in 10 L opaque carboys and processed immediately after collection. 1.87 mL of seawater was mixed with 0.125 mL 16% paraformaldehyde yielding a final paraformaldehyde concentration of 1%. Mixing was carried out using vortex, after which samples were left for 10 minutes at room temperature in the dark before transfer to a $-80\text{ }^{\circ}\text{C}$ freezer. Samples will be analysed on a FACSort flow cytometer (Beckton-Dickinson, UK) following the method of e.g. Davey et al. (2008), with the intention of analysing for nanophytoplankton, picophytoplankton, *Synechococcus*, *Prochlorococcus* and total bacterial cell counts.

High Performance Liquid Chromatography (HPLC): 4 L seawater was filtered onto Fisher MF300 glass fibre filter pads and placed directly into a $-80\text{ }^{\circ}\text{C}$ freezer. These will be analysed on return to GEOMAR following the method of e.g. Gibb et al. (2000).

POC/PON: Water was collected in 10 L opaque carboys and processed immediately after collection. 4 L was filtered onto pre-combusted Advantec glass fibre filters (25 mm) and frozen at $-80\text{ }^{\circ}\text{C}$.

Virus (surface samples only): Water was collected in 10 L opaque carboys and processed immediately after collection. 50 mL of seawater was filtered through an 0.25/0.45 μm syringe filter and kept in a $4\text{ }^{\circ}\text{C}$ refrigerator. Samples will be transported at $\sim 4\text{-}10\text{ }^{\circ}\text{C}$ to Laboratoire Arago (France) for analysis.

Metagenomics: Samples were collected in ~ 4 L amber Nalgene LDPE bottles. ~ 4 L seawater samples for DNA extractions were filtered onto 0.22 μm pore-sized PES membrane filters

(Supor200, Pall Gelman, NY, USA for Stations 1–30 and Millipore GPWP after Station 30) using a Masterflex peristaltic pump and then frozen and stored in cryovials at -80°C . Samples will be sent on dry ice to Prof. Julie LaRoche at Dalhousie University for extraction and metagenomics analyses following Willis et al. (2019).

Fast repetition rate fluorometry: Fast repetition rate fluorescence measurements enable the calculation of e.g., the so called “normalized variable fluorescence” (F_v/F_m), which can be used as a diagnostic for nutrient stress, especially for iron limitation. A FASTOcean fluorometer (Sensor ID: 14-9740-003) with integrated FASTact laboratory system (both Chelsea Technologies LTD., UK) was used to measure in vitro variable fluorescence of phytoplankton samples. Fluorescence light curves were also run for surface and some DCM samples following a protocol of progressively increasing light intensities between 20 and 2000 $\mu\text{mol photons m}^{-2} \text{s}^{-1}$ (as described in Browning et al., 2014). Blank filtrates (0.2 μm filtrates) were measured for virtually all samples. All FRRf data will be blank-corrected and fluorescence parameters recalculated upon return to GEOMAR. In addition to discrete samples from the CTD-rosette, fluorescence measurements with the FRRf device were conducted by using the pump system on the RV Sonne which enables continuous supply of near surface seawater.

5.7.1 Nitrogen fixation and primary production

(Z. Wen, T. Browning)

Biological N_2 fixation is a key process which provides bioavailable nitrogen for the growth of phytoplankton that live in the euphotic zone. In some areas of the oligotrophic open ocean, such “new nitrogen” derived by the N_2 fixers can equal to the nitrogen diffused from the deep water, which substantially supports primary production and subsequently export production. Despite its importance, few efforts have been conducted to understand the spatial and temporal distribution of N_2 fixation, and a mechanistic understanding of its controlling factors is still lacking, presenting a major barrier to making accurate projections. To address this, N_2 fixation rate incubations were conducted, alongside DNA sampling for the analysis of the abundances of key diazotrophic phylotypes. These efforts were also accompanied by a diverse range of ancillary environmental parameters, alongside several nutrient amendment experiments directly testing the response of N_2 fixation rates to supply of potentially limiting nutrients (Fe and P).

Biology Ti-CTD sampling: Samples were collected at exactly the same depths and stations as for the phytoplankton parameters previously described for the determination of *nifH* gene abundance and for N_2 fixation and primary production incubations (42 stations, Station numbers 1-3, 5-21, 23-44, at 3 depths (Station 1) or 6 depths (all remaining stations) on a dedicated cast throughout the upper water column (surface to a maximum of 225 m) using the Ti trace-metal-clean CTD).

Samples were collected for analysis of the following:

- **N_2 fixation and primary production measurements:** N_2 fixation rates were determined by the $^{15}\text{N}_2$ gas dissolution method (Mohr et al., 2010), combined with a primary production assay using $\text{NaH}^{13}\text{CO}_3$ (99 atom% ^{13}C , Cambridge Isotope Laboratories). The N_2 fixation and primary production incubations were conducted in duplicate 4 L Nalgene polycarbonate bottles. Samples were spiked with 100 mL $^{15}\text{N}_2$ enriched filtered seawater from the same site and incubated on-deck for 24 h. The final $^{15}\text{N}_2$ enriched seawater concentration in the incubation

bottles was ~3 atom%. $\text{NaH}^{13}\text{CO}_3$ solution was added at a concentration of 100 μM . After that, the bottles were incubated for 24 h in an on-deck incubator covered with neutral density screen to adjust the light to the approximate levels at sampling depths, and continuously flushed with surface seawater. The incubation was ended by filtration onto pre-combusted Advantec glass fibre filters after 24 h.

- nifH gene abundance: ~4 L seawater samples for DNA extractions were filtered onto 0.22 μm pore-sized PES membrane filters (Supor200, Pall Gelman, NY, USA for Stations 1–30 and Millipore GPWP after Station 30) and stored at -80°C . DNA will be extracted using the QIAamp® DNA Mini Kit (Qiagen) follow the manufacturer's protocol. The quantitative polymerase chain reaction (qPCR) analysis was targeted on the nifH phylotypes of *Trichodesmium* spp., unicellular cyanobacterial UCYN-A1, UCYN-A2, and UCYN-B, *Richelia* spp. (het-1), and a gamma-proteobacterium (γ -24774A11), using previously designed primers and probe sets (Church et al., 2005a; 2005b; Moisander et al., 2008; Thompson et al., 2014).

Bioassay incubation: 11 x 48-hour duration on-deck incubation experiments were carried out in 4 L trace-metal-clean polycarbonate bottles. Seawater was collected at using the trace-metal-clean towed fish. Bottled seawater was spiked with the following treatments: control, +P, +Fe and +Fe+P. Final incubation concentrations of iron was 2 nM and 100 nM phosphate. Bottles were placed in on-deck incubators connected to the ships underway flow-through system to continuously maintain temperatures at that of sea surface waters. Incubators were screened with Blue Lagoon screening (Lee Filters), which maintained irradiance at ~30% of that of the surface. After 24 hours incubation, all bottles were carried back to the lab, added with $^{15}\text{N}_2$ enriched water and $\text{NaH}^{13}\text{CO}_3$ for the incubations of N_2 fixation and primary production rates. After another 24 hours incubation, experiments were taken down and sampling made for analysis of POC and PON concentrations and their ^{13}C and ^{15}N stable isotopic abundances, and nifH gene abundances of six major diazotrophs.

5.7.2 Nutrient enrichment bioassay experiments

(H. Liu, T. Browning)

Experiments were conducted to assess the main nutrients limiting to the overall phytoplankton community throughout the transect (e.g., Browning et al., 2017). 12 x ~48-hour duration on-deck incubation experiments were carried out in 1 L trace-metal-clean polycarbonate bottles. Seawater was collected using the trace-metal-clean towed-fish. Filling times were approximately ~30 minutes for 1 L bottle experiments (total volume = 42 L). Bottled seawater was spiked with the following combination of nutrients/trace metals:

Control, N, Fe, Co, NFe, NCo, FeCo, NFeCo, NCoZn, NaOH, Control + Stn. 5 5m seawater, N+ Stn. 5 5m seawater, Fe + Stn.5 5 m seawater and NFe + Stn. 5 5m seawater

Final incubation added concentrations of N were 2 μM , Fe were 2 nM, Co and Zn 0.5/0.1 nM, and Stn. 5 5m seawater 10 mL. The NaOH addition was made to a final added concentration of 500 μM .

Initial conditions were sampled in 1 L bottles for all experiments at 3 time points throughout the bottle filling procedure. Triplicate control bottles (1 L) with no nutrients added were also

collected alongside all treatment experiments. Bottles were placed in on-deck incubators connected to the ship's underway flow-through system to continuously maintain temperatures at that of sea surface waters. Incubators were screened with Blue Lagoon screening (Lee Filters), which maintained irradiance at ~30% of that of the surface. After 48 hours incubation, experiments were taken down and measurements made for: Chlorophyll-a concentrations (1 replicate per treatment bottle), FRRf (single acquisitions for each triplicate bottle), analytical flow cytometry, community structure, total alkalinity and pH (for control and NaOH treatments only).

5.7.3 Dilution experiments

(Z. Yuan, T. Browning)

A total of 12 on-deck incubation experiments were carried out in 1 L trace-metal-clean polycarbonate bottles. Seawater was collected using the trace-metal-clean towed-fish into an acid-washed 60 L HDPE carboy, first collecting 16 L unfiltered seawater and then collecting 44 L of filtered (0.2 μm , Pall Acropak) resulting in a ~27% dilution. Total filling times were approximately ~30 minutes. Incubation bottles were spiked in triplicate with a spectrum of (i) $\text{NO}_3^- + \text{NH}_4^+$ (0, 0.1 μM , 0.2 μM , 0.4 μM , 0.8 μM) and Fe (0, 0.1 nM, 0.2 nM, 0.4 nM, 0.8 nM) for Experiments 1, 2, 3, 4, 5, (ii) $\text{NO}_3^- + \text{NH}_4^+$ (0, 0.05 μM , 0.1 μM , 0.2 μM , 0.4 μM) and Fe (0, 0.05 nM, 0.1 nM, 0.2 nM, 0.4 nM) for Experiments 6, 7, 8, (iii) $\text{NO}_3^- + \text{NH}_4^+$ (0, 0.025 μM , 0.05 μM , 0.1 μM , 0.2 μM) and Fe (0, 0.025 nM, 0.05 nM, 0.1 nM, 0.2 nM) for Experiments 9, 10, and (iv) $\text{NO}_3^- + \text{NH}_4^+$ (0, 0.025 μM , 0.05 μM , 0.1 μM , 0.2 μM) and P (0, 5 nM, 10 nM, 20 nM, 40 nM) for Experiments 11, 12 to provide 25 treatments. Bottles were capped, and placed in on-deck incubators connected to the ships underway flow-through system to continuously maintain temperatures at that of sea surface waters. Incubators were screened with Blue Lagoon screening (Lee Filters), which maintained irradiance at ~30% of that of the surface. After 30-48 h incubation, experiments were taken down and each triplicate replicate was subsampled for collection/analysis of chlorophyll-a and flow cytometry.

5.7.4 Photophysiological assessment of phytoplankton to Fe and N supply

(J. Tammen, T. Browning)

To supplement the depth profile and semi-continuous underway Fast Repetition Rate fluorometry (FRRf) measurements, nutrient addition experiments were conducted to assess the short-term (24h) photophysiological responses of phytoplankton to nutrient supply.

Surface and DCM layer incubation experiments were conducted. Acid washed 500 mL polycarbonate bottles were used. Incubation was undertaken in on-deck incubators at ~30% and ~1% of surface irradiance for simulating surface mixed layer and DCM light levels respectively. Incubators were connected to the ship's underway flow through system to continuously maintain temperatures at that of sea surface waters. Sample collection and nutrient addition were conducted in trace-metal-clean environment (over-pressurized with HEPA-filtered air).

Surface incubations: Four different treatments, consisting of control (no amendment), single addition of Fe (50 μL 2nM FeCl_3 in 0.1 M HCl), single addition of N (50 μL 1 μM nitrate and 50 μL 1 μM ammonium) and combined addition of Fe and N (50 μL of each, 2nM FeCl_3 in 0.1 M HCl, 1 μM nitrate and 1 μM ammonium) were conducted simultaneously, each consisting

of 3 replicates. Trace-metal-clean surface water samples (supplied by using the previously described towed fish) were taken at night time and Fv/Fm values were measured for initial samples and following nutrient addition/incubation after 24 h (single acquisitions made for each triplicate bottle). A total of 21 experiments were conducted throughout the transect.

DCM incubations: A total of 17 incubation experiments using water samples from the DCM (sampled with trace-metal-clean CTD) were conducted to test for Fe limitation at this depth layer. Therefore, the experiment only consisted of a control and Fe amended treatments, each with 3 replicates. The procedure was similar to the incubation experiments of surface waters. Fv/Fm values were measured for initial samples as well after 24 h of incubation. Furthermore, fluorescence light curves were also conducted for initial, control and Fe-amended samples.

5.7.5 Nickel addition bioassay experiments

(T. Browning)

A total of 6 experiments were undertaken to assess the impact of nickel (Ni) supply on microbial urea uptake and N₂ fixation rates. Six 4.3 L acid-washed polycarbonate bottles (Nalgene) were filled with surface water from the tow fish. Three bottles were sealed with no amendment and three were spiked to a final added Ni concentration of 2 nM. Bottles were incubated for 48 hours in an on-deck incubator screened to ~25% of surface light levels. In the final 11-18 hours, an addition of 12.5–50 nM ¹⁵N-labelled urea (Sigma-Aldrich) was added to the bottles. After 48 hours, bottles were sub-sampled for flow cytometry (~2 mL) and chlorophyll (0.2 L; see earlier sections) and for ¹⁵N-labelled urea uptake. For the latter, the full remaining volume (4.1 L) was filtered over a pre-combusted Adventec glass fibre filter and frozen directly at –80 °C. Upon return to the laboratory the particulate ¹⁵N enrichment will be analysed using an elemental analyzer coupled to a mass spectrometer (EA-IRMS, Thermo Fisher Flash HT 2000-Delta V plus). These experiments were matched with the N₂ fixation bioassay start points (see N₂ fixation and primary production section, where Ni (2 nM addition) was also included as part of the standard set of nutrient additions (control, +phosphate, +Fe, +Fe+phosphate).

At experimental start points, filtered (0.2 µm Acropak) seawater samples were also collected for later determination of Ni isotope composition (4 L acid-washed LDPE; sample stored at room temperature), Ni ligand concentrations (125 mL acid-washed LDPE; sample frozen directly at –20 °C), and urea concentrations (2 x 50 mL acid-washed PP vials; sample frozen directly at –20 °C).

5.8 Assessment of marine aggregates-associated bacterial and archaeal life and diversity of extracellular vesicles in marine waters

(E. Fadeev)

5.8.1 Sampling of marine aggregates

Sedimentation of organic matter from the surface to deep ocean is part of the biological carbon pump. Sedimentation largely occurs via formation and gravitational settling of aggregates, which include decaying phytoplankton, faecal pellets and other forms of particulate matter, distributing energy and chemical compounds throughout the water column. Marine aggregates are hotspots of microbial activity and are colonized by a variety of microorganisms. The

colonizing microorganisms, mostly bacteria, recycle the particulate organic matter in the aggregates using hydrolytic enzymes, which releases dissolved organic matter and nutrients into the surrounding water. This process forms diverse micro-niches in the aggregates, allowing taxonomic and functional succession of the aggregate-associated communities in the water column. In this cruise, we aimed at sampling marine aggregates from the mesopelagic layer for taxonomic and functional characterization of their bacterial and archaeal communities using molecular techniques.

To sample marine aggregates from the mesopelagic, we deployed McLane Large Volume Water Transfer Systems (ISP) with sequentially mounted 142 mm 3 μm pore size (Millipore) and 0.22 μm pore size filters (Millipore) (Table 12.7). This approach separates between the aggregate-associated ($> 3 \mu\text{m}$) and free-living (0.22-3 μm) bacteria and archaea. Additional water samples were obtained using Niskin bottles housed on a stainless-steel rosette equipped with SBE conductivity–temperature–depth (CTD) sensors. Samples were collected from the deep chlorophyll maximum depth ($< 200 \text{ m}$) and mesopelagic depths (540-750 m; Table 12.7). Similar to the in-situ pump sampling, each seawater sample was sequentially filtered using peristaltic pump through 47 mm, 3 μm and 0.22 μm pore size filters (Millipore). All sampled filters were stored at $-80 \text{ }^\circ\text{C}$ for further analysis in the lab.

5.8.2 Sampling of extracellular vesicles

The dissolved organic matter (DOM) is a major component of oceanic biogeochemical cycles that are driven mostly by marine microorganisms. Due to its operational definition (size cut-off of $< 0.22 \mu\text{m}$), the DOM contains not only “truly” dissolved organic molecules, but also a large portion of other biological-nanostructures like viruses and extracellular vesicles (EVs). While the diversity of marine viruses has been extensively studied, the biogeography of EVs in the ocean remain unknown. Therefore, despite likely being a ubiquitous biological feature in the ocean, we have essentially no knowledge on the functional roles of EVs in the ocean or their contribution to the oceanic microbial food web and the marine DOM pool. In this cruise, I aimed at sampling EVs from surface waters to investigate their abundance and diversity across the SPO.

Water samples of 60 L each were collected using the membrane seawater pump of the vessel, which pumps seawater from ca. 6.5 m depth. Each water sample was pre-filtered via 3 and 0.22 μm 142 mm filter to capture the aggregates-associated and free-living microbial communities, respectively (see section 5.8.1). The filtrate was then concentrated by tangential flow filtration with a 100 kDa cut-off (Vivaflow, Germany) to 500 mL of concentrated sample. From each sample 250 mL of the concentrated EVs (100 kDa – 0.22 μm) and 100 mL of the outflow ($< 100\text{KDa}$) were stored at $-20 \text{ }^\circ\text{C}$ for further analysis in the lab. Additional subsample of 50 mL was collected from each fraction for nutrients analysis (see section 5.21), as well as subsample of ca. 40 mL for dissolved organic carbon (DOC) concentration measurements (see section 5.10).

5.8.3 Further analysis and data management

Collected samples for both marine aggregates and EVs will be used for extraction of DNA and proteins, and then analysed using molecular techniques (metagenomics and metaproteomics, respectively). Additionally, the EVs samples will be used for quantification

using nanoparticle tracking analysis (NTA). All produced data will be made available to the broader scientific community. The molecular ('omics') data will be archived and accessible at the European Nucleotide Archive (ENA), the proteomics data will be archived at the PRoteomics IDentifications database (PRIDE). The NTA data will be deposited on the EV-TRACK platform (<https://https://evtrack.org/>), nutrients and DOC will be included in the scientific publication.

5.9 Full depth water collection with trace metal clean CTD/Rosette

(K. Gosnell, S. Pöhle, D. Jasinski, E. O'Sullivan)

5.9.1 Seawater collection

A Ti rosette frame equipped with 24 trace metal clean 12 L Niskin bottles was used for the collection of trace metal clean seawater samples (TM-clean CTD). The TM-clean CTD was also furnished with sensors for conductivity, temperature, depth (CTD), turbidity and oxygen (Seabird Electronics). The TM-clean CTD was attached and operated using a conducting plastic-coated Kevlar wire and deployed over the side of the ship using a trace metal clean LEBUS winch system. As soon as the TM-clean rosette was recovered and secured on deck, all 24 Niskin bottles were quickly unloaded and hand-carried into the trace metal clean sampling container where sampling was to occur. Clean vinyl gloves were placed on all Niskin bottle taps in order to minimize contamination risk during movement, and then removed once bottles were in the van.

5.9.2 Clean lab Unfiltered seawater sampling

Unfiltered samples were always collected first. The first samples were for dissolved oxygen, which were obtained from only 3 different depths covering the concentration range of dissolved oxygen. Dissolved oxygen samples were taken without any bubbles using a silicon tubing into a 100 mL glass bottle. The overflowing glass bottle was handed outside the sampling van for chemical treatment for Winkler analysis. This was quickly followed by 3 salinity samples (300 mL) from the same 3 depths (both GEOMAR). The next bubble free unfiltered samples collected were for Hg speciation (GEOMAR and Mediterranean Institute for Oceanography (MIO)). Three different samples were collected for Hg; dissolved gaseous Hg sample from approximately every other depth (150 mL); methylmercury from every depth (150 mL), and total Hg from every depth (60 mL). These samples were all collected from nearly every station.

At superstations additional unfiltered samples (~2 L) were collected for sequential filtration for trace metals (Jacobs University Bremen) from 3 depths. Unfiltered samples (1 L) were also collected for Pb isotopes from approximately 8 depths per profile at each superstation (MPI Mainz). Also, unfiltered 2 L samples were filled into Flexboys (bloodbags) using a silicon tube and adaptor from 3 to 6 depths at each superstation, to be used for particulate and dissolved siderophore assessments (GEOMAR). All samples collected were first triple rinsed with the targeted sample water prior to being filled (excluding those for oxygen and siderophores).

5.9.3 Clean lab Filtered seawater sampling

Filtered samples were collected by passing water through a 0.8/0.2 μm filter cartridge (AcroPak 500, Pall). Samples were all triple rinsed with filtered target water prior to sampling. Dissolved aluminum (50 mL), nutrients (10 mL), dissolved cations (5 mL), and dissolved trace

metals (125 mL) were collected from every station and every depth of the transect (all GEOMAR; 44 total stations). Selenium samples (50 mL; University of Zurich) were collected with filtered seawater from every station and depth until Station 22. After that, Se speciation was collected as 3 unfiltered and 3 filtered samples from the chlorophyll max of each station, and from approximately every depth for superstations, or the top 3-4 depths of regular stations.

Additional filtered samples were also collected at superstations. Dissolved chromium samples (1 L; University of Lausanne) were collected from approximately 8 spaced out depths up until station 23. One Niskin bottle was dedicated to collect 8-10 L of filtered seawater for ultrafiltration processing at the chlorophyll max (Jacobs University Bremen). Filtered samples were also collected for dissolved trace metals (100 mL), high-field strength elements (HFSE; 100 mL), organic ligands (125 mL and 250 mL), and Cr and V speciation (100 mL each) at approximately 20 of the superstation depths (all Jacobs University Bremen). These samples were also collected at approximately every third normal station, depending on spacing in the station scheme (see section 5.19 for further detail). Fluorine samples (60 mL) were also collected from every depth (GEOMAR). A 1 L sample for Fe-Cd isotopes (University of Florida and GEOMAR) was further collected from every superstation depth. Additionally, filtered subsamples were collected for the analysis of the soluble fraction of trace metals from 12-22 depths. These samples were initially collected in 125 mL bottles, and then the water was further filtered through 0.02 μm filters (25 mm, Anapore) via syringe filtration under a laminar flow bench outside the clean lab container.

All LDPE bottles used to collect respective trace metal clean samples were cleaned prior to the cruise in accordance with GEOTRACES cleaning approval. Further information on this is provided in the GEOTRACES cookbook (<https://www.geotraces.org/methods-cookbook/>.)

5.9.4 Particulate filter samples

After AcroPak sample filtering was finished, the Niskin bottles were all opened up and connected to pressurized nitrogen gas lines (~0.5 bar; 99.999% AlphagazTM 1) for trace metals in particulate matter (>0.2 μm) collection. Each Niskin bottle had its own gas line and tubing setup which could be manually opened or closed as needed. For superstations every depth would have a particulate matter sample, while 12-16 filter depths were collected for particulate material at normal stations. For these samples; an acid-cleaned and milliQ rinsed polyethersulfone (PES) filter (25 mm, Pall) was placed in an acid-cleaned Swinnex filter holder, then directly attached to the Niskin bottle tap. After ensuring that the bottles were secure under pressure, the taps were opened up and water was allowed to filter out. A 2 L volumetric pitcher was placed below each filter to collect and record how much water volume passed through each filter. Water volumes were variable depending on the depths and region, however typically 2-8 L would pass through each filter. After collection the filter was gently removed via Teflon tweezers and placed in a petri dish or small clean bag, then stored in the freezer prior to shipment back to GEOMAR.

5.10 On-deck sampling for He and DOC

(L. Blum)

³Helium is a conservative tracer for vent supply, which allows us to trace hydrothermal vents of the EPR. Helium is a low-density gas, samples for helium isotopes were sampled first from

the Niskins of the SS-CTD. Seawater samples for helium were collected in a copper pipe, which was connected to the Niskin bottle, with water flowing until bubbles in the tube were removed. While the water was flowing, the pipe was closed using an electrical drill and a ratchet to ensure it is tight enough. Helium isotopes will be analysed at the University of Bremen. In addition, 0.5 L samples for tritium analyses were collected at 3 full depth CTD casts (Station 27, Station 34, Station 40). The samples will be analysed in Bremen too, and the data will serve to correct the He isotope measurements for tritium present in the deep-water. Dissolved oxygen samples were taken bubble free in 100 mL glass bottles for subsequent Winkler analysis.

DOC samples were taken and acidified to pH 2 in the lab. Shallow samples from 400 m upward were filtered through an ashed GF/F filter. DOC samples will be analysed at GEOMAR using a Shimadzu TOC/TDN instrument.

5.11 Oxygen

(L. Blum)

Oxygen concentrations of the different CTD casts were measured by oxygen sensors attached onto the rosette frames. 254 discrete oxygen samples were collected from different depths of the water column and the CTD casts to calibrate these sensors. For the trace-metal-clean CTD, three samples were taken at the deep cast, starting at station 15. For the stainless-steel CTD, there were up to five samples taken, including the oxygen minimum zone. Oxygen concentration samples were analysed during the cruise using the Winkler (1888) Method.

5.12 Particulate and dissolved siderophores

(L. Blum)

Siderophores are organic ligands that show specificity for iron and are assumed to play an important role in keeping seawater iron in solution. Two litre samples have been collected in FlexBoys from the Niskin bottles of the Trace metal clean CTD at super stations and additional coastal stations. Six samples were taken in the shallow cast, including the deep chlorophyll maximum (DCM) and the different light levels. Four evenly spread samples were taken in the deep cast. After adding the internal Standard (160 pM H-Riboflavin concentration) to the samples, the samples were filtered using Sterivex PVDF filters and Bond Elut ENV 500 mg columns by gravity. The filters were frozen at $-80\text{ }^{\circ}\text{C}$ and the columns at $-20\text{ }^{\circ}\text{C}$ to be analysed via HPLC-MS after the cruise. The FlexBoys, filters and columns were cleaned with methanol, HCl (0.1 M) and MQ before sampling. In total there were 130 samples taken.

5.13 Sampling and analysis of dissolved Al

(T. Liu)

Aluminum (Al) is a scavenged-type trace metal in the oceans whose concentrations tend to be highest near its major sources such as river, atmospheric dust, seafloor sediments and hydrothermal vents. Dissolved Al has been used as a tracer of atmospheric inputs in surface waters (Barraqueta et al., 2019) and shown to trace water mass mixing at depth (Middag et al., 2011). Filtered seawater samples were collected from the Ti-CTD rosette and an underway Towed-Fish system (Table 12.22). The analyses of dissolved Al were performed on shipboard following Ren et al., (2001) using a Carey Eclipse fluorimeter. Dissolved Al concentrations

were calibrated using standard additions from a 1 μM Al stock solution (in 1M HNO_3) to filtered acidified seawater that was collected in the SPO with a Towed-Fish system. An eight-point calibration line (0, 1, 2, 4, 8, 12, 15, 20 nM Al standard additions), blank determination and an internal reference sample were measured every batch. Blank contributions were determined as two separate parts, the manifold blank and the reagent blank. The manifold blank was assessed by the average counts of two acidified seawater samples (one is the surface water and the other is the deep water) without reagents. The reagent blank was determined using two different methods. One was by the analysis of three acidified seawater samples spiked with 1x, 2x and 3x volume of reagent. The other method was using two series of calibration line with 1x and 2x volume of reagent, respectively. The reagent blank was assessed by the difference in the intercepts of two series of calibration lines.

Samples for dissolved Al concentrations were taken and analyzed from all the Ti-CTD casts and underway tow-fish sampling.

Preliminary results for the entire water column show generally high concentrations of dissolved Al in the surface water and bottom depth, indicating aeolian dust and sediment input in the South Pacific. Relatively higher dissolved Al (up to 10 nM - 15nM) was observed at the hydrothermal vent station and decrease with increasing distance to the vent (Fig. 5.6). Relatively high surface dissolved Al concentrations were observed close to the South American and Australian continents (Fig. 5.7).

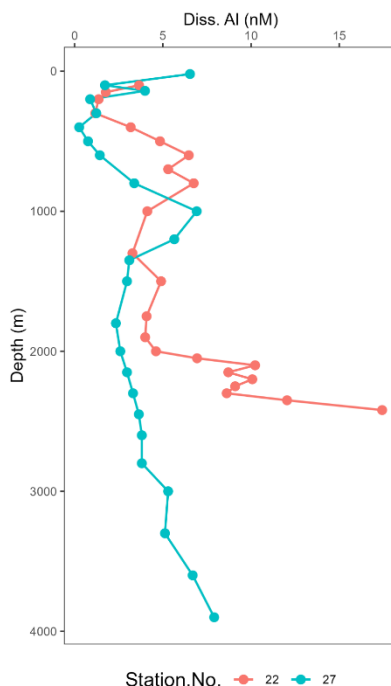
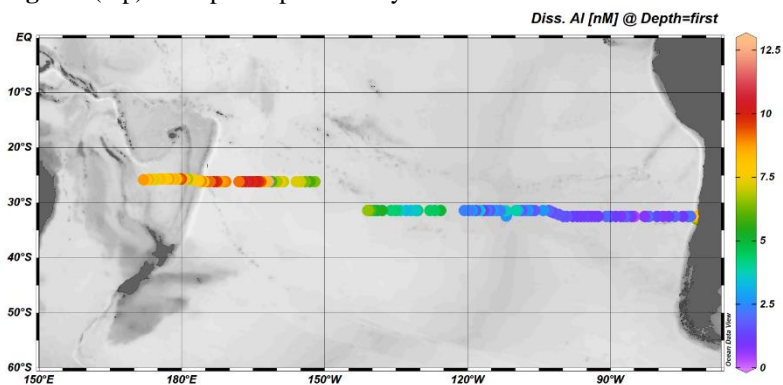


Fig. 5.6 (top) Example of preliminary dissolved aluminum concentrations



at the hydrothermal vent station (Station 22) and Station 27 that is ~570 km west of the vent site.

Fig. 5.7 (left) Preliminary dissolved aluminum concentrations of the surface waters along the transect.

5.14 N_2O - CH_4 - CO and Nitrate-isotopes

(G. Li)

For N_2O and CH_4 , bubble-free triplicate water samples were collected from Niskins of the SS-CTD and immediately sealed by means of butyl stoppers and aluminum crimps. Saturated mercuric chloride (HgCl_2) solution was added to poison the samples. The samples will be

analyzed by means of a headspace equilibrium method and gas chromatography at GEOMAR. In order to decipher nitrogen cycling, Nitrate-isotope samples were collected at selected locations and the same depths at which N₂O samples were collected. Samples were collected in 100 ml sampling bottles, which were immediately frozen at –20 °C.

In order to assess the rate of CO photo-production under different wavelengths in the SPO, samples for determining the apparent quantum yields (AQYs) of CO photoproduction were sequentially passed through polyethersulfone membrane filters, transferred into acid-cleaned 10 L clear containers, and stored in the dark at 4 °C. The samples were brought back to a land-based laboratory and irradiated within two months of sample collection.

The field work conducted during the SO289 cruise will provide:

- a. High resolution measurements of trace gases (N₂O, and CH₄) in SPO, thereby leading to a regional estimate of the rate of transfer between ocean and atmosphere and its overall importance.
- b. Comprehensive view of the large-scale water column distribution of N₂O and CH₄, which in combination with hydrographic and chemical information collected by other groups will help elucidating its transport pathways towards and from the South Pacific, and its main production/consumption processes.
- c. Revealed the significant role of the SPO in global oceanic CO photochemical process.

5.15 Radiogenic Isotopes (neodymium, hafnium) and Rare Earth Elements

(Z. Zhang, A. Xu, M. Frank)

Radiogenic neodymium (Nd) and hafnium (Hf) isotopes are a set of tracers that provide information about water mass mixing and erosional input into seawater. The isotopic signatures in continental rocks vary as a function of type and age of the rocks, which release these signatures during weathering and transfer them to seawater via riverine and dust inputs, but also via exchange with shelf sediments (Frank, 2002). Water masses therefore acquire their radiogenic Nd and Hf isotope signatures through weathering of rocks with characteristic isotopic compositions. The Nd residence time between 400 and 2000 y allows the tracing of deep-water mixing from different sources using their isotopic values. Hf is released incongruently from rocks as a function of both rock composition and the degree mechanical weathering (van de Flierdt et al., 2002), and has a shorter residence time than Nd. Hf isotopes are consequently more indicative of regional continental weathering inputs (Rickli et al., 2009; Stichel et al., 2012). The combination of Nd and Hf isotopes thus allows tracing water mass mixing as well as exchange with the continents and dust.

During cruise SO289, our primary goal was to obtain water samples to investigate the inflowing deep waters from the Southern Ocean and North Pacific in the SPO, as well as removal processes of REEs near the EPR. Besides water mass mixing, we will also investigate the influence of boundary exchange on the dissolved Nd and Hf isotope compositions at the SPO margins, including dissolved and particulate riverine inputs, shelf exchange off South America and New Zealand, as well as dust input from Australia.

For the radiogenic Nd and Hf isotope measurements a total of 181 samples were taken covering the entire cruise track (Table 12.21). Samples from the full water column were collected with 10 L Niskin bottles attached to a stainless steel CTD rosette. Starting at Station 18, 40 L of surface seawater were taken per sample from the fish pump (trace-metal clean) right before or after the station in order to allow measurements of the isotopic composition at the expected low concentrations. The samples were then treated in the onboard laboratory strictly following recommended GEOTRACES protocols. Each 20 L sample was filtered through a nitro-cellulose acetate filter (0.45 μm pore diameter) into an acid-cleaned LDPE-cubitainer (20 L) with a peristaltic pump within 2 h after sample collection, and subsequently acidified with 1 mL/L concentrated, distilled HCl. For determination of Nd/Hf concentrations, REE concentrations, Silicon isotope and Barium isotope measurements, 1-2 L aliquots from each filtered sample were collected in acid-cleaned 1 or 2 L PE-bottles and acidified. To each large volume sample, 25 $\mu\text{L/L}$ FeCl_3 solution (~ 200 mg Fe/mL) were added and the sample was left to equilibrate for 24 h. Ammonia solution (25%, Merck Suprapur®) was then added to raise the pH from about 2 to 7.8-8.2. After 48 h, the trace elements co-precipitated with the iron hydroxide precipitates settled to the bottom of the cubitainers and the supernatant was syphoned off. The precipitates were then transferred into 2 L PE-bottles, and were transported to the home laboratory at GEOMAR for further ion-chromatographic cleaning and measurement via MC-ICPMS.

At several stations, for example those close to the East Pacific Rise (Sta. 22) and continuous fish samples in the Fiji Basin (Sta. 39-44), additional 106 water samples were taken for REEs measurements. Samples were collected into either 125 mL LDPE or 1 L or 2 L PE-bottles via AcroPak online filtration and subsequently acidified.

5.16 Stable Silicon isotopes and Barium isotopes

(Z. Zhang, A. Xu, M. Frank)

The stable isotope composition of silicon ($\delta^{30}\text{Si}$) is a powerful tool to investigate the cycling of dissolved silicon (Si). It is primarily used to trace Si utilization and diatom productivity in the surface waters (Reynolds et al., 2006). Its utility to trace water mass mixing has also been investigated throughout the global ocean (De Souza et al., 2012a; 2012b). At high southern latitudes, the uptake and associated isotope fractionation of Si by diatoms result in highly elevated $\delta^{30}\text{Si}$ values, which can be introduced into the ocean interior by the subduction of Subantarctic Mode Water (SAMW) and AAIW, whose northward spreading result in a strong isopycnal control on lower-thermocline and intermediate $\delta^{30}\text{Si}$ values at lower latitudes.

The stable isotope composition of barium ($\delta^{138/134}\text{Ba}$) is a novel tracer for biogeochemical cycling of barium (Ba) (Horner et al., 2015). It has also been tested to trace water mass mixing in the Atlantic (Bates et al., 2017). Distinct $\delta^{138/134}\text{Ba}$ signals in different deep-water end-members facilitate the applicability of $\delta^{138/134}\text{Ba}$ to trace water mixing in the deep ocean, as well as to identify non-conservative behavior of Ba, revealing additional inputs or sinks of Ba during transport (Hsieh and Henderson, 2017).

During cruise SO289, we aim to test the utility of both $\delta^{30}\text{Si}$ and $\delta^{138/134}\text{Ba}$ as water mass tracers in the intermediate and deep water of the SPO. Our sampling transect spans a large gradient in primary productivity from the upwelling region off Chile to the oligotrophic

subtropical gyre. Therefore, besides water mass mixing, we will also apply $\delta^{30}\text{Si}$ to investigate Si utilization and diatom productivity in the euphotic zone and apply $\delta^{138/134}\text{Ba}$ to better understand organic matter degradation in the twilight zone, especially in the oxygen minimum zone in the eastern SPO. In addition, we will also evaluate the influence of the hydrothermal plume from the EPR on the deep $\delta^{30}\text{Si}$ and $\delta^{138/134}\text{Ba}$ distribution.

In total, 180 water sample aliquots for stable Si and Ba isotopes were taken from the large volume samples for Nd/Hf isotopes, via nitro-cellulose acetate filter (0.45 μm pore diameter) filtration (see section 5.15). In addition, another set of 45 water samples were taken from the upper 200 m in the Chilean upwelling region (Sta.1 to Sta.8) for stable Si and Ba isotopes analyses. They were collected in 125 mL LDPE-bottles via AcroPak online filtration from the trace-metal clean titanium CTD (BIO-CAST) and stored in the dark. These samples were transported to the home laboratory at GEOMAR for further pre-concentration, ion-chromatographic cleaning and measurement via MC-ICPMS.

5.17 Transient Tracers in the South Pacific Ocean: ^{129}I and ^{236}U

(N. Casacuberta Arola)

Transient tracers generally stand for artificial substances that human activities have generated and ultimately released to the marine environment. Depending on their biological, chemical and physical characteristics, they are capable of labeling different ocean processes (Jenkins and Smethie, 1996). In particular, those behaving conservatively in seawater, either because they are soluble or gases, have been used as powerful tools that provide with a unique opportunity to study the effects of the changing climate on the ocean. Good examples of transient tracers are the CFCs and SF_6 gas tracers, and radionuclides of either natural or artificial origin (^{14}C , ^{137}Cs , ^3H , etc.). The long-lived (i.e. $T_{1/2}$ of millions of years) artificial radionuclides ^{129}I and ^{236}U are two novel oceanographic transient tracers that have emerged in the last 20 years thanks to advancements in Accelerator Mass Spectrometry (AMS) techniques (Smith et al., 2011; Casacuberta et al., 2014). Both radionuclides have been introduced to the marine environment either from controlled releases from the Nuclear Reprocessing Plants (NRPs) of Sellafield (UK) and La Hague (France) and/or atmospheric weapon tests (global fallout) (Christl et al., 2015). Given their recent input to the oceans (from 1950s) and due to the different release history (input functions), they are used today as excellent markers to understand the origin of water masses, their circulation timescales and the mixing regimes of waters (advection and diffusion processes) (Casacuberta et al., 2018; Wefing et al., 2021).

In 2013, the US GEOTRACES Eastern Pacific Zonal Transect (GP16) performed a few observations of ^{236}U in the coast of Perú (Villa-Alfageme et al., 2019) proving the potential of ^{236}U in identifying and resolving the origin of water masses. During the GEOTRACES GP21 in the South Pacific Ocean, we aim at performing a more comprehensive transect of both ^{236}U and ^{129}I along the 32°S line to add to the 2013 data. On one hand, we aim at having a broader overview of the distribution of weapon-test derived radionuclides to constrain their sources and use their distribution to understand circulation patterns and mixing regimes. On the other hand, this study will set the base for “background” concentrations of both radionuclides in the South Pacific, before the European reprocessing plant’s signal penetrates into these basins. To this aim, 200 samples were collected for the analysis of ^{129}I (250 mL) and 100 samples for ^{236}U (3

L), corresponding to 10 stations along the 32°S line. Full profiles were taken at stations 6, 9, 13, 17, 25, 29, 32, 34, 37 and 43. Samples were taken from the CTD rosette, rinsed three times with seawater and then filled up in 250 mL dark bottles and 3 L cubitainers, respectively for ^{129}I and ^{236}U . Samples will be sent to Zürich where they will be analyzed and measured in the following months upon their arrival.

5.18 Mercury collection and analysis from the South Pacific

(K. Gosnell, A. Kleindienst)

5.18.1 Project overview

Mercury (Hg) is delivered to the surface ocean through atmospheric deposition while deep water reservoirs tend to show increases of concentrations with depth due to particle remineralization. Most atmospheric Hg comes from anthropogenic sources (i.e coal fired power plants and cement manufacturing), while volcanos and hydrothermal vents contribute natural atmosphere and deep-water sources. No measurements of Hg have yet been completed for the SPO, with a transect completed just south of the equatorial Pacific (Bowman et al., 2016). Accordingly, the SO289 cruise will provide the first Hg speciation data transect for the SPO. Measuring the Hg biogeochemistry and speciation cycling in the water column in high resolution depth profiles of total Hg (THg), methylmercury (MeHg) and dissolved gaseous mercury (DGM) will provide data to complete a circulation link for global evaluations as well as to the different models and other investigations completed throughout the greater Pacific.

5.18.2 Mercury sampling

Unfiltered seawater was collected directly from the TM Clean Niskin bottle for Hg speciation samples. Each sample was filled with ~5% of the water volume and triple rinsed. Bottles were filled until slightly overflowing, with care taken to limit the amount of bubbles in the water. Caps were attached tightly and bottles were placed in separate boxes for transport and lab analysis. Three bottles were used to collect samples for the 3 different mercury speciation measurements. DGM was always collected first into a 125 mL PET bottle from 12-14 alternating depths (including surface tow fish) of each profile. This was followed by MeHg samples into a separate 125 mL PET bottle, and the THg sample into an acid-cleaned 60 mL Teflon (PFA/FEP) bottle. Triplicate sample collection was conducted at several stations for quality control. The MeHg and THg samples were collected from every depth, as well as surface tow fish samples. The THg sample bottles were used repetitively throughout the cruise for collection and analysis, while DGM and MeHg bottles were always fresh. Complete mercury profiles were collected from every station excluding: 4, 7, 9, 13-15, 21, 26 and 44. DGM was furthermore not collected at stations 20 and 27.

5.18.3 Particulate mercury filters

Superstations (14 total) were sampled for particulate Hg (pHg) at specific target depths (e.g. surface, 50-60 m, max chl, OMZ, within plume). Cut-outs of QMA filters of ~25 mm were collected at all superstations for THg analysis (LECO, AMA 254) at MIO Marseille.

The remaining filter material (QMA) was preserved for particulate THg isotope analysis at all superstations. A preconcentration step is required before analysis using MC-ICP-MS. Preconcentration is realized by thermal combustion (all Hg converted to gaseous elemental Hg)

followed by oxidative trapping (Jiskra et al., 2021). Obtained samples will be checked for THg concentrations, as a minimum of 10 ng/L of Hg is required for each measurement.

5.18.4 At-Sea Analytical work and sample processing

All ship-board analysis was completed on a Brooks Rand Model-III instrument that was modified for streamlined and mobile ‘on-line’ analysis (US EPA method 1631; Heimbürger et al., 2015). The Hg amount was quantified by Cold Vapor Automatic Fluorescence Spectrometry (CVAFS) via a lamp and quartz cuvette (US EPA method 1631). Argon gas flow was set to 1 Bar, and was additionally regulated into the instrument using an AALBORG mass Flow Controller set to 0.15 mL/min. The Model-III sensitivity PMT was set to 900 V. Gold traps were replaced when the sensitivity dropped significantly (<90%), which was typically after 5-7 days of continuous use.

5.18.4.1 Methylmercury (MeHg)

Upon reception the MeHg samples were acidified using concentrated HCl (620 μ L) and placed in a plastic bag, then put in a box for storage. Methylmercury analysis will be completed using isotope dilution (Monperrus et al., 2005) via an ICPMS in the laboratory at MIO within the next 8 months. In total 34 profiles were collected for MeHg.

5.18.4.2 Total Hg (THg)

The analytical reagents bromine monochloride (BrCl) and Stannous chloride (SnCl_2) were prepared at the beginning of the cruise following US EPA Method 1631. To start the analytical day ~30-40 mL of BrCl treated seawater was added to the sparging tube, followed by 1 drop of SnCl_2 , and the plunger cap was quickly and tightly sealed. Water was repetitively sparged until blank levels were consistent for ~3 peaks. Each THg run would be sparged for 240 sec (4 min). Every day a working standard curve was created by pipetting increasing concentrations of NIST Hg standard into the purged water of the sparging tube until satisfactory ($r^2 = 0.99xx$).

The BrCl was pipetted directly into each THg sample bottle (105 μ L) at minimum 0.5 hour before analysis. For analysis; approximately 30 mL of the sample was poured into the sparging tube and 1 drop of SnCl_2 (~30 μ L) was added just before tightening. Sample peak area was recorded and quantified after ending each run. Purged water was poured into a measuring tube after analysis had ended in order to record sample volume. Duplicate analyses were completed for THg on a minimum of 6 samples per station by analyzing the remaining sample volume. A 50 pg Hg NIST reference standard was analyzed every ~6 samples and at the end of the analysis to track potential drift. Total Hg analysis was completed on 34 profiles for the cruise.

5.18.4.3 Dissolved Gaseous Mercury (DGM)

DGM is volatile and mobile, and rapidly escapes out of collected samples. Accordingly, DGM samples were always analyzed first and as soon as possible. As DGM samples provoke quicker Au trap deterioration, and require more time, approximately 12-14 depths (out of 24/25) were analyzed for DGM per each station.

For DGM analysis a standard curve was first completed as described for THg measurements. The introduction setup and settings were then switched and adjusted for DGM analysis by attaching a bottle cap and sparging bulb directly to the first valve loop. DGM samples were

measured as collected using no chemical treatment. Adequate head space was formed in each sample by quickly pouring out water immediately before attaching it to the sparging cap for analysis. Water was typically adjusted until sample volume met 125 mL. Each sample was then attached directly to the online sparging cap for analysis. DGM samples were sparged for 752 s (~12.5 min) with Ar. DGM sample analysis was bracketed by standard measurements of 50 μ L Hg (NIST) to assess potential drift during the run. Every DGM sample was acidified with concentrated HCl (500 μ L) after analysis and placed in a plastic bag, then storage box until future MeHg analysis could be completed via isotope dilution (Heimbürger et al., 2015; Monperrus et al., 2005) at MIO. A total of 32 profiles were completed for DGM samples during the cruise.

5.18.4.4 Mercury Methylation and demethylation incubation experiments (3 stations)

Species-specific enriched stable isotope incubation experiments (10 pM $^{199}\text{Hg(II)}$, 1 pM $^{201}\text{MMHg}$) were completed in order to determine methylation and demethylation rates following established protocols (Rodriguez-Gonzalez et al. 2013) for 3 stations at chosen depths (eg. surface, max chl, OMZ, bottom-waters). The relative importance of (a-)biotic transformations was addressed by incubating unfiltered and filtered (AcroPak 500, 0.2 μ m) waters under dark and light conditions for 24 hours. Incubations were stopped by addition of 0.5 % (v/v) HCl. Samples will be analyzed at the University of Pau by double-double spike species specific isotope dilution.

5.18.5 Preliminary Results Overview:

The THg profiles were relatively consistent throughout the transect, displaying low surface THg, a subsurface minimum typically coinciding with the chlorophyll maximum, then a gradual increase in concentrations with depth (Figs. 5.8). DGM was consistently lowest in surface and increased with depth (Fig. 5.8). Average deep-water values for THg ranged up to ~1 pM, while deep water DGM was approximately half at 0.5 pM. A distinct higher THg hydrothermal plume signal was measured next to the mid-ocean ridge spreading axis (Station 22; Fig. 5.9). This signal coincided with a distinctive drop in DGM values, and prominent turbidity measurements.

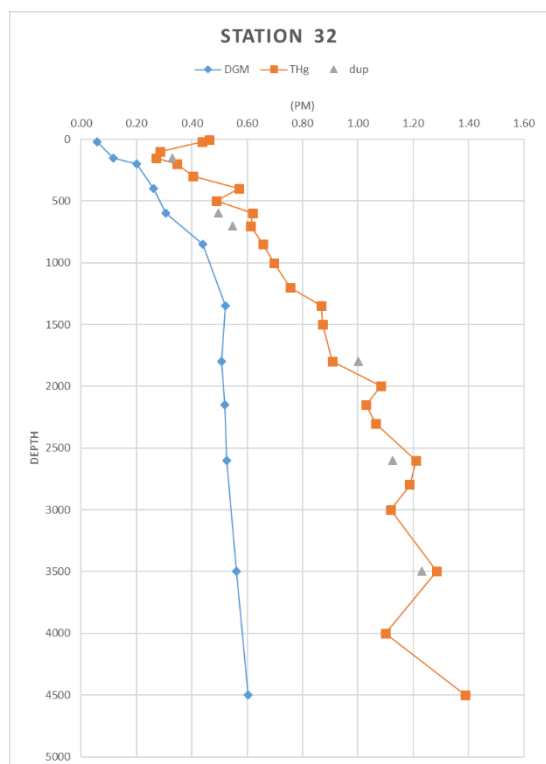


Fig. 5.8 Results from a typical total mercury (THg; orange) and dissolved gaseous mercury (DGM; blue) profile measured during the South Pacific SO289 transect. Station 32 is displayed.

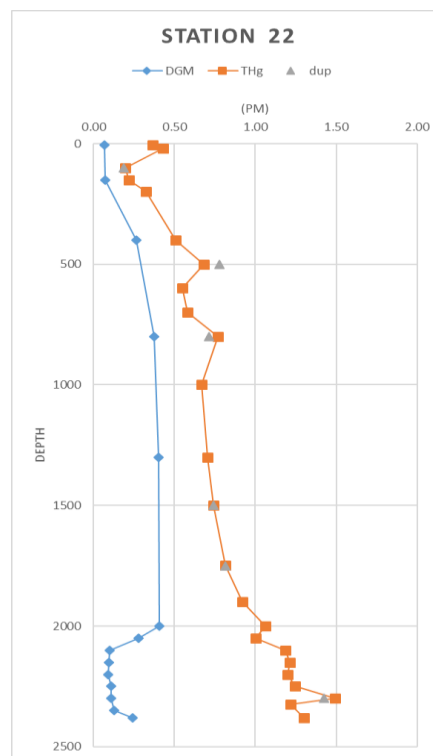


Fig. 5.9 Total mercury (THg; orange) and dissolved gaseous mercury profile (DGM; blue) profile collected around the mid-ridge spreading axis (Station 22) of the SPO289 cruise.

5.19 Investigation of trace-metals, HFSE, Cr and V redox speciation and organic Fe, and Cu ligands in different size fractions

(S. Pöhle, N. Fröhberg, C. Gürses, I. Pedre)

5.19.1 Areas of interest

In order to study the distribution and the physico-chemical speciation of trace metals in the South Pacific, our sampling strategy was based on a series of 11 normal stations (0.2 μm filtered samples only) and 15 superstations (including sequential filtration and ultrafiltration procedures), during which we acquired a total of 2436 samples.

The cruise track offers three areas of investigation for our study: 1. The pronounced oxygen minimum zone (OMZ) off Chile; 2. The hydrothermal plume at the East Pacific Rise (EPR) and 3. The Australian dust input in the western South Pacific.

5.19.2 Elements of interest

Molybdenum (Mo) and uranium (U) were chosen as representatives for commonly known conservative metals for this investigation. Recent studies reported deviations from the conservative behaviour of dissolved Mo in anoxic environments such as tidal flats (Dellwig et al. 2007) warranting more detailed investigations in the area influenced by the OMZ in the eastern part of the transect. Chromium (Cr) and vanadium (V), on the other hand, represent

redox-sensitive trace metals in the marine environment. Since the redox species of the four aforementioned trace metals differ in their particle reactivity, the abundance of the dissolved trace metals in different size fractions might be affected by the dissolved oxygen concentration and the presence of particulate matter to sorb onto. Hence, the pronounced OMZ off Chile is of particular interest to investigate the depth distribution of the selected metals with respect to their size fractionation.

Besides these trace metals, we also investigate the so-called high field strength elements (HFSE) like zirconium (Zr), hafnium (Hf), niobium (Nb) and tantalum (Ta). The ratios of Zr/Hf and Nb/Ta have been suggested to serve as a paleoproxy for water masses (Frank, 2011). However, their analysis is challenging since their concentration in seawater is very low (pmol/L) and a preconcentration step is necessary prior to their analytical determination (Poehle et al., 2015). The HFSE are known to be very particle-reactive and therefore easily sorb onto particulate matter either from biogenic or mineral source. The pronounced OMZ off Chile with high bioproductivity as well as the area influenced by Australian dust input are therefore of high interest for our study on these HFSE.

Finally, fate and biological availability of trace metals is not only controlled by their concentration and inorganic speciation but also highly dependent on the complexation by organic ligands. These molecules can be decay products of organic matter or be actively produced by marine micro-organisms to control the solubility and biological uptake of trace metals like for example iron (Fe) or nickel (Ni) as micronutrients or copper (Cu) that can be both limiting growth factors at low concentrations or show toxicity at high levels. Throughout the transect, we sampled for analysis of Fe-binding ligands (FeL) and took additional samples for Cu-binding ligands (CuL) during the eastern part of the transect affected by the OMZ.

To summarize, filtered seawater samples were collected for the analysis of selected trace metals (TM), HFSE, Cr- and V redox species, and Fe- and Cu binding ligands in different size fractions.

5.19.3 Sampling Procedure

Sampling was done with 24 x 12 L Niskin water samplers attached to a titanium rosette equipped with sensors for conductivity, temperature and depth (CTD). This CTD-set-up comes with its own winch and a polyethylene coated KevlarTM cable to avoid metal contamination. After the completed up-cast, the Niskin bottles were immediately transferred to a clean-lab container, where they were filtered through 0.8/0.2 μm AcroPak (Pall) filters. Among aliquots for other workgroups subsamples for trace metals, HFSE, redox speciation of Cr and V, and Fe- and Cu binding ligands (for more information on sampling, see section 5.9) were collected for this study and transferred to the chemical lab for processing.

At each superstation, we collected three unfiltered samples from pre-defined depths for the sequential filtration approach (see subsection 5.19.6). We used membranes of 0.8 μm , 0.2 μm and 0.015 μm pore sizes. Close to the Chilean coast, where we observed the pronounced OMZ, seawater samples were filtered sequentially through the three different pore sizes for three different depths; one in the surface layer, one in the OMZ (approx. 800 m) and one in deep waters. The selection of the water depths to be sampled changed according for the area of the hydrothermal plume input (EPR) where we collected one sample above the plume, one within

and one below the plume. In the area of the Australian dust input, where higher bioproductivity might be initiated due to the deposition of mineral particles, we selected one sample in the surface layer, one in the depth range of the deep chlorophyll maximum (around 120-140 m) and one in deep waters. Hence, the size fractionation approach applies to all three areas of interest in this study although different research questions initiated the depth selection.

One sample from the same depth as a sequential filtration (either water layer of OMZ, within the plume, or within deep chlorophyll maximum) was chosen per superstation to be collected for an ultrafiltration treatment (please refer to subsection 5.19.7) using a 10 kDa membrane which corresponds to a pore size of approx. 3 nm.

Additionally, we collected surface water samples for HFSE and TM from the tow-fish at every superstation.

In total, 2436 samples were collected, of which a detailed count is given in Table 12.23.

5.19.4 Sample storage

All sample containers were acid cleaned prior to the cruise following the GEOTRACES cleaning protocol (GTU) or the JUB-TM protocol (Table 12.14).

Samples for dissolved trace metal concentrations and HFSE were stored in 100 mL GTU cleaned LDPE bottles, acidified to $\text{pH} < 1.7$ (using 1.5 mL/L ultrapure hydrochloric acid [HCl, 34%, RothTM]), stored at 4 °C on board and transported to Bremen in the shipping containers. Samples for Mo/U concentrations were stored in 5 mL JUB-TM cleaned LDPE vials, acidified in the same manner and transported via flight luggage. The acidification of samples on board was carried out in the laboratory within a laminar flow bench.

Samples for CuL were collected in 125 mL JUB-cleaned LDPE and samples for FeL in 250 mL GTU cleaned fluorinated HDPE bottles. Samples for Cr and V speciation were collected in 100 mL LDPE bottles and the respective cleaning procedure was selected based on the expected concentration ranges for the different working areas and documented in the sample protocol. All speciation and ligand samples were frozen on board to -20 °C and transported frozen to the home laboratory.

The filter membranes used during sequential filtration were collected in Petri dishes and stored and transported frozen at -20 °C for analysis.

5.19.5 Sequential filtration

To determine the different size fractions in the pre-defined water layers according to the area of investigation, three samples at each superstation were chosen for the sequential filtration. In this procedure, 2 L aliquots of the original unfiltered samples were taken from the clean lab to the chemical lab, where they were successively filtered through 47 mm diameter Nuclepore (Whatman) membrane filters with decreasing pore size (0.8, 0.2 and 0.015 μm) and subsampled after each filtration step. Filtrations were carried out inside a laminar flow-bench using 10% HNO_3 pre-cleaned filter towers (at least 12 h). A separate tower was used for each size fraction. Prior to filtration, each filter-tower and membrane filter were rinsed with approx. 30 mL of 0.5 M ultrapure HCl (Roth) and two times with 100 mL pure water provided by a Milli-Q unit (>18.2 M Ω , MilliQ[®] Merck). To increase filtration speed, the filter-towers were pressurized (0.5

to 1 bar) with nitrogen gas (N₂ 99.999 % Alphagaz™) as shown in Fig. 12.67. The approximate volumes filtered were 1650 mL for the 0.8 µm pore size, 1100 mL for 0.2 µm and 550 mL for the 0.015 µm fraction. In all cases, the real volumes (± 50 mL) were documented in the filtration protocol.

After each filtration step, aliquots of the filtrates were stored in different bottles for their future analysis in the land-based laboratory. The parameters to be determined are trace metals, HFSE and Fe-binding ligands. At some stations, aliquots for the determination of Cu-binding ligands (125 mL HDPE) and the analysis of Mo and U (5 mL) were also collected.

As a quality control, blanks for analysis of HFSE and dissolved trace metals were processed using pure water (>18.2 M Ω , MillQ® Merck). The first blank was done prior to the first sample processing and repeated after each area of interest resulting in four blanks for this research expedition. The treatment for the blank procedure was the same as for the samples.

5.19.6 Ultrafiltration

We further conducted a cross-flow ultrafiltration (Millipore Pellicon 2 tangential flow ultrafiltration unit) with a molecular weight cut-off (MWCO) of 10 kDa. By following this approach, we will receive information about the distribution between the colloidal (<0.2 µm) and the truly dissolved (<10 kDa) pool through separating and preconcentrating the colloidal fraction larger than 10 kDa.

In an acid-cleaned 10 L LDPE carboy approx. 7-8 L of a 0.8/0.2 µm filtered seawater sample (AcroPak, Pall) was collected in the clean lab container and then transferred to the chemical lab. The ultrafiltration set-up consists of a peristaltic pump (Millipore Masterflex I/P) and the ultrafiltration (UF) membrane unit (Fig. 12.68).

Samples were processed at a flow rate <250 mL/min. The permeate was collected in a separate acid-cleaned 10 L carboy while the retentate was transported back to the sample bottle. We aim to a concentration factor (CF = volume sample/volume retentate) of at least 8 before the ultrafiltration process was stopped, which allows the retentate volume to be at least 8 times smaller compared to the initial sample volume.

In order to collect the colloidal fraction from the UF-membrane, a 30 mM HCl solution (ultrapure grade, Roth) was recirculated through the system for 10 minutes.

The same membrane was used throughout the expedition with complete cleaning cycles (flushing and recirculation of the following solution in consecutive order: pure water – 0.1 M NaOH – pure water – 0.1 M HCl – pure water) after each sample processing. A blank sample was processed before we processed the first seawater sample, one after the area of pronounced OMZ, and finally one after the last sample. During sample, blank and cleaning procedure, the inlet pressure was monitored and kept at 2 bar by adjusting the pump speed whenever necessary. Subsamples for trace metals (U, Mo, V), HFSE, and ligand analysis were collected from the resulting permeate and retentate volume from all processed samples and blanks.

5.19.7 Analyses

After the samples are transported back to the home laboratory in Bremen, all samples in their respective size fractions will be measured by different analytical procedures. Samples dedicated

for the analysis of trace metals (e.g. Mo and U) will be measured with a quadrupole inductively coupled plasma-mass spectrometer (ICP-MS) while the HFSE samples will be pre-concentrated by an offline-seaFAST system prior to the ICP-MS analysis. Chromium redox species will be measured voltammetrically (Sander and Koschinsky, 2000) and V redox species will be determined after solid-phase separation via ICP-MS (modified after Wang & Sañudo-Wilhelmy, 2008). Ligands for Fe and Cu will be analyzed by competitive ligand exchange cathodic stripping voltammetry (Buck et al., 2015; Kleint et al., 2016). The filters obtained from the sequential filtrations will be analysed on the ICP-MS following an HF digestion step.

5.20 Major elements

(E. O’Sullivan, Z. Steiner)

Despite being among the most abundant elements present in the global ocean, the concentration and distribution of some dissolved major elements (Ca, Sr, Li and F) have been largely understudied. Traditionally considered not to vary by analytically measurable quantities as they are so high, their salinity-normalised concentrations do in fact vary by measurable quantities (de Villiers 1998, 1999; Brass and Turekian 1974; Steiner et al., 2020, 2021; Fabricand 1967). A major element of particular interest to this survey is fluorine, which has been traditionally thought not to vary beyond the 1% margin of error commonly reported (Warner, 1971). However, larger variations in seawater F concentrations were reported in regions affected by large inputs from continental runoff (Windom, 1971), hydrothermal activity (Edmond et al., 1979), undetermined deep-sea processes (Brewer et al., 1970; Greenhalgh and Riley, 1963; Riley, 1965) and in early diagenesis of marine sediments (Froelich et al., 1983; Rude and Aller, 1991, 1994). This is distinct from profiles of Sr concentrations, which often increase with depth in the top 1000 m of the water column due to uptake of Sr in the surface ocean during precipitation of calcium carbonate and strontium sulfate skeletons, and dissolution of these skeletons at depth (Bernstein et al., 1987; de Villiers, 1999). The distribution coefficients of Sr and F into calcium carbonate minerals are similar but incorporation of these elements in other marine minerals is widely different (Rude and Aller 1994; Milliman 1970), hence it should be possible to calculate the relative importance of various biomineralization and dissolution processes in the ocean by combining measurements of Ca, Sr and F concentrations.

Lithium is studied along the SO289 transect as an additional proxy for dust supply and scavenging processes, alongside Fe and Al. Similar to Al, Li can be supplied to the ocean with aerosol clays either adsorbed or in the crystal structure of the clays. Lithium does not tend to be incorporated into organic tissues or biogenic skeletons, hence it is hypothesized that if Li fluxes from Australian dust are high enough to increase surface water Li concentrations by a measurable degree, the fate of these Li can be used as an additional tracer to the fate of aerosol delivered elements in the ocean.

We collected samples for the analyses of major cation concentrations at all stations, and F concentrations from 24 stations along the cruise track. We also collected water samples from the surface mixed layer at each sampling station, as well as 130 underway tow-fish samples for major dissolved cations. High volume samples were collected on 0.4 μm polyethersulfone (PES) filters using in-situ pumps for quantification of major element concentrations in particulate phases and for microscopical observations of the suspended phases. Major cation

water samples were filtered in the clean laboratory and stored in acid cleaned bottles. The major cation samples were acidified to pH ~1.8 with ultrapure HCl. The samples for F analysis were also filtered in the clean laboratory, but stored in non-acid cleaned bottles and were not acidified. The ratios of the major dissolved cations magnesium, calcium, strontium, lithium and potassium to sodium will be analysed at GEOMAR using a Varian-720 ICP-OES, using a sample-standard bracketing method (Steiner et al., 2020). Fluorine concentrations will be analysed using the spectrophotometric method described by Kremling (1999).

5.21 Nutrient distribution

(T. von Keitz, A. Mutzberg)

The distribution of nutrients in seawater is key for understanding the biogeochemical processes, and their signatures allow the differentiation between the various water masses in the ocean. In addition, they are used to identify leaking bottles due to their well-defined and oceanographically consistent distributions.

Every Niskin bottle fired from every single cast and depth was sampled for nutrient analysis onboard. The seawater was collected in 15 mL polypropylene sample vials. Containers and caps were rinsed three times with the sample water before the actual sampling. Samples were placed in the fridge immediately after collection (4 °C in dark), in case they could not be immediately analyzed. Analysis of macro nutrients was undertaken on board by segmented flow injection analysis using a QUAATRO39 (Seal Analytical) auto-analyzer including a XY2-autosampler unit. For nano-molar nutrient samples, a modified detector set up with 1000 mm flow cells has been used. The system set-up included 4 channels for nitrate + nitrite (TON), silicate, nitrite, and phosphate. The analytical methods followed during the cruise correspond to those described by QuAAtro Applications: Method No. Q-068-05 Rev. 11 for TON, Q-066-05 Rev. 5 for Silicate, Q-070-05 Rev. 6 for Nitrite and Q-064-05 Rev. 8 for Phosphate.

A total of ~2400 macro molar samples collected by all Ti-geo-CTD-casts, by all Ti-biology-CTD-casts in depths between ~5 and 200 m and collected by all SS-CTD-casts were measured.

Additionally, ~120 samples for dissolved organic Nitrogen and Phosphorous (DON / DOP) collected by all GEOMAR titanium-biology-CTD-casts and were also measured after digestion on board.

~120 tow-fish samples from oceanic surface with expected concentration values lower than ~100 nM for mainly nitrate + nitrite were stored like the nano molar nutrient samples from the titanium-biology-CTD-casts at -20 °C to be analyzed on board with the modified QUAATRO39 (Seal Analytical) auto-analyzer.

~35 Seawater samples from oceanic surface in a depth of 6.7 m collected from the ship's own membrane / sinus pump were stored, similar the nano molar nutrient samples from the titanium-biology-CTD-casts at -20 °C, to be analyzed on board with the QUAATRO39 (Seal Analytical) auto-analyzer.

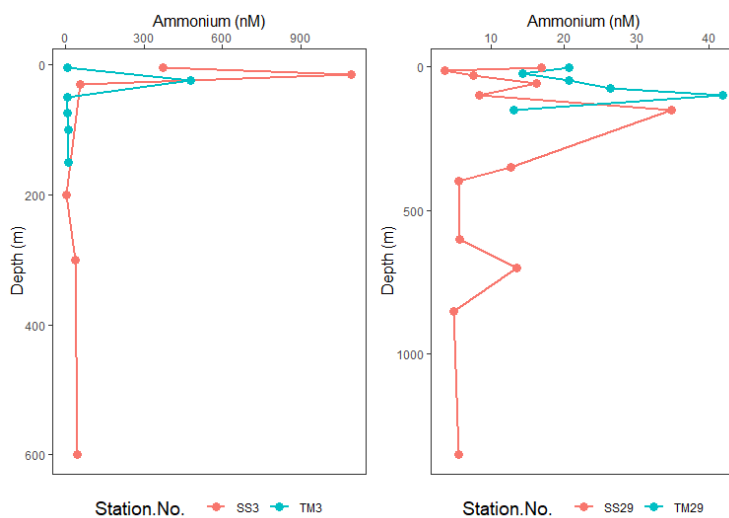
Certified Reference Material for Nutrients in Seawater (RMNS) was used for every run in order to I) guarantee repeatability and reproducibility between analytical runs and to II) validate the data set in terms of compatibility within the scientific community. Nutrient analyses were

validated with KANSO CRM, Lot-No. CC, CL for macro molar Nutrients and CK for nano molar nutrient concentrations.

5.22 Sampling and analysis of Ammonium

(E. Achterberg, T. Liu)

Samples for ammonium were taken from Niskin bottles deployed on the SS-CTD, and also the Ti-CTD for the biology cast. Analysis of ammonium was conducted using the OPA method for all samples from the biology cast (5 m, 25 m, 50 m, 75 m, 100 m and 150 m), and for samples from the stainless steel CTD at depths < 1000 m. Samples were stored in the fridge directly for a short period and the fluorescent OPA reagent was added followed by a 24 h incubation time, during which the samples were kept in the dark at room temperature with caps tightly closed. Subsequent detection of ammonium was performed on a Carey Eclipse fluorimeter. Calibration was carried out using the external standard addition method using ammonium-free deep ocean waters (> 600 m).



Preliminary results of ammonium from SS- and Ti-CTD rosette frames showed good agreement. Enhanced concentrations of ammonium were typically observed below the surface mixed layer, ranging from 30 - 1500 nM, as a result of bacterial breakdown of phytoplankton (Fig. 5.10). The nearshore stations showed higher ammonium concentrations compared with the open ocean stations (Fig. 5.10).

Fig. 5.10 Preliminary results of ammonium profiles. Station SS3 and SS29 are nearshore and open ocean stations, respectively, sampled using SS-CTD. Station TM3 and TM29 are nearshore and open ocean stations, respectively, sampled using Ti-CTD.

5.23 Suspended particles and radiogenic tracers

5.23.1 Sampling particulate matter with in-situ pumps

(D. Köhler)

Up to eleven in-situ pumps (ISP) were deployed at stations 5, 8, 12, 16, 19, 22, 24, 28, 31, 33, 36, 39, 40 and 42. Three dual head pumps McLane WTS LVDF (AWI, PIS020, PIS021), five mono head pumps McLane TWS LV (PIS007, PIS007, PIS010, PIS011, PIS012) and two mono head prototype pumps AWI/Fielax (AWI-CTD, AWI-MiniCTD) with external CTD sensors were used. Pump heads were deployed with acid-washed 0.8 μm polyethersulfone (PES) and pre-combusted Quartz filters. In addition, manganese cartridges were used to sample

radium at selected depths. One additional mono head pump McLane TWS LV (E. Fadeev) was operated by Vienna for sampling marine aggregates (see section 5.8).

After recovering the ISP, filters were immediately subsampled with PTFE punches and tools. 25 mm PES filters were punched for BSi, major ions, metals, Cd isotopes, Si isotopes, Ba isotopes, Ni isotopes, REE, metabolites, microscopy, Selenium and Synchrotron analysis, remaining parts of PES filters will be used for metagenomic analysis at Vienna. Quartz filters were subsampled with 25 mm punches for ^{234}Th , POC/PIC/PON, POP, pHg and CN isotopes and remains for Hg isotopes. Subsamples were either stored at $-20\text{ }^{\circ}\text{C}$ (Hg) and $-80\text{ }^{\circ}\text{C}$ (metabolites, metagenomic analysis) or were directly dried at $60\text{ }^{\circ}\text{C}$ (^{234}Th , BSi, POP, POC/PIC/PON, major ions, metals, Cd isotopes, Si isotopes, Ba isotopes, Ni isotopes, REE) to preserve them for measurement on land. Only ^{234}Th was measured onboard. All work steps followed the Sampling and Sample-handling Protocols for GEOTRACES Cruises Version 3.

5.23.2 Metal mineralogy sampling (suspended particles)

(D. Köhler)

Sediments and deep-sea hydrothermal vents are a source of dissolved and particulate metals to the ocean; however, the overall transport potential, speciation, and bioavailability of hydrothermally derived metals is largely unknown. It is important to determine the fate of hydrothermally derived particulate metals with increasing distance from the source, including an assessment of changes in physical and chemical particulate forms.

Metal mineralogy samples were handled, sealed and stored under anoxic conditions using a Captair portable glove bag purged with N_2 gas. Three layers of gloves were worn at operation, 1) cotton gloves on hands to absorb moisture; 2) glove bag attached white gloves; 3) nitrile gloves over the top to keep attached gloves clean and improve dexterity.

Samples were operated, sealed and stored based on following steps: (step 1) filter and all packaging put into glove bag with N_2 (g); (step 2) filter piece goes in petri slide; (step 3) petri slide goes in plastic bag; (step 4) plastic bag goes in mylar and is heat sealed; (step 5) sealed mylar pouch stored at $-20\text{ }^{\circ}\text{C}$. Filter samples were sealed immediately after sampling. Sediment samples were all sealed at the end of the cruise; they had first been stored frozen in an Eppendorf that had been flushed with N_2 . The samples will be shipped to Brandy Toner's working group at U. Minnesota, US for synchrotron analysis.

5.24 Radium 226, 228 isotopes

(L. H. Vieira, P. Battermann)

Radium isotopes are produced by the decay of particle-bound thorium isotopes in sediments and are soluble in seawater. As they present a large range of half-lives, they can be applied to study the age of water masses, shelf-ocean mixing processes, ocean circulation, and as traces of element inputs into the oceans. Radium-226 has a half-life of 1600 years, low particle reactivity, and is principally produced by the decay of ^{230}Th in marine sediments, which makes this isotope a suitable tracer of water masses. Radium-228, with a half-life of 5.7 years, is a suitable tool to study coastal and open ocean processes and can be used as tracers of shelf sediment and river water inputs into the oceans. The decrease in its concentration from its source can be used together with its relatively short half-life to constrain flux rates. Thus, ^{228}Ra

can be coupled with trace elements to identify their sources and quantify their fluxes to offshore regions.

Approximately 1000 L of surface seawater were collected from 3 m depth from the ship's seawater intake and filtered through MnO₂-impregnated acrylic fiber (Mn-fibers) at a flow rate <1 L/min to quantitatively extract Ra isotopes. Surface samples were collected from all stations and between stations during transit.

In addition, 5-7 in-situ pumps (McClane) were used to collect depth profiles of dissolved Ra isotopes at every superstation deployed between 100 to 2300 m. The in-situ pumps were equipped with a polyethersulfone membrane filter (PES) and Quartz filters, alternately, to collect suspended particles; the filtrate then passed through MnO₂-coated polypropylene filter cartridges (Mn-cartridges) to extract the Ra isotopes (Henderson et al., 2013). The Mn-fibers and cartridges were rinsed with radium-free fresh water and excess moisture was removed using compressed air. Small-volume samples (1 litre) were also collected from the CTD casts for high-resolution ²²⁶Ra depth profiles. The chosen depths from the CTD casts included the corresponding in-situ pump depths for determining the radium extraction efficiency of the Mn-cartridges. Following collection from the CTD, samples were acidified with 1 mL of sub-boiled nitric acid, double-bagged, and stored at room temperature. Radium-226 concentrations from the 1 L seawater samples will be determined by mass spectrometry.

5.25 ²³⁴Th, ²³⁰Th and ²³⁸U

(S. Hamisch)

²³⁴Th is the surface-active daughter isotope of the ubiquitous radiogenic ²³⁸U. Therefore, it can be used to calculate particle fluxes such as export of POC to deeper depths, an important aspect of quantifying organic carbon export rates in open ocean waters.

Sampling of dissolved ²³⁴Th and ²³⁸U occurred at all super-stations (Stations 5, 8, 12, 16, 19, 22, 24, 28, 31, 33, 40, 42). Between seven and twelve 4 L samples of unfiltered seawater were collected from the stainless steel CTD. Samples were collected in 0-400 m depth for analyses of ²³⁴Th activity to calculate POC flux. For stations 22, 24 and 28, additional deep-water samples were taken to quantify particle flux caused by hydrothermal vent activity at the mid-oceanic ridge. At Stations 31, 36 and 42, additional single deep-water samples have been taken for reference. Additionally, Station 33 contained a high-resolution surface profile from surface to 400 m depth consisting of 10 samples for each dissolved and particulate ²³⁴Th samples.

All ²³⁴Th samples were acidified to pH <1.5 (~1.3) using 6.2 mL of concentrated nitric acid directly after sampling. Further, 100 µl of yield standard solution was added. After 8 h, the pH was neutralized to pH 8.2-8.5 (~8.3) using 10 ml of concentrated ammonium solution. 50 µL of KMnO₄-solution and 50 µl of MnCl₂-solution were added to co-precipitate ²³⁴Th with MnO₂. After waiting for 12 h, the precipitate was filtered onto 3 µm pore size silver filters, rinsed with pH 9 MQ water and dried at 60 °C for 3h. Sampling bottles were cleaned with 100 mL of H₂O₂/HNO₃-solution and rinsed three times with MQ. Before sampling, the bottles were rinsed three times with seawater from the according Niskin-bottle. As the silver filters have shown to have relatively low recovery rates in comparison to QMA filters, QM-A filters (25mm 2.2µm pore size) were used for Stations 40 and 42.

At each station, five individual 25 mm QM-A-filter cuts were taken from in-situ pumps deployed over the same range of depths as the dissolved ^{234}Th and ^{238}U samples. Filters cuts were dried at 60 °C for 3h. After drying, each filter was covered in plastic foil and wrapped with aluminium foil onto the sample holder. For all samples of dissolved and particulate ^{234}Th , total beta activity was measured using a Risø low-level beta GM multiscaler until the error of the measurement reached values $< \pm 4\%$ ($\sim \pm 2.5\%$ most often). Measurement time ranged from ~ 12 h for the particulate ^{234}Th samples to ~ 36 h for the dissolved ^{234}Th samples. Once QM-A filters were used for the dissolved ^{234}Th sampling, measurement times went down to 5 to 10 h. After the beta counting, the samples were stored at room temperature. All ^{234}Th samples will be measured after 6 months for baseline radioactivity correction. ICP-MS analysis of ^{230}Th will be conducted to determine the individual yield for Thorium recovery rates.

From every depth of ^{234}Th sampling, 12 mL of filtered seawater were sampled for analysis of ^{238}U . Samples were collected in 15 mL screw-lid vials, acidified with 20 μL of concentrated HCl (32%) and stored at room temperature. The concentration of ^{238}U will be determined at GEOMAR using ICP-MS.

5.26 Sampling for Pa/Th and Ac

(D. Köhler, W. Geibert)

Uranium naturally present in seawater constantly produces the isotopes ^{231}Pa and ^{230}Th at a known rate (Anderson et al., 1983). These isotopes are therefore exceptional tracers, because their supply rate is much better constrained than that of any other isotope, making them unique tools to study removal rates (Hayes et al., 2021, Costa et al., 2020, Geibert, 2018). In addition to their use for particle removal processes, their slightly different reactivity towards particles leads to a different sensitivity for large-scale ocean circulation in present and past.

GEOTRACES has delivered a number of well intercalibrated sections from various oceanic regions, which led for example to surprising discoveries on the large-scale role of mid-ocean ridges for trace metal cycles (Pavia et al., 2017).

However, a gap in our data distribution existed in the SPO - crucial for modelling, and also in the center of attention for understanding the re-organisation of ocean circulation in the last glacial (Ronge et al., 2021). This cruise now allows to fill in this gap, with 89 samples of 20 L, spread across the SPO.

Their analysis is planned at the AWI. In addition, we will explore the possibility to measure ^{227}Ac on the same samples (Levier et al., 2021), a unique tracer for deep upwelling, for which no data from the region exist. The $^{230}\text{Th}/^{231}\text{Pa}$ data will be intercalibrated according to GEOTRACES standards and form part of a future GEOTRACES data product. We expect to see the effects of hydrothermal scavenging, effect of trenches, and to get a better understanding of particle removal and other TEIs.

5.27 Aerosol sampling using high volume collector

(E. Achterberg)

We deployed one high volume aerosol collector (MCV CAV-A/Mb), which sampled the PM10 dry aerosol fraction during the cruise. The flow rate of the aerosol collector was set to

60 m³ h⁻¹. The collector was placed on the monkey island of the vessel, and away from areas where personnel were smoking. The collectors switched off automatically during periods of unfavourable wind directions, when stack contamination was a possibility. A wind vane was attached to the collector to allow the directional sampling.

We employed Whatmann 41 filter (acid-cleaned, 203 mm x 254 mm) for trace elements and isotope sampling. Filters were changed every 48 h, and stored frozen (-20 °C). A total of 14 filters each were collected during the cruise (with additional instrumental blanks). The sampling protocol followed the GEOTRACES recommendations.

5.28 Assessing plastic pollution along the South Pacific

(M. d. l. A. Amenábar)

We run two different protocols in order to assess plastic pollution along a longitudinal gradient in the South Pacific Ocean, one focused on floating debris that were visible from deck during the ship's movement, and the second focused on microplastic samples at subsurface waters.

For floating macro debris, we did a visual survey from the uppermost deck spending as many hours as possible during day light in order to cover most of the transect. Every time we spotted a floating item, we took a photo and noted the coordinates and characteristics of the object (size, color, shape, type of debris, percentage of the volume that is floating, whether the object was biofouled or not). All notes of the survey were written on a paper sheet on deck during litter spotting, the work of digitalizing the data is still pending.

In parallel, and in order to compare if microplastic follows the same abundance and distribution trends as macroplastic and other floating debris, we installed a setup filtration system with an intake of subsurface seawater coming from a membrane pump fixed on the ship's hull, approximately 6 meters under-water. The pumped water passed through a flowmeter to measure the volume filtered, and then through the setup system with a 10 µm mesh to retain all larger particles. The pump was running as long as possible during stations, and also during travel, but distinguishing whether samples were collected during station or transit (Column: Station/Underway in Table 12.17). Each sample consisted of the particles retained on top of the mesh after draining the water. The sample was rinsed with milliQ water and transferred to a glass jar for storage at room temperature. A total of 79 samples were collected during the cruise, with 38 of them during underway movement, and 41 of them on stations. Detail of the samples is provided in Table 12.17.

7 Station List MXX/Y

7.1 Overall Station List

ISP= in situ pumps. CTD used: Sonne stainless steel CTD (SS CTD) and GEOMAR Ultra Clean Titanium CTD for biology or geochemistry (Ti BIO CTD and Ti GEOCHEM CTD).

Station	Device Operation	Event Date and Time	Event Comment	Latitude	Longitude	Seafloor Depth (m)

1	SO289_1-1	2022/02/23 16:28:42	Ti GEO-BIO CTD	33° 36,455' S	071° 43,741' W	108
0	SO289_0_Underway-1	2022/02/23 16:30:12	ADCP start	33° 36,454' S	071° 43,743' W	109
0	SO289_0_Underway-2	2022/02/23 16:30:42	EM122 start	33° 36,454' S	071° 43,745' W	117
1	SO289_1-2	2022/02/23 17:08:29	SS CTD	33° 36,454' S	071° 43,742' W	111
0	SO289_0_Underway-3	2022/02/23 17:39:43	TMF	33° 36,239' S	071° 43,968' W	112
2	SO289_2-1	2022/02/23 21:00:45	Ti GEO-BIO-CTD	33° 05,403' S	071° 49,514' W	162
2	SO289_2-2	2022/02/23 22:01:49	SS CTD	33° 05,412' S	071° 49,518' W	163
3	SO289_3-1	2022/02/24 00:29:03	Ti BIO-CTD	32° 58,042' S	071° 51,840' W	840
3	SO289_3-2	2022/02/24 08:36:19	SS-CTD	32° 58,035' S	071° 51,833' W	832
3	SO289_3-3	2022/02/24 11:26:24	Ti GEO CTD	32° 58,038' S	071° 51,831' W	833
4	SO289_4-1	2022/02/24 14:07:12	SS-CTD	32° 52,394' S	071° 53,532' W	1749
5	SO289_5-1	2022/02/24 18:37:45	SS-CTD	32° 29,954' S	071° 59,906' W	2449
5	SO289_5-2	2022/02/24 20:43:43	Ti GEO CTD	32° 29,964' S	071° 59,904' W	2450
5	SO289_5-3	2022/02/25 01:29:01	SS CTD + ISP	32° 29,964' S	071° 59,902' W	2450
5	SO289_5-4	2022/02/25 06:43:01	Ti BIO-CTD	32° 29,966' S	071° 59,910' W	2451
6	SO289_6-1	2022/02/25 11:06:35	Ti GEO CTD	32° 30,004' S	072° 48,015' W	5488
6	SO289_6-2	2022/02/25 16:04:24	SS-CTD	32° 30,002' S	072° 47,990' W	5486
6	SO289_6-3	2022/02/25 22:22:02	Ti BIO CTD	32° 29,998' S	072° 47,995' W	5486
7	SO289_7-1	2022/02/26 03:14:36	TI GEO CTD	32° 29,985' S	073° 48,002' W	4060
7	SO289_7-2	2022/02/26 06:07:13	SS-CTD	32° 29,998' S	073° 47,997' W	4062
7	SO289_7-3	2022/02/26 10:00:39	Ti BIO CTD	32° 30,002' S	073° 47,996' W	4060
8	SO289_8-1	2022/02/26 21:50:24	Ti BIO CTD	32° 30,004' S	076° 36,039' W	3887
8	SO289_8-2	2022/02/26 22:28:03	SS CTD	32° 30,006' S	076° 36,026' W	3881
8	SO289_8-3	2022/02/27 01:25:12	TI GEO CTD	32° 30,002' S	076° 36,029' W	3885
8	SO289_8-4	2022/02/27 04:25:37	SS CTD + ISP	32° 30,000' S	076° 36,017' W	3886
9	SO289_9-1	2022/02/27 20:25:39	Ti BIO CTD	32° 30,001' S	079° 00,082' W	4030
9	SO289_9-2	2022/02/27 20:52:40	SS CTD	32° 29,999' S	079° 00,075' W	4030
9	SO289_9-3	2022/02/28 00:11:17	TI GEO CTD	32° 30,003' S	079° 00,057' W	4035
10	SO289_10-1	2022/02/28 16:36:52	Ti BIO CTD	32° 29,876' S	081° 59,950' W	3984
10	SO289_10-2	2022/02/28 17:00:00	SS-CTD	32° 29,884' S	081° 59,954' W	3992
10	SO289_10-3	2022/02/28 20:00:52	Ti GEO CTD	32° 29,890' S	081° 59,949' W	3992
11	SO289_11-1	2022/03/01 12:21:24	Ti BIO CTD	32° 30,015' S	085° 00,026' W	3840
11	SO289_11-2	2022/03/01 12:47:00	SS CTD	32° 30,009' S	085° 00,020' W	3824
11	SO289_11-3	2022/03/01 15:54:27	TI GEO CTD	32° 30,015' S	085° 00,031' W	3841
12	SO289_12-1	2022/03/02 07:24:48	Ti BIO-CTD	32° 29,868' S	087° 59,964' W	3713
12	SO289_12-2	2022/03/02 07:48:47	SS-CTD	32° 29,871' S	087° 59,974' W	3711
12	SO289_12-3	2022/03/02 10:46:30	Ti GEO CTD	32° 29,877' S	087° 59,970' W	3720
12	SO289_12-4	2022/03/02 13:58:45	SS CTD + ISP	32° 29,880' S	087° 59,995' W	3712
13	SO289_13-1	2022/03/03 08:20:53	Ti BIO CTD	32° 30,010' S	090° 59,900' W	3611
13	SO289_13-2	2022/03/03 08:44:27	SS CTD	32° 29,998' S	090° 59,900' W	3612
13	SO289_13-3	2022/03/03 11:42:20	Ti GEO CTD	32° 30,001' S	090° 59,896' W	3612

14	SO289_14-1	2022/03/04 02:23:10	Ti BIO CTD	32° 29,977' S	094° 00,050' W	3928
14	SO289_14-2	2022/03/04 02:49:32	SS CTD	32° 29,975' S	094° 00,049' W	3927
14	SO289_14-3	2022/03/04 05:56:38	Ti GEO CTD	32° 29,978' S	094° 00,050' W	3926
15	SO289_15-1	2022/03/04 22:15:03	Ti BIO CTD	32° 30,024' S	097° 00,049' W	3850
15	SO289_15-2	2022/03/04 22:38:08	SS CTD	32° 30,018' S	097° 00,063' W	3852
15	SO289_15-3	2022/03/05 01:56:03	Ti GEO CTD	32° 30,009' S	097° 00,054' W	3857
16	SO289_16-1	2022/03/05 16:57:12	Ti BIO CTD	32° 30,010' S	100° 00,024' W	3742
16	SO289_16-2	2022/03/05 17:18:53	SS CTD	32° 30,009' S	100° 00,025' W	3745
16	SO289_16-3	2022/03/05 20:51:14	Ti GEO CTD	32° 30,010' S	100° 00,015' W	3745
16	SO289_16-4	2022/03/05 23:31:37	SS CTD + ISP	32° 30,007' S	100° 00,012' W	3748
17	SO289_17-1	2022/03/06 18:34:05	TI BIO CTD	31° 25,650' S	102° 59,925' W	3564
17	SO289_17-2	2022/03/06 18:57:24	SS CTD	31° 25,646' S	102° 59,922' W	3563
17	SO289_17-3	2022/03/06 21:50:52	TI GEO CTD	31° 25,652' S	102° 59,927' W	3564
18	SO289_18-1	2022/03/07 12:56:44	TI BIO CTD	31° 25,829' S	106° 00,006' W	3403
18	SO289_18-2	2022/03/07 13:20:16	SS CTD	31° 25,832' S	106° 00,003' W	3401
18	SO289_18-3	2022/03/07 16:03:59	TI GEO CTD	31° 25,816' S	106° 00,009' W	3404
19	SO289_19-1	2022/03/08 03:03:53	TI BIO CTD	31° 25,794' S	107° 59,996' W	3114
19	SO289_19-2	2022/03/08 03:26:03	SS CTD + ISP	31° 25,793' S	107° 59,995' W	3114
19	SO289_19-3	2022/03/08 10:12:32	Ti GEO CTD	31° 25,793' S	107° 59,996' W	3114
19	SO289_19-4	2022/03/08 12:41:17	SS CTD	31° 25,798' S	107° 59,992' W	3113
20	SO289_20-1	2022/03/08 22:00:24	Ti BIO CTD	31° 25,808' S	110° 00,001' W	2670
20	SO289_20-2	2022/03/08 22:26:03	SS CTD	31° 25,811' S	110° 00,014' W	2667
20	SO289_20-3	2022/03/09 00:43:12	Ti GEO CTD	31° 25,811' S	110° 00,017' W	2678
21	SO289_21-1	2022/03/09 14:19:04	Ti BIO CTD	32° 30,039' S	111° 59,969' W	2703
22	SO289_22-1	2022/03/09 19:37:45	SS CTD	31° 25,826' S	111° 59,362' W	2382
22	SO289_22-2	2022/03/09 20:30:00	SS CTD	31° 25,823' S	111° 59,376' W	2387
22	SO289_22-3	2022/03/09 21:16:50	TI GEO CTD	31° 25,815' S	111° 59,388' W	2387
22	SO289_22-4	2022/03/09 23:02:00	CTD + ISP	31° 25,816' S	111° 59,382' W	2385
23	SO289_23-1	2022/03/10 13:48:25	Ti BIO CTD	31° 25,784' S	114° 00,016' W	2920
23	SO289_23-2	2022/03/10 14:13:09	SS CTD	31° 25,788' S	114° 00,015' W	2919
23	SO289_23-3	2022/03/10 16:35:10	TI GEO CTD	31° 25,799' S	114° 00,013' W	2918
24	SO289_24-1	2022/03/11 06:48:01	TI BIO CTD	31° 25,808' S	116° 00,025' W	3312
24	SO289_24-2	2022/03/11 07:19:25	SS CTD + ISP	31° 25,813' S	116° 00,012' W	3312
24	SO289_24-3	2022/03/11 14:02:52	Ti GEO CTD	31° 25,804' S	116° 00,008' W	3314
24	SO289_24-4	2022/03/11 16:24:54	SS CTD	31° 25,806' S	116° 00,009' W	3315
25	SO289_25-1	12/03/2022 06:35	TI BIO CTD	31° 25,792' S	119° 00,007' W	3719
25	SO289_25-2	12/03/2022 06:59	SS CTD	31° 25,800' S	118° 59,995' W	3719
25	SO289_25-3	12/03/2022 10:05	Ti GEO CTD	31° 25,798' S	119° 00,007' W	3719
26	SO289_26-1	13/03/2022 02:00	Ti Bio CTD	31° 25,794' S	121° 59,988' W	3676
26	SO289_26-2	13/03/2022 02:24	SS-CTD	31° 25,795' S	121° 59,987' W	3679
26	SO289_26-3	13/03/2022 05:22	TI GEO CTD	31° 25,800' S	122° 00,004' W	3677

27	SO289_27-1	13/03/2022 20:56	Ti Bio CTD	31° 25,767' S	125° 00,003' W	3848
27	SO289_27-2	13/03/2022 21:24	SS-CTD	31° 25,769' S	125° 00,013' W	3849
27	SO289_27-3	14/03/2022 00:27	Ti GEO CTD	31° 25,767' S	125° 00,002' W	3839
28	SO289_28-1	14/03/2022 17:07	TI BIO CTD	31° 25,800' S	128° 00,014' W	3705
28	SO289_28-2	14/03/2022 17:35	SS CTD	31° 25,795' S	128° 00,010' W	3764
28	SO289_28-3	14/03/2022 19:05	TI GEO CTD	31° 25,801' S	127° 59,995' W	3753
28	SO289_28-4	14/03/2022 21:39	SS CTD + ISP	31° 25,798' S	127° 59,996' W	3690
29	SO289_29-1	15/03/2022 16:31	TI BIO CTD	31° 25,816' S	131° 00,047' W	4250
29	SO289_29-2	15/03/2022 16:58	SS CTD	31° 25,813' S	131° 00,030' W	4248
29	SO289_29-3	15/03/2022 20:17	TI GEO CTD	31° 25,801' S	131° 00,023' W	4250
30	SO289_30-1	16/03/2022 11:59	TI BIO CTD	31° 25,793' S	134° 00,005' W	4172
30	SO289_30-2	16/03/2022 12:24	SS CTD	31° 25,798' S	134° 00,001' W	4167
30	SO289_30-3	16/03/2022 15:48	Ti GEO CTD	31° 25,804' S	133° 59,995' W	4184
31	SO289_31-1	17/03/2022 17:59	TI BIO CTD	31° 25,797' S	137° 59,990' W	4348
31	SO289_31-2	17/03/2022 18:20	SS CTD	31° 25,804' S	137° 59,998' W	4349
31	SO289_31-3	17/03/2022 19:41	TI GEO CTD	31° 25,798' S	137° 59,995' W	4348
31	SO289_31-4	17/03/2022 23:09	SS CTD + ISP	31° 25,809' S	137° 59,994' W	4345
32	SO289_32-1	18/03/2022 18:44	TI BIO CTD	31° 25,779' S	140° 59,999' W	4665
32	SO289_32-2	18/03/2022 19:07	SS CTD	31° 25,789' S	140° 59,995' W	4663
32	SO289_32-3	18/03/2022 22:47	Ti GEO CTD	31° 25,802' S	140° 59,996' W	4663
33	SO289_33-1	23/03/2022 18:30	TI BIO CTD	26° 10,182' S	152° 00,010' W	4658
33	SO289_33-2	23/03/2022 18:55	SS CTD	26° 10,191' S	152° 00,009' W	4654
33	SO289_33-3	23/03/2022 23:08	Ti GEO CTD	26° 10,189' S	152° 00,010' W	4661
33	SO289_33-4	24/03/2022 02:36	SS CTD + ISP	26° 10,187' S	151° 59,999' W	4656
34	SO289_34-1	25/03/2022 00:33	TI BIO CTD	26° 10,112' S	155° 59,927' W	5087
34	SO289_34-2	25/03/2022 00:59	SS CTD	26° 10,107' S	155° 59,921' W	5091
34	SO289_34-3	25/03/2022 04:42	Ti GEO CTD	26° 10,111' S	155° 59,924' W	5094
35	SO289_35-1	26/03/2022 02:27	BIO CTD	26° 10,208' S	159° 59,967' W	4952
35	SO289_35-2	26/03/2022 02:52	SS CTD	26° 10,204' S	159° 59,985' W	4959
35	SO289_35-3	26/03/2022 06:44	TI GEO CTD	26° 10,198' S	159° 59,995' W	4954
36	SO289_36-1	27/03/2022 02:07	Ti BIO CTD	26° 10,196' S	163° 59,975' W	5606
36	SO289_36-2	27/03/2022 02:30	SS CTD (shallow)	26° 10,202' S	163° 59,977' W	5606
36	SO289_36-3	27/03/2022 03:51	Ti GEO CTD	26° 10,198' S	163° 59,980' W	5606
36	SO289_36-4	27/03/2022 08:03	SS CTD + ISP	26° 10,197' S	163° 59,986' W	5607
37	SO289_37-1	28/03/2022 07:45	TI BIO CTD	26° 10,206' S	168° 00,024' W	5477
37	SO289_37-2	28/03/2022 08:07	SS CTD	26° 10,194' S	168° 00,005' W	5509
37	SO289_37-3	28/03/2022 12:30	TI GEO CTD	26° 10,213' S	168° 00,029' W	5473
38	SO289_38-1	29/03/2022 09:05	TI BIO CTD	26° 10,202' S	172° 00,003' W	5192
38	SO289_38-2	29/03/2022 09:26	SS CTD	26° 10,208' S	172° 00,005' W	5446
38	SO289_38-3	29/03/2022 13:28	TI GEO CTD	26° 10,202' S	172° 00,003' W	5192
38	SO289_38-4	29/03/2022 17:02	SS CTD (shallow)	26° 10,196' S	172° 00,000' W	5197

39	SO289_39-1	30/03/2022 08:52	TI BIO CTD	26° 09,996' S	175° 23,792' W	7681
39	SO289_39-2	30/03/2022 09:14	SS CTD + ISP	26° 10,002' S	175° 23,795' W	7680
39	SO289_39-3	30/03/2022 15:21	TI GEO CTD	26° 09,999' S	175° 23,792' W	7688
40	SO289_40-1	31/03/2022 04:37	Ti GEO CTD	25° 52,491' S	177° 10,997' W	526
40	SO289_40-2	31/03/2022 05:22	TI GEO CTD	25° 52,498' S	177° 10,998' W	526
40	SO289_40-3	31/03/2022 10:16	TI BIO CTD	25° 52,501' S	177° 11,002' W	527
41	SO289_41-1	31/03/2022 18:49	Ti BIO CTD	25° 43,093' S	178° 42,893' W	2353
41	SO289_41-2	31/03/2022 19:18	SS CTD	25° 43,093' S	178° 42,891' W	2356
41	SO289_41-3	31/03/2022 21:15	TI GEO CTD	25° 43,090' S	178° 42,895' W	2350
42	SO289_42-1	01/04/2022 11:48	TI BIO CTD	25° 43,101' S	178° 59,986' E	3763
42	SO289_42-2	01/04/2022 12:16	CTD-SS	25° 43,106' S	178° 59,987' E	3761
42	SO289_42-3	01/04/2022 13:31	TI GEO CTD	25° 43,094' S	178° 59,985' E	3760
42	SO289_42-4	01/04/2022 16:03	SS CTD + ISP	25° 43,094' S	178° 59,983' E	3763
43	SO289_43-1	02/04/2022 16:49	Ti BIO CTD	25° 43,218' S	175° 29,873' E	4492
43	SO289_43-2	02/04/2022 17:20	SS CTD	25° 43,114' S	175° 29,987' E	4488
43	SO289_43-3	02/04/2022 20:48	TI GEO CTD	25° 43,099' S	175° 30,003' E	4507
44	SO289_44-1	03/04/2022 15:36	Ti BIO CTD	25° 49,979' S	171° 59,942' E	3396
44	SO289_44-2	03/04/2022 15:59	SS CTD	25° 49,979' S	171° 59,943' E	3407
44	SO289_44-3	03/04/2022 18:43	Ti GEO CTD	25° 49,977' S	171° 59,943' E	3317
0	SO289_0_Underway-4	03/04/2022 21:33		25° 49,972' S	171° 59,941' E	0

8 Data and Sample Storage and Availability

A cruise summary report (CSR) has been compiled and submitted to DOD (Deutsches Ozeanographisches Datenzentrum), BSH, Hamburg, immediately after the cruise. Part of the cruise was performed in waters under jurisdiction of Chile. As requested, the CTD data and this cruise report have been transferred to the respective authorities.

All hydrographic data acquired during the cruise are transferred to BSH, and also stored at the GEOTRACES data base at BODC, Liverpool, U.K., and will be made available to the PANGAEA data base. All trace metal and isotope data to be acquired will also be fed into these data bases and will be made publicly available within 3 years after cruise end (1st quarter of 2025). All water and particulate and sediment samples are stored at the respective laboratories, where the measurements will be carried out. The Kiel Data Management Team (KDMT) provides an information and data archival system where metadata of the onboard DSHIP-System are collected and are made publicly available. This Ocean Science Information System (OSIS-Kiel) is accessible for all project participants and can be used to share and edit field information (<https://portal.geomar.de/metadata/>).

Availability of metadata in OSIS, 2 weeks after completion of the cruise and related experiments. Availability of data in OSIS (<https://portal.geomar.de/osis/>): 6 months after completion of the cruise and related experiments.

Table 8.1 lists the target data bases, tentative availability times and responsible scientists.

Hydrography - CTD and ADCP and multibeam data are held at DAM and GEOMAR Helmholtz Centre for Ocean Research Kiel and are publicly available immediately after cruise (responsible: Prof. E. Achterberg).

Dissolved trace metals - samples and data are held at GEOMAR, Kiel (responsible: Prof. E. Achterberg).

Particulate trace metals - samples and data are held at GEOMAR, Kiel (responsible: Prof. E. Achterberg).

Trace element and isotopes (REE, Ba) - samples and data are held at GEOMAR, Kiel (responsible: Prof. M. Frank).

Stable Fe isotopes - samples and data are held at GEOMAR, Kiel (responsible: Prof. E. Achterberg).

Radium isotopes - samples and data are held at GEOMAR (responsible Prof. E. Achterberg).

High Field Strength Elements and trace element speciation – samples and data are held at the Jacobs University Bremen (responsible Prof. A. Koschinsky).

Phytoplankton/productivity – samples and data are held at GEOMAR, Kiel (responsible Dr. T. Browning).

Nitrogen cycling and fixation - samples and data are held at GEOMAR (responsible Dr. T. Browning).

Nutrients, DOC, DOC, alkalinity, carbon cycle - samples and data are held at GEOMAR, Kiel (responsible Prof. E. Achterberg).

Table 8.1 Overview of data availability

Type	Database	Available	Contact
Hydrography	BODC/PANGAEA	June 2022	eachterberg@geomar.de
Nutrients	BODC/PANGAEA	March 2025	eachterberg@geomar.de
Dissolved trace metals	BODC/PANGAEA	March 2025	eachterberg@geomar.de
Particulate trace metals	BODC/PANGAEA	March 2025	eachterberg@geomar.de
High field strength elements / metal speciation	BODC/PANGAEA	March 2025	a.koschinsky@jacobs-university.de
REEs and Ba isotopes	BODC/PANGAEA	March 2025	mfrank@geomar.de
Stable Fe isotopes	BODC/PANGAEA	March 2025	eachterberg@geomar.de
Radium isotopes	BODC/PANGAEA	March 2025	eachterberg@geomar.de
Nitrogen cycling and fixation	BODC/PANGAEA	March 2025	tbrowning@geomar.de
Phytoplankton/productivity	BODC/PANGAEA	March 2025	tbrowning@geomar.de
Carbonate chemistry, DOC	BODC/PANGAEA	March 2025	eachterberg@geomar.de

9 Acknowledgements

All the members of the SO289 GEOTRACES South Pacific team are very grateful to the BMBF, the German Research Fleet Coordination Centre at the Universität Hamburg, the shipping company BRIESE RESEARCH and LPL Projects + Logistics GmbH for providing their outstanding support to science and ship logistics, which made this cruise possible. The careful managing of the COVID situation was outstanding, and allowed us to conduct our successful cruise. We also like to sincerely thank the captain, officers and crew on the RV Sonne who did a fantastic job at facilitating our research and making our life as pleasant as possible on board.

10 References

- Anderson, R.F., Bacon, M.P., Brewer, P.G., 1983. Removal of ^{230}Th and ^{231}Pa at ocean margins. *Earth and Planetary Science Letters* 66, pp.73-90.
- Bates, S.L., Hendry, K.R., Pryer, H.V., Kinsley, C.W., Pyle, K.M., Woodward, E.M.S. Horner, T.J., 2017. Barium isotopes reveal role of ocean circulation on barium cycling in the Atlantic. *Geochimica et Cosmochimica Acta* 204, 286–299.
- Bernstein, R.E., Betzer, P.R., Feely, R.A., Byrne, R.H., Lamb, M.F., Michaels, A.F., 1987. Acantharian fluxes and strontium to chlorinity ratios in the north Pacific Ocean. *Science* 237, 1490-1494.
- Bowman, K.L., Hammerschmidt, C.R., Lamborg, C.H., Swarr, G.J., Agather, A.M., 2016. Distribution of mercury species across a zonal section of the eastern tropical South Pacific Ocean (US GEOTRACES GP16). *Marine Chemistry*, 186, pp.156-166.
- Brass, G.W., Turekian, K.K., 1974. Strontium distribution in GEOSECS oceanic profiles. *Earth and Planetary Science Letters* 23, 141-148.
- Brewer, P.G., Spencer, D.W., Wilkniss, P.E., 1970. Anomalous fluoride concentrations in the North Atlantic. *Deep Sea Research and Oceanographic Abstracts* 17, 1-7.
- Browning, T.J., Achterberg, E.P., Rapp, I., Engel, A., Bertrand, E.M., Tagliabue, A., Moore, C.M., 2017. Nutrient co-limitation at the boundary of an oceanic gyre. *Nature* 551(7679), 242-246.
- Browning, T.J., Bouman, H.A., Moore, C.M., 2014. Satellite-detected fluorescence: decoupling nonphotochemical quenching from iron stress signals in the South Atlantic and Southern Ocean. *Global Biogeochemical Cycles* 28, 510–524.
- Buck, K.N., Sohst, B., Sedwick, P.N., 2015. The organic complexation of dissolved iron along the U.S. GEOTRACES (GA03) North Atlantic section. *Deep Sea Research part II: Topical Studies in Oceanography* 116, 152-165.
- Caress, D.W., Chayes, D.N., 2017. MB-System: Mapping the Seafloor, <https://www.mbari.org/products/research-software/mb-system>.
- Casacuberta, N., Christl, M., Lachner, J., van der Loeff, M.R., Masque, P., Synal, H.A., 2014. A first transect of U-236 in the North Atlantic Ocean. *Geochimica et Cosmochimica Acta* 133, 34-46.

- Casacuberta, N., Christl, M., Vockenhuber, C., Wefing, A.-M., Wacker, L., Masqué, P., Synal, H.-A., van der Loeff, M.R., 2018. Tracing the Three Atlantic Branches Entering the Arctic Ocean With ^{129}I and ^{236}U . *Journal of Geophysical Research: Oceans* 123(9), 6909-6921.
- Castrillejo, M., Casacuberta, N., Christl, M., Vockenhuber, C., Synal, H.A., García-Ibáñez, M.I., Lherminier, P., Sarthou, G., Garcia-Orellana, J., Masqué, P., 2018. Tracing water masses with ^{129}I and ^{236}U in the subpolar North Atlantic along the GEOTRACES GA01 section. *Biogeosciences*, 15(18), 5545-5564
- Christl, M., Casacuberta, N., Vockenhuber, C., Elsässer, C., Bois, P.B.d., Herrmann, J., Synal, H.A., 2015. Reconstruction of the ^{236}U input function for the Northeast Atlantic Ocean: Implications for $^{129}\text{I}/^{236}\text{U}$ and $^{236}\text{U}/^{238}\text{U}$ -based tracer ages. *Journal of Geophysical Research: Oceans*.
- Church, M.J., Jenkins, B.D., Karl, D.M., Zehr, J.P., 2005a. Vertical distributions of nitrogen fixing phylotypes at Stn ALOHA in the oligotrophic North Pacific Ocean. *Aquatic Microbial Ecology* 38, 3–14.
- Church, M.J., Short, C.M., Jenkins, B.D., Karl, D.M., Zehr, J.P., 2005b. Temporal patterns of nitrogenase gene (*nifH*) expression in the oligotrophic North Pacific Ocean. *Applied and Environmental Microbiology* 71, 5362–5370.
- Costa, K.M., Hayes, C.T., Anderson, R.F., Pavia, F.J., Bausch, A., Deng, F., Dutay, J.C., Geibert, W., Heinze, C., Henderson, G., Hillaire-Marcel, C., 2020. ^{230}Th normalization: New insights on an essential tool for quantifying sedimentary fluxes in the modern and Quaternary ocean. *Paleoceanography and Paleoclimatology* 35(2), e2019PA003820.
- Davey, M., Tarran, G. A., Mills, M.M., Ridame, C., Geider, R.J., La Roche, J., 2008. Nutrient limitation of picophytoplankton photosynthesis and growth in the tropical North Atlantic. *Limnology and Oceanography* 53, 1722–1733.
- Dellwig, O., Beck, M., Lemke, A., Lunau, M., Kolditz, K., Schnetger, B., Brumsack, H.-J., 2007. Non-conservative behaviour of molybdenum in coastal waters: Coupling geochemical, biological, and sedimentological processes. *Geochimica et Cosmochimica Acta* 71, 2745-2761.
- De Souza, G.F., Reynolds, B.C., Johnson, G.C., Bullister, J.L., Bourdon, B., 2012a. Silicon stable isotope distribution traces Southern Ocean export of Si to the eastern South Pacific thermocline. *Biogeosciences* 9, 4199–4213.
- De Souza, G.F., Reynolds, B.C., Rickli, J., Frank, M., Saito, M.A., Gerringa, L.J.A., Bourdon, B., 2012b. Southern Ocean control of silicon stable isotope distribution in the deep Atlantic Ocean. *Global Biogeochemical Cycles* 26, 1–13.
- de Villiers, S., 1998. Excess dissolved Ca in the deep ocean: a hydrothermal hypothesis. *Earth and Planetary Science Letters* 164, 627-641.
- de Villiers, S., 1999. Seawater strontium and Sr/Ca variability in the Atlantic and Pacific oceans. *Earth and Planetary Science Letters* 171, 623-634.
- Edmond, J.M., Measures, C., McDuff, R.E., Chan, L.H., Collier, R., Grant, B., Gordon, L.I., Corliss, J.B., 1979. Ridge crest hydrothermal activity and the balances of the major and minor elements in the ocean: The Galapagos data. *Earth and Planetary Science Letters* 46, 1-18.

- Fabricand, B.P., Imbimbo, E.S., Brey, M.E., 1967. Atomic absorption analyses for Ca, Li, Mg, K, Rb and Sr at two Atlantic Ocean stations. *Deep-Sea Research* 14, 785-789.
- Frank, M., 2002. Radiogenic isotopes: Tracers of past ocean circulation and erosional input. *Reviews in Geophysics* 40(1), 1–38.
- Frank, M., 2011. Chemical twins, separated. *Nature Geoscience* 4, 220-221.
- Froelich, P.N., Kim, K.H., Jahnke, R., Burnett, W.C., Soutar, A., Deakin, M., 1983. Pore water fluoride in Peru continental margin sediments: Uptake from seawater. *Geochimica et Cosmochimica Acta* 47, 1605-1612.
- GEBCO Compilation Group, 2021. GEBCO 2021 Grid.
- Geibert, W., 2018. Processes that regulate trace element distribution in the ocean. *Elements: An International Magazine of Mineralogy, Geochemistry, and Petrology* 14(6), 391-396.
- Gibb, S.W., Barlow, R.G., Cummings, D.G., Rees, N.W., Trees, C.C., Holligan, P., Suggett, D., 2000. Surface phytoplankton pigment distributions in the Atlantic Ocean: an assessment of basin scale variability between 50 degrees N and 50 degrees S. *Progress in Oceanography* 45, 339–368.
- Gorsky, G., Ohman, M. D., Picheral, M., Gasparini, S., Stemann, L., Romagnan, J. B., Cawood, A., Pesant, S., García-Comas, C., Prejger, F., 2010. Digital zooplankton image analysis using the ZooScan integrated system. *Journal of Plankton Research*, 32(3), 285–303.
- Greenhalgh, R., Riley, J.P., 1963. Occurrence of abnormally high fluoride concentrations at depth in the oceans. *Nature* 197, 371-372.
- Hayes, C., Costa, K., Anderson, R., Calvo, E., Chase, Z., Demina, L., Dutay, J.C., German, C., Heimbürger, L.E., Jaccard, S., Jacobel, A., 2021. Global ocean sediment composition and burial flux in the deep sea. *Global biogeochemical cycles* 35, e2020GB006769.
- Heimbürger, L.E., Sonke, J.E., Cossa, D., Point, D., Lagane, C., Laffont, L., Galfond, B.T., Nicolaus, M., Rabe, B., van der Loeff, M.R., 2015. Shallow methylmercury production in the marginal sea ice zone of the central Arctic Ocean. *Scientific Reports*, 5(1), 1-6.
- Henderson, P.B., Morris, P.J., Moore, W.S., Charette, M.A., 2013. Methodological advances for measuring low-level radium isotopes in seawater. *Journal of Radioanalytical and Nuclear Chemistry* 296, 357–362.
- Horner, T.J., Kinsley, C.W., Nielsen, S.G., 2015. Barium-isotopic fractionation in seawater mediated by barite cycling and oceanic circulation. *Earth and Planetary Science Letters* 430, 511–522.
- Hsieh, Y.T., Henderson, G.M., 2017. Barium stable isotopes in the global ocean: Tracer of Ba inputs and utilization. *Earth and Planetary Science Letters* 473, 269–278.
- Jiskra, M., Heimbürger-Boavida, L.E., Desgranges, M.M., Petrova, M.V., Dufour, A., Ferreira-Araujo, B., Masbou, J., Chmeleff, J., Thyssen, M., Point, D., Sonke, J.E., 2021. Mercury stable isotopes constrain atmospheric sources to the ocean. *Nature*, 597(7878), 678-682.
- Jenkins, W.J., Smethie, W.M., 1996. Transient Tracers Track Ocean Climate Signals. *OCAENUS- Woods Hole Mass.* 39, 29-32.

- Kleint, C., Hawkes, G.A., Sander, S.G., Koschinsky, A., 2016. Voltammetric investigation of hydrothermal iron speciation. *Frontiers in Marine Science* 3, 75.
- Kremling, K., 1999. Determination of the major constituents, in: K. Grasshoff, K.K.a.M.E. (Ed.), *Methods of Seawater Analysis*. WILEY-VCH Verlag GmbH, Weinheim, pp. 229-251.
- Levier, M., Roy-Barman, M., Colin, C., Dapoigny, A., 2021. Determination of low level of actinium 227 in seawater and freshwater by isotope dilution and mass spectrometry. *Marine Chemistry* 233, 103986.
- Leybourne, M. I., Schwarz-Schampera, U., De Ronde, C. E. J., Baker, E. T., Faure, K., Walker, S. L., Butterfield, D. A., Resing, J. A., Lupton, J. E., Hannington, M. D., Gibson, H. L., Massoth, G. J., Embley, R. W., Chadwick, W. W., Clark, M. R., Timm, C., Graham, I. J., Wright, I. C., 2012. Submarine magmatic-hydrothermal systems at the monowai volcanic center, Kermadec Arc. *Economic Geology*, 107(8), 1669–1694.
- Li, X., Gilhooly III, W.P., Zerkle, A.L., Lyons, T.W., Farquhar, J., Werne, J.P., Varela, R., Scranton, M.I., 2010. Stable sulfur isotopes in the water column of the Cariaco Basin. *Geochimica et Cosmochimica Acta* 74, 6764–6778.
- Menzel Barraqueta, J.L., Klar, J., Gledhill, M., Schlosser, C., Shelley, R., Planquette, H.F., Wenzel, B., Sarthou, G., Achterberg, E.P., 2019. Atmospheric deposition fluxes over the Atlantic Ocean: A GEOTRACES case study. *Biogeosciences*, 16(7), 1525–1542.
- Middag, R., van Slooten, C., de Baar, H. J. W., Laan, P., 2011. Dissolved aluminium in the Southern Ocean. *Deep-Sea Research Part II: Topical Studies in Oceanography* 58(25–26), 2647–2660.
- Milliman, J.D., 1974. *Marine carbonates*. Springer-Verlag, Berlin.
- Mohr, W., Großkopf, T., Wallace, D.W., LaRoche, J., 2010. Methodological underestimation of oceanic nitrogen fixation rates. *PLoS One* 5, e12583.
- Moisander, P.H., Beinart, R.A., Voss, M., Zehr, J.P., 2008. Diversity and abundance of diazotrophic microorganisms in the South China Sea during intermonsoon. *The ISME Journal* 2, 954–967.
- Monperrus, M., Tessier, E., Veschambre, S., Amouroux, D., Donard, O., 2005. Simultaneous speciation of mercury and butyltin compounds in natural waters and snow by propylation and species-specific isotope dilution mass spectrometry analysis. *Analytical and Bioanalytical Chemistry*, 381(4), 854-862.
- Ono, S., Keller, N.S., Rouxel, O., Alt, J.C., 2012. Sulfur-33 constraints on the origin of secondary pyrite in altered oceanic basement: *Geochimica et Cosmochimica Acta* 87, 323–340.
- Pavia, F., Anderson, R., Vivancos, S., Fleisher, M., Lam, P., Lu, Y., Cheng, H., Zhang, P., Edwards, R.L., 2018. Intense hydrothermal scavenging of ²³⁰Th and ²³¹Pa in the deep Southeast Pacific. *Marine Chemistry* 201, 212-228.
- Picheral, M., Guidi, L., Stemmann, L., Karl, D. M., Iddaoud, G., Gorsky, G., 2010. The underwater vision profiler 5: An advanced instrument for high spatial resolution studies of particle size spectra and zooplankton. *Limnology and Oceanography: Methods*, 8(SEPT), 462–473.

- Poehle, S., Schmidt, K., Koschinsky, A., 2015. Determination of Ti, Zr, Nb, V, W and Mo in seawater by a new online-preconcentration method and subsequent ICP-MS analysis. *Deep-Sea Research Part I: Oceanographic Research Papers* 98, 83-93.
- QGIS Development Team, 2022. QGIS Geographic Information System. Open Source Geospatial Foundation Project. <http://qgis.osgeo.org>.
- Ren, J.L., Zhang, J., Luo, J.Q., Pei, X.K., Jiang, Z.X., 2001. Improved fluorimetric determination of dissolved aluminium by micelle-enhanced lumogallion complex in natural waters. *The Analyst*, 126(5), 698–702.
- Reynolds, B.C., Frank, M., Halliday, A.N., 2006. Silicon isotope fractionation during nutrient utilization in the North Pacific. *Earth and Planetary Science Letters* 244, 431–443.
- Rickli, J., Frank, M., Halliday, A.N., 2009. The hafnium-neodymium isotopic composition of Atlantic seawater. *Earth and Planetary Science Letters* 280, 118–127.
- Riley, J.P., 1965. The occurrence of anomalously high fluoride concentrations in the North Atlantic. *Deep-Sea Research and Oceanographic Abstracts* 12, 219-220.
- Rodriguez-Gonzalez, P., Bouchet, S., Monperrus, M., Tessier, E., Amouroux, D., 2013. In situ experiments for element species-specific environmental reactivity of tin and mercury compounds using isotopic tracers and multiple linear regression. *Environmental Science and Pollution Research*, 20(3), 1269-1280.
- Ronge, T.A., Lippold, J., Geibert, W., Jaccard, S.L., Mieruch-Schnülle, S., Sufke, F., Tiedemann, R., 2021. Deglacial patterns of South Pacific overturning inferred from ^{231}Pa and ^{230}Th . *Scientific Reports* 11(1), 1-11.
- Rude, P.D., Aller, R.C., 1991. Fluorine mobility during early diagenesis of carbonate sediment: An indicator of mineral transformations. *Geochimica et Cosmochimica Acta* 55, 2491-2509.
- Rude, P.D., Aller, R.C., 1994. Fluorine uptake by Amazon continental shelf sediment and its impact on the global fluorine cycle. *Continental Shelf Research* 14, 883-907.
- Sander, S., Koschinsky, A., 2000. Onboard-ship redox speciation of chromium in diffuse hydrothermal fluids from the North Fiji Basin. *Marine Chemistry* 71, 83-102.
- Smith, J.N., McLaughlin, F.A., Smethie, W.M., Moran, S.B., Lepore, K., 2011. Iodine-129, ^{137}Cs , and CFC-11 tracer transit time distributions in the Arctic Ocean. *Journal of Geophysical Research: Oceans*, 116(C4), C04024.
- Steiner, Z., Sarkar, A., Prakash, S., Vinayachandran, P.N., Turchyn, A.V., 2020. Dissolved strontium, Sr/Ca ratios, and the abundance of Acantharia in the Indian and Southern Oceans. *ACS Earth and Space Chemistry*.
- Stichel, T., Frank, M., Rickli, J., Haley, B.A., 2012. The hafnium and neodymium isotope composition of seawater in the Atlantic sector of the Southern Ocean. *Earth and Planetary Science Letters* 317–318, 282–294.
- Thompson, A.W., Carter, B.J., Turk-Kubo, K., Malfatti, F., Azam, F., Zehr, J.P., 2014. Genetic diversity of the unicellular nitrogen-fixing cyanobacteria UCYN-A and its prymnesiophyte host. *Environmental Microbiology* 16, 3238–3249.

US Environmental Protection Agency (EPA) method 1631.

van de Flierdt, T., Frank, M., Lee, D.C., Halliday, A.N., 2002. Glacial weathering and the hafnium isotope composition of seawater. *Earth and Planetary Science Letters* 201, 639–647.

Villa-Alfageme, M., Chamizo, E., Kenna, T.C., López-Lora, M., Casacuberta, N., Chang, C., Masqué, P., Christl, M., 2019. Distribution of ^{236}U in the U.S. GEOTRACES Eastern Pacific Zonal Transect and its use as a water mass tracer. *Chemical Geology* 517, 44-57.

Wang, D., Sañudo-Wilhelmy, S., 2008. Development of an analytical protocol for the determination of V(IV) and V(V) in seawater: Application to coastal environments. *Marine Chemistry* 112, 72-80.

Warner, T.B., 1971. Normal fluoride content of seawater. *Deep Sea Research and Oceanographic Abstracts* 18, 1255-1263.

Wefing, A.-M., Casacuberta, N., Christl, M., Gruber, N., Smith, J.N., 2021. Circulation timescales of Atlantic Water in the Arctic Ocean determined from anthropogenic radionuclides. *Ocean Science* 17(1), 111-129.

Welschmeyer, N.A., 1994. Fluorometric analysis of chlorophyll-a in the presence of chlorophyll-b and pheopigments. *Limnology and Oceanography* 39: 1985–1992.

Wessel, P., Luis, J.F., Uieda, L., Scharroo, R., Wobbe, F., Smith, W.H.F., Tian, D., 2019. The Generic Mapping Tools Version 6. *Geochemistry, Geophysics, Geosystems*, 20(11), 5556–5564.

Willis, C., Desai, D. and LaRoche, J., 2019. Influence of 16S rRNA variable region on perceived diversity of marine microbial communities of the Northern North Atlantic. *FEMS microbiology letters* 366(13), fnz152.

Windom, H.L., 1971. Fluoride concentration in coastal and estuarine waters of Georgia. *Limnology and Oceanography* 16, 806-810.

Winkler, L.W., 1888. The determination of dissolved oxygen in water. *Berlin DeutChem Gas* 21, 2843-2855.

11 Abbreviations

AAIW	Antarctic Intermediate Water
ADCP	Acoustic Doppler Current Profiler
AMS	Accelerator Mass spectrometry
AQY	Apparent Quantum Yields
BIO-CTD	Shallow trace metal clean water sampling
BODC	British Oceanographic Data Centre
BSH	Bundesamts für Seeschifffahrt und Hydrographie
BSi	Biogenic silica
CFCs	Chlorofluorocarbons
Chl	Chlorophyll
CO	Carbon monoxide
CRM	Certified Reference Material
CSR	Cruise Summary Report
CTD	Conductivity, Temperature and Depth

CVAFS	Cold Vapor Automatic Fluorescence Spectrometry
DAM	Deutsche Allianz für Meeresforschung
DCM	Deep Chlorophyll Maximum
DGM	Dissolved Gaseous Mercury
DIC	Dissolved Inorganic Carbon
DOC	Dissolved Organic Carbon
DOD	Deutsches Ozeanographisches Datenzentrum
DOM	Dissolved Organic Matter
DON	Dissolved Organic Nitrogen
DWBC	Deep Western Boundary Current
EAC	East Australian Current
EEZ	Exclusive Economic Zone
ENA	European Nucleotide archive
EPR	East Pacific Rise
EVs	Extracellular Vesicles
FEP	Fluorinated ethylene propylene
FRRf	Fast Repetition Rate Fluorometry
GEO-CTD	Deep trace metal clean water sampling
GF/F	Glass Fibre Filter
HDPE	High-density Polyethylene
HFSE	High-Field Strength Elements
HPLC	High Performance Liquid Chromatography
ICP-MS	Inductively Coupled Plasma Mass Spectrometry
ICP-OES	Inductively Coupled Plasma Optical Emission Spectroscopy
ISP	In-situ Pump
KDMT	Kiel Data Management Team
LDPE	Low-density Polyethylene
MC-ICP-MS	Multi-Collector Inductively Coupled Plasma Mass Spectrometry
MeHg	Methylmercury
MIO	Mediterranean Institute of Oceanography
MWCO	Molecular Weight Cut-Off
NIST	National Institute of Standards and Technology
NPRs	Nuclear Rprocessing Plants
NTA	Nanoparticle Tracking Analysis
OMZ	Oxygen Minimum Zone
OPA	o-Phtaladiadehyde
OSIS	Ocean Science Information System
PC	Polycarbonate
PCC	Peru Chile Current
PES	Polyethersulfone
PET	Polyethylene terephthalate
PFA	Perfluoroalkoxy Alkane
PMT	Photomultiplier Tube
PO	Pacific Ocean
POC	Particulate organic carbon
PON	Particulate organic nitrogen
PRIDE	PRoteomics IDentifications database
PVDF	Polyvinylidene fluoride
QMA	Quartz Microfiber
qPCR	Quantitative Polymerase Chain Reaction

REE	Rare Earth Elements
SAMW	Subantarctic Mode Water
SEC	South Equatorial Current
SPC	South Pacific Current
SPO	South Pacific Ocean
SRP	Soluble Reactive Phosphorous
SS	Stainless Steel
SS-CTD	Stainless Steel CTD
TA	Total Alkalinity
TDN	Total Dissolved Nitrogen
TE	Trace elements
TEIs	Trace elements and their isotopes
THg	Total mercury
Ti-CTD	Titanium CTD (trace metal clean)
TM	Trace Metals
TOC	Total Organic Carbon
TON	Total Oxidised Nitrogen (nitrate + nitrite)
TSG	Thrmosalinograph
UVP	Underwater Vision Profiler

12 Appendices

12.1 SS-CTD

(C. Galley)

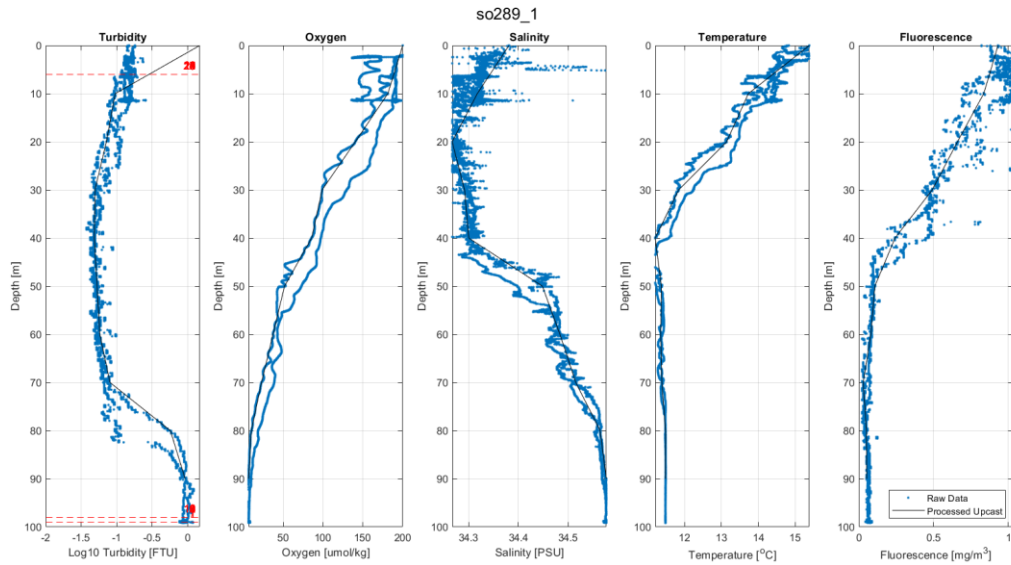


Fig. 12.1 Station 1's cast data, showing the raw down and upcast data in blue, along with the processed upcast data in black, for the turbidity, oxygen, salinity, temperature, and fluorescence data from the SS-CTD. Bottles were fires at the depths indicated with a red dotted line in the turbidity plot.

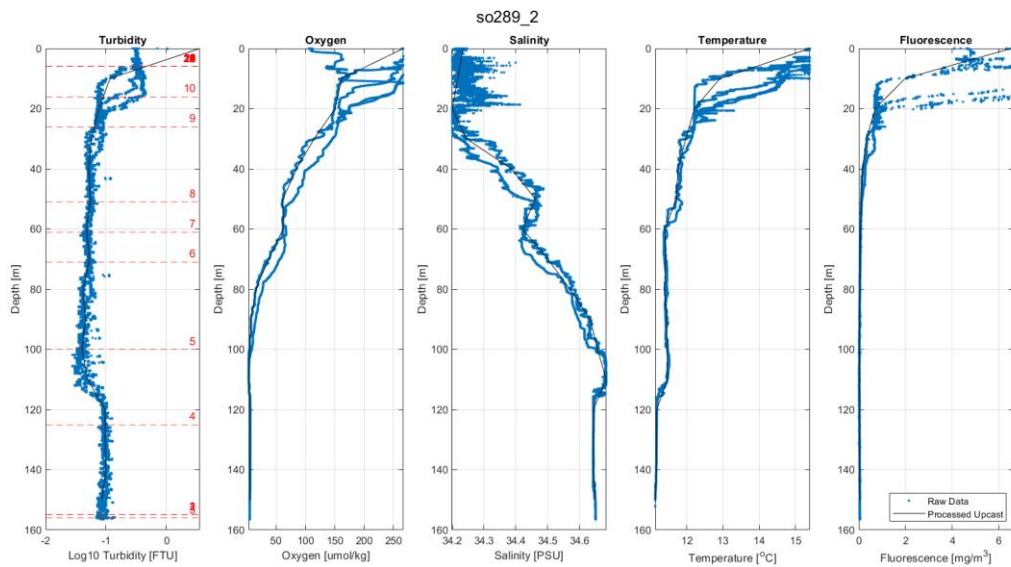


Fig. 12.2 Station 2's cast data, showing the raw down and upcast data in blue, along with the processed upcast data in black, for the turbidity, oxygen, salinity, temperature, and fluorescence data from the SS-CTD. Bottles were fires at the depths indicated with a red dotted line in the turbidity plot.

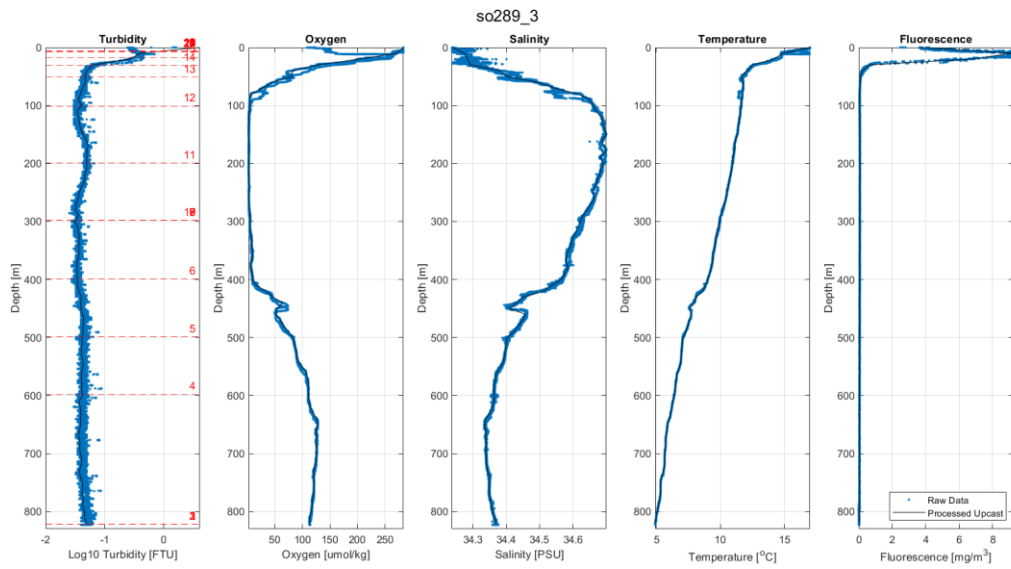


Fig. 12.3 Station 3's cast data, showing the raw down and upcast data in blue, along with the processed upcast data in black, for the turbidity, oxygen, salinity, temperature, and fluorescence data from the SS-CTD. Bottles were fired at the depths indicated with a red dotted line in the turbidity plot.

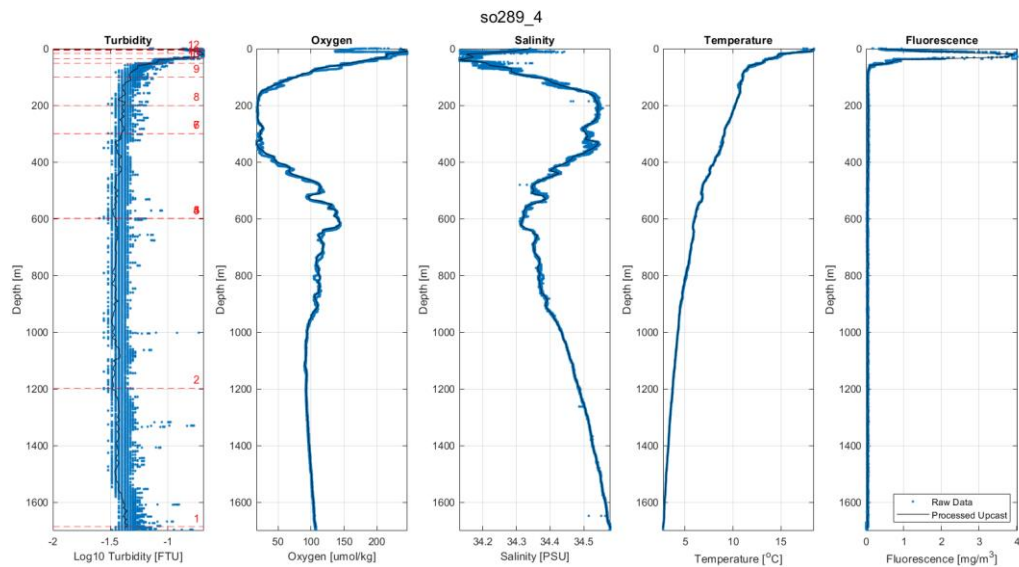


Fig. 12.4 Station 4's cast data, showing the raw down and upcast data in blue, along with the processed upcast data in black, for the turbidity, oxygen, salinity, temperature, and fluorescence data from the SS-CTD. Bottles were fired at the depths indicated with a red dotted line in the turbidity plot.

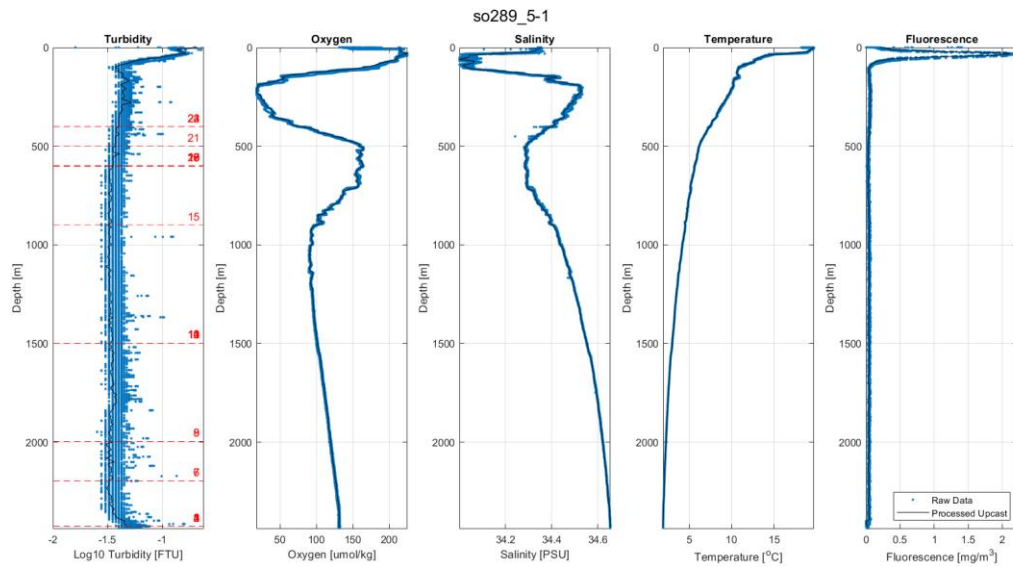


Fig. 12.5 Station 5-1's cast data, showing the raw down and upcast data in blue, along with the processed upcast data in black, for the turbidity, oxygen, salinity, temperature, and fluorescence data from the SS-CTD. Bottles were fired at the depths indicated with a red dotted line in the turbidity plot.

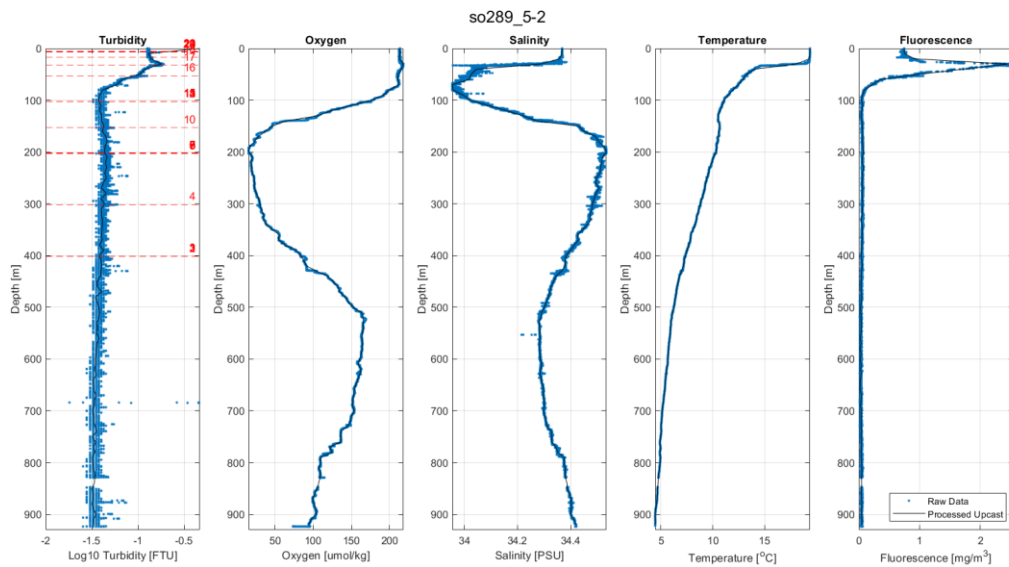


Fig. 12.6 Station 5-2's cast data, showing the raw down and upcast data in blue, along with the processed upcast data in black, for the turbidity, oxygen, salinity, temperature, and fluorescence data from the SS-CTD. Bottles were fired at the depths indicated with a red dotted line in the turbidity plot.

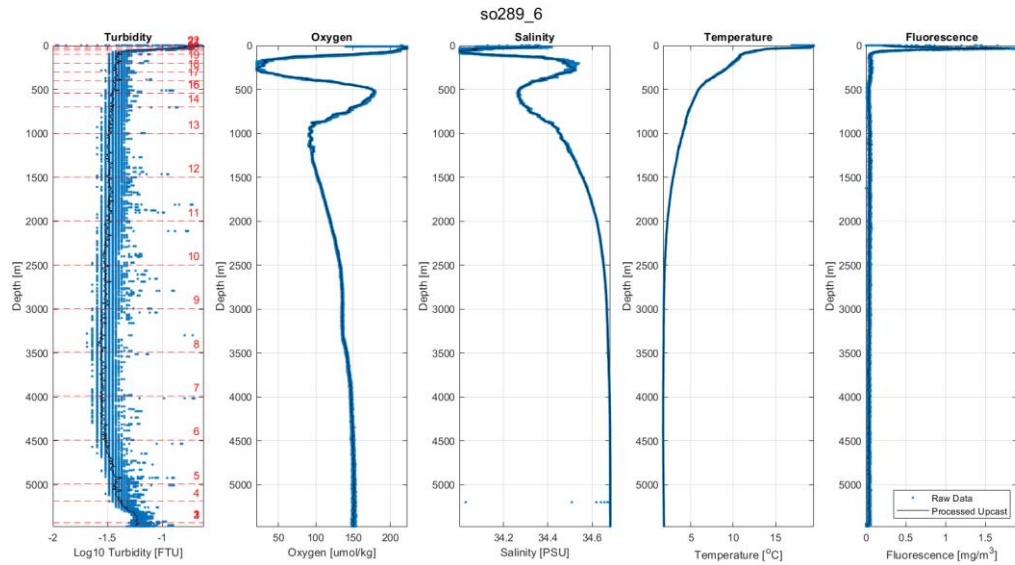


Fig. 12.7 Station 6's cast data, showing the raw down and upcast data in blue, along with the processed upcast data in black, for the turbidity, oxygen, salinity, temperature, and fluorescence data from the SS-CTD. Bottles were fired at the depths indicated with a red dotted line in the turbidity plot.

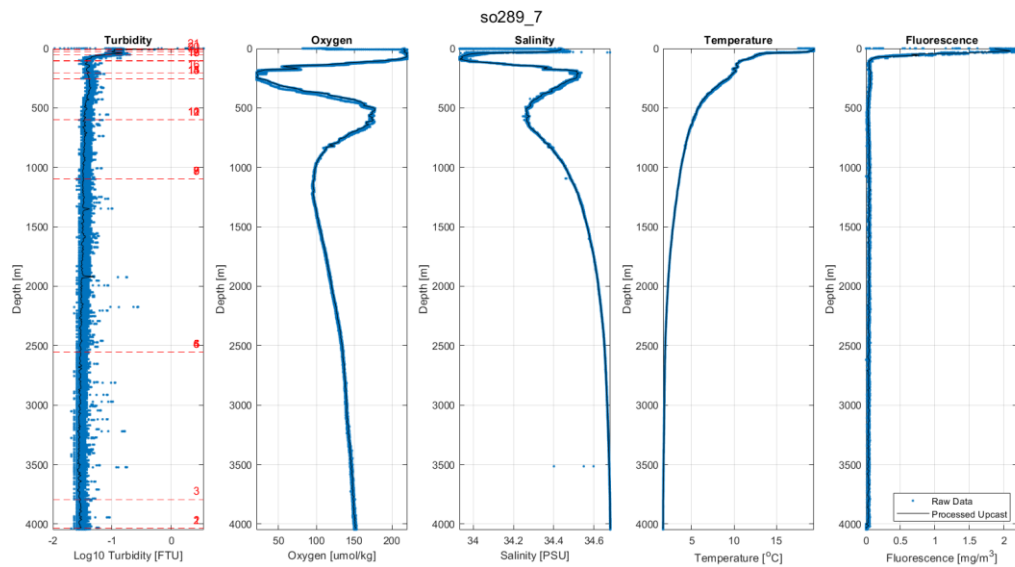


Fig. 12.8 Station 7's cast data, showing the raw down and upcast data in blue, along with the processed upcast data in black, for the turbidity, oxygen, salinity, temperature, and fluorescence data from the SS-CTD. Bottles were fired at the depths indicated with a red dotted line in the turbidity plot.

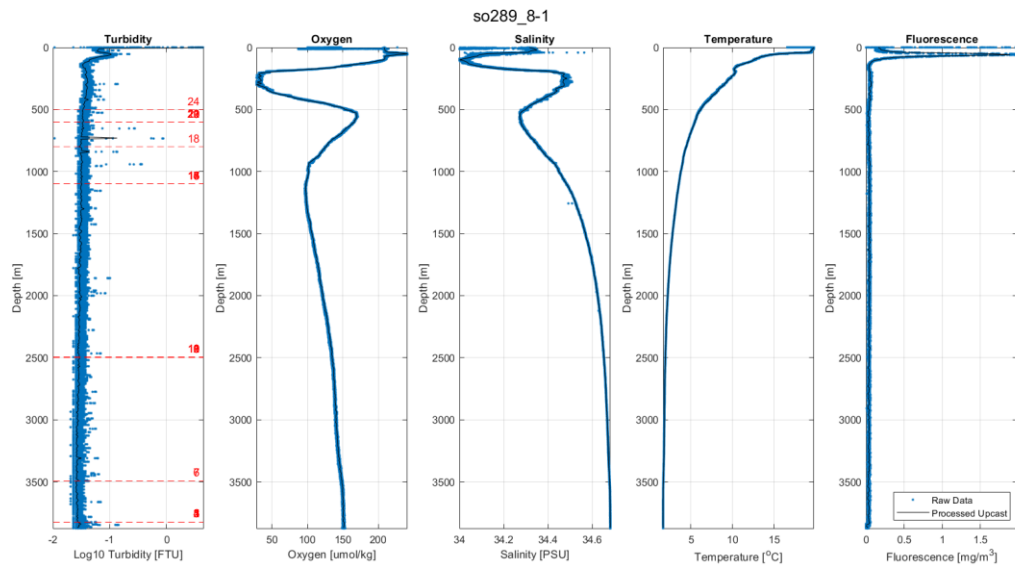


Fig. 12.9 Station 8-1's cast data, showing the raw down and upcast data in blue, along with the processed upcast data in black, for the turbidity, oxygen, salinity, temperature, and fluorescence data from the SS-CTD. Bottles were fired at the depths indicated with a red dotted line in the turbidity plot.

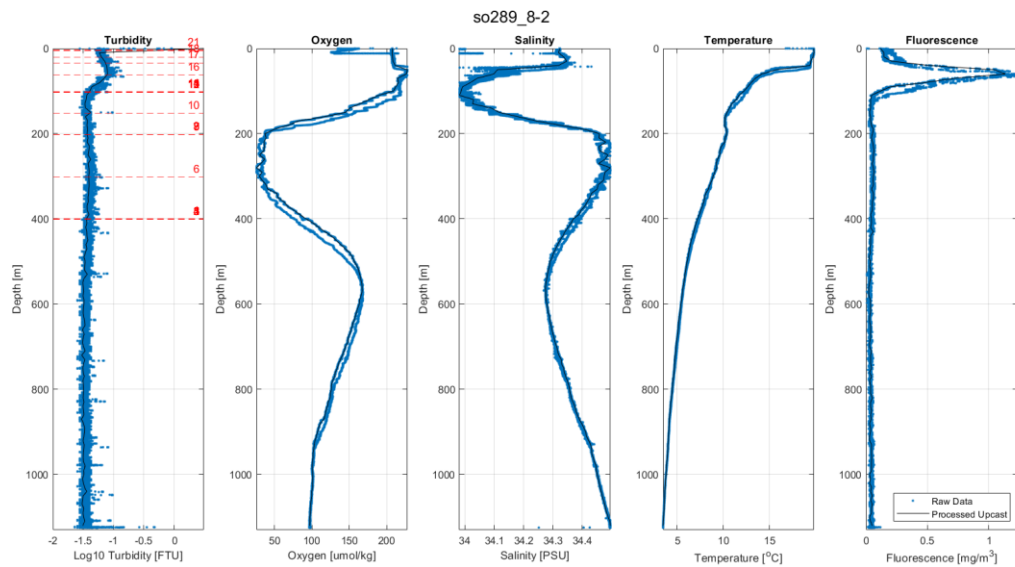


Fig. 12.10 Station 8-2's cast data, showing the raw down and upcast data in blue, along with the processed upcast data in black, for the turbidity, oxygen, salinity, temperature, and fluorescence data from the SS-CTD. Bottles were fired at the depths indicated with a red dotted line in the turbidity plot.

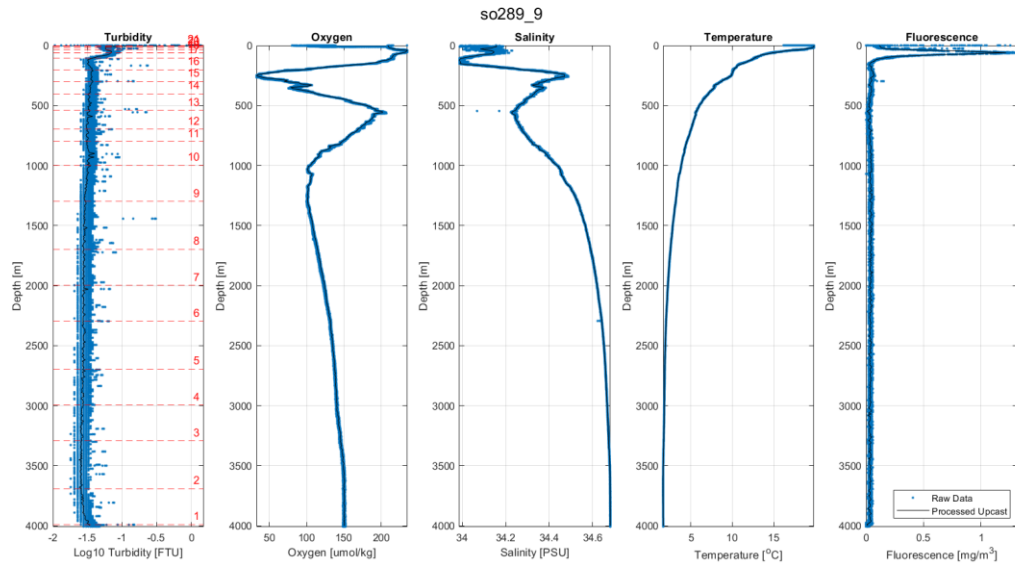


Fig. 12.11 Station 9's cast data, showing the raw down and upcast data in blue, along with the processed upcast data in black, for the turbidity, oxygen, salinity, temperature, and fluorescence data from the SS-CTD. Bottles were fired at the depths indicated with a red dotted line in the turbidity plot.

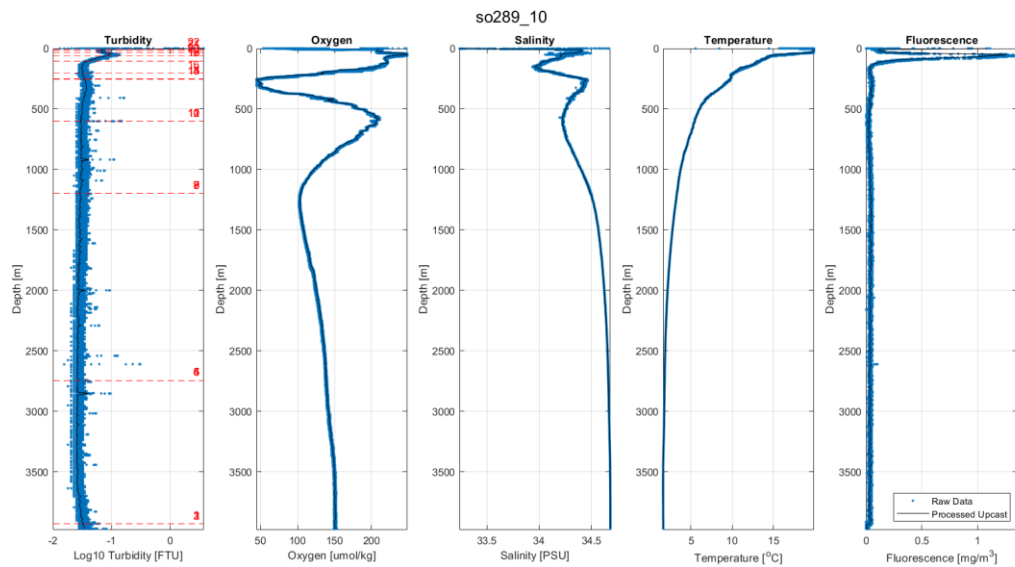


Fig. 12.12 Station 10's cast data, showing the raw down and upcast data in blue, along with the processed upcast data in black, for the turbidity, oxygen, salinity, temperature, and fluorescence data from the SS-CTD. Bottles were fired at the depths indicated with a red dotted line in the turbidity plot.

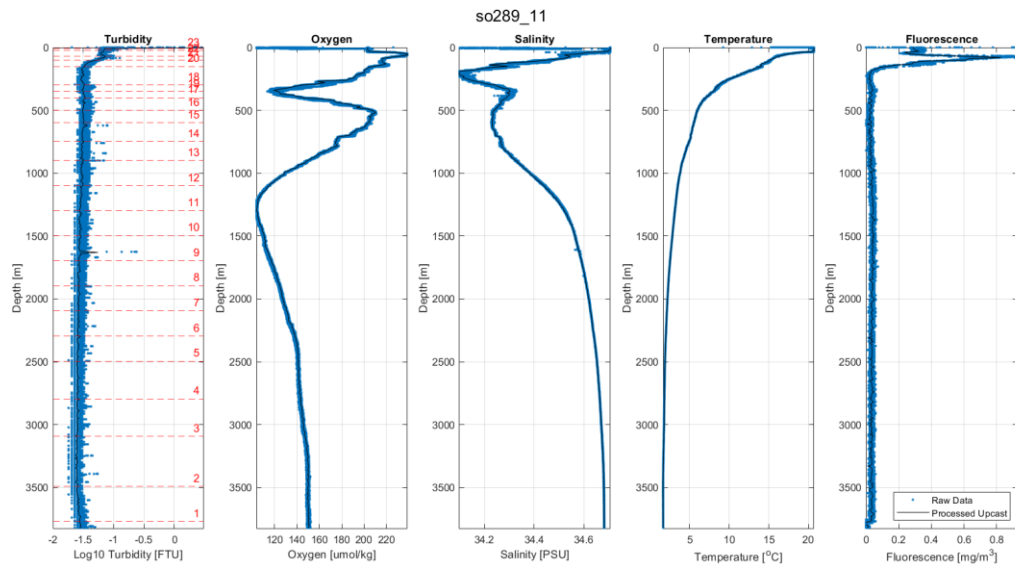


Fig. 12.13 Station 11's cast data, showing the raw down and upcast data in blue, along with the processed upcast data in black, for the turbidity, oxygen, salinity, temperature, and fluorescence data from the SS-CTD. Bottles were fired at the depths indicated with a red dotted line in the turbidity plot.

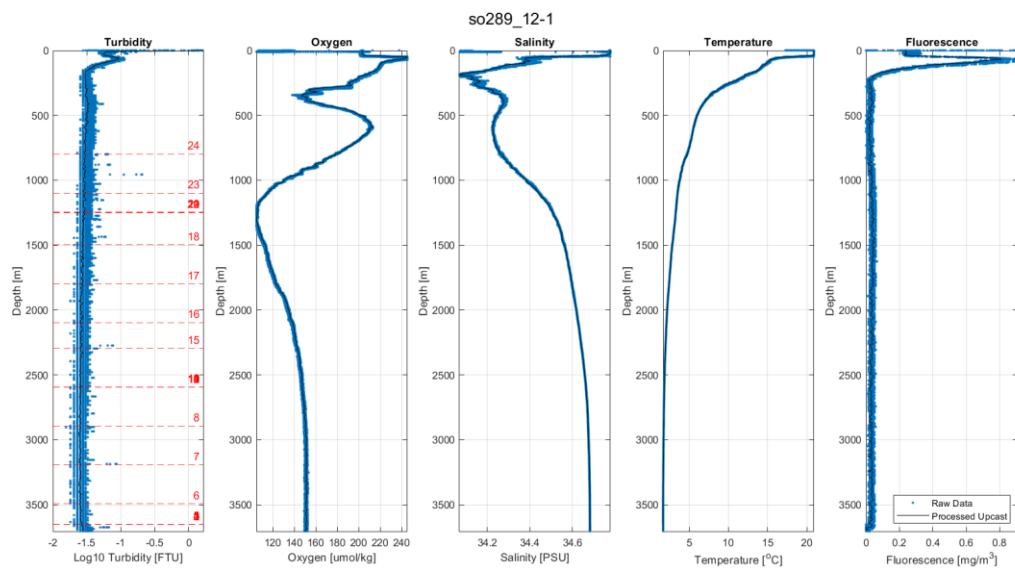


Fig. 12.14 Station 12-1's cast data, showing the raw down and upcast data in blue, along with the processed upcast data in black, for the turbidity, oxygen, salinity, temperature, and fluorescence data from the SS-CTD. Bottles were fired at the depths indicated with a red dotted line in the turbidity plot.

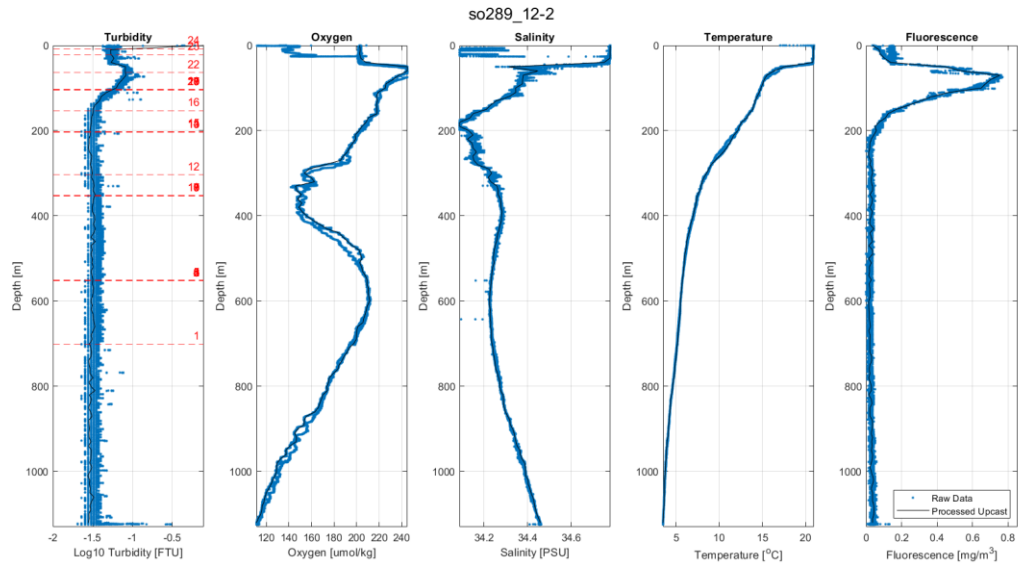


Fig. 12.15 Station 12-2's cast data, showing the raw down and upcast data in blue, along with the processed upcast data in black, for the turbidity, oxygen, salinity, temperature, and fluorescence data from the SS-CTD. Bottles were fired at the depths indicated with a red dotted line in the turbidity plot.

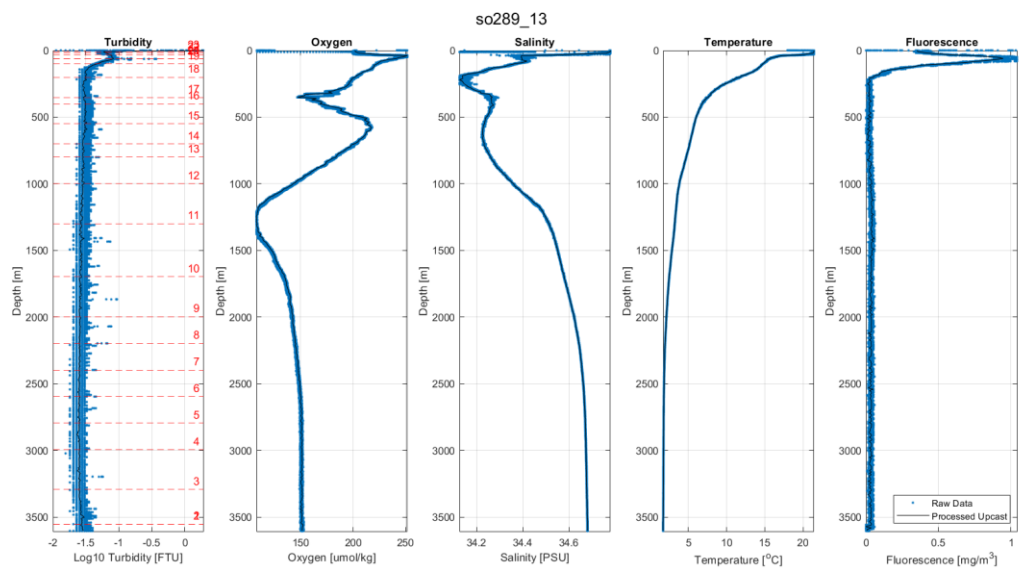


Fig. 12.16 Station 13's cast data, showing the raw down and upcast data in blue, along with the processed upcast data in black, for the turbidity, oxygen, salinity, temperature, and fluorescence data from the SS-CTD. Bottles were fired at the depths indicated with a red dotted line in the turbidity plot.

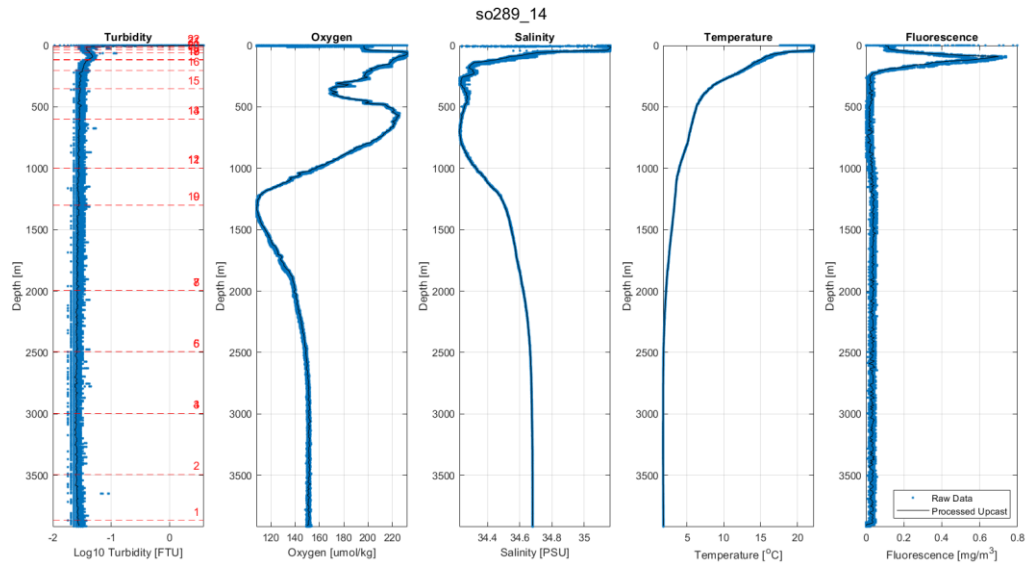


Fig. 12.17 Station 14's cast data, showing the raw down and upcast data in blue, along with the processed upcast data in black, for the turbidity, oxygen, salinity, temperature, and fluorescence data from the SS-CTD. Bottles were fired at the depths indicated with a red dotted line in the turbidity plot.

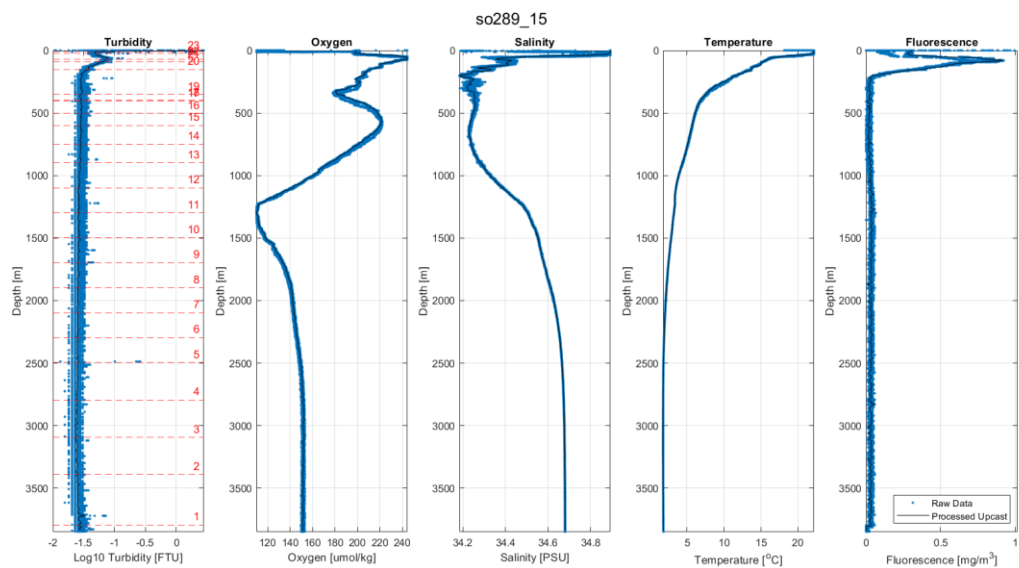


Fig. 12.18 Station 15's cast data, showing the raw down and upcast data in blue, along with the processed upcast data in black, for the turbidity, oxygen, salinity, temperature, and fluorescence data from the SS-CTD. Bottles were fired at the depths indicated with a red dotted line in the turbidity plot.

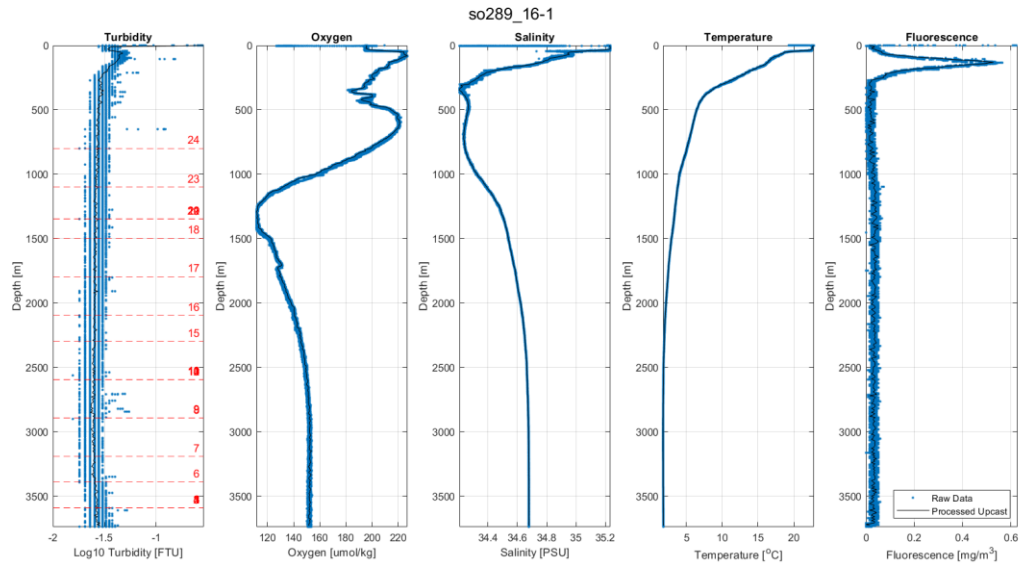


Fig. 12.19 Station 16-1's cast data, showing the raw down and upcast data in blue, along with the processed upcast data in black, for the turbidity, oxygen, salinity, temperature, and fluorescence data from the SS-CTD. Bottles were fired at the depths indicated with a red dotted line in the turbidity plot.

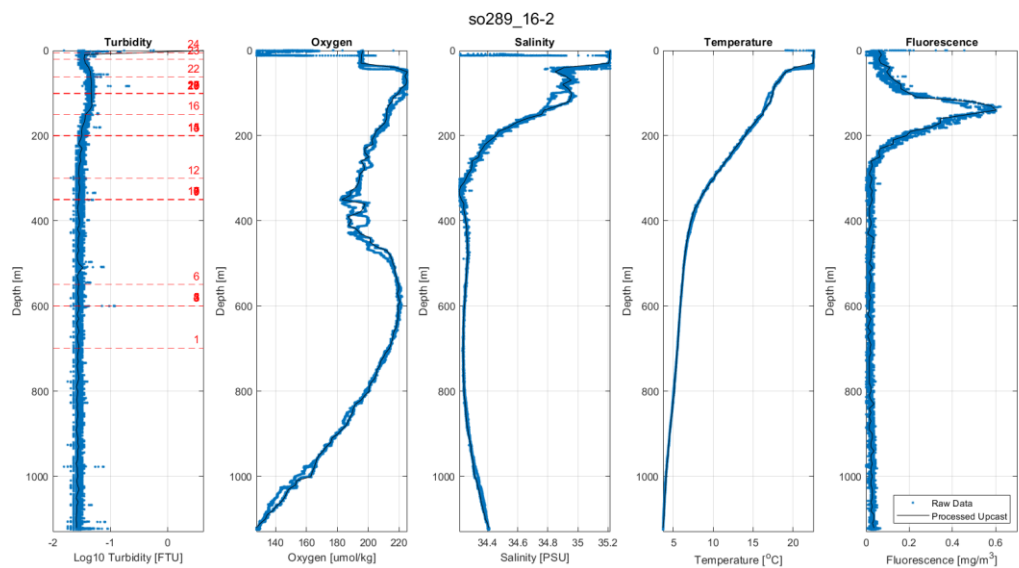


Fig. 12.20 Station 16-2's cast data, showing the raw down and upcast data in blue, along with the processed upcast data in black, for the turbidity, oxygen, salinity, temperature, and fluorescence data from the SS-CTD. Bottles were fired at the depths indicated with a red dotted line in the turbidity plot.

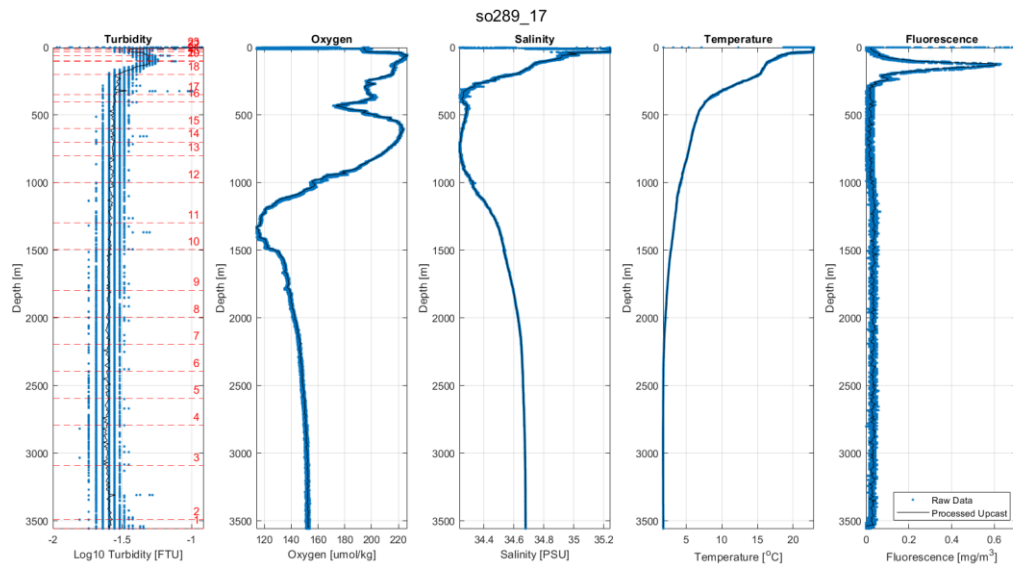


Fig. 12.21 Station 17's cast data, showing the raw down and upcast data in blue, along with the processed upcast data in black, for the turbidity, oxygen, salinity, temperature, and fluorescence data from the SS-CTD. Bottles were fired at the depths indicated with a red dotted line in the turbidity plot.

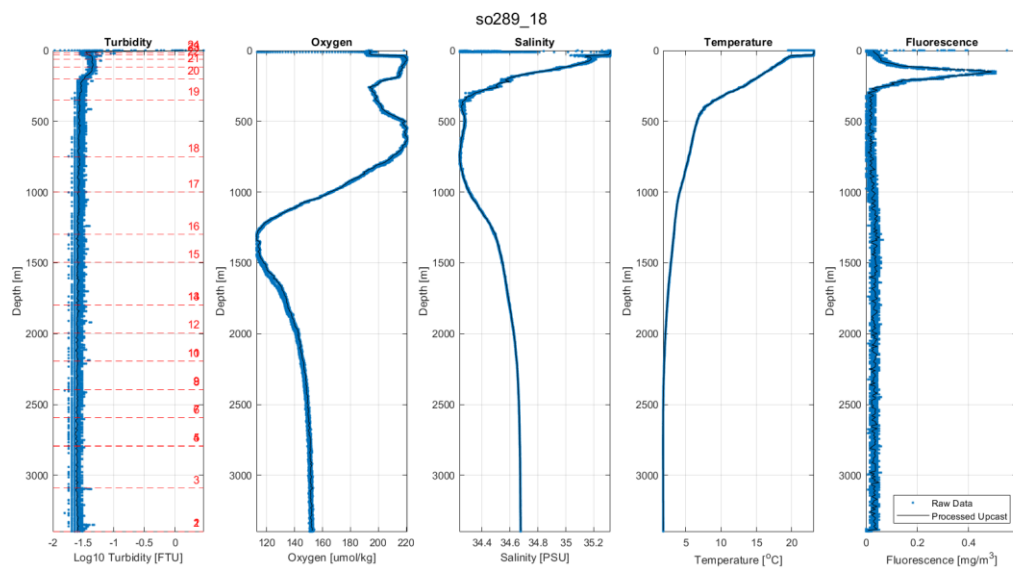


Fig. 12.22 Station 18's cast data, showing the raw down and upcast data in blue, along with the processed upcast data in black, for the turbidity, oxygen, salinity, temperature, and fluorescence data from the SS-CTD. Bottles were fired at the depths indicated with a red dotted line in the turbidity plot.

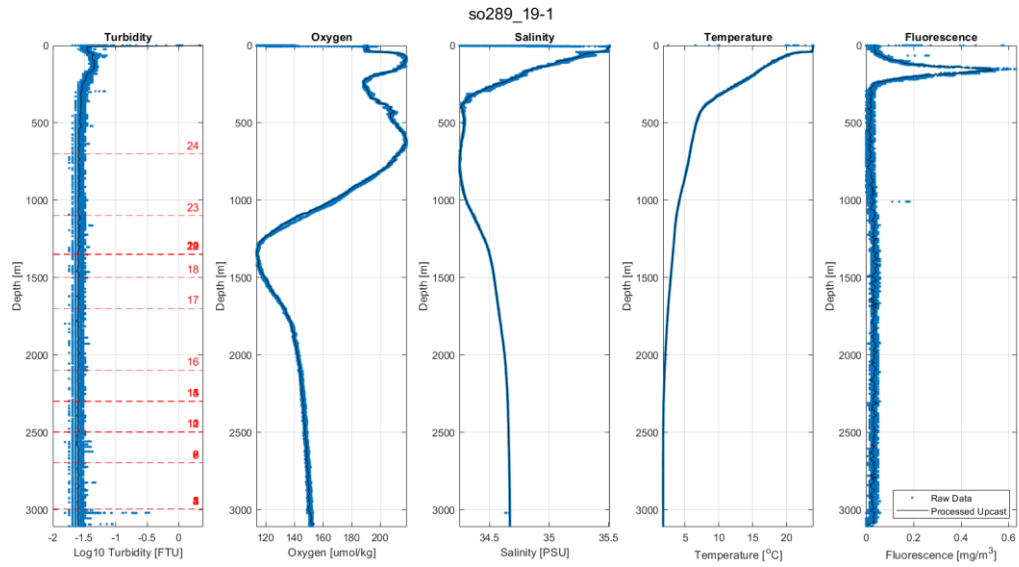


Fig. 12.23 Station 19-1's cast data, showing the raw down and upcast data in blue, along with the processed upcast data in black, for the turbidity, oxygen, salinity, temperature, and fluorescence data from the SS-CTD. Bottles were fired at the depths indicated with a red dotted line in the turbidity plot.

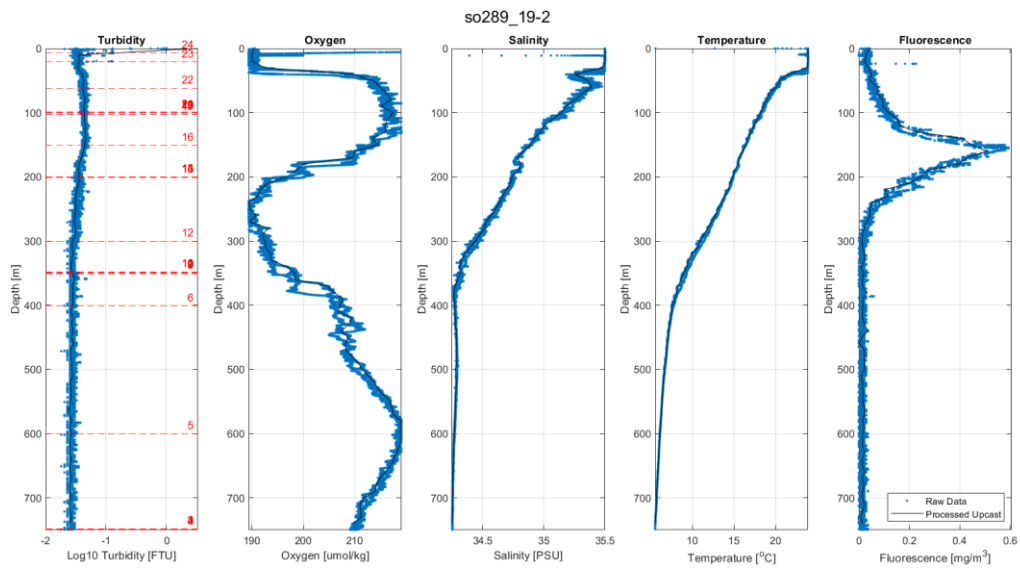


Fig. 12.24 Station 19-2's cast data, showing the raw down and upcast data in blue, along with the processed upcast data in black, for the turbidity, oxygen, salinity, temperature, and fluorescence data from the SS-CTD. Bottles were fired at the depths indicated with a red dotted line in the turbidity plot.

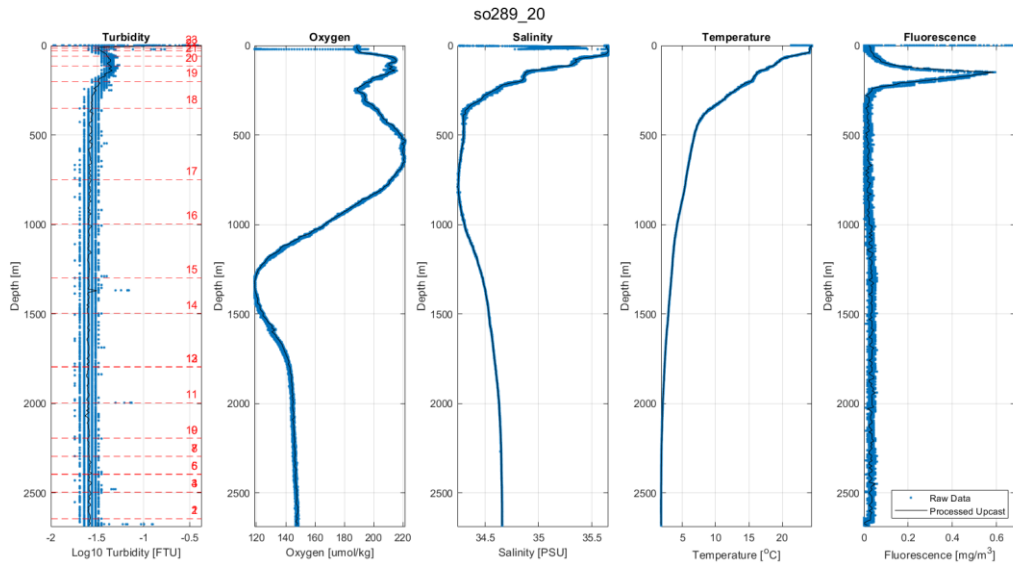


Fig. 12.25 Station 20's cast data, showing the raw down and upcast data in blue, along with the processed upcast data in black, for the turbidity, oxygen, salinity, temperature, and fluorescence data from the SS-CTD. Bottles were fired at the depths indicated with a red dotted line in the turbidity plot.

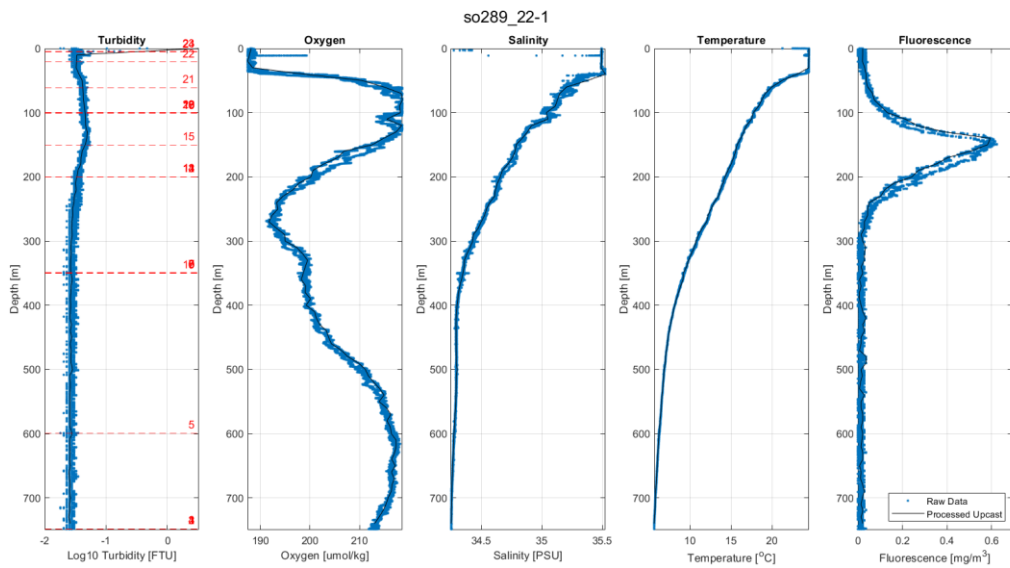


Fig. 12.26 Station 22-1's cast data, showing the raw down and upcast data in blue, along with the processed upcast data in black, for the turbidity, oxygen, salinity, temperature, and fluorescence data from the SS-CTD. Bottles were fired at the depths indicated with a red dotted line in the turbidity plot.

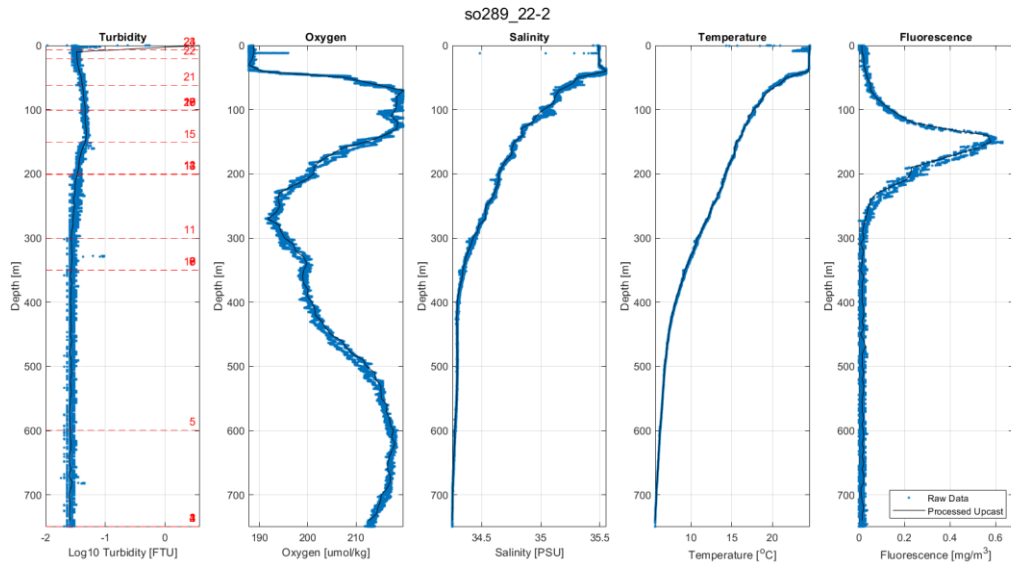


Fig. 12.27 Station 22-2's cast data, showing the raw down and upcast data in blue, along with the processed upcast data in black, for the turbidity, oxygen, salinity, temperature, and fluorescence data from the SS-CTD. Bottles were fired at the depths indicated with a red dotted line in the turbidity plot.

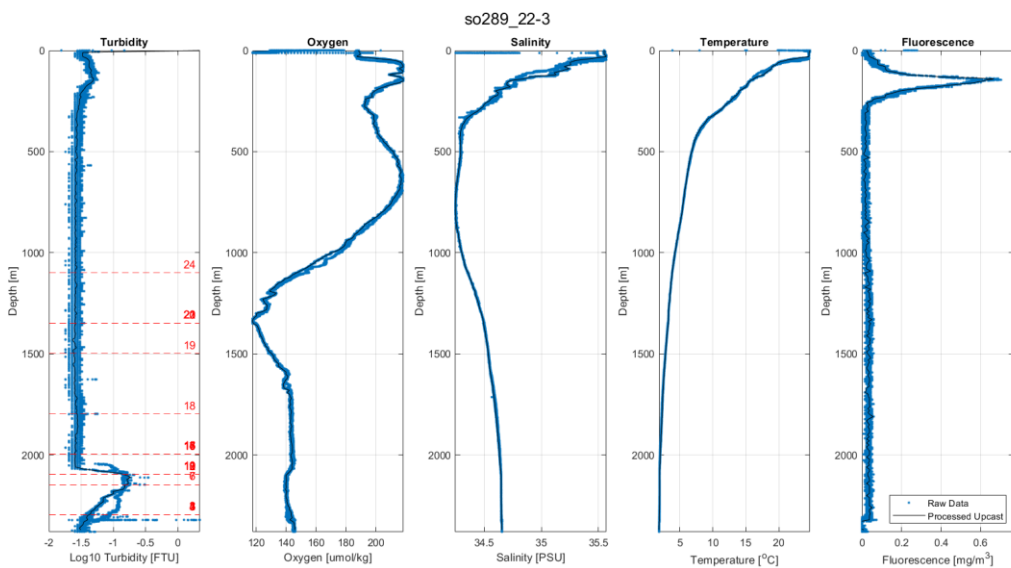


Fig. 12.28 Station 22-3's cast data, showing the raw down and upcast data in blue, along with the processed upcast data in black, for the turbidity, oxygen, salinity, temperature, and fluorescence data from the SS-CTD. Bottles were fired at the depths indicated with a red dotted line in the turbidity plot.

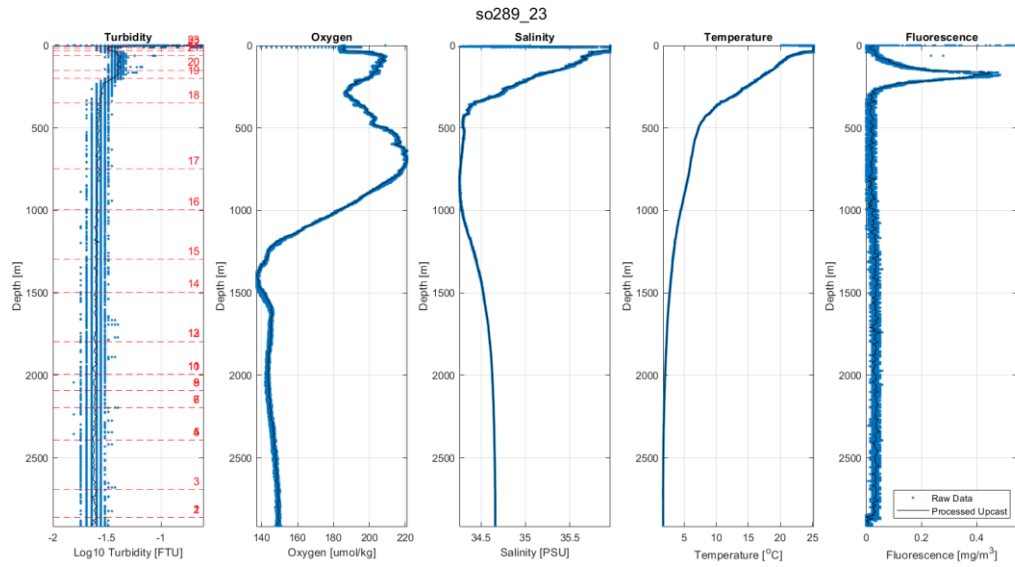


Fig. 12.29 Station 23's cast data, showing the raw down and upcast data in blue, along with the processed upcast data in black, for the turbidity, oxygen, salinity, temperature, and fluorescence data from the SS-CTD. Bottles were fired at the depths indicated with a red dotted line in the turbidity plot.

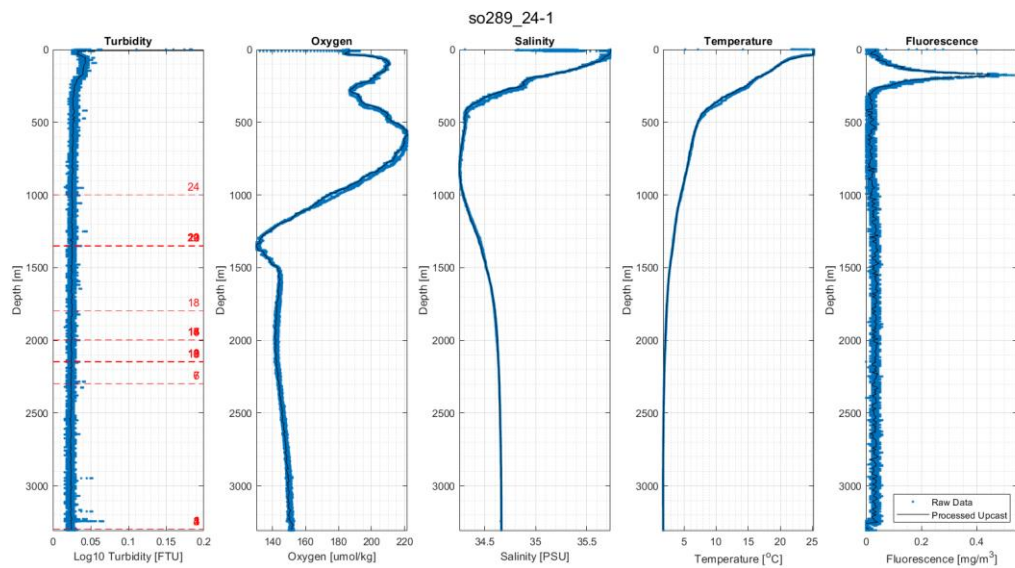


Fig. 12.30 Station 24-1's cast data, showing the raw down and upcast data in blue, along with the processed upcast data in black, for the turbidity, oxygen, salinity, temperature, and fluorescence data from the SS-CTD. Bottles were fired at the depths indicated with a red dotted line in the turbidity plot.

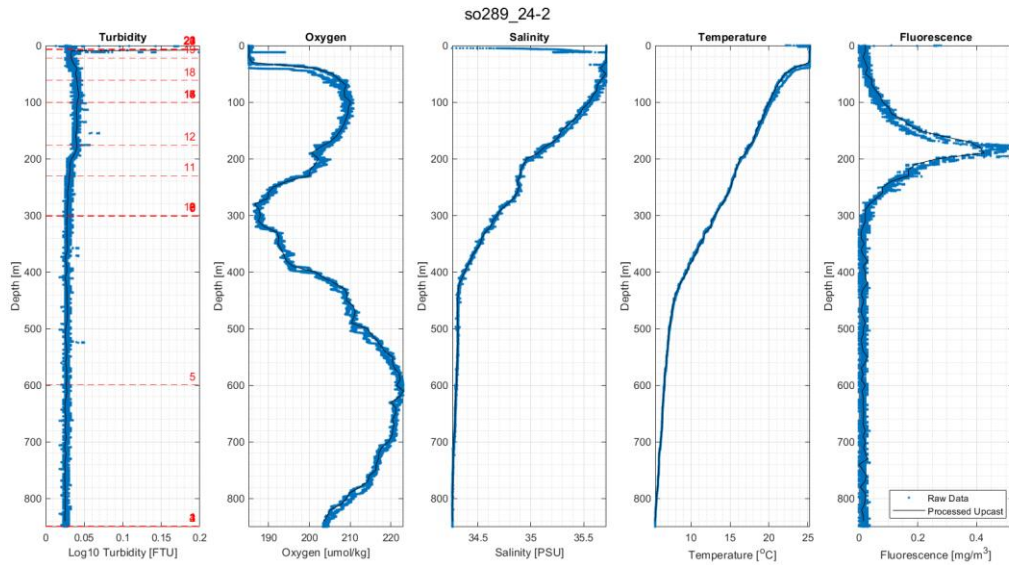


Fig. 12.31 Station 24-2's cast data, showing the raw down and upcast data in blue, along with the processed upcast data in black, for the turbidity, oxygen, salinity, temperature, and fluorescence data from the SS-CTD. Bottles were fired at the depths indicated with a red dotted line in the turbidity plot.

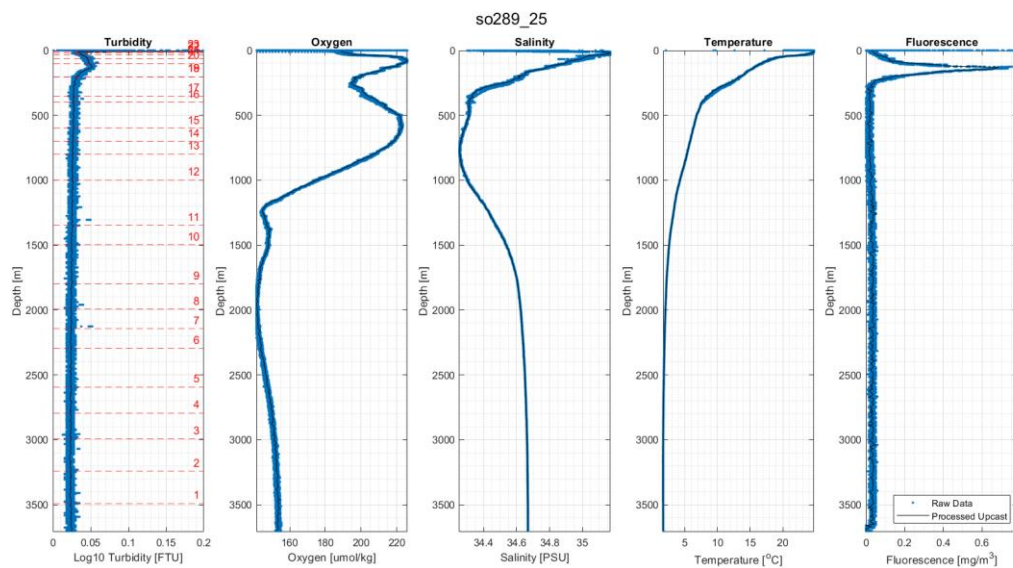


Fig. 12.32 Station 25's cast data, showing the raw down and upcast data in blue, along with the processed upcast data in black, for the turbidity, oxygen, salinity, temperature, and fluorescence data from the SS-CTD. Bottles were fired at the depths indicated with a red dotted line in the turbidity plot.

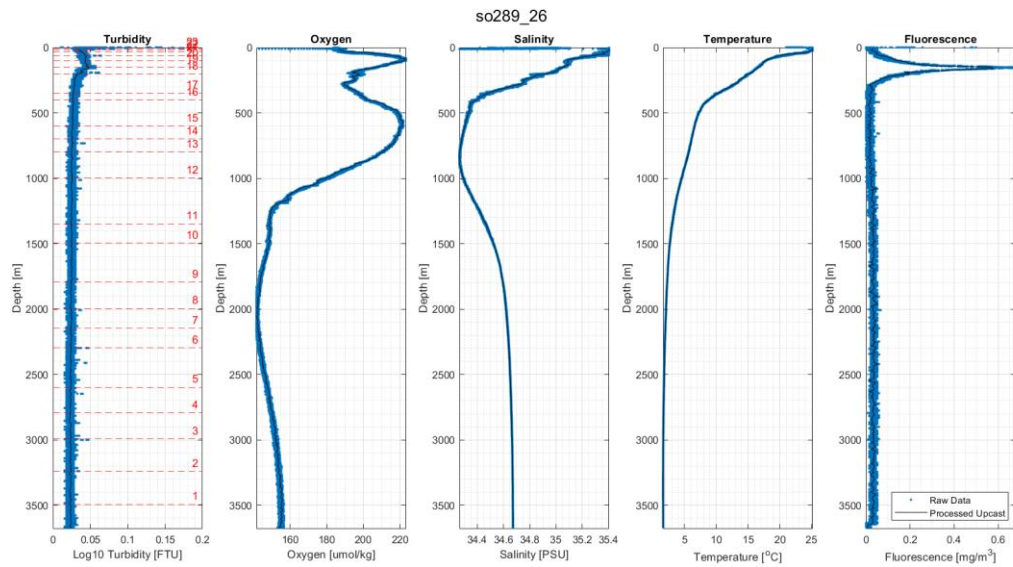


Fig. 12.33 Station 26's cast data, showing the raw down and upcast data in blue, along with the processed upcast data in black, for the turbidity, oxygen, salinity, temperature, and fluorescence data from the SS-CTD. Bottles were fired at the depths indicated with a red dotted line in the turbidity plot.

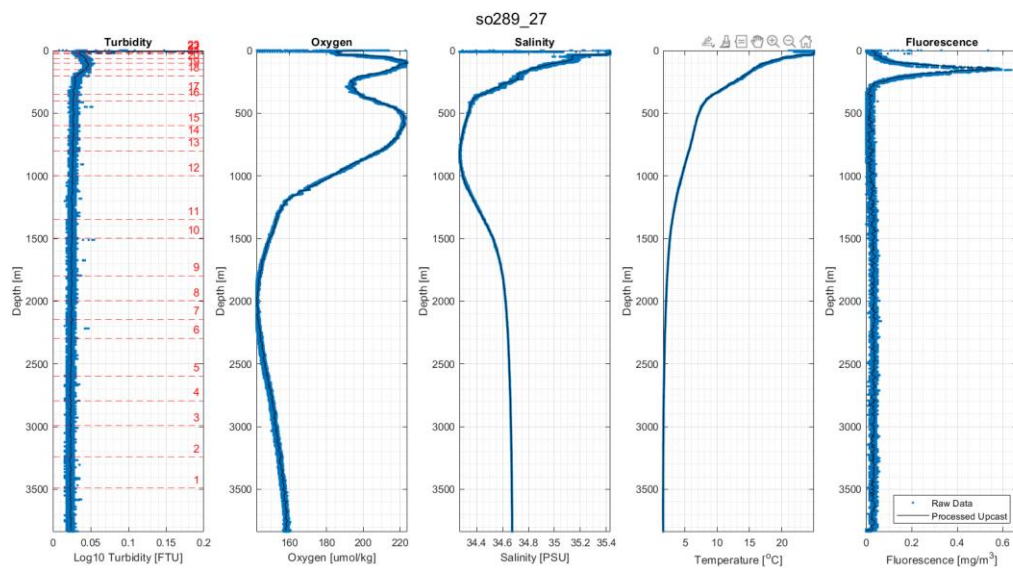


Fig. 12.34 Station 27's cast data, showing the raw down and upcast data in blue, along with the processed upcast data in black, for the turbidity, oxygen, salinity, temperature, and fluorescence data from the SS-CTD. Bottles were fired at the depths indicated with a red dotted line in the turbidity plot.

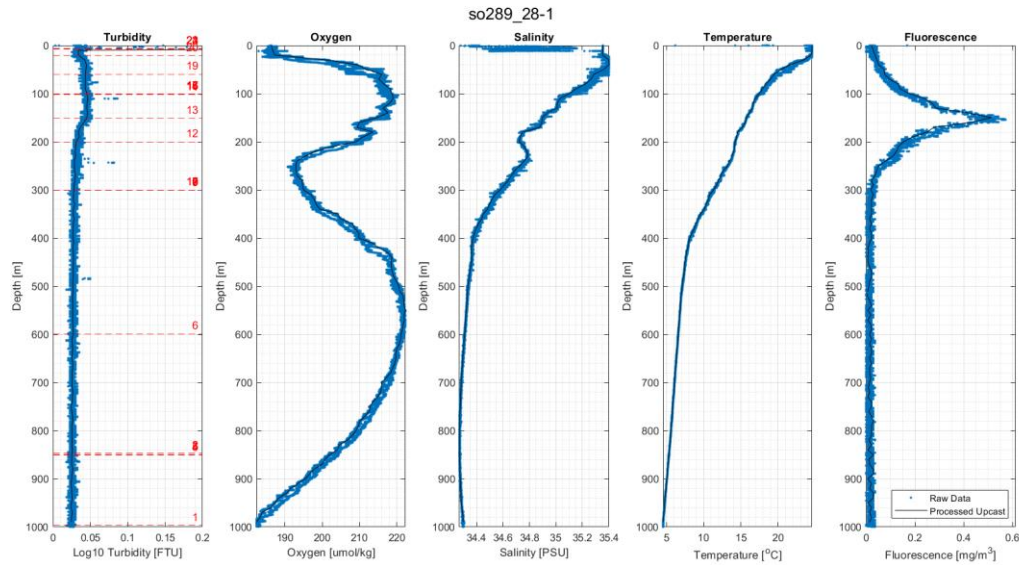


Fig. 12.35 Station 28-1's cast data, showing the raw down and upcast data in blue, along with the processed upcast data in black, for the turbidity, oxygen, salinity, temperature, and fluorescence data from the SS-CTD. Bottles were fired at the depths indicated with a red dotted line in the turbidity plot.

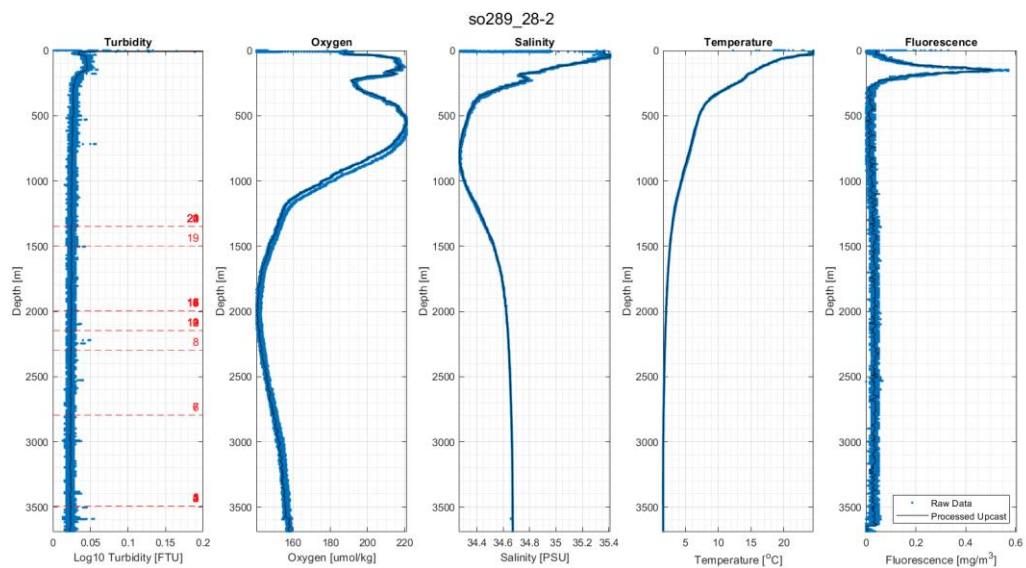


Fig. 12.36 Station 28-2's cast data, showing the raw down and upcast data in blue, along with the processed upcast data in black, for the turbidity, oxygen, salinity, temperature, and fluorescence data from the SS-CTD. Bottles were fired at the depths indicated with a red dotted line in the turbidity plot.

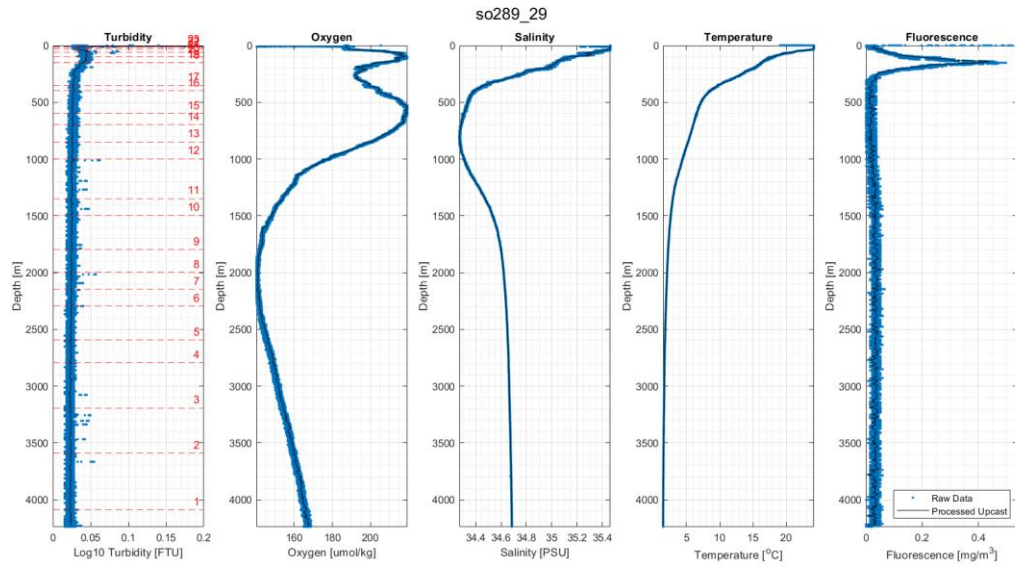


Fig. 12.37 Station 29's cast data, showing the raw down and upcast data in blue, along with the processed upcast data in black, for the turbidity, oxygen, salinity, temperature, and fluorescence data from the SS-CTD. Bottles were fired at the depths indicated with a red dotted line in the turbidity plot.

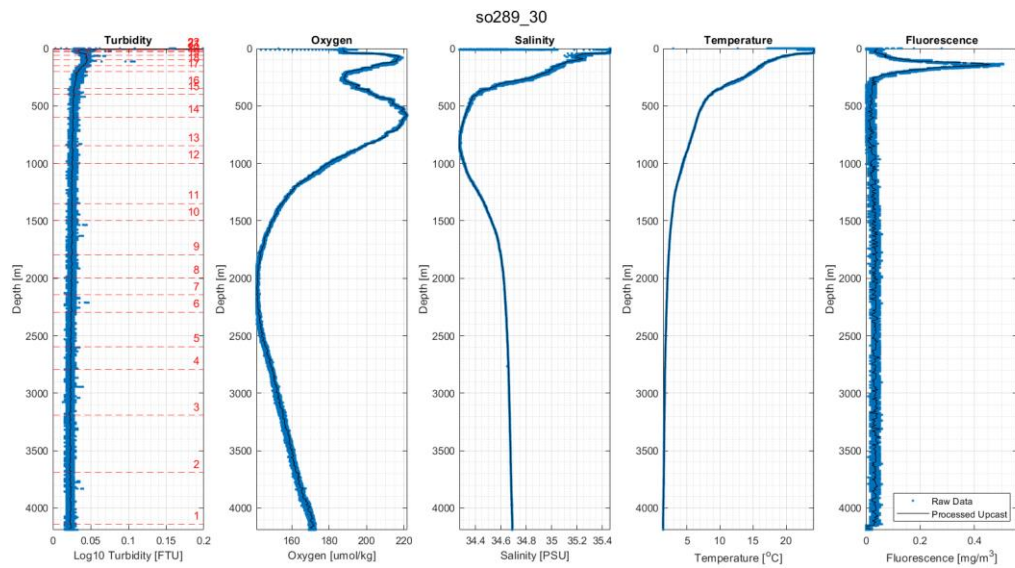


Fig. 12.38 Station 30's cast data, showing the raw down and upcast data in blue, along with the processed upcast data in black, for the turbidity, oxygen, salinity, temperature, and fluorescence data from the SS-CTD. Bottles were fired at the depths indicated with a red dotted line in the turbidity plot.

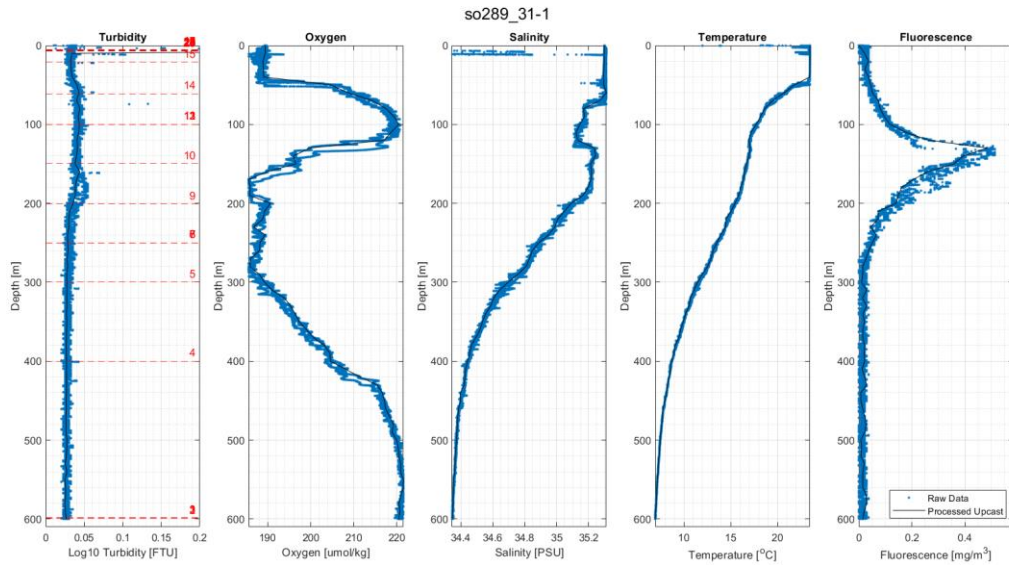


Fig. 12.39 Station 31-1's cast data, showing the raw down and upcast data in blue, along with the processed upcast data in black, for the turbidity, oxygen, salinity, temperature, and fluorescence data from the SS-CTD. Bottles were fired at the depths indicated with a red dotted line in the turbidity plot.

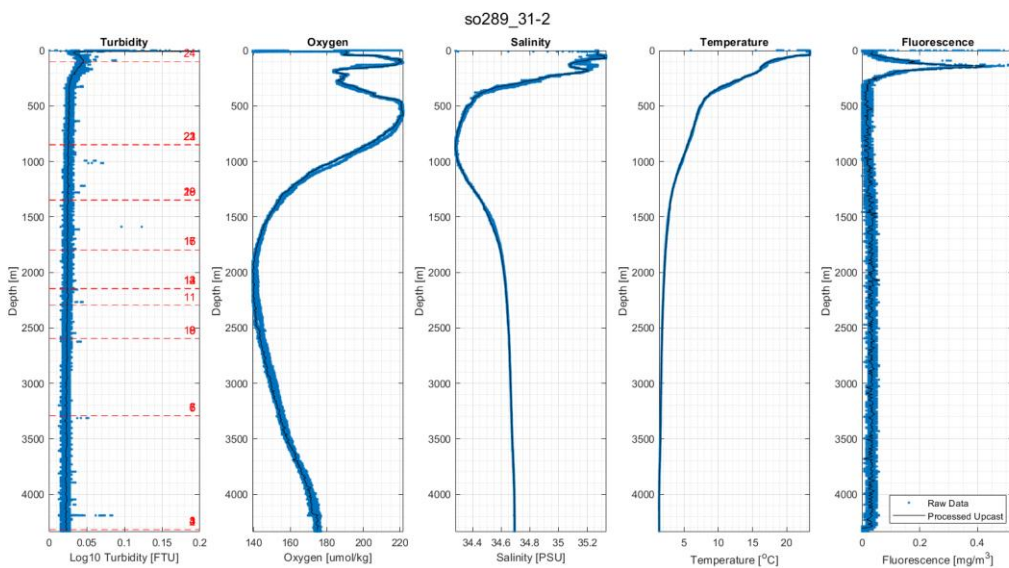


Fig. 12.40 Station 31-2's cast data, showing the raw down and upcast data in blue, along with the processed upcast data in black, for the turbidity, oxygen, salinity, temperature, and fluorescence data from the SS-CTD. Bottles were fired at the depths indicated with a red dotted line in the turbidity plot.

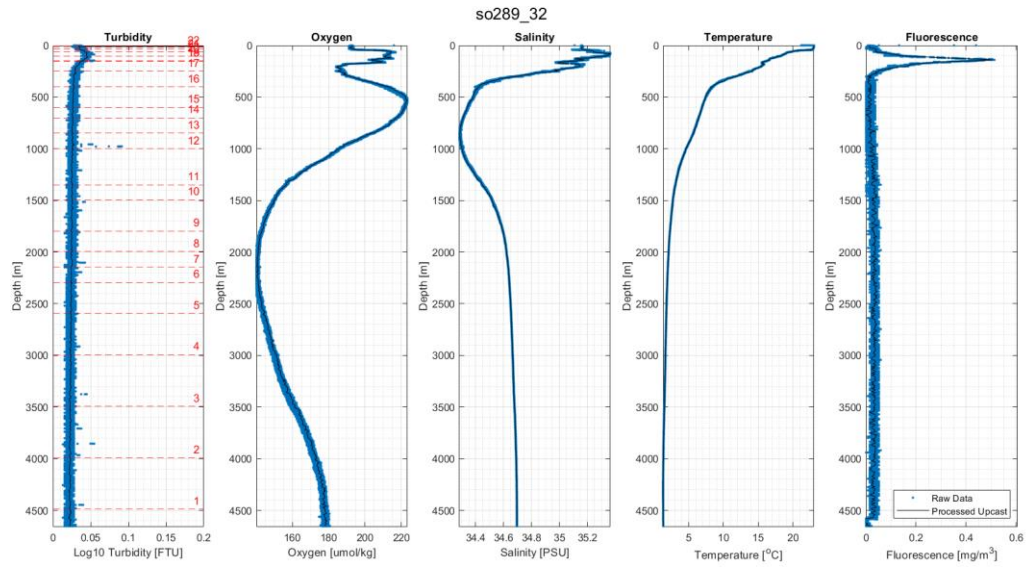


Fig. 12.41 Station 32's cast data, showing the raw down and upcast data in blue, along with the processed upcast data in black, for the turbidity, oxygen, salinity, temperature, and fluorescence data from the SS-CTD. Bottles were fired at the depths indicated with a red dotted line in the turbidity plot.

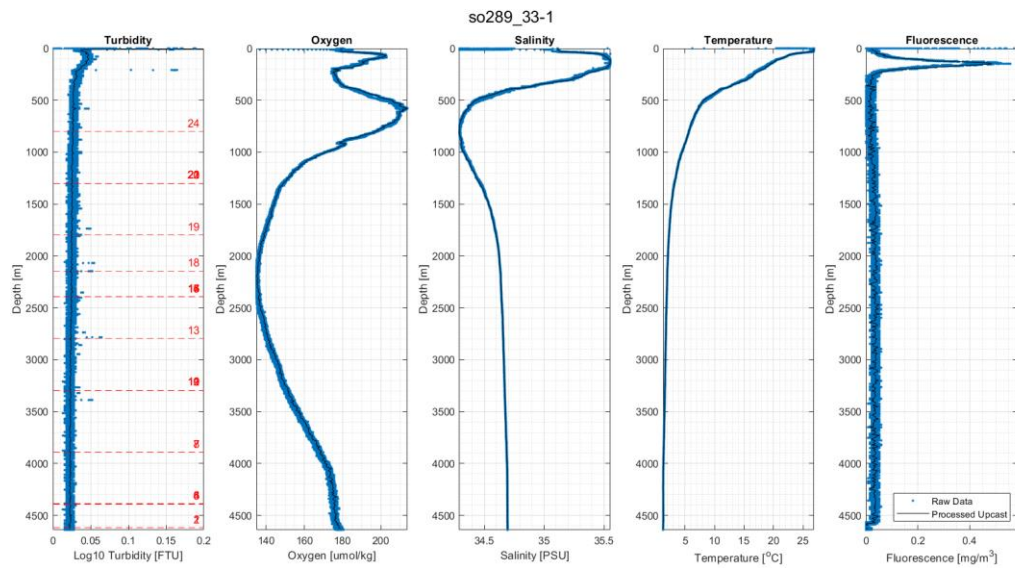


Fig. 12.42 Station 33-1's cast data, showing the raw down and upcast data in blue, along with the processed upcast data in black, for the turbidity, oxygen, salinity, temperature, and fluorescence data from the SS-CTD. Bottles were fired at the depths indicated with a red dotted line in the turbidity plot.

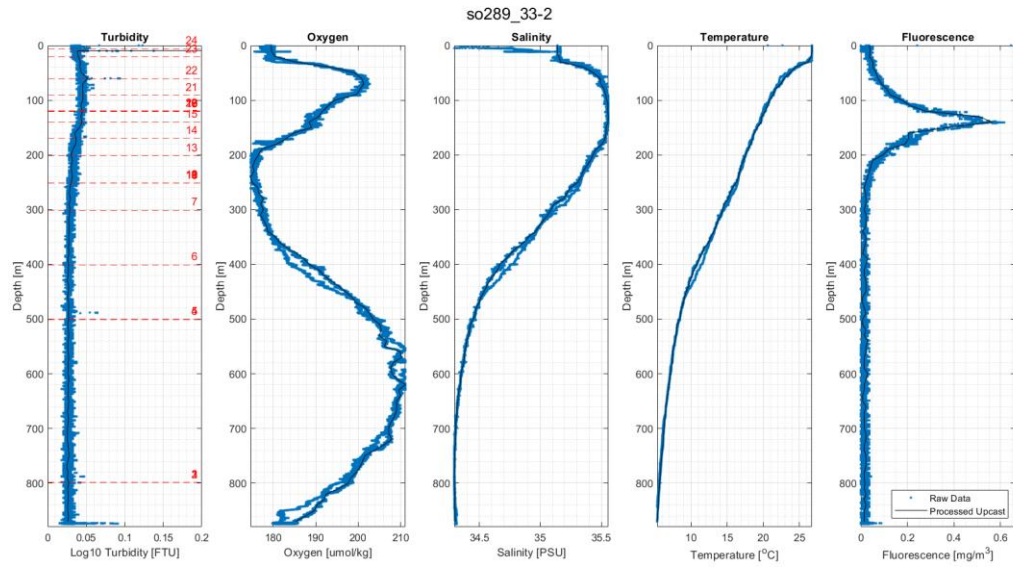


Fig. 12.43 Station 33-2's cast data, showing the raw down and upcast data in blue, along with the processed upcast data in black, for the turbidity, oxygen, salinity, temperature, and fluorescence data from the SS-CTD. Bottles were fired at the depths indicated with a red dotted line in the turbidity plot.

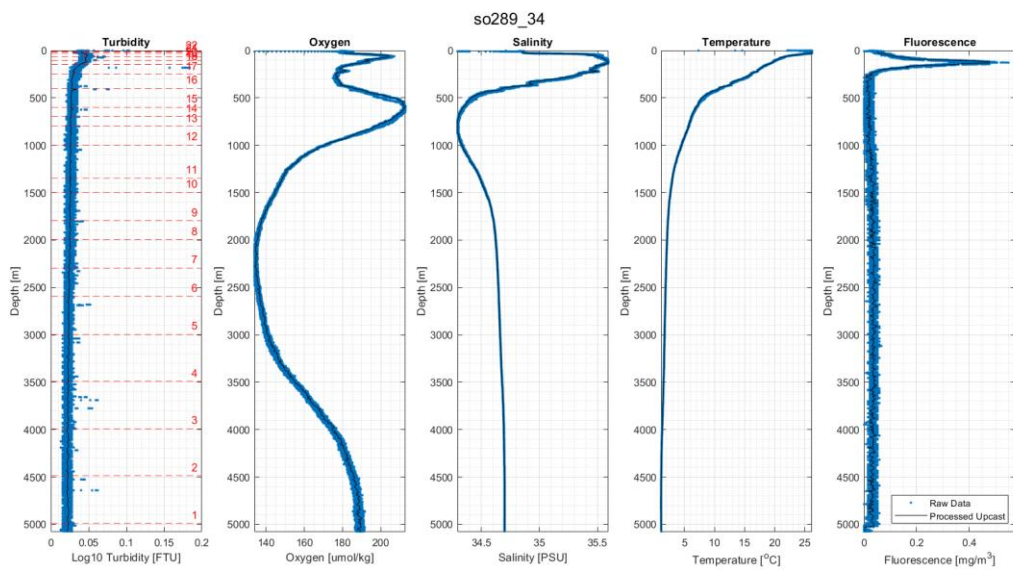


Fig. 12.44 Station 34's cast data, showing the raw down and upcast data in blue, along with the processed upcast data in black, for the turbidity, oxygen, salinity, temperature, and fluorescence data from the SS-CTD. Bottles were fired at the depths indicated with a red dotted line in the turbidity plot.

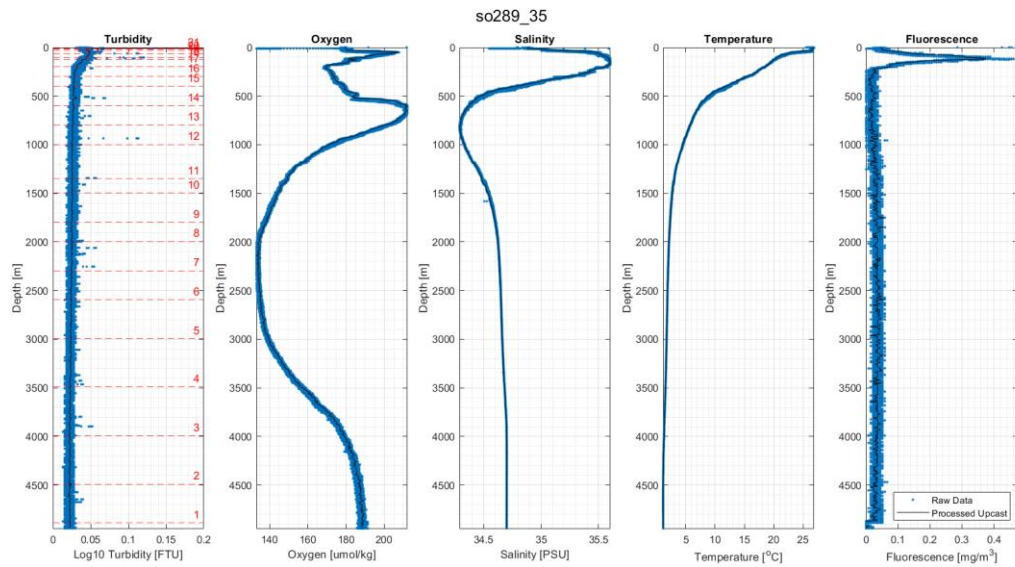


Fig. 12.45 Station 35's cast data, showing the raw down and upcast data in blue, along with the processed upcast data in black, for the turbidity, oxygen, salinity, temperature, and fluorescence data from the SS-CTD. Bottles were fired at the depths indicated with a red dotted line in the turbidity plot.

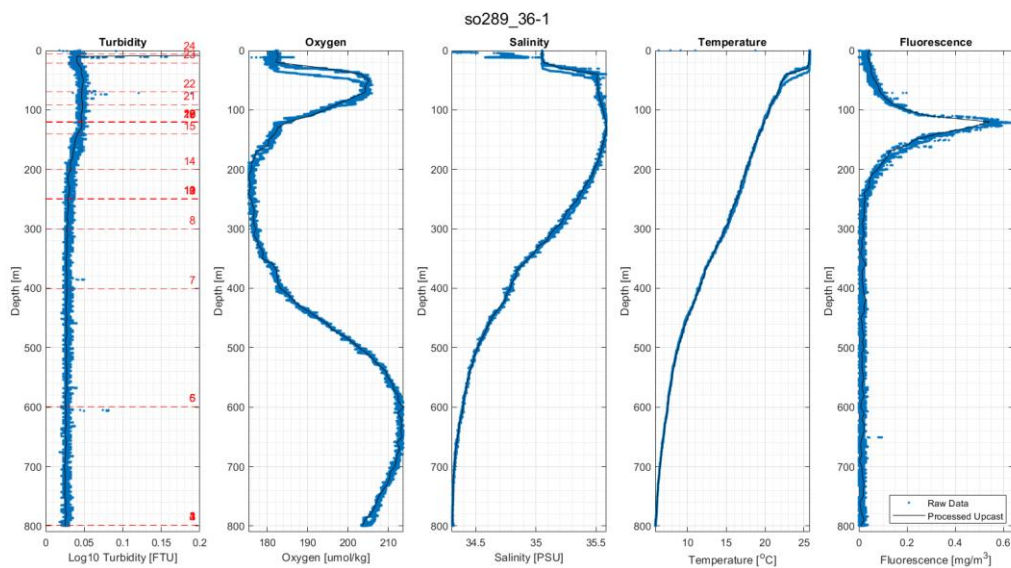


Fig. 12.46 Station 36-1's cast data, showing the raw down and upcast data in blue, along with the processed upcast data in black, for the turbidity, oxygen, salinity, temperature, and fluorescence data from the SS-CTD. Bottles were fired at the depths indicated with a red dotted line in the turbidity plot.

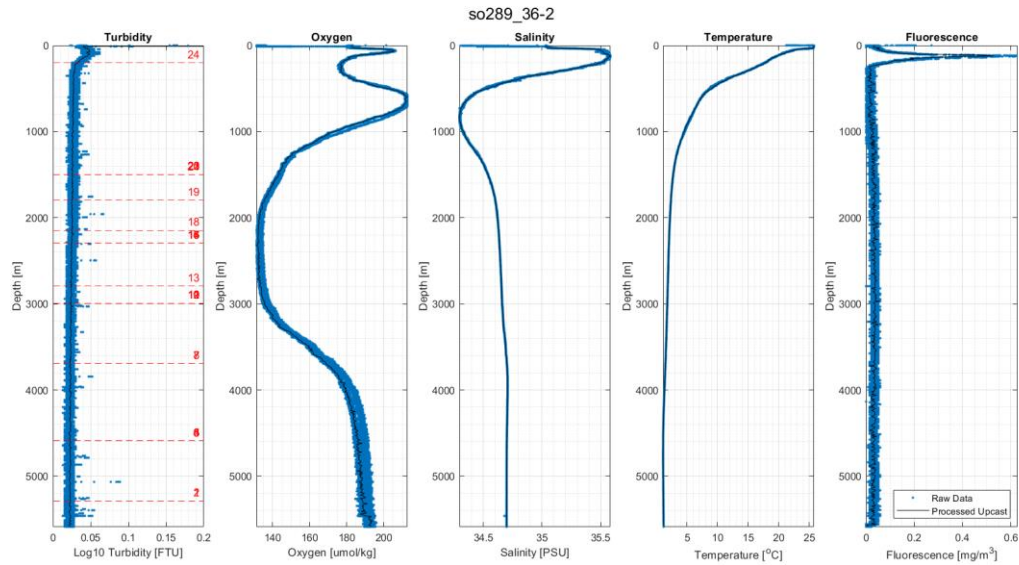


Fig. 12.47 Station 36-2's cast data, showing the raw down and upcast data in blue, along with the processed upcast data in black, for the turbidity, oxygen, salinity, temperature, and fluorescence data from the SS-CTD. Bottles were fired at the depths indicated with a red dotted line in the turbidity plot.

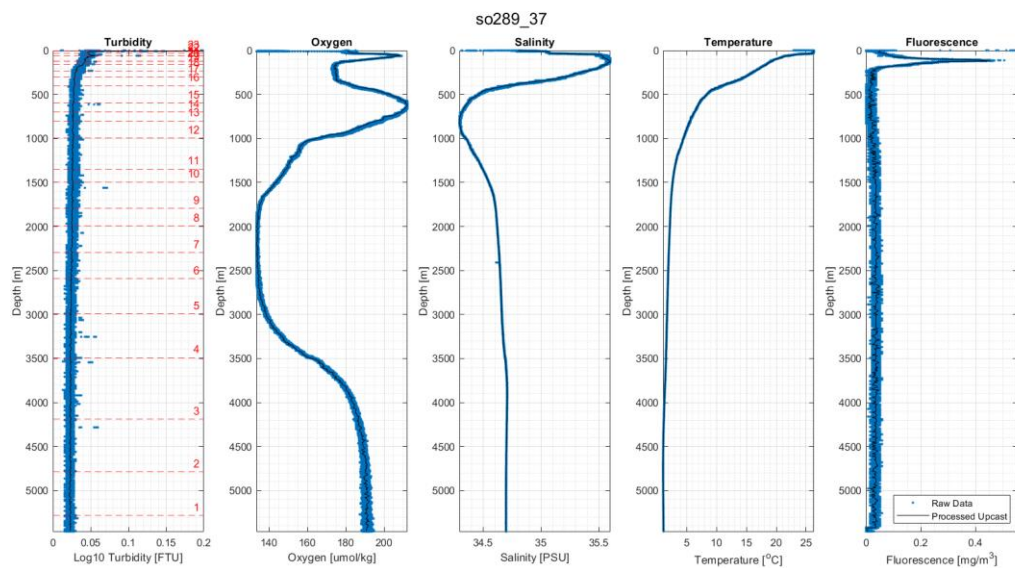


Fig. 12.48 Station 37's cast data, showing the raw down and upcast data in blue, along with the processed upcast data in black, for the turbidity, oxygen, salinity, temperature, and fluorescence data from the SS-CTD. Bottles were fired at the depths indicated with a red dotted line in the turbidity plot.

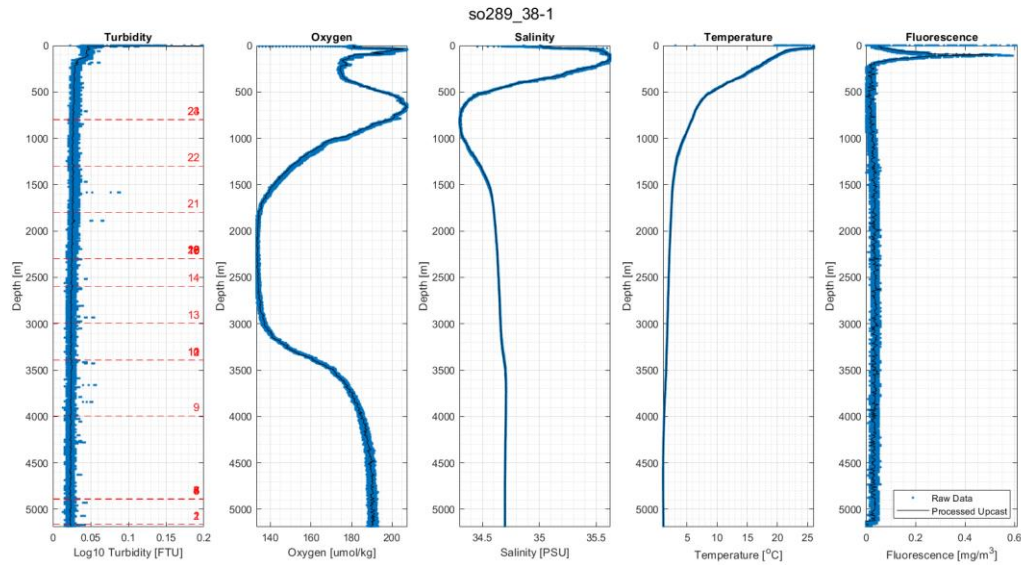


Fig. 12.49 Station 38-1's cast data, showing the raw down and upcast data in blue, along with the processed upcast data in black, for the turbidity, oxygen, salinity, temperature, and fluorescence data from the SS-CTD. Bottles were fired at the depths indicated with a red dotted line in the turbidity plot.

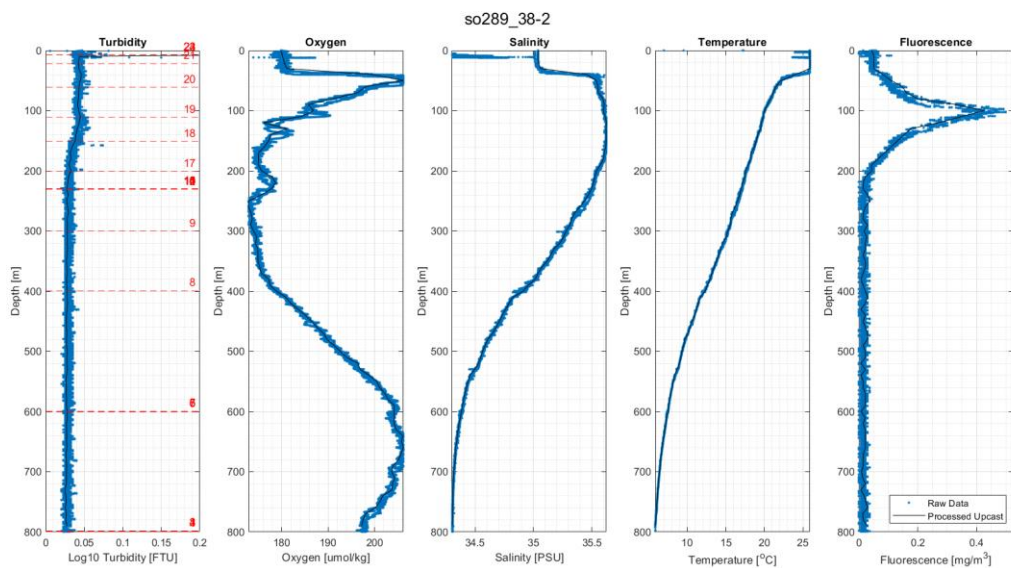


Fig. 12.50 Station 38-2's cast data, showing the raw down and upcast data in blue, along with the processed upcast data in black, for the turbidity, oxygen, salinity, temperature, and fluorescence data from the SS-CTD. Bottles were fired at the depths indicated with a red dotted line in the turbidity plot.

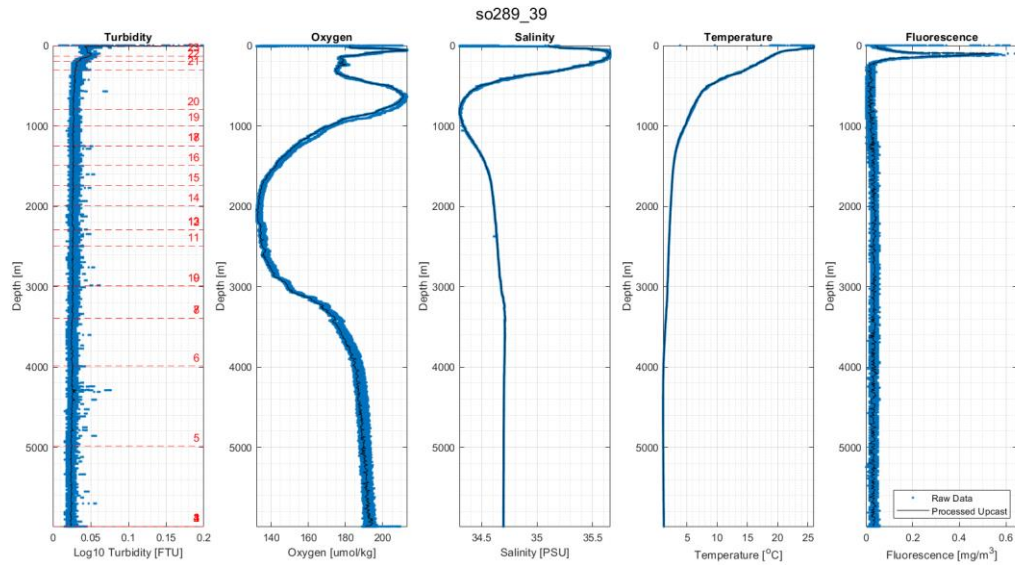


Fig. 12.51 Station 39's cast data, showing the raw down and upcast data in blue, along with the processed upcast data in black, for the turbidity, oxygen, salinity, temperature, and fluorescence data from the SS-CTD. Bottles were fired at the depths indicated with a red dotted line in the turbidity plot.

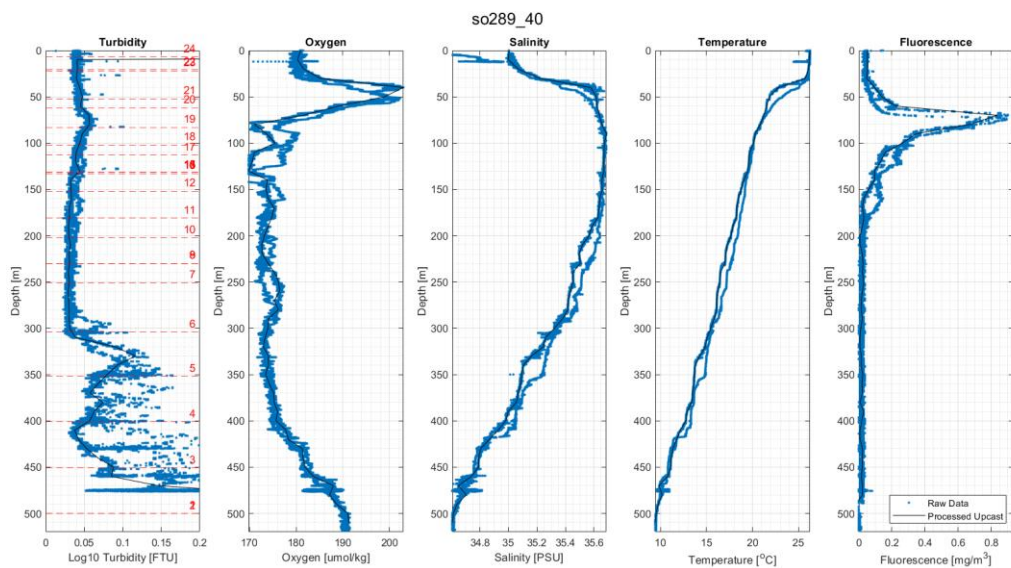


Fig. 12.52 Station 40's cast data, showing the raw down and upcast data in blue, along with the processed upcast data in black, for the turbidity, oxygen, salinity, temperature, and fluorescence data from the SS-CTD. Bottles were fired at the depths indicated with a red dotted line in the turbidity plot.

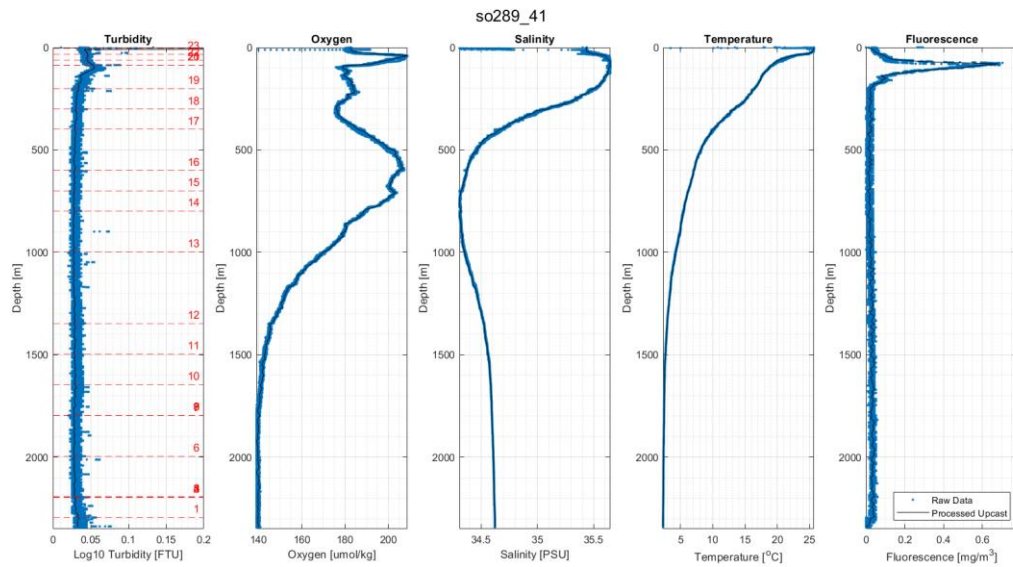


Fig. 12.53 Station 41's cast data, showing the raw down and upcast data in blue, along with the processed upcast data in black, for the turbidity, oxygen, salinity, temperature, and fluorescence data from the SS-CTD. Bottles were fired at the depths indicated with a red dotted line in the turbidity plot.

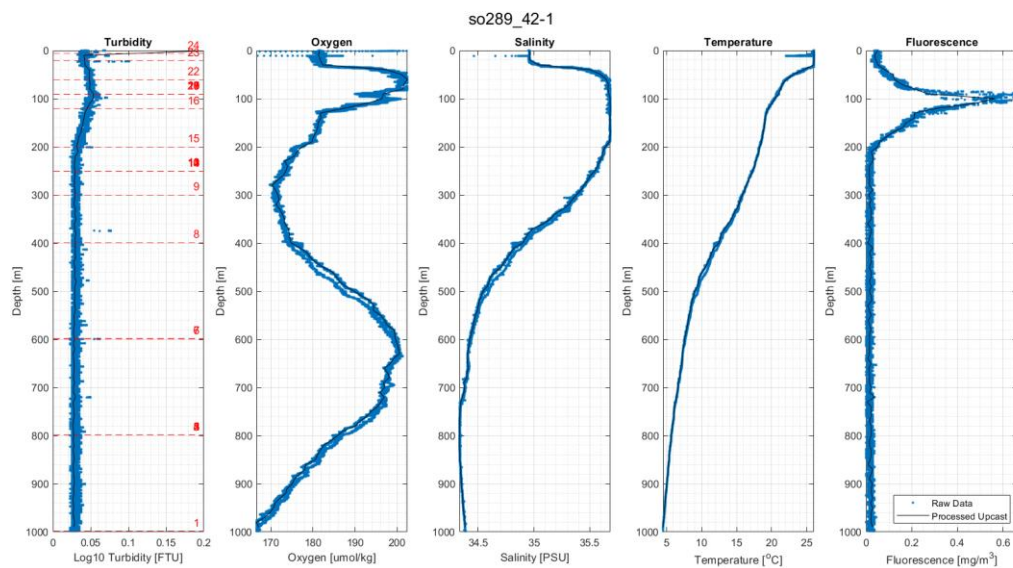


Fig. 12.54 Station 42-1's cast data, showing the raw down and upcast data in blue, along with the processed upcast data in black, for the turbidity, oxygen, salinity, temperature, and fluorescence data from the SS-CTD. Bottles were fired at the depths indicated with a red dotted line in the turbidity plot.

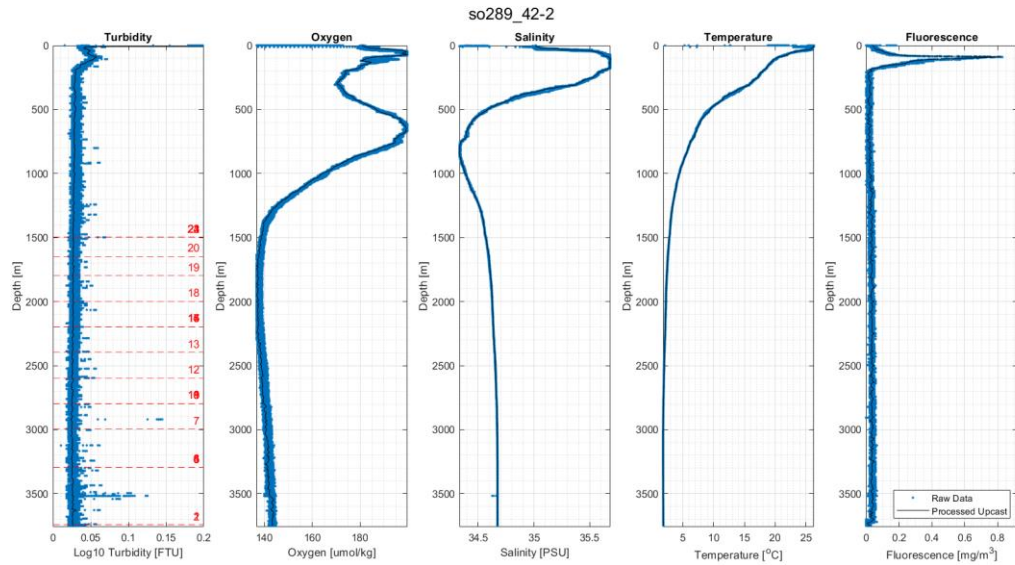


Fig. 12.55 Station 42-2's cast data, showing the raw down and upcast data in blue, along with the processed upcast data in black, for the turbidity, oxygen, salinity, temperature, and fluorescence data from the SS-CTD. Bottles were fired at the depths indicated with a red dotted line in the turbidity plot.

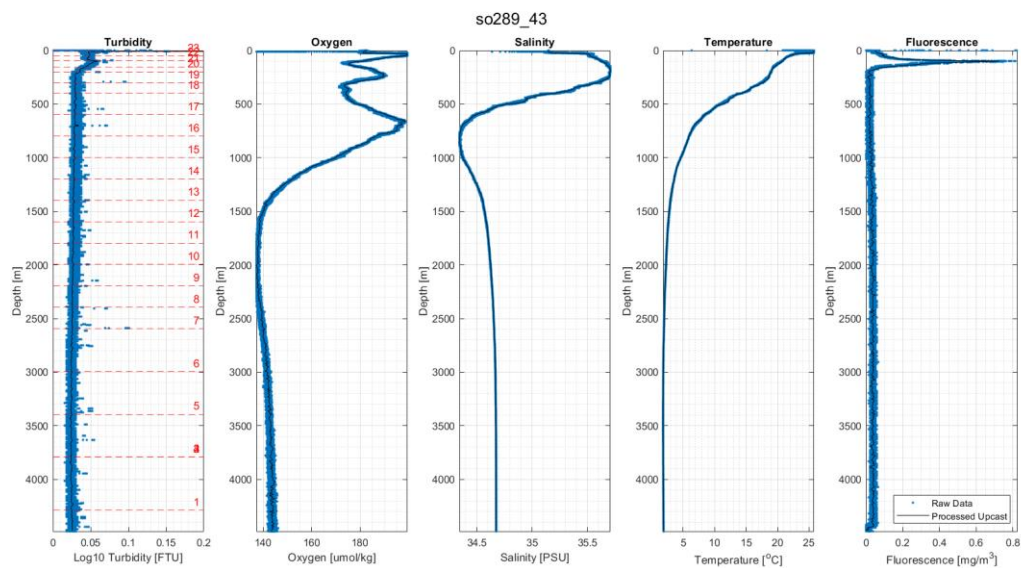


Fig. 12.56 Station 43's cast data, showing the raw down and upcast data in blue, along with the processed upcast data in black, for the turbidity, oxygen, salinity, temperature, and fluorescence data from the SS-CTD. Bottles were fired at the depths indicated with a red dotted line in the turbidity plot.

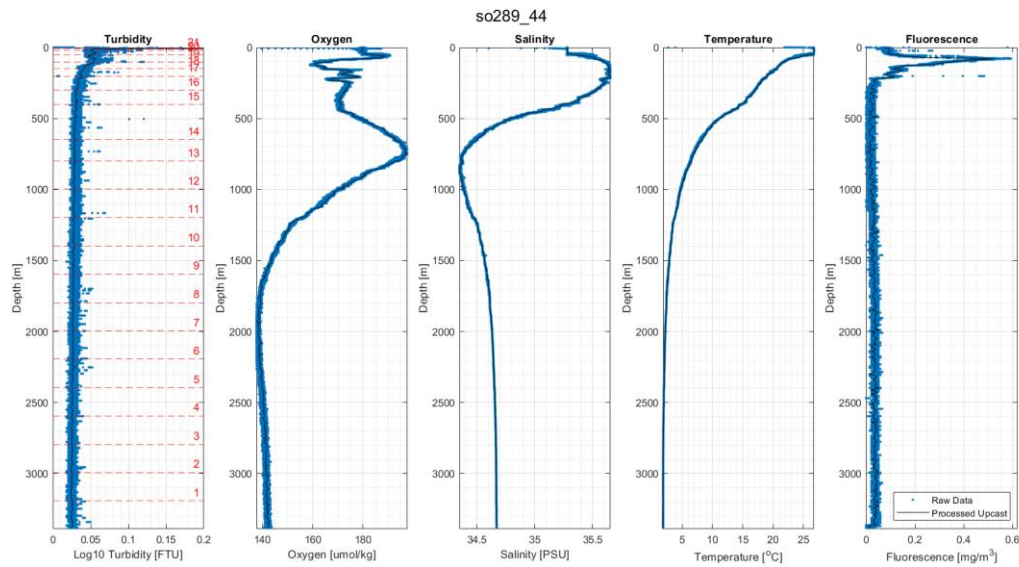


Fig. 12.57 Station 44's cast data, showing the raw down and upcast data in blue, along with the processed upcast data in black, for the turbidity, oxygen, salinity, temperature, and fluorescence data from the SS-CTD. Bottles were fired at the depths indicated with a red dotted line in the turbidity plot.

12.2 UVP data (C. Galley)

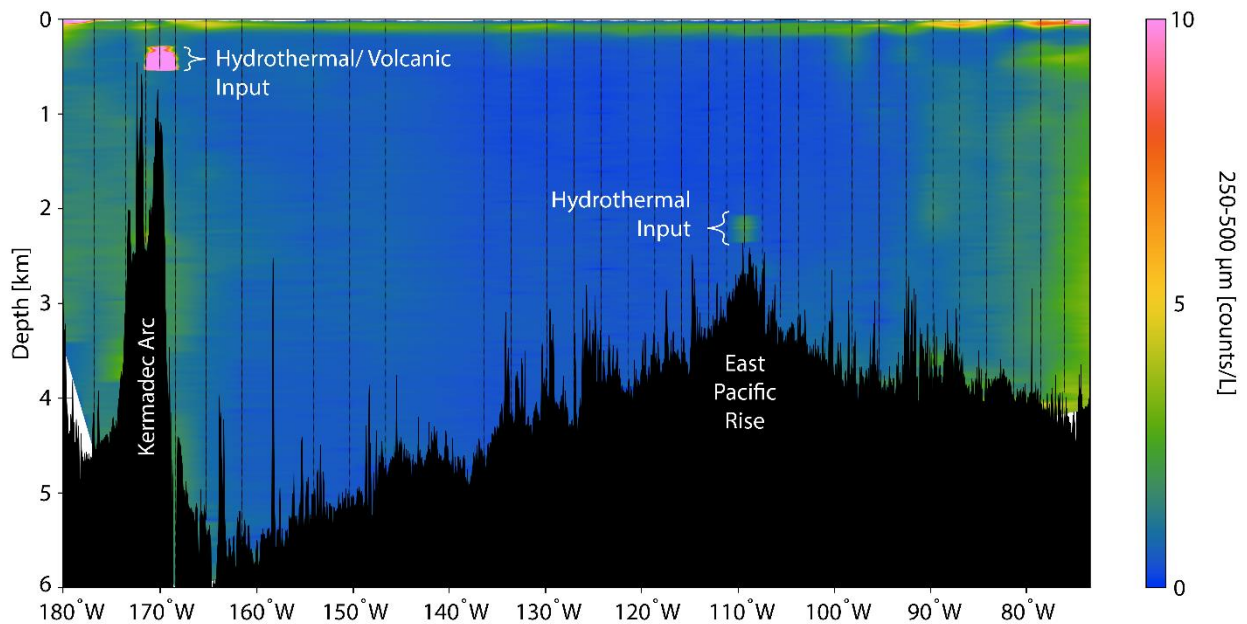


Fig. 12.58 UVP profile for 125-250 μm particle density.

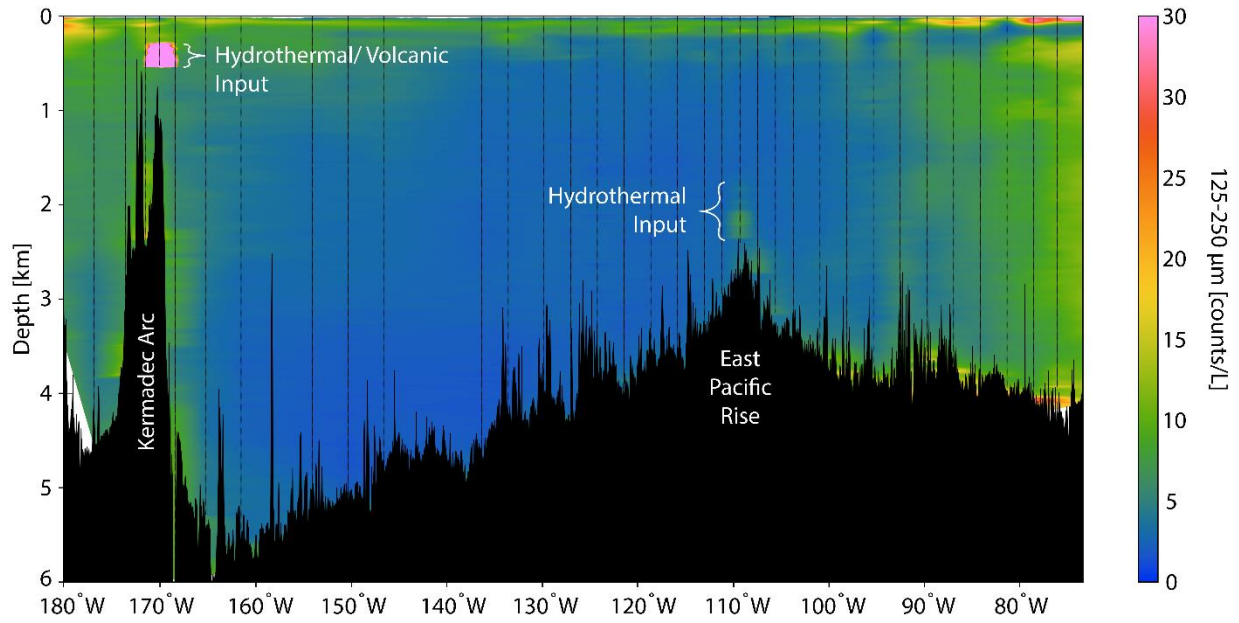


Fig. 12.59 UVP profile for 250-500 µm particle density.

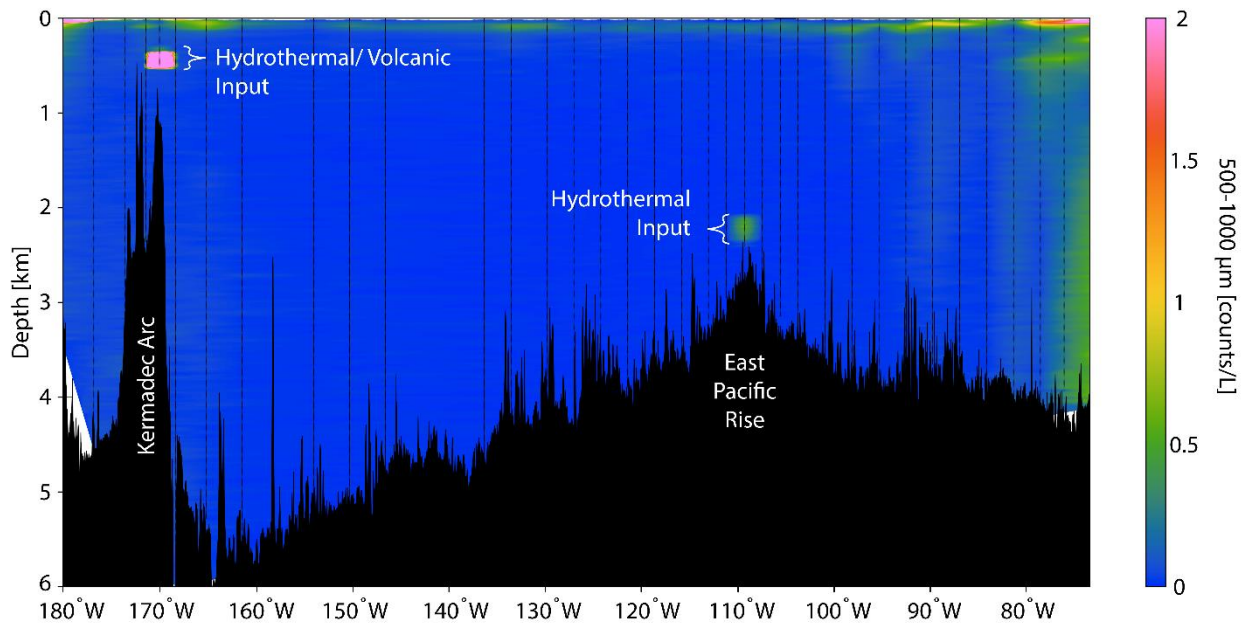


Fig. 12.60 UVP profile for 500-1000 µm particle density.

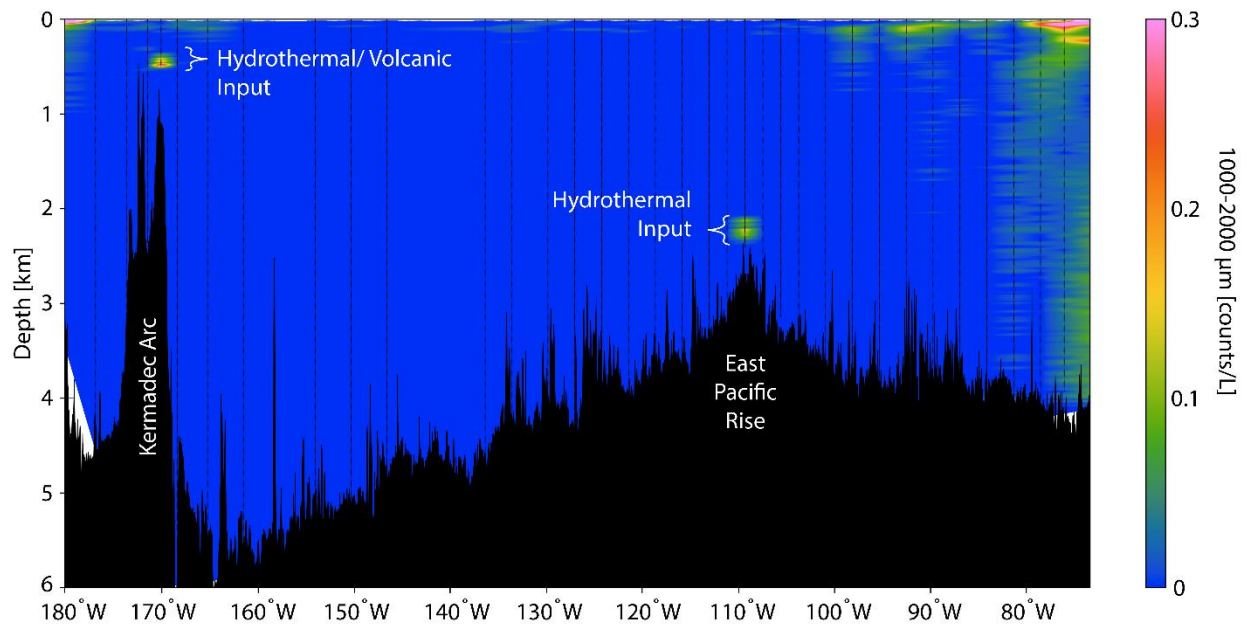


Fig. 12.61 UVP profile for 1000-2000 μm particle density.

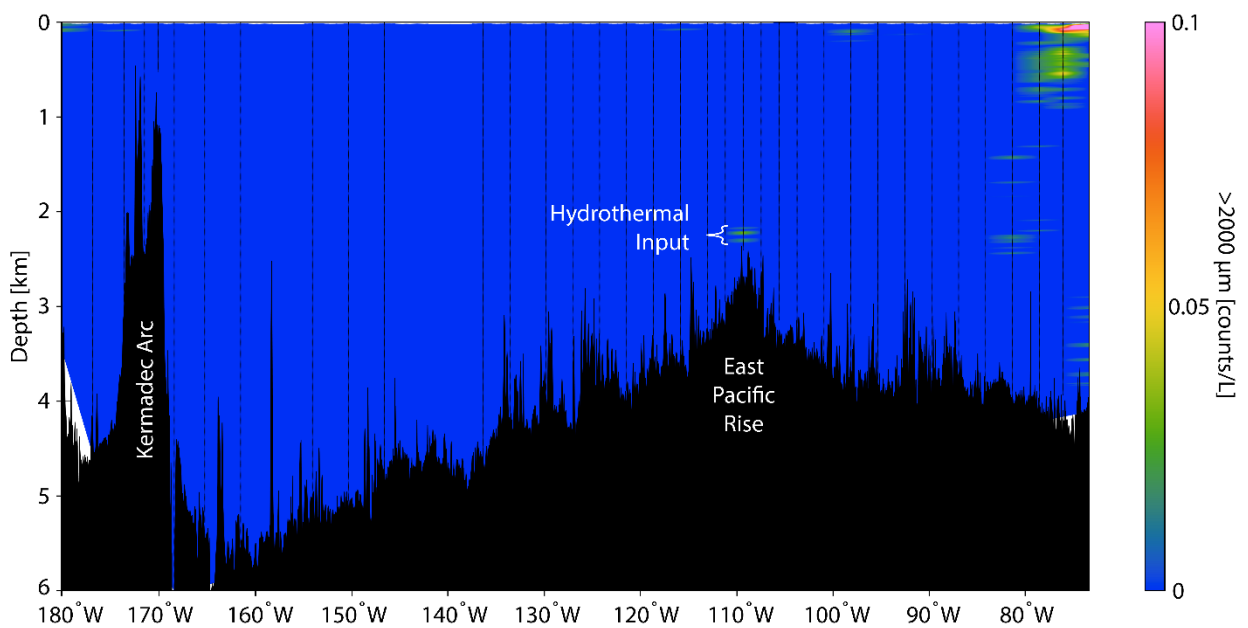


Fig. 12.62 UVP profile for $>2000 \mu\text{m}$ particle density.

12.3 Phytoplankton experiments

(Z. Yuan, H. Liu, J. Tammen, Z. Wen, J. LaRoche, T. Browning)

Table 12.1 Nitrogen fixation experiments dates and times

Experiment number	UTC Date	UTC Time
1	25.02.2022	17:05
2	28.02.2022	22:00
3	03.03.2022	20:11
4	07.03.2022	04:40
5	10.03.2022	21:28

6	14.03.2022	22:26
7	18.03.2022	22:50
8	24.03.2022	00:14
9	27.03.2022	08:50
10	30.03.2022	06:02
11	01.04.2022	01:55

Table 12.2 Nutrient enrichment bioassay experiments dates and times

Experiment number	UTC Date	UTC Time
1	26.02.2022	01:30
2	01.03.2022	02:20
3	04.03.2022	01:47
4	07.03.2022	02:03
5	10.03.2022	05:09
6	14.03.2022	04:58
7	17.03.2022	04:46
8	19.03.2022	01:49
9	24.03.2022	06:02
10	27.03.2022	06:42
11	30.03.2022	06:42
12	01.04.2022	04:01

Table 12.3 Dilution experiments dates and times

Experiment number	UTC Date	UTC Time
1	25.02.2022	23:01
2	27.02.2022	19:20
3	02.03.2022	00:38
4	04.03.2022	00:08
5	06.03.2022	15:10
6	10.03.2022	02:28
7	15.03.2022	03:36
8	18.03.2022	23:52
9	24.03.2022	02:23
10	28.03.2022	05:05
11	31.03.2022	04:55
12	02.04.2022	04:16

Table 12.4 List of surface incubation sampling dates and times

Experiment number	UTC Date	UTC Time
1	26.02.2022	02:44
2	27.02.2022	02:16
3	01.03.2022	03:14
4	02.03.2022	04:58
5	03.03.2022	05:19
6	05.03.2022	05:18
7	06.03.2022	06:03
8	08.03.2022	05:49

9	09.03.2022	05:26
10	10.03.2022	06:57
11	11.03.2022	05:35
12	14.03.2022	07:46
13	15.03.2022	07:14
14	16.03.2022	09:07
15	18.03.2022	08:44
16	24.03.2022	09:53
17	26.03.2022	10:33
18	27.03.2022	10:29
19	29.03.2022	11:35
20	01.04.2022	11:02
21	02.04.2022	10:46

Table 12.5 List of DCM incubation sampling dates and times

Experiment number	UTC Date	UTC Time
1	27.02.2022	20:40
2	01.03.2022	13:50
3	03.03.2022	09:51
4	04.03.2022	23:40
5	06.03.2022	20:04
6	08.03.2022	23:27
7	10.03.2022	15:42
8	13.03.2022	05:16
9	15.03.2022	18:05
10	18.03.2022	20:08
11	23.03.2022	20:40
12	25.03.2022	02:01
13	26.03.2022	04:19
14	28.03.2022	09:07
15	30.03.2022	10:33
16	31.03.2022	20:19

Table 12.6 Nickel addition bioassay experiment sampling dates and times

Experiment number	UTC Date	UTC Time
1	25.02.2022	16:30
2	03.03.2022	17:05
3	10.03.2022	20:35
4	18.03.2022	21:50
5	23.03.2022	23:09
6	30.03.2022	04:56

12.4 Samples collected for assessment of marine aggregates-associated bacterial and diversity of extracellular vesicles

(E. Fadeev)

Table 12.7 Seawater samples for microbial analysis, collected using in-situ pump and Niskin bottles.

Station ID	Depths (m)	Sampling method
SO289_5	700	In-situ pump
SO289_6	25, 540	Niskin
SO289_8	700	In-situ pump
SO289_9	50, 700	Niskin
SO289_12	700	In-situ pump
SO289_13	50, 700	Niskin
SO289_16	700	In-situ pump
SO289_17	100, 700	Niskin
SO289_19	700	In-situ pump
SO289_20	100, 750	Niskin
SO289_21	700	In-situ pump
SO289_23	150, 750	Niskin
SO289_24	700	In-situ pump
SO289_28	700	In-situ pump
SO289_31	700	In-situ pump
SO289_32	150, 700	Niskin
SO289_33	700	In-situ pump
SO289_34	150, 700	Niskin
SO289_36	700	In-situ pump
SO289_40	200	In-situ pump
SO289_41	85, 700	Niskin
SO289_42	700	In-situ pump
SO289_43	150, 700	Niskin

Table 12.8 EVs samples for quantification and molecular analysis, collected using on-board membrane pump.

StationID	Additional measurements
SO289_1	nutrients, DOC

SO289_3	-
SO289_6	nutrients, DOC
SO289_9	nutrients, DOC
SO289_12	-
SO289_13	nutrients, DOC
SO289_16	-
SO289_17	nutrients, DOC
SO289_20	nutrients, DOC
SO289_23	nutrients
SO289_27	nutrients, DOC
SO289_30	-
SO289_32	nutrients, DOC
SO289_33	-
SO289_34	nutrients, DOC
SO289_37	-
SO289_39	nutrients, DOC
SO289_41	nutrients, DOC
SO289_43	-
SO289_44	-

12.5 In-situ pump deployments and samples for natural level radiogenic elements

(D. Köhler, L.H. Viera, P. Battermann, S. Hamisch)

Table 12.9 ISP deployments. P = PES filter, Q = QMA filter

Station	5	8	12	16	19	22	24
Depth (m)	20 (Q/P)	20 (Q/P)	20 (Q/P)	20 (Q/P)	20 (Q/P)	20 (Q)	20 (Q)
	50 (Q/P)	60 (Q/P)	60 (Q)	60 (Q)	100 (Q)	150 (Q/P)	175 (Q/P)
	100 (Q)	100 (Q)	100 (Q/P)	100 (Q/P)	150 (Q/P)	200 (Q)	230 (Q)
	120 (P)	150 (P)	150 (P)	150 (P)	200 (Q/P)	300 (Q/P)	300 (Q/P)
	200 (Q/P)	200 (Q/P)	200 (Q/P)	200 (Q/P)	300 (Q)	600 (P)	600 (P)
	300 (Q)	300 (Q)	300 (Q)	300 (Q)	400 (P)	700 (PC)	700 (PC)
	500 (P)	400 (P)	350 (P)	350 (P)	600 (P)	1500 (P)	1000 (P)
	700 (PC)	600 (P)	550 (P)	550 (P)	700 (PC)	2000 (P)	1350 (P)
	900 (P)	700 (PC)	700 (PC)	700 (PC)	1100 (P)	2100 (Q/P)	2000 (P)
		800 (P)	800 (P)	800 (P)	1700 (P)	2150 (P)	2150 (Q/P)

		1100 (P)	1100 (P)	1100 (P)	2300 (P)	2300 (P)	2300 (P)
--	--	----------	----------	----------	----------	----------	----------

Station	28	31	33	36	39	40	42
Depth (m)	20 (Q)	20 (Q)	20 (Q)	20 (Q)	5975 (P)	20 (Q/P)	20 (Q)
	150 (Q/P)	100 (Q/P)	60 (Q/P)	70 (Q/P)		50 (Q)	60 (Q/P)
	200 (Q)	150 (Q/P)	90 (Q)	120 (Q/P)		80 (Q/P)	90 (Q/P)
	300 (Q/P)	200 (Q/P)	120 (Q/P)	200 (Q/P)		130 (Q/P)	200 (Q/P)
	600 (P)	300 (Q)	140 (Q)	300 (Q)		175 (P)	300 (Q)
	700 (PC)	400 (P)	170 (Q)	400 (P)		200 (PC)	400 (P)
	1000 (P)	600 (P)	200 (Q/P)	600 (P)		250 (P)	600 (P)
	1500 (P)	700 (PC)	250 (Q)	700 (PC)		300 (Q)	700 (PC)
	2000 (P)	850 (P)	300 (Q)	800 (P)		450 (P)	1000 (P)
	2150 (Q/P)	1350 (P)	400 (Q)	1500 (P)			1650 (P)
	2300 (P)	2300 (P)	700 (PC)				

Table 12.10 Samples collected from the In-situ pumps for Ra-228 and Ra-226 analysis.

	Station 5	Station 8	Station 12	Station 16	Station 19	Station 22	Station 24
Depth (m)	100	50	60	60	100	20	230
	300	100	150	150	300	200	600
	500	150	300	300	400	600	1000
	900	300	350	350	600	1500	1350
		400	550	550	1100	2000	2000
		600	800	800	1700	2200	2300
		800	1100	1100	2300	2300	
		1100					
	Station 28	Station 31	Station 33	Station 36	Station 39	Station 40	Station 42
Depth (m)	150	150	120	120	5950	100	90
	600	300	250	300		175	300
	1000	400	300	400		250	400
	1500	600		600		300	600
	2000	850		800		450	1000
	2300	1350		1500			1650
		2300					

Table 12.11 Pa/Th samples collected

Station	5	8	12	16	19	22	24	28	33	36	42
---------	---	---	----	----	----	----	----	----	----	----	----

Depth (m)	5	5	5	5	5	5	5	5	5	5	5
	100	100	100	100	100	100	100	100	100	120	90
	200	400	350	350	350	350	300	300	250	200/250	250
	400	600	550	600	750	750	850	850	800	800	800
	600	1100	1250	1350	1350	1350	1350	1350	1300	1500	1500
	1500	2500	2600	2600	2500	2000	2000	2000	2400	2300	2200
	2000	3500	2900	2900	2700	2100	2150	2150	3300	3000	2800
	2185	3830	3660	3600	3000	2300	3300	3500	4400	4600	3300
	2425										

Table 12.12 Samples of dissolved ^{234}Th and ^{238}U were taken according to the table below. Preliminary activity values (beta counts per minute) are included.

Station	Depth	Label ID	volume ^{238}U [mL]	volume ^{234}Th [mL]	beta [cpm]	annotation
Station 05	400	40093	12	4000	1.04	
Station 05	300	40099	12	4000	1.43	
Station 05	200	40104	12	4000	1.84	OMZ
Station 05	150	40105	12	4000	1.85	
Station 05	100	40108	12	4000	1.62	
Station 05	50	40111	12	4000	3.13	chlorophyll max.
Station 05	30	40112	12	4000	2.54	chlorophyll max.
Station 05	15	40113	12	4000	2.18	
Station 05	5	40119	12	4000	2.29	
Station 08	400	40194	12	4000	1.62	
Station 08	300	40197	12	4000	0.93	
Station 08	200	40200	12	4000	1.42	OMZ
Station 08	150	40201	12	4000	1.4	
Station 08	100	40202	12	4000	2.47	
Station 08	60	40207	12	4000	1.42	chlorophyll max.
Station 08	30	40208	12	4000	1.77	
Station 08	20	40209	12	4000	1.81	
Station 08	5	40215	12	4000	2.4	
Station 12	350	40318	12	4000	1.41	
Station 12	300	40321	12	4000	1.67	
Station 12	200	40324	12	4000	1.74	
Station 12	150	40325	12	4000	1.29	
Station 12	100	40326	12	4000	1.43	
Station 12	60	40331	12	4000	1.86	
Station 12	5	40333	12	4000	1.24	
Station 16	350	40438	12	4000	0.95	
Station 16	300	40441	12	4000	1.29	
Station 16	200	40444	12	4000	1.43	
Station 16	150	40445	12	4000	1.25	
Station 16	100	40446	12	4000	1.56	
Station 16	60	40451	12	4000	1.62	
Station 16	20	40452	12	4000	1.35	

Station 16	5	40453	12	4000	1.4	
Station 19	400	40531	12	4000	1.35	
Station 19	350	40534	12	4000	1.29	
Station 19	300	40537	12	4000	1.68	
Station 19	200	40540	12	4000	1.16	
Station 19	150	40541	12	4000	1.44	
Station 19	100	40542	12	4000	1.78	
Station 19	60	40547	12	4000	1.88	
Station 19	20	40548	12	4000	1.72	
Station 19	5	40549	12	4000	1.52	
Station 22	2300	40578	12	4000	1.13	below turb. Max.
Station 22	2150	40579	12	4000	0.9	turb. Max.
Station 22	2100	40585	12	4000	1.05	turb. Max.
Station 22	2000	40588	12	4000	1.21	above turb. Max
Station 22	1500	40592	12	4000	1.02	
Station 22	300	40608	12	4000	1.39	
Station 22	200	40611	12	4000	1.11	
Station 22	150	40612	12	4000	1.47	chlorophyll max.
Station 22	100	40613	12	4000	1.61	
Station 22	60	40618	12	4000	1.69	
Station 22	20	40619	12	4000	1.37	
Station 22	5	40620	12	4000	1.98	
Station 24	3300	40649	12	4000	0.91	
Station 24	2300	40650	12	4000	0.79	
Station 24	2150	40656	12	4000	1.15	
Station 24	2000	40659	12	4000	1.12	
Station 24	1350	40663	12	4000	1.07	
Station 24	300	40678	12	4000	0.81	
Station 24	230	40679	12	4000	1.42	
Station 24	175	40680	12	4000	1.39	chlorophyll max.
Station 24	20	40687	12	4000	1.62	
Station 24	5	40688	12	4000	1.64	
Station 28	3500	40793	12	4000	1.14	
Station 28	2800	40794	12	4000	1.04	
Station 28	2300	40796	12	4000	2	
Station 28	2150	40801	12	4000	1.55	
Station 28	2000	40804	12	4000	1.24	
Station 28	300	40775	12	4000	1.28	
Station 28	200	40776	12	4000	1.32	
Station 28	150	40777	12	4000	1.49	chlorophyll max.
Station 28	20	40784	12	4000	2	
Station 28	5	40785	12	4000	1.78	
Station 31	600	40863	12	4000	1.03	
Station 31	400	40864	12	4000	1.32	
Station 31	300	40865	12	4000	1.22	
Station 31	250	40868	12	4000	0.95	
Station 31	200	40869	12	4000	1.17	
Station 31	150	40870	12	4000	1.2	chlorophyll max.
Station 31	100	40871	12	4000	1.43	

Station 31	60	40874	12	4000	1.6	
Station 31	5	40876	12	4000	1.79	
Station 33	400	40958	12	4000	1.06	
Station 33	300	40959	12	4000	1.89	
Station 33	250	40960	12	4000	1.71	
Station 33	170	40966	12	4000	1.32	
Station 33	140	40967	12	4000	1.22	
Station 33	120	40968	12	4000	1.76	chlorophyll max.
Station 33	90	40973	12	4000	1.75	
Station 33	60	40974	12	4000	2.05	
Station 33	20	40975	12	4000	1.56	
Station 33	5	40976	12	4000	2.01	
Station 36	1800	41067	12	4000	0.92	
Station 36	400	41031	12	4000	0.92	
Station 36	300	41032	12	4000	1.5	
Station 36	250	41033	12	4000	1.14	
Station 36	200	41072	12	4000	1.06	
Station 36	140	41039	12	4000	1.92	
Station 36	120	41040	12	4000	1.31	chlorophyll max.
Station 36	90	41045	12	4000	1.64	
Station 36	70	41046	12	4000	1.52	
Station 36	20	41047	12	4000	1.42	
Station 36	5	41048	12	4000	1.38	
Station 40	300	41174	12	4000	4.31	
Station 40	200	41178	12	4000	4.64	
Station 40	130	41184	12	4000	3.05	Ag filter
Station 40	130	41184	12	4000	4.82	QMA filter
Station 40	110	41185	12	4000	4.53	
Station 40	100	41186	12	4000	4.47	
Station 40	80	41187	12	4000	3.26	
Station 40	60	41188	12	4000	3.99	
Station 40	50	41189	12	4000	4.25	
Station 40	20	41190	12	4000	3.6	Ag filter
Station 40	20	41190	12	4000	4.67	QMA filter
Station 40	5	41192	12	4000	4.26	
Station 42	1000	41217	12	4000	4.11	
Station 42	300	41225	12	4000	4.29	
Station 42	200	41231	12	4000	4.44	
Station 42	120	41232	12	4000	4.48	
Station 42	90	41237	12	4000	4.4	chlorophyll max.
Station 42	60	41238	12	4000	4.25	
Station 42	20	41239	12	4000	3.54	
Station 42	5	41240	12	4000	4.33	

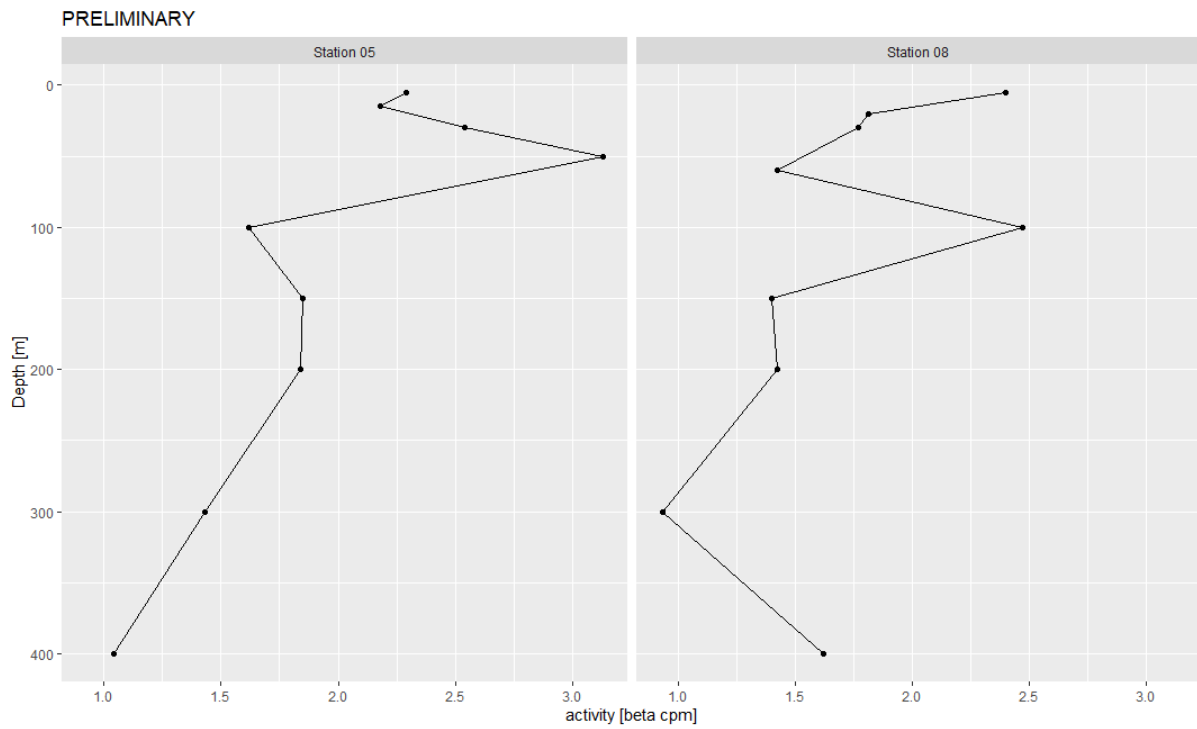


Fig. 12.63 Preliminary results for dissolved ^{234}Th activities [cpm].

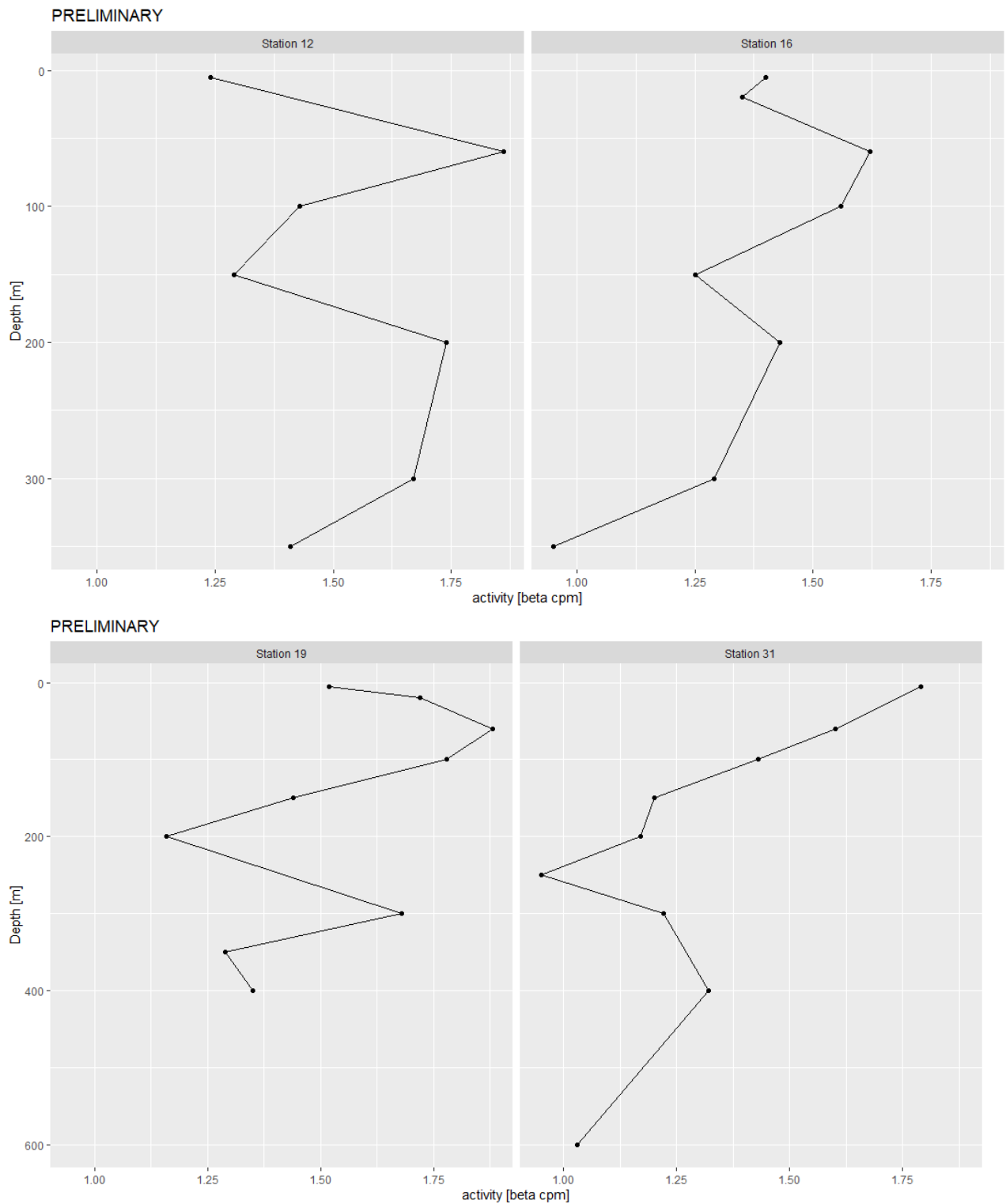


Fig. 12.64 Preliminary results for dissolved ^{234}Th activities [cpm].

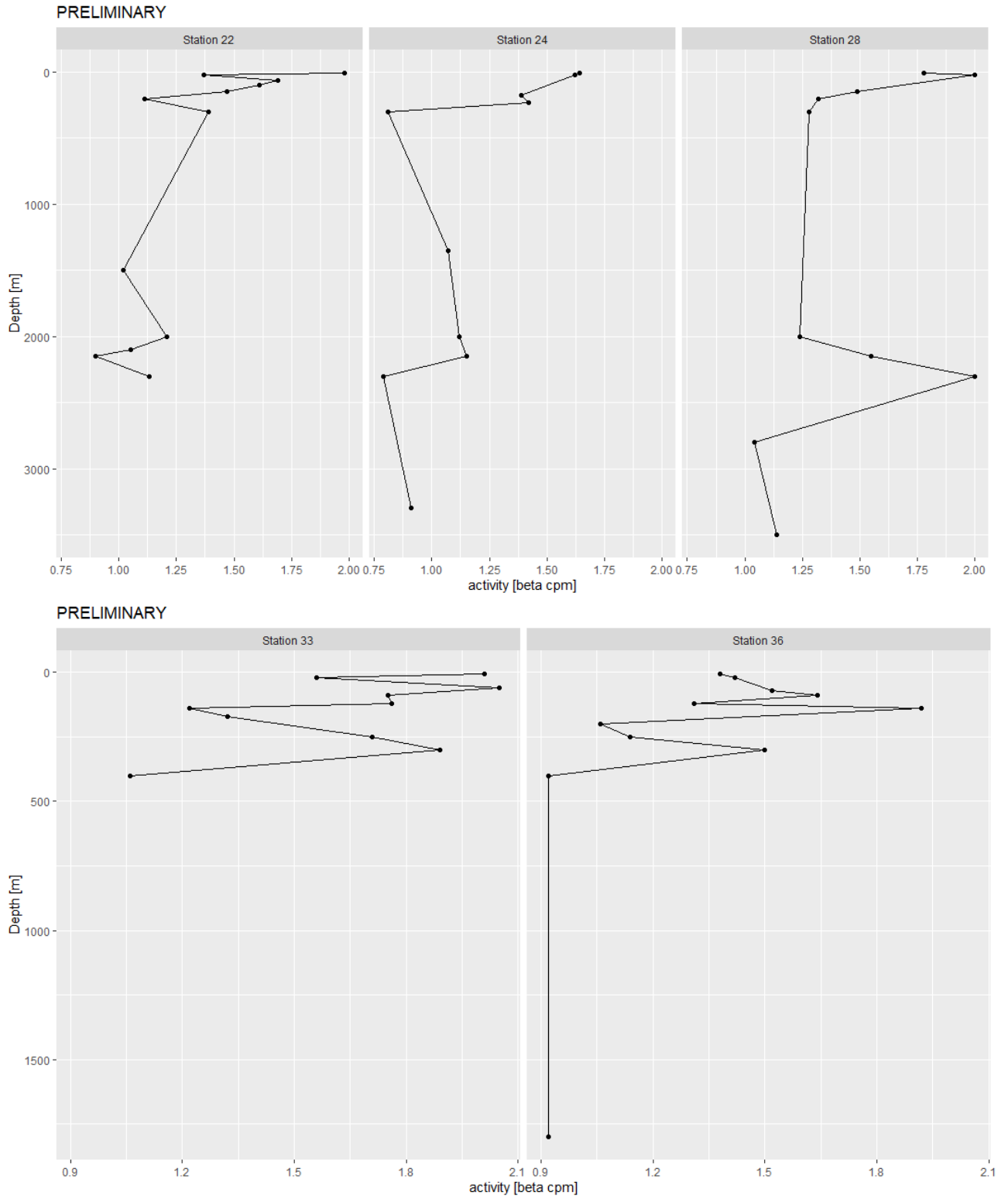


Fig. 12.65 Preliminary results for dissolved ^{234}Th activities [cpm].

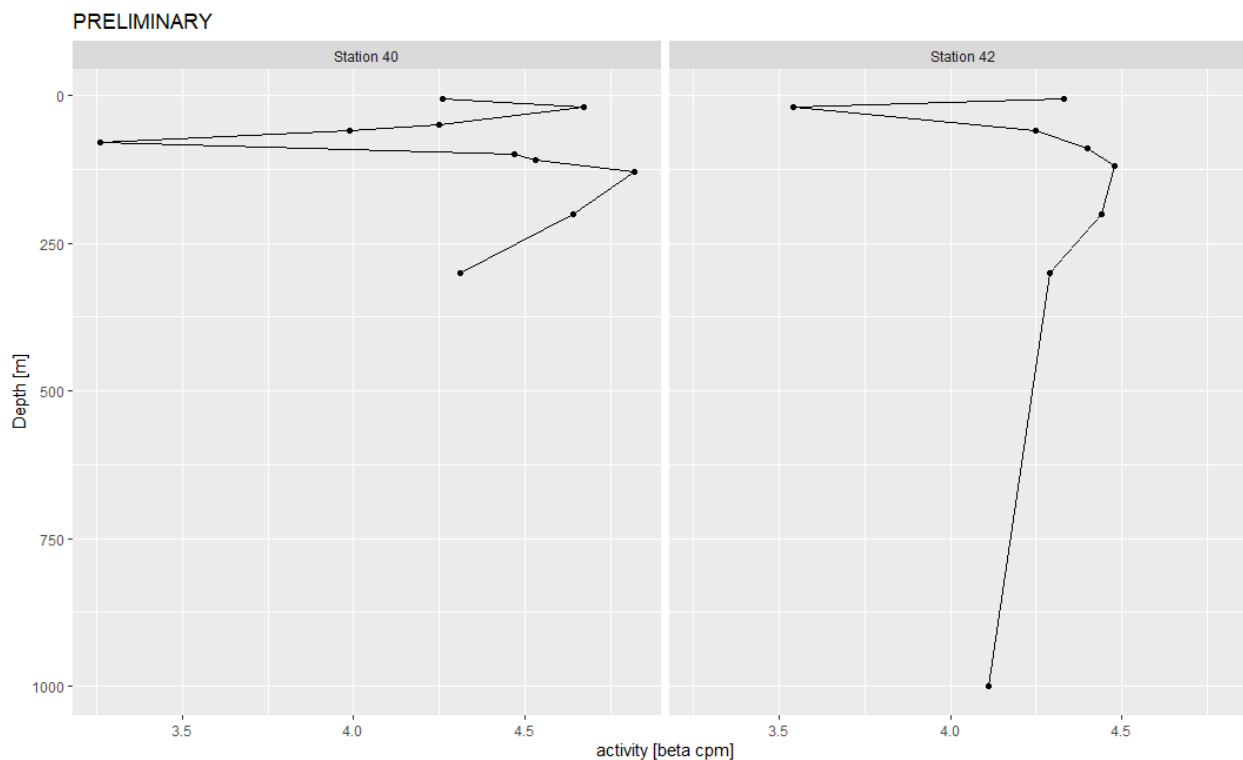


Fig. 12.66 Preliminary results for dissolved ^{234}Th activities [cpm].

Table 12.13 Samples of particulate ^{234}Th were taken according to the table below. Preliminary activity values (beta counts per minute) are included.

sample	Station	filtertype	depth [m]	pumptime [min]	activity [beta cpm]	counts
50001	Station 5	QM-A	20	120	2.69	2871
50003	Station 5	QM-A	50	120	3.61	3860
50005	Station 5	QM-A	100	120	6.82	7286
50007	Station 5	QM-A	200	120	3.56	3803
50009	Station 5	QM-A	300	120	5.52	5899
50013	Station 8	QM-A	20	180	3.63	4728
50015	Station 8	QM-A	50	180	4.13	5389
50017	Station 8	QM-A	100	180	8.18	10663
50019	Station 8	QM-A	200	180	0.33	435
50021	Station 8	QM-A	300	180	8.08	10539
50027	Station 12	QM-A	20	180	7.14	4830
50029	Station 12	QM-A	60	180	5.09	3448
50030	Station 12	QM-A	100	180	6.97	4721
50033	Station 12	QM-A	200	180	3.15	2130
50035	Station 12	QM-A	300	180	4.32	2923
50041	Station 16	QM-A	20	180	8.69	12639
50043	Station 16	QM-A	60	180	6.49	9445
50044	Station 16	QM-A	100	180	8.92	12974
50047	Station 16	QM-A	200	180	3.11	4519
50049	Station 16	QM-A	300	180	3.51	5112
50055	Station 19	QM-A	20	180	5.44	7564
50057	Station 19	QM-A	100	180	5.85	8135
50058	Station 19	QM-A	150	180	8.91	12393
50060	Station 19	QM-A	200	180	3.73	5188

50062	Station 19	QM-A	300	180	2.4	3332
50069	Station 21	QM-A	20	180	6.67	2185
50070	Station 21	QM-A	150	180	10.07	3299
50072	Station 21	QM-A	200	180	5.77	1891
50073	Station 21	QM-A	300	180	2.26	740
50079	Station 21	QM-A	2100	180	9.28	3041
50083	Station 24	QM-A	20	180	5.24	3464
50084	Station 24	QM-A	175	180	7.67	5063
50086	Station 24	QM-A	230	180	6.93	4576
50087	Station 24	QM-A	300	180	3.13	2066
50094	Station 24	QM-A	2150	180	0.97	641
50097	Station 28	QM-A	20	180	5.29	4220
50098	Station 28	QM-A	150	180	10.33	8239
50100	Station 28	QM-A	200	180	8.74	6965
50101	Station 28	QM-A	300	180	2.35	1877
50108	Station 28	QM-A	2150	180	0.86	684
50111	Station 31	QM-A	20	180	5.05	6195
50112	Station 31	QM-A	100	180	5.94	7281
50114	Station 31	QM-A	150	180	6.82	8364
50116	Station 31	QM-A	200	180	1.72	2105
50118	Station 31	QM-A	300	180	3.64	4459
50125	Station 33	QM-A	20	150	4.67	2433
50126	Station 33	QM-A	60	150	4.12	3910
50128	Station 33	QM-A	90	150	8.99	8522
50129	Station 33	QM-A	120	150	6.1	3177
50131	Station 33	QM-A	140	150	8.41	7977
50132	Station 33	QM-A	170	150	0.74	701
50133	Station 33	QM-A	200	150	2.67	2536
50135	Station 33	QM-A	250	150	3.93	2047
50136	Station 33	QM-A	300	150	2.53	1318
50137	Station 33	QM-A	400	150	2.77	1442
50139	Station 36	QM-A	20	180	4.65	5516
50140	Station 36	QM-A	70	180	4.03	4773
50142	Station 36	QM-A	120	180	7.61	9018
50144	Station 36	QM-A	200	180	2.94	3483
50146	Station 36	QM-A	300	180	2.83	3357
50153	Station 40	QM-A	20	180	1.98	1893
50155	Station 40	QM-A	60	180	2.62	2508
50156	Station 40	QM-A	100	180	3.58	3431
50158	Station 40	QM-A	130	180	2.43	2330
50163	Station 40	QM-A	300	180	3.19	3058
50165	Station 42	QM-A	20	180	2.62	1306
50166	Station 42	QM-A	60	180	2.25	1121
50168	Station 42	QM-A	90	180	4.15	2066
50170	Station 42	QM-A	200	180	2.46	1222
50172	Station 42	QM-A	300	180	2.54	1263

12.6 Jacobs University cleaning and sampling procedures

(S. Pöhle, N. Fröhberg, C. Gürses, I. Pedre)

Table 12.14 Cleaning procedures applied for Jacobs University sampling bottles used during cruise SO289.

Procedure Cleaning step	GEOTRACES cleaning (GTU)	JUB Trace metal cleaning (JUB-TM)
1	Dishwasher	Dishwasher
2	Filled with 6 M HCl, soaked in 2 M HCl for 28 days at room temperature	Filled with HNO ₃ (2% / 0.2%), stored for 2 days at 45°C
3	Four times rinse with pure water	Triple rinse with pure water
4	Filled with HCl/HF (1 M/0.1 M, both of ultrapure grade) for 28 days at room temperature	Filled with 1 M HCl (suprapure), stored for 2 days at 45°C
5	Triple rinse with pure water	Triple rinse with pure water
6	Filled with pure water, stored for 2 days at room temperature	Filled with pure water, stored for 2 days at room temperature
7	Triple rinse with pure water	Triple rinse with pure water

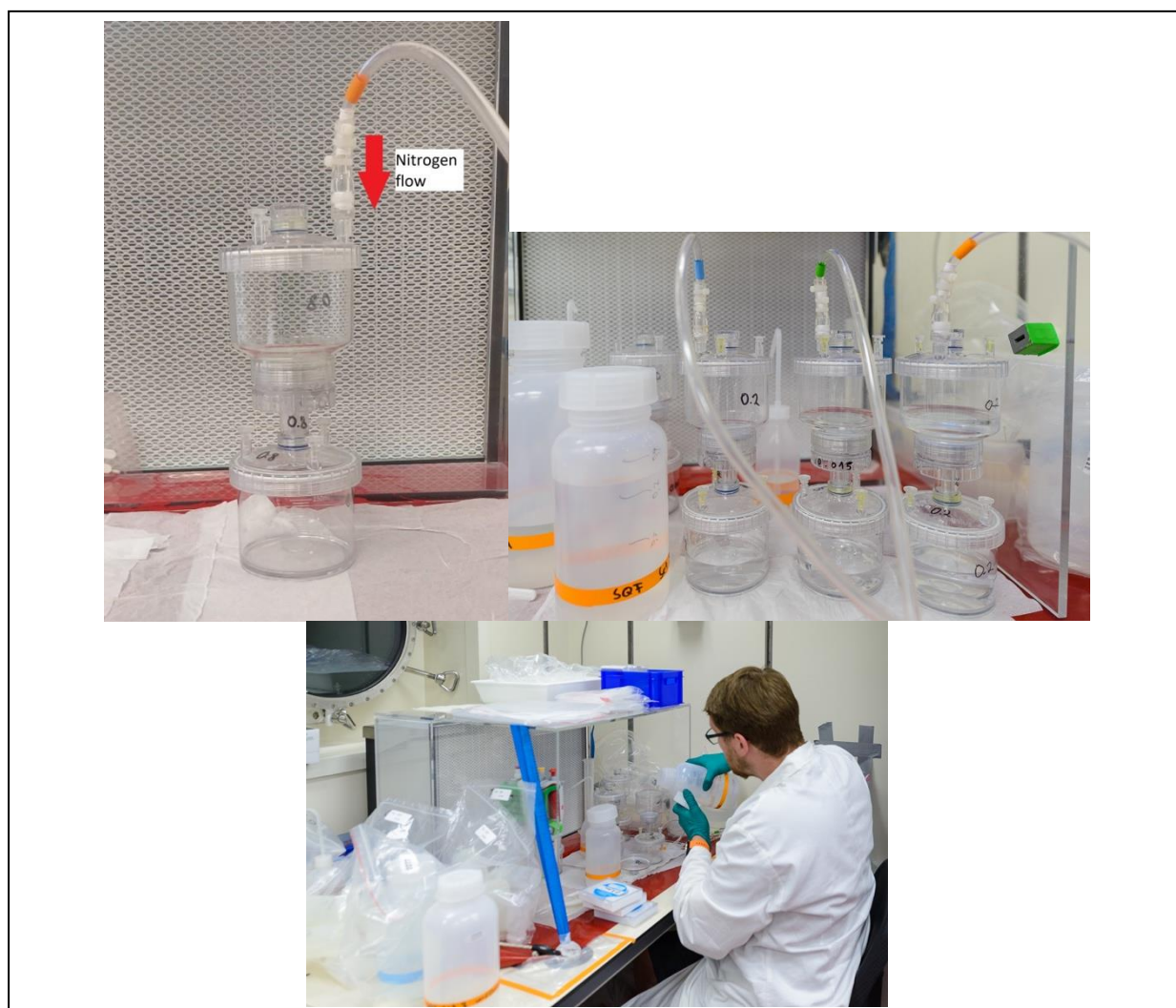


Fig. 12.67 Filtration Set-up used by the Jacobs University team for sequential filtration of up to three seawater samples simultaneously using filter towers with positive gas pressure inside a laminar flow bench.



Fig. 12.68 Ultrafiltration in the on-board laboratory.

12.7 Oxygen, siderophores and microplastic samples

(L. Blum, M. d. I. A. Amenábar)

Table 12.15 Total oxygen samples taken, including station numbers and casts and the results of the Winkler titration.

Date	Station No.	Profile/Cast	Bedford No.	Bottle No.	Bottle factor	Factor Sodium thiosulphate	titr. mL Sodium thiosulphate	mL O ₂ [μmol/L]
05.03.2022	15	TM CTD	20550	152	49.468	0.10107544	3.455	17.28
05.03.2022	15	TM CTD	20566	156	50.276	0.09945103	5.290	26.45
05.03.2022	15	TM CTD	20573	187	49.631	0.10074349	4.620	23.10
05.03.2022	16	TM CTD	20593	229	46.530	0.10745755	3.730	18.65
05.03.2022	16	TM CTD	20608	228	46.910	0.10658708	4.555	22.78
05.03.2022	16	TM CTD	20615	194	50.064	0.09987216	4.620	23.10
06.03.2022	17	TM CTD	20634	175	50.044	0.09991208	3.418	17.09
06.03.2022	17	TM CTD	20650	177	49.969	0.10006204	5.165	25.83
06.03.2022	17	TM CTD	20657	174	50.352	0.09930092	4.482	22.41
07.03.2022	18	TM CTD	20670	190	46.910	0.10658708	3.45	17.25
07.03.2022	18	TM CTD	20688	104	46.360	0.1078516	4.92	24.60
07.03.2022	18	TM CTD	20693	187	49.631	0.10074349	4.588	22.94
08.03.2022	19	TM CTD	20712	177	49.969	0.10006204	3.422	17.11
08.03.2022	19	TM CTD	20722	175	50.044	0.09991208	2.6	13.00
08.03.2022	19	TM CTD	20735	174	50.352	0.09930092	4.383	21.92
08.03.2022	20	TM CTD	20754	190	46.910	0.10658708	3.343	16.72
08.03.2022	20	TM CTD	20764	194	50.064	0.09987216	2.68	13.40
08.03.2022	20	TM CTD	20777	187	49.631	0.10074349	4.58	22.90
09.03.2022	22	TM CTD	20819	125	49.844	0.10031298	4.63	23.15

09.03.2022	22	TM CTD	20796	167	49.989	0.100022	3.283	16.42
09.03.2022	22	TM CTD	20806	104	46.360	0.1078516	3.495	17.48
10.03.2022	23	TM CTD	20834	194	50.064	0.09987216	3.36	16.80
10.03.2022	23	TM CTD	20845	167	49.989	0.100022	3.232	16.16
10.03.2022	23	TM CTD	20857	187	49.631	0.10074349	4.41	22.05
11.03.2022	24	TM CTD	20876	228	46.910	0.10658708	3.623	18.12
11.03.2022	24	TM CTD	20887	229	46.530	0.10745755	3.498	17.49
11.03.2022	24	TM CTD	20899	234	46.630	0.10722711	4.603	23.02
12.02.2022	25	TM CTD	20912	125	49.844	0.10031298	3.663	18.32
12.02.2022	25	TM CTD	20923	229	46.530	0.10745755	3.587	17.94
12.02.2022	25	TM CTD	20935	177	49.969	0.10006204	4.607	23.04
12.02.2022	26	TM CTD	20954	151	46.580	0.10734221	3.75	18.75
12.02.2022	26	TM CTD	20964	156	50.276	0.09945103	3.473	17.37
12.02.2022	26	TM CTD	20977	167	49.989	0.100022	4.413	22.07
13.03.2022	27	TM CTD	20996	155	50.393	0.09922013	3.538	17.69
13.03.2022	27	TM CTD	21012	234	46.630	0.10722711	5.376	26.88
13.03.2022	27	TM CTD	21019	228	46.910	0.10658708	4.688	23.44
14.03.2022	28	TM CTD	21038	104	46.360	0.1078516	3.828	19.14
14.03.2022	28	TM CTD	21052	187	49.631	0.10074349	4.732	23.66
14.03.2022	28	TM CTD	21061	177	49.969	0.10006204	4.49	22.45
15.03.2022	29	TM CTD	21080	167	49.989	0.100022	3.748	18.74
15.03.2022	29	TM CTD	21094	125	49.844	0.10031298	4.708	23.54
15.03.2022	29	TM CTD	21103	229	46.530	0.10745755	4.798	23.99
16.03.2022	30	TM CTD	21122	174	50.352	0.09930092	3.808	19.04
16.03.2022	30	TM CTD	21136	175	50.044	0.09991208	4.49	22.45
16.03.2022	30	TM CTD	21145	177	49.969	0.10006204	4.4	22.00
17.03.2022	31	TM CTD	21164	167	49.989	0.100022	3.873	19.37
17.03.2022	31	TM CTD	21176	172	49.739	0.10052474	4.663	23.32
17.03.2022	31	TM CTD	21187	187	49.631	0.10074349	4.598	22.99
18.03.2022	32	TM CTD	21215	229	46.530	0.10745755	3.455	17.28
18.03.2022	32	TM CTD	21224	156	50.276	0.09945103	5.11	25.55
18.03.2022	32	TM CTD	21228	234	46.630	0.10722711	5.218	26.09
23.03.2022	33	TM CTD	21256	228	46.910	0.10658708	4.02	20.10
23.03.2022	33	TM CTD	21265	229	46.530	0.10745755	4.418	22.09
23.03.2022	33	TM CTD	21277	234	46.630	0.10722711	4.45	22.25
24.03.2022	34	TM CTD	21302	151	46.580	0.10734221	3.245	16.23
24.03.2022	34	TM CTD	21309	152	49.468	0.10107544	4.495	22.48
24.03.2022	34	TM CTD	21318	155	50.393	0.09922013	4.595	22.98
25.03.2022	35	TM CTD	21344	187	49.631	0.10074349	3.1	15.50
25.03.2022	35	TM CTD	21351	190	46.910	0.10658708	4.588	22.94
25.03.2022	35	TM CTD	21360	194	50.064	0.09987216	4.625	23.13
26.03.2022	36	TM CTD	21387	156	50.276	0.09945103	3.27	16.35
26.03.2022	36	TM CTD	21394	167	49.989	0.100022	4.87	24.35
26.03.2022	36	TM CTD	21402	172	49.739	0.10052474	4.71	23.55

27.03.2022	37	TM CTD	21428	228	46.910	0.10658708	3.258	16.29
27.03.2022	37	TM CTD	21437	229	46.530	0.10745755	5.19	25.95
27.03.2022	37	TM CTD	21444	234	46.630	0.10722711	5.04	25.20
28.03.2022	38	TM CTD	21470	172	49.739	0.10052474	3.078	15.39
28.03.2022	38	TM CTD	21479	174	50.352	0.09930092	4.668	23.34
28.03.2022	38	TM CTD	21486	175	50.044	0.09991208	4.57	22.85
29.02.2022	39	TM CTD	21514	152	49.468	0.10107544	3.19	15.95
29.02.2022	39	TM CTD	21521	151	46.580	0.10734221	4.845	24.23
29.02.2022	39	TM CTD	21529	155	50.393	0.09922013	4.768	23.84
30.03.2022	40	TM CTD	21550	172	49.739	0.10052474	4.18	20.90
30.03.2022	40	TM CTD	21555	174	50.352	0.09930092	4.06	20.30
30.03.2022	40	TM CTD	21566	175	50.044	0.09991208	4.433	22.17
31.03.2022	41	TM CTD	21588	172	49.739	0.10052474	3.238	16.19
31.03.2022	41	TM CTD	21605	174	50.352	0.09930092	4.192	20.96
31.03.2022	41	TM CTD	21609	175	50.044	0.09991208	4.888	24.44
02.04.2022	42	TM CTD	21634	228	46.910	0.10658708	3.363	16.82
02.04.2022	42	TM CTD	21641	229	46.530	0.10745755	4.843	24.22
02.04.2022	42	TM CTD	21651	234	46.630	0.10722711	5	25.00
03.04.2022	43	TM CTD	21678	172	49.739	0.10052474	3.183	15.92
03.04.2022	43	TM CTD	21683	174	50.352	0.09930092	4.285	21.43
03.04.2022	43	TM CTD	21690	175	50.044	0.09991208	4.178	20.89
03.04.2022	44	TM CTD	21713	228	46.910	0.10658708	3.357	16.79
03.04.2022	44	TM CTD	21720	229	46.530	0.10745755	4.763	23.82
03.04.2022	44	TM CTD	21728	234	46.630	0.10722711	4.515	22.58
08.03.2022	19	SS CTD	40549	156	50.276	0.09945103	4.732	23.66
08.03.2022	20	SS CTD	40557	229	46.530	0.10745755	3.520	17.60
08.03.2022	20	SS CTD	40567	228	46.910	0.10658708	4.838	24.19
08.03.2022	20	SS CTD	40573	234	46.630	0.10722711	4.708	23.54
09.03.2022	22-2	SS CTD	40605	151	46.580	0.10734221	4.855	24.28
09.03.2022	22-2	SS CTD	40620	152	49.468	0.10107544	4.433	22.17
09.03.2022	22-3	SS CTD	40579	172	49.739	0.10052474	3.150	15.75
09.03.2022	22-3	SS CTD	40595	155	50.393	0.09922013	2.652	13.26
10.03.2022	23	SS CTD	40629	174	50.352	0.09930092	3.223	16.12
10.03.2022	23	SS CTD	40638	175	50.044	0.09991208	4.378	21.89
10.03.2022	23	SS CTD	40644	177	49.969	0.10006204	4.425	22.13
11.03.2022	24-1	SS CTD	40650	104	46.360	0.1078516	3.573	17.87
11.03.2022	24-1	SS CTD	40666	125	49.844	0.10031298	3.143	15.72
11.03.2022	24-2	SS CTD	40688	151	46.580	0.10734221	4.595	22.98
12.03.2022	25	SS CTD	40693	187	49.631	0.10074349	3.480	17.40
12.03.2022	25	SS CTD	40703	155	50.393	0.09922013	3.297	16.49
12.03.2022	25	SS CTD	40707	104	46.360	0.1078516	5.410	27.05
12.03.2022	25	SS CTD	40709	152	49.468	0.10107544	4.652	23.26
12.03.2022	25	SS CTD	40716	190	46.910	0.10658708	4.447	22.24
12.03.2022	26	SS CTD	40717	194	50.064	0.09987216	3.473	17.37

12.03.2022	26	SS CTD	40727	175	50.044	0.09991208	3.353	16.77
12.03.2022	26	SS CTD	40733	174	50.352	0.09930092	4.442	22.21
12.03.2022	26	SS CTD	40740	172	49.739	0.10052474	4.428	22.14
13.03.2022	27	SS CTD	40741	229	46.530	0.10745755	3.808	19.04
13.03.2023	27	SS CTD	40751	190	46.910	0.10658708	3.473	17.37
13.03.2024	27	SS CTD	40757	152	49.468	0.10107544	4.543	22.72
13.03.2025	27	SS CTD	40764	125	49.844	0.10031298	4.567	22.84
14.03.2022	28-1	SS CTD	40785	151	46.580	0.10734221	4.688	23.44
14.03.2022	28-2	SS CTD	40794	152	49.468	0.10107544	3.650	18.25
14.03.2022	28-2	SS CTD	40811	156	50.276	0.09945103	3.698	18.49
15.03.2022	29	SS CTD	40813	172	49.739	0.10052474	3.732	18.66
15.03.2022	29	SS CTD	40829	174	50.352	0.09930092	4.487	22.44
15.03.2022	29	SS CTD	40836	175	50.044	0.09991208	4.378	21.89
16.03.2022	30	SS CTD	40837	190	46.910	0.10658708	3.850	19.25
16.03.2023	30	SS CTD	40844	194	50.064	0.09987216	3.200	16.00
16.03.2024	30	SS CTD	40852	228	46.910	0.10658708	4.720	23.60
16.03.2022	30	SS CTD	40859	234	46.630	0.10722711	4.718	23.59
17.03.2022	31-1	SS CTD	40876	104	46.360	0.1078516	4.860	24.30
17.03.2022	31-2	SS CTD	40888	125	49.844	0.10031298	3.490	17.45
18.03.2022	32	SS CTD	40905	155	50.393	0.09922013	3.940	19.70
18.03.2022	32	SS CTD	40921	151	46.580	0.10734221	4.593	22.97
18.03.2022	32	SS CTD	40928	152	49.468	0.10107544	4.505	22.53
23.03.2022	33-1	SS CTD	40932	172	49.739	0.10052474	3.982	19.91
23.03.2022	33-2	SS CTD	40955	174	50.352	0.09930092	4.445	22.23
24.03.2022	34	SS CTD	40977	175	50.044	0.09991208	4.195	20.98
24.03.2022	34	SS CTD	40993	177	49.969	0.10006204	4.077	20.39
24.03.2022	34	SS CTD	40100	125	49.844	0.10031298	4.531	22.66
25.03.2022	35	SS CTD	41001	228	46.910	0.10658708	4.475	22.38
25.03.2022	35	SS CTD	41016	229	46.530	0.10745755	4.295	21.48
25.03.2022	35	SS CTD	41023	234	46.630	0.10722711	4.445	22.23
26.03.2022	36	SS CTD	41038	125	49.844	0.10031298	4.413	22.07
26.03.2022	36	SS CTD	41048	104	46.360	0.1078516	4.688	23.44
26.03.2022	36	SS CTD	41052	174	50.352	0.09930092	4.253	21.27
27.03.2022	37	SS CTD	41073	151	46.580	0.10734221	4.615	23.08
27.03.2022	37	SS CTD	41079	152	46.580	0.10734221	3.095	15.48
27.03.2022	37	SS CTD	41087	155	50.393	0.09922013	4.820	24.10
27.03.2022	37	SS CTD	41090	187	49.631	0.10074349	4.143	20.72
28.03.2022	38-1	SS CTD	41111	190	46.910	0.10658708	3.093	15.47
28.03.2022	38-2	SS CTD	41125	194	50.064	0.09987216	4.683	23.42
28.03.2022	38-2	SS CTD	41136	104	46.360	0.1078516	4.480	22.40
28.03.2022	38-2	SS CTD	41142	125	49.844	0.10031298	4.527	22.64
29.02.2022	39	SS CTD	41156	228	46.910	0.10658708	3.305	16.53
29.02.2022	39	SS CTD	41165	229	46.530	0.10745755	4.360	21.80
29.02.2022	39	SS CTD	41168	234	46.630	0.10722711	4.563	22.82

30.03.2022	40	SS CTD	41186	167	49.989	0.100022	4.138	20.69
30.03.2022	40	SS CTD	41192	187	49.631	0.10074349	4.433	22.17
31.03.2022	41	SS CTD	41210	151	46.580	0.10734221	4.388	21.94
31.03.2022	41	SS CTD	41216	155	50.393	0.09922013	4.335	21.68
02.04.2022	42-1	SS CTD	41226	152	46.580	0.10734221	4.060	20.30
02.04.2022	42-1	SS CTD	41240	156	50.276	0.09945103	4.655	23.28
02.04.2022	42-2	SS CTD	41244	190	46.910	0.10658708	3.263	16.32
02.04.2022	42-2	SS CTD	41257	194	50.064	0.09987216	3.185	15.93
03.04.2022	43	SS CTD	41265	151	46.580	0.10734221	3.523	17.62
03.04.2022	43	SS CTD	41273	155	50.393	0.09922013	3.430	17.15
03.04.2022	43	SS CTD	41281	167	49.989	0.100022	4.423	22.12
03.04.2022	43	SS CTD	41288	187	49.631	0.10074349	4.420	22.10
03.04.2022	44	SS CTD	41298	152	46.580	0.10734221	3.385	16.93
03.04.2022	44	SS CTD	41302	156	50.276	0.09945103	4.758	23.79
03.04.2022	44	SS CTD	41307	190	46.910	0.10658708	3.964	19.82
03.04.2022	44	SS CTD	41310	194	50.064	0.09987216	4.293	21.47

Table 12.16 Total samples to analyze particulate and dissolved siderophores including the sample volumes.

Station	Label ID	sample volume in L	cast
1	20005	2.00	bio
1	20013	1.95	bio
2	20027	2.00	bio
2	20029	1.89	bio
2	20033	1.88	bio
3	20052	2.00	bio
3	20055	2.20	bio
3	20061	2.40	bio
5	20119	1.69	bio
5	20122	1.60	bio
5	20125	1.80	bio
5	20128	1.75	bio
5	20131	1.80	bio
5	20134	1.70	bio
6	20160	2.10	bio
6	20162	2.00	bio
6	20164	1.90	bio
6	20166	2.10	bio
6	20168	1.90	bio
6	20170	2.10	bio
7	20196	1.80	bio
7	20199	1.70	bio
7	20202	1.80	bio
7	20205	1.80	bio

7	20208	1.60	bio
7	20211	2.00	bio
9	20280	1.90	bio
9	20283	1.65	bio
9	20286	1.82	bio
9	20289	1.90	bio
9	20292	1.70	bio
9	20295	1.90	bio
12	20406	1.72	bio
12	20409	1.62	bio
12	20412	1.80	bio
12	20415	1.80	bio
12	20418	1.75	bio
12	20421	2.05	bio
12	20425	2.00	geo
12	20428	2.20	geo
12	20432	1.90	geo
12	20439	2.00	geo
16	20574	1.68	bio
16	20577	1.62	bio
16	20580	1.80	bio
16	20583	1.45	bio
16	20586	1.60	bio
16	20589	1.70	bio
16	20593	1.80	geo
16	20596	2.10	geo
16	20600	2.00	geo
16	20607	2.00	geo
19	20694	1.60	bio
19	20697	1.70	bio
19	20700	1.62	bio
19	20703	1.62	bio
19	20706	1.88	bio
19	20709	1.75	bio
19	20713	1.70	geo
19	20716	1.70	geo
19	20721	1.70	geo
19	20728	1.70	geo
24	20858	2.10	bio
24	20861	2.00	bio
24	20864	1.90	bio
24	20867	2.10	bio
24	20870	2.02	bio
24	20883	1.70	geo

24	20887	1.70	geo
24	20894	1.60	geo
28	21020	1.80	bio
28	21023	1.70	bio
28	21026	1.70	bio
28	21029	1.75	bio
28	21032	1.75	bio
28	21035	1.80	bio
28	21039	1.80	geo
28	21044	1.70	geo
28	21050	1.70	geo
28	21056	1.60	geo
31	21146	1.80	bio
31	21149	1.80	bio
31	21152	1.70	bio
31	21155	1.60	bio
31	21158	1.70	bio
31	21161	1.80	bio
31	21165	1.70	geo
31	21170	1.80	geo
31	21176	1.85	geo
31	21182	1.80	geo
33	21230	1.70	bio
33	21236	1.70	bio
33	21242	1.70	bio
33	21245	1.70	bio
33	21248	1.70	bio
33	21251	1.70	bio
33	21255	1.60	geo
33	21260	1.50	geo
33	21266	1.60	geo
33	21272	1.60	geo
36	21362	1.80	bio
36	21365	1.60	bio
36	21368	1.60	bio
36	21371	1.65	bio
36	21374	1.60	bio
36	21377	1.65	bio
36	21381	1.85	geo
36	21386	1.80	geo
36	21392	1.85	geo
36	21398	1.70	geo
40	21530	1.62	bio
40	21533	1.80	bio

40	21536	1.50	bio
40	21539	1.69	bio
40	21542	1.90	bio
40	21545	1.80	bio
40	21549	1.90	geo
40	21551	1.88	geo
40	21554	1.70	geo
40	21558	1.90	geo
42	21611	1.60	bio
42	21614	2.00	bio
42	21617	1.50	bio
42	21620	1.80	bio
42	21623	1.80	bio
42	21626	1.70	bio
42	21630	1.90	geo
42	21635	1.80	geo
42	21641	1.90	geo
42	21647	1.90	geo

Table 12.17 Microplastic samples.

Sample ID	Latitude start	Longitude start	Latitude End	Longitude End	Station/ Underway (S/U)	Volume filtered (L)
70001	33°36.351'S	71°43.876'W	33°28.644'S	71°49.512'W	U	528.2
70002	33°05.406'S	71°49.515'W	33°04.951'S	71°49.678'W	S_02	370.3
70003	32°58.037'S	71°51.835'W	32°58.039'S	71°51.829'W	S_03	3703.3
70004	32°52.338'S	71°53.550'W	32°49.468'S	71°54.377'W	S_04	826
70005	32°45.836'S	71°55.436'W	32°29.955'S	71°59.905'W	U	739.9
70006	32°29.958'S	71°59.912'W	32°29.984'S	71°59.911'W	S_05	5502.1
70007	32°29.997'S	72°47.995'W	32°30.152'S	72°48.735'W	S_06	2747
70008	32°29.998'S	72°53.015'W	32°29.999'S	73°48.000'W	U	2603.9
70009	32°30.000'S	73°48.002'W	32°30.004'S	73°47.999'W	S_07	1233.5
70010	32°30.000'S	74°35.790'W	32°30.005'S	76°36.029'W	U	4125.4
70011	32°30.005'S	76°36.025'W	32°29.998'S	76°36.042'W	S_08	4463.8
70012	32°30.001'S	77°44.656'W	32°30.001'S	79°00.086'W	U	2298.7
70013	32°30.022'S	79°00.079'W	32°30.017'S	79°00.053'W	S_09	2795.5
70014	32°29.998'S	79°30.002'W	32°29.998'S	81°59.143'W	U	4857.5
70015	32°29.892'S	81°59.943'W	32°29.892'S	81°59.949'W	S_10	1999
70016	32°29.892'S	81°59.949'W	32°29.998'S	82°36.577'W	U	1162.2
70017	32°30.014'S	85°00.032'W	32°30.031'S	85°00.022'W	S_11	1622.9
70018	32°29.898'S	85°20.737'W	32°30.001'S	87°18.746'W	U	3673.5
70019	32°29.880'S	87°59.985'W	32°30.146'W	88°01.212'W	S_12	1274.8
70020	32°30.003'S	88°05.576'W	32°30.002'S	89°51.721'W	U	3441.8
70021	32°29.992'S	90°59.901'W	32°30.002'S	91°02.327'W	S_13	869.2

70022	32°30.005'S	91°13.787'W	32°29.980'S	94°00.057'W	U	4692.2
70023	32°29.979'S	94°00.052'W	32°29.991'S	94°00.033'W	S_14	2085.9
70024	32°29.998'S	95°26.500'W	32°29.992'S	6,000000	U	2830
70025	32°30.012'S	97°00.044'W	32°30.030'S	97°00.042'W	S_15	2681.9
70026	32°30.001'S	99°22.237'W	32°30.011'S	100°00.035'W	U	1363.6
70027	32°30.011'S	100°00.016'W	32°30.004'S	100°00.004'W	S_16	5038.7
70028	31°39.555'S	102°21.647'W	31°25.643'S	102°59.924'W	U	1435.8
70029	31°25.650'S	102°59.931'W	31°26.081'S	103°02.634'W	S_17	2688.9
70030	31°25.802'S	103°56.285'W	31°25.847'S	105°59.993'W	U	3803.9
70031	31°25.816'S	105°59.998'W	31°25.947'S	106°01.242'W	S_18	546.3
70032	31°25.914'S	106°05.510'W	31°25.793'S	107°59.996'W	U	4738.7
70033	31°25.796'S	107°59.996'W	31°25.819'S	108°00.001'W	S_19	4122.5
70034	31°25.801'S	108°32.208'W	31°25.780'S	109°59.940'W	U	3105.5
70035	31°25.809'S	110°00.014'W	31°25.822'S	110°.00.024' W	S_20	1513.3
70036	31°38.587'S	110°23.782'W	32°29.939'S	111°59.946'W	U	3560.1
70037	31°25.810'S	111°59.384'W	31°25.793'S	111°59.375	S_22	3598.4
70038	31°25.810'S	112°02.861'W	31°25.791'S	114°00.015'W	U	3413.1
70039	31°25.798'S	114°00.014'W	31°25.800'S	114°05.350'W	S_23	1150.4
70040	31°25.796'S	114°07.020'W	31°25.797'S	115°45.671'W	U	4017.6
70041	31°25.809'S	116°00.014'W	31°25.803'S	116°00.003'W	S_24	2951.3
70042	31°25.908'S	116°00.123'W	31°25.794'S	119°00.005'W	U	5336.5
70043	31°25.799'S	118°59.994'W	31°25.784'S	118°59.997'W	S_25	5165.5
70044	31°25.799'S	119°50.405'W	31°25.780'S	122°00.002'W	U	6367.5
70045	31°25.801'S	122°00.009'W	31°25.784'S	122°00.018'W	S_26	1337.5
70046	31°25.805'S	124°01.830'W	31°25.770'S	125°00.009'W	U	1454.9
70047	31°25.771'S	125°00.008'W	31°25.792'S	124°59.996'W	S_27	3952.9
70048	31°25.806'S	125°32.052'W	31°25.797'S	128°00.011'W	U	4121.1
70049	31°25.797'S	128°00.010'W	31°25.815'S	127°59.990'W	S_28	4226.8
70050	31°25.803'S	128°10.053'W	31°25.835'S	131°00.045'W	U	3456.9
70051	31°25.805'S	131°00.030'W	31°25.801'S	131°00.062'W	S_29	2272.4
70052	31°25.799'S	131°06.123'W	31°25.811'S	133°59.987'W	U	3819
70053	31°25.803'S	133°59.987'W	31°25.896'S	134°04.590'W	S_30	1869.7
70054	31°25.892'S	134°04.806'W	31°.25.797'S	137°59.998'W	U	7124.6
70055	31°25.799'S	138.00.000'W	31°25.800'S	137°59.998'W	S_31	4111.7
70056	31°26.057'S	137°59.845'W	31°25.794'S	140°59.994'W	U	4924.8
70057	31°25.796'S	140°59.996'W	31°25.788'S	140°59.973'W	S_32	3632.6
70058	26°10.189'S	152°00.014'W	26°10.219'S	152°00.012'W	S_33	6715.2
70059	26°10.276'S	152°01.054'W	26°10.114'S	155°59.932'W	U	4696.1
70060	26°10.107'S	155°59.920'W	26°10.011'S	156°02.392'W	S_34	4012.9
70061	26°10.194'S	158°22.621'W	26°10.206'S	159°59.972'W	U	2655.6
70062	26°10.194'S	159°59.981'W	26°10.203'S	159°59.995'W	S_35	3201.4
70063	26°10.105'S	160°00.284'W	26°10.208'S	163°59.981'W	U	8476.8
70064	26°10.206'S	163°59.980'W	26°10.186'S	163°59.966'W	S_36	6471.3

70065	26°10.201'S	165°07.889'W	26°10.197'S	168°00.002'W	U	5594.7
70066	26°10.196'S	168°00.006'W	26°10.177'S	168°00.019'W	S_37	4619.3
70067	26°10.200'S	169°05.520'W	26°10.164'S	171°59.956'W	U	6475.7
70068	26°10.200'S	172°00.002'W	26°10.249'S	172°02.374'W	S_38	4929.7
70069	26°10.155'S	172°47.581'W	26°10.000'S	175°23.799'W	U	5779
70070	26°10.004'S	175°23.801'W	26°10.004'S	175°23.793'W	S_39	5601.7
70071	26°07.120'S	175°41.531'W	25°52.495'S	177°10.994'W	U	3784.3
70072	25°52.497'S	177°10.997'W	25°52.240'S	177°13.572'W	S_40	3238.1
70073	25°51.908'S	177°16.849'W	25°43.094'S	178°42.893'W	U	4349.4
70074	25°43.097'S	178°42.889'W	25°43.100'S	178°42.900'W	S_41	2585.1
70075	25°43.101'S	179°04.532'W	25°43.100'S	179°13.091'E	U	5217.9
70076	25°43.101'S	178°59.986'E	25°43.304'S	178°59.241'E	S_42	6195.9
70077	25°43.097'S	178°55.429'E	25°43.194'S	175°29.900'E	U	9057.8
70078	25°43.100'S	175°30.006'E	25°43.100'S	175°30.00'E	S_43	1785.1
70079	25°44.789'S	174°38.536'E	25°49.556'S	172°00.428'E	U	7056.7

12.8 Sulfur isotopes and carbonate chemistry samples

(C. Galley, S. Moriarty, P. Battermann)

Table 12.18 Sulfur isotope samples collected during the cruise

Sample_no.	Stn_no.	Latitude_N	Longitude_E	Depth_m
40003	1	-33.60487	-71.6884892	98
40027	2	-33.0912	-71.8258	155
40041	3	-32.9674	-71.8639	823
40058	4	-32.8722	-71.8924	1686
40065	4	-32.8722	-71.8924	200
40076	5	-32.3	-72	2425
40086	5	-32.3	-72	900
40098	5	-32.3	-72	400
40104	5	-32.3	-72	200
40120	6	-32.3	-72.8	5434
40138	6	-32.3	-72.8	200
40146	7	-32.3	-73.8	3800
40162	7	-32.3	-73.8	100
40172	8	-32.3	-76.6	3830
40179	8	-32.3	-76.6	2500
40184	8	-32.3	-76.6	1100
40185	8	-32.3	-76.6	800
40194	8	-32.3	-76.6	400
40200	8	-32.3	-76.6	200
40216	9	-32.3	-79	4000
40231	9	-32.3	-79	200
40240	10	-32.3	-82	3928
40256	10	-32.3	-82	100
40262	11	-32.3	-85	3780
40277	11	-32.3	-85	500

40280	11	-32.3	-85	350
40290	12	-32.3	-88	3700
40299	12	-32.3	-88	2600
40304	12	-32.3	-88	1100
40308	12	-32.3	-88	1100
40309	12	-32.3	-88	800
40315	12	-32.3	-88	550
40318	12	-32.3	-88	350
40324	12	-32.3	-88	200
40334	13	-32.3	-90.99	3660
40344	13	-32.3	-90.99	1300
40348	13	-32.3	-90.99	550
40348	13	-32.3	-90.99	350
40351	13	-32.3	-90.99	200
40382	15	-32.3	-97	3800
40386	15	-32.3	-97	250
40396	15	-32.3	-97	600
40412	16	-32.3	-100	3200
40428	16	-32.3	-100	1100
40454	17	-31.43	-103	3557
40455	17	-31.43	-103	3500
40476	17	-31.43	-103	15
40479	18	-31.43	-106	3396
40495	18	-31.43	-106	700
40496	18	-31.43	-106	350
40501	18	-31.43	-106	15
40506	19	-31.43	-108	3000
40513	19	-31.43	-108	2500
40523	19	-31.43	-108	1350
40527	19	-31.43	-108	700
40534	19	-31.43	-108	350
40551	20	-31.43	-110	2650
40560	20	-31.43	-110	2000
40564	20	-31.43	-110	1300
40567	20	-31.43	-110	350
40573	20	-31.43	-110	5
40602	22	-31.43	-111.99	600
40612	22	-31.43	-111.99	150
40578	22	-31.43	-111.99	2420
40579	22	-31.43	-111.99	2300
40585	22	-31.43	-111.99	2100
40588	22	-31.43	-111.99	2000
40593	22	-31.43	-111.99	1350
40623	23	-31.43	-114	2860
40625	23	-31.43	-114	2400
40627	23	-31.43	-114	2200
40629	23	-31.43	-114	2100
40631	23	-31.43	-114	2000
40633	23	-31.43	-114	1800

40634	23	-31.43	-114	1500
40649	24	-31.43	-116	3300
40656	24	-31.43	-116	2150
40662	24	-31.43	-116	1800
40663	24	-31.43	-116	1350
40678	24	-31.43	-116	300
40693	25	-31.43	-119	3500
40709	25	-31.43	-119	350
40741	27	-31.43	-125	3500
40745	27	-31.43	-125	2600
40757	27	-31.43	-125	350
40763	27	-31.43	-125	15
40813	29	-31.43	-131	4100
40829	29	-31.43	-131	350
40837	30	-31.43	-134	4150
40838	30	-31.43	-134	3700
40848	30	-31.43	-134	1000
40859	30	-31.43	-134	5
40887	31	-31.43	-138	3300
40905	32	-31.43	-141	4500
40921	32	-31.43	-141	250
40930	33	-26.17	-152	4630
40936	33	-26.17	-152	3900
40968	33	-26.17	-152	120
40977	34	-26.17	-156	5000
40981	34	-26.17	-156	3000
40989	34	-26.17	-156	800
40994	34	-26.17	-156	150
41001	35	-31.43	-160	4900
41003	35	-31.43	-160	4000
41006	35	-31.43	-160	2600
41009	35	-31.43	-160	1800
41020	35	-31.43	-160	60
41039	36	-26.17	-164	140
41056	36	-26.17	-164	3700
41061	36	-26.17	-164	2800
41073	37	-26.17	-168	5300
41074	37	-26.17	-168	4800
41084	37	-26.17	-168	1000
41105	38	-26.17	-172	4000
41106	38	-26.17	-172	3400
41118	38	-26.17	-172	1300
41139	38	-26.17	-172	110
41146	39	-26.17	-175.4	6000
41149	39	-26.17	-175.4	5000
41150	39	-26.17	-175.4	4000
41155	39	-26.17	-175.4	2500
41159	39	-26.17	-175.4	1750
41160	39	-26.17	-175.4	1500

41169	40	-25.88	-177.18	500
41171	40	-25.88	-177.18	450
41173	40	-25.88	-177.18	350
41174	40	-25.88	-177.18	300
41175	40	-25.88	-177.18	250
41178	40	-25.88	-177.18	200
41179	40	-25.88	-177.18	175
41180	40	-25.88	-177.18	150
41181	40	-25.88	-177.18	130
41185	40	-25.88	-177.18	110
41189	40	-25.88	-177.18	50
41192	40	-25.88	-177.18	5
41193	41	-25.718	-178.715	2300
41205	41	-25.718	-178.715	1000
41212	41	-25.718	-178.715	100
41222	42	-25.718	179	600
41224	42	-25.718	179	400
41240	42	-25.718	179	5
41253	42	-25.718	179	2200
41258	42	-25.718	179	2000
41260	42	-25.718	179	1650
41265	43	-25.718	175.5	4300
41266	43	-25.718	175.5	3800
41271	43	-25.718	175.5	2600
41273	43	-25.718	175.5	2200
41275	43	-25.718	175.5	1800
41277	43	-25.718	175.5	1400
41279	43	-25.718	175.5	1000
41281	43	-25.718	175.5	600
41284	43	-25.718	175.5	200
41286	43	-25.718	175.5	90
41288	43	-25.718	175.5	5
41289	44	-25.83	172	3200
41290	44	-25.83	172	3000
41291	44	-25.83	172	2800
41296	44	-25.83	172	1800
41300	44	-25.83	172	1000
41302	44	-25.83	172	650
41307	44	-25.83	172	100

Table 12.19 Carbonate chemistry samples collected during the cruise

Sample_no.	Stn_no.	Latitude_N	Longitude_E	Depth_m
40003	1	-33.60487	-71.6884892	98
40015	1	-33.60487	-71.6884892	6
40027	2	-33.0912	-71.8258	155
40037	2	-33.0912	-71.8258	5
40041	3	-32.9674	-71.8639	823
40042	3	-32.9674	-71.8639	600

40047	3	-32.9674	-71.8639	300
40050	3	-32.9674	-71.8639	100
40056	3	-32.9674	-71.8639	5
40058	4	-32.8722	-71.8924	1686
40059	4	-32.8722	-71.8924	1200
40060	4	-32.8722	-71.8924	600
40063	4	-32.8722	-71.8924	300
40065	4	-32.8722	-71.8924	200
40066	4	-32.8722	-71.8924	100
40070	4	-32.8722	-71.8924	5
40076	5	-32.5	-72	2425
40085	5	-32.5	-72	1500
40086	5	-32.5	-72	900
40091	5	-32.5	-72	600
40098	5	-32.5	-72	400
40104	5	-32.5	-72	200
40106	5	-32.5	-72	100
40118	5	-32.5	-72	5
40120	6	-32.5	-72.8	5434
40126	6	-32.5	-72.8	4000
40130	6	-32.5	-72.8	2000
40131	6	-32.5	-72.8	1500
40133	6	-32.5	-72.8	700
40136	6	-32.5	-72.8	400
40138	6	-32.5	-72.8	200
40139	6	-32.5	-72.8	100
40143	6	-32.5	-72.8	5
40146	7	-32.5	-73.8	3800
40149	7	-32.5	-73.8	2750
40152	7	-32.5	-73.8	1100
40155	7	-32.5	-73.8	600
40158	7	-32.5	-73.8	250
40159	7	-32.5	-73.8	200
40162	7	-32.5	-73.8	100
40166	7	-32.5	-73.8	5
40172	8	-32.5	-76.6	3830
40179	8	-32.5	-76.6	2500
40184	8	-32.5	-76.6	1100
40185	8	-32.5	-76.6	800
40190	8	-32.5	-76.6	600
40194	8	-32.5	-76.6	400
40200	8	-32.5	-76.6	200
40202	8	-32.5	-76.6	100
40214	8	-32.5	-76.6	5
40216	9	-32.5	-79	4000
40219	9	-32.5	-79	3000
40222	9	-32.5	-79	2000
40224	9	-32.5	-79	1300
40229	9	-32.5	-79	400

40231	9	-32.5	-79	200
40232	9	-32.5	-79	100
40237	9	-32.5	-79	5
40240	10	-32.5	-82	3928
40243	10	-32.5	-82	2750
40246	10	-32.5	-82	1200
40249	10	-32.5	-82	600
40252	10	-32.5	-82	250
40253	10	-32.5	-82	200
40256	10	-32.5	-82	100
40262	11	-32.5	-85	3780
40268	11	-32.5	-85	2100
40273	11	-32.5	-85	1100
40276	11	-32.5	-85	600
40280	11	-32.5	-85	350
40283	11	-32.5	-85	70
40290	12	-32.5	-88	3660
40299	12	-32.5	-88	2600
40308	12	-32.5	-88	1100
40309	12	-32.5	-88	800
40315	12	-32.5	-88	550
40318	12	-32.5	-88	350
40324	12	-32.5	-88	200
40326	12	-32.5	-88	100
40333	12	-32.5	-88	5
40334	13	-32.5	-91	3560
40339	13	-32.5	-91	2600
40340	13	-32.5	-91	2400
40344	13	-32.5	-91	1300
40349	13	-32.5	-91	400
40351	13	-32.5	-91	200
40352	13	-32.5	-91	100
40357	13	-32.5	-91	5
40359	14	-32.5	-94	3500
40372	14	-32.5	-94	350
40377	14	-32.5	-94	60
40380	14	-32.5	-94	5
40382	15	-32.5	-97	3800
40388	15	-32.5	-97	2100
40393	15	-32.5	-97	1100
40396	15	-32.5	-97	600
40400	15	-32.5	-97	350
40403	15	-32.5	-97	70
40410	16	-32.5	-100	3600
40419	16	-32.5	-100	2600
40428	16	-32.5	-100	1100
40429	16	-32.5	-100	800
40435	16	-32.5	-100	550
40438	16	-32.5	-100	350

40444	16	-32.5	-100	200
40446	16	-32.5	-100	100
40453	16	-32.5	-100	5
40454	17	-31.43	-103	3557
40459	17	-31.43	-103	2400
40460	17	-31.43	-103	2200
40464	17	-31.43	-103	1300
40469	17	-31.43	-103	400
40471	17	-31.43	-103	200
40472	17	-31.43	-103	100
40477	17	-31.43	-103	5
40479	18	-31.43	-105	3396
40496	18	-31.43	-105	350
40499	18	-31.43	-105	60
40506	19	-31.43	-108	3000
40513	19	-31.43	-108	2500
40524	19	-31.43	-108	1100
40525	19	-31.43	-108	700
40530	19	-31.43	-108	600
40534	19	-31.43	-108	350
40540	19	-31.43	-108	200
40542	19	-31.43	-108	100
40549	19	-31.43	-108	5
40551	20	-31.43	-110	2650
40567	20	-31.43	-110	350
40570	20	-31.43	-110	60
40602	22	-31.43	-111.99	600
40605	22	-31.43	-111.99	350
40611	22	-31.43	-111.99	200
40613	22	-31.43	-111.99	100
40620	22	-31.43	-111.99	5
40578	22	-31.43	-111.99	2300
40588	22	-31.43	-111.99	2000
40597	22	-31.43	-111.99	1100
40622	23	-31.43	-114	2860
40638	23	-31.43	-114	350
40641	23	-31.43	-114	60
40649	24	-31.43	-116	3300
40659	24	-31.43	-116	2000
40668	24	-31.43	-116	1000
40673	24	-31.43	-116	600
40679	24	-31.43	-116	230
40688	24	-31.43	-116	5
40693	25	-31.43	-119	3500
40698	25	-31.43	-119	2300
40703	25	-31.43	-119	1350
40708	25	-31.43	-119	400
40710	25	-31.43	-119	200
40712	25	-31.43	-119	100

40716	25	-31.43	-119	5
40717	26	-31.43	-122	3500
40722	26	-31.43	-122	2300
40727	26	-31.43	-122	1350
40732	26	-31.43	-122	400
40736	26	-31.43	-122	100
40740	26	-31.43	-122	5
40741	27	-31.43	-125	3500
40746	27	-31.43	-125	2300
40751	27	-31.43	-125	1350
40756	27	-31.43	-125	400
40760	27	-31.43	-125	100
40764	27	-31.43	-125	5
40765	28	-31.43	-128	1000
40770	28	-31.43	-128	600
40776	28	-31.43	-128	200
40785	28	-31.43	-128	5
40793	28	-31.43	-128	3500
40804	28	-31.43	-128	2000
40813	29	-31.43	-131	4100
40818	29	-31.43	-131	2300
40823	29	-31.43	-131	1350
40828	29	-31.43	-131	400
40830	29	-31.43	-131	150
40832	29	-31.43	-131	100
40836	29	-31.43	-131	5
40837	30	-31.43	-134	4150
40842	30	-31.43	-134	2300
40847	30	-31.43	-134	1350
40851	30	-31.43	-134	400
40855	30	-31.43	-134	100
40859	30	-31.43	-134	5
40863	31	-31.43	-138	600
40868	31	-31.43	-138	250
40876	31	-31.43	-138	5
40887	31	-31.43	-138	3300
40895	31	-31.43	-138	1800
40905	32	-31.43	-141	4500
40910	32	-31.43	-141	2300
40915	32	-31.43	-141	1350
40920	32	-31.43	-141	400
40922	32	-31.43	-141	150
40924	32	-31.43	-141	100
40928	32	-31.43	-141	5
40930	33	-26.17	-152	4630
40932	33	-26.17	-152	4400
40937	33	-26.17	-152	3300
40941	33	-26.17	-152	2800
40942	33	-26.17	-152	2400

40946	33	-26.17	-152	2150
40947	33	-26.17	-152	1800
40950	33	-26.17	-152	1300
40952	33	-26.17	-152	800
40957	33	-26.17	-152	500
40958	33	-26.17	-152	400
40959	33	-26.17	-152	300
40960	33	-26.17	-152	250
40965	33	-26.17	-152	200
40966	33	-26.17	-152	170
40967	33	-26.17	-152	140
40968	33	-26.17	-152	120
40975	33	-26.17	-152	20
40976	33	-26.17	-152	5
40977	34	-26.17	-156	5000
40978	34	-26.17	-156	4500
40979	34	-26.17	-156	4000
40980	34	-26.17	-156	3500
40981	34	-26.17	-156	3000
40982	34	-26.17	-156	2600
40983	34	-26.17	-156	2300
40984	34	-26.17	-156	2000
40985	34	-26.17	-156	1800
40986	34	-26.17	-156	1500
40987	34	-26.17	-156	1350
40988	34	-26.17	-156	1000
40989	34	-26.17	-156	800
40991	34	-26.17	-156	600
40992	34	-26.17	-156	400
40993	34	-26.17	-156	250
40994	34	-26.17	-156	150
40996	34	-26.17	-156	100
40997	34	-26.17	-156	60
40998	34	-26.17	-156	30
40999	34	-26.17	-156	15
41000	34	-26.17	-156	5
41001	35	-31.43	-160	4900
41002	35	-31.43	-160	4500
41003	35	-31.43	-160	4000
41004	35	-31.43	-160	3500
41005	35	-31.43	-160	3000
41006	35	-31.43	-160	2600
41007	35	-31.43	-160	2300
41008	35	-31.43	-160	2000
41009	35	-31.43	-160	1800
41010	35	-31.43	-160	1500
41011	35	-31.43	-160	1350
41012	35	-31.43	-160	1000
41013	35	-31.43	-160	800

41014	35	-31.43	-160	600
41015	35	-31.43	-160	400
41016	35	-31.43	-160	300
41017	35	-31.43	-160	200
41018	35	-31.43	-160	120
41019	35	-31.43	-160	100
41020	35	-31.43	-160	60
41021	35	-31.43	-160	30
41022	35	-31.43	-160	15
41023	35	-31.43	-160	5
41030	36	-26.17	-164	600
41031	36	-26.17	-164	400
41032	36	-26.17	-164	300
41033	36	-26.17	-164	250
41038	36	-26.17	-164	200
41039	36	-26.17	-164	140
41040	36	-26.17	-164	120
41045	36	-26.17	-164	90
41046	36	-26.17	-164	70
41047	36	-26.17	-164	20
41048	36	-26.17	-164	5
41050	36	-26.17	-164	5300
41052	36	-26.17	-164	4600
41057	36	-26.17	-164	3000
41061	36	-26.17	-164	2800
41062	36	-26.17	-164	2300
41066	36	-26.17	-164	2150
41067	36	-26.17	-164	1800
41070	36	-26.17	-164	1500
41073	37	-26.17	-168	5300
41074	37	-26.17	-168	4800
41075	37	-26.17	-168	4200
41076	37	-26.17	-168	3500
41077	37	-26.17	-168	3000
41078	37	-26.17	-168	2600
41079	37	-26.17	-168	2300
41080	37	-26.17	-168	2000
41081	37	-26.17	-168	1800
41082	37	-26.17	-168	1500
41083	37	-26.17	-168	1350
41084	37	-26.17	-168	1000
41085	37	-26.17	-168	800
41087	37	-26.17	-168	600
41088	37	-26.17	-168	400
41089	37	-26.17	-168	300
41090	37	-26.17	-168	230
41091	37	-26.17	-168	160
41093	37	-26.17	-168	120
41094	37	-26.17	-168	60

41095	37	-26.17	-168	30
41096	37	-26.17	-168	5
41097	38	-26.17	-172	5170
41099	38	-26.17	-172	4900
41105	38	-26.17	-172	4000
41106	38	-26.17	-172	3400
41109	38	-26.17	-172	3000
41110	38	-26.17	-172	2600
41111	38	-26.17	-172	2300
41116	38	-26.17	-172	2300
41117	38	-26.17	-172	1800
41118	38	-26.17	-172	1300
41119	38	-26.17	-172	800
41125	38	-26.17	-172	600
41128	38	-26.17	-172	400
41129	38	-26.17	-172	300
41136	38	-26.17	-172	230
41137	38	-26.17	-172	200
41138	38	-26.17	-172	150
41139	38	-26.17	-172	110
41140	38	-26.17	-172	60
41141	38	-26.17	-172	20
41142	38	-26.17	-172	5
41146	39	-26.17	-175.397	6000
41149	39	-26.17	-175.397	5000
41150	39	-26.17	-175.397	4000
41152	39	-26.17	-175.397	3400
41153	39	-26.17	-175.397	3000
41155	39	-26.17	-175.397	2500
41157	39	-26.17	-175.397	2300
41158	39	-26.17	-175.397	2000
41159	39	-26.17	-175.397	1750
41160	39	-26.17	-175.397	1500
41162	39	-26.17	-175.397	1250
41163	39	-26.17	-175.397	1000
41164	39	-26.17	-175.397	800
41165	39	-26.17	-175.397	300
41166	39	-26.17	-175.397	200
41167	39	-26.17	-175.397	130
41168	39	-26.17	-175.397	5
41169	40	-25.875	-177.183	500
41171	40	-25.875	-177.183	450
41172	40	-25.875	-177.183	400
41173	40	-25.875	-177.183	350
41174	40	-25.875	-177.183	300
41175	40	-25.875	-177.183	250
41176	40	-25.875	-177.183	225
41178	40	-25.875	-177.183	200
41179	40	-25.875	-177.183	175

41180	40	-25.875	-177.183	150
41181	40	-25.875	-177.183	130
41185	40	-25.875	-177.183	110
41186	40	-25.875	-177.183	100
41187	40	-25.875	-177.183	80
41188	40	-25.875	-177.183	60
41189	40	-25.875	-177.183	50
41191	40	-25.875	-177.183	20
41192	40	-25.875	-177.183	5
41193	41	-25.718	-178.715	2300
41194	41	-25.718	-178.715	2200
41198	41	-25.718	-178.715	2000
41199	41	-25.718	-178.715	1800
41203	41	-25.718	-178.715	1500
41204	41	-25.718	-178.715	1350
41205	41	-25.718	-178.715	1000
41206	41	-25.718	-178.715	800
41208	41	-25.718	-178.715	600
41209	41	-25.718	-178.715	400
41210	41	-25.718	-178.715	300
41211	41	-25.718	-178.715	200
41212	41	-25.718	-178.715	85
41214	41	-25.718	-178.715	60
41215	41	-25.718	-178.715	30
41216	41	-25.718	-178.715	5
41217	42	-25.718	179	1000
41221	42	-25.718	179	800
41223	42	-25.718	179	600
41224	42	-25.718	179	400
41225	42	-25.718	179	300
41226	42	-25.718	179	250
41231	42	-25.718	179	200
41232	42	-25.718	179	120
41233	42	-25.718	179	90
41238	42	-25.718	179	60
41239	42	-25.718	179	20
41240	42	-25.718	179	5
41242	42	-25.718	179	3740
41244	42	-25.718	179	3300
41247	42	-25.718	179	3000
41250	42	-25.718	179	2800
41252	42	-25.718	179	2600
41257	42	-25.718	179	2400
41253	42	-25.718	179	2200
41258	42	-25.718	179	2000
41259	42	-25.718	179	1800
41260	42	-25.718	179	1650
41261	42	-25.718	179	1500
41265	43	-25.718	175.5	4300

41266	43	-25.718	175.5	3800
41269	43	-25.718	175.5	3400
41270	43	-25.718	175.5	3000
41271	43	-25.718	175.5	2600
41272	43	-25.718	175.5	2400
41273	43	-25.718	175.5	2200
41274	43	-25.718	175.5	2000
41275	43	-25.718	175.5	1800
41276	43	-25.718	175.5	1600
41277	43	-25.718	175.5	1400
41278	43	-25.718	175.5	1200
41279	43	-25.718	175.5	1000
41280	43	-25.718	175.5	800
41281	43	-25.718	175.5	600
41282	43	-25.718	175.5	400
41283	43	-25.718	175.5	300
41284	43	-25.718	175.5	200
41285	43	-25.718	175.5	150
41286	43	-25.718	175.5	90
41287	43	-25.718	175.5	50
41288	43	-25.718	175.5	5
41289	44	-25.833	172	3200
41290	44	-25.833	172	3000
41291	44	-25.833	172	2800
41292	44	-25.833	172	2600
41293	44	-25.833	172	2400
41294	44	-25.833	172	2200
41295	44	-25.833	172	2000
41296	44	-25.833	172	1800
41297	44	-25.833	172	1600
41298	44	-25.833	172	1400
41299	44	-25.833	172	1200
41300	44	-25.833	172	1000
41301	44	-25.833	172	800
41302	44	-25.833	172	650
41303	44	-25.833	172	400
41304	44	-25.833	172	300
41305	44	-25.833	172	200
41306	44	-25.833	172	150
41307	44	-25.833	172	100
41308	44	-25.833	172	50
41309	44	-25.833	172	20
41310	44	-25.833	172	5

12.9 Sampling tables Ra, REE, tow-fish, ISP

(L.H. Viera, S. Pöhle, Z. Zhang, Z. Steiner, D. Köhler)

Table 12.20 Samples collected from the CTD for Ra-226 analysis by mass spectrometry.

	Station 2	Station 3	Station 4	Station 5	Station 6	Station 7	Station 8	Station 10	Station 12	Station 14	Station 16	Station 17	Station 18	Station 19	Station 20
Depth (m)	5	5	5	5	5	100	100	50	60	100	60	100	115	100	115
	70	100	100	100	100	300	200	100	100	350	100	200	350	200	350
	170	300	200	200	300	600	300	250	150	600	150	350	700	300	750
		600	400	300	400	1500	400	600	200	1000	200	600	1300	400	1300
		830	800	500	540	2750	500	1100	350	1300	300	1300	1800	600	1800
			1200	600	1500	3800	600	2750	550	2000	350	1800	2000	700	2000
			1500	900	2000		800	4000	800	2500	550	2800	2200	1100	2200
				1500	4000		1100		1100	3000	700	3900	2400	1700	2400
				2425	5900		1500		2600	3500	800		2600	2100	2600
							2500		3700			1100	2800	2500	2800
						4150					2600	3500	2900	2950	
											3600		3200		
	Station 22	Station 23	Station 24	Station 25	Station 28	Station 31	Station 33	Station 36	Station 39	Station 40	Station 41	Station 42	Station 43	Station 44	
Depth (m)	100	150	100	200	150	100	120	5	5	20	5	5	150	5	
	200	350	230	400	200	200	4630	5300	130	60	100	80	600	100	
	350	750	300	600	600	400	250	120	200	100	300	200	800	200	
	600	1300	600	800	1000	600	300	300	300	130	600	300	1400	400	
	1100	1800	1000	1350	1500	850	500	400	800	175	800	400	2000	800	
	1350	2000	1350	1800	2000	1350	850	600	1500	200	1350	600	2400	1400	
	1500	2100	1800	2150	2150	1800	1300	1500	2000	250	1500	1000	3400	2000	
	1700	2200	2000	2300	2300	2300	2400	2300	2500	300	1650	1650	4300	2600	
	2000	2400	2150	2800	2800	2600	2800	3000	3000	350	1800	2000		3200	
	2100	2700	2300	3500	3500	3300	3300	4600	3400	400	2000	2600			
2200	3000	3300				4080			4000	450	2200	3000			
2300									5000	500	2300	3500			

				5													
--	--	--	--	---	--	--	--	--	--	--	--	--	--	--	--	--	--

Table 12.22 Surface water samples taken using the two-fish.

Sample ID	UTC date (dd:mm:yy)	Nutrients	diss TMs	Al	Major elements	TM (JUB)	HFSE (JUB)	Pb iso	Fe iso	AWI Th230/Pa231	Nd iso/ Si iso+ REE	CO incubations	Latitude (deg N)	Longitude (deg E)	Salinity psu	T deg C	Note
10001	23.02.2022		22:40	22:40	22:40								-33,09	-71,83	34,236	16,13	Stn 2
10002	24.02.2022		13:05	13:05	13:05								-32,94	-71,90	34,284	17,19	Stn 3
10003	24.02.2022		16:00	16:00	16:00								-32,87	-71,89	34,361	18,50	Stn 4
10004	24.02.2022		18:20	18:20	18:20	18:20	18:20	18:27	18:30				-32,51	-71,99	34,379	19,66	Stn 5
10005	25.02.2022		08:18	08:18	08:18								-32,50	-72,17	34,322	19,37	
10006	25.02.2022		10:49	10:49	10:49								-32,50	-72,77	34,373	19,31	Stn 6
10007	26.02.2022		00:46	00:46	00:46								-32,50	-73,26	34,417	19,36	
10008	26.02.2022		02:56	02:56	02:56								-32,50	-73,77	34,477	19,58	Stn 7
10009	26.02.2022		14:43	14:43	14:43								-32,50	-74,86	34,468	19,72	
10010	26.02.2022	21:35	21:34	21:34	21:35	21:32	21:31	21:30	21:26				-32,50	-76,53	34,330	20,13	Stn 8
10011	27.02.2022	15:17	15:14	15:16	15:17								-32,50	-77,80	34,042	19,51	
10012	27.02.2022	20:07	20:09	20:08	20:07								-32,50	-78,96	34,155	19,94	Stn 9
10013	28.02.2022	08:23	08:21	08:22	08:20								-32,50	-80,23	34,725	20,40	
10014	28.02.2022	16:02	16:00	16:02	16:00								-32,50	-81,93	34,421	19,89	stn 10
10015	01.03.2022	00:31	00:33	00:32	00:31								-32,50	-82,31	34,413	19,80	
10016	01.03.2022	02:53	02:51	02:53	02:53								-32,50	-82,84			
10017	01.03.2022	13:01	13:03	13:02	13:01								-32,50	-85,00		20,13	Stn 11
10018	01.03.2022	21:39	21:40	21:39	21:39								-32,50	-85,67	34,823	20,80	
10019	02.03.2022	01:24	01:23	01:23	01:24								-32,50	-86,59	34,764	20,93	

10043	07.03.2022	21:25	21:23	21:24	21:25									-31,43	-106,67	35,629	24,05	
10044	08.03.2022	00:05	00:06	00:08	00:08									-31,43	-107,32	35,583	24,24	
10045	08.03.2022	02:27	02:26	02:27	02:28	02:29	02:30	02:23	02:18	02:36		02:46-02:54		-31,43	-107,85	35,555	24,13	Stn 19
10046	08.03.2022	16:30	16:28	16:29	16:30									-31,43	-108,69	35,372	23,86	
10047	08.03.2022	19:19	19:21	19:20	19:20									-31,43	-109,38	35,133	23,43	
10048	08.03.2022	21:38	21:40	21:39	21:37									-31,43	-109,92	35,501	23,95	Stn 20
10049	09.03.2022	13:06	13:08	13:09	13:06							13:25-13:50		-32,45	-111,90	35,379	24,23	Stn 21
10050	09.03.2022	19:04	19:03	19:01	19:04	18:59	19:01	19:32	19:27	19:11		19:17-19:54		-31,46	-111,99	35,414	24,45	Stn 22
10051	10.03.2022	10:17	10:15	10:16	10:17									-31,43	-113,11	35,556	24,71	
10052	10.03.2022	13:21	13:23	13:22	13:21									-31,43	-113,92	35,877	24,94	Stn 23
10053	10.03.2022	22:37	22:35	22:36	22:37									-31,43	-114,62	35,694	25,00	
10054	11.03.2022	03:18	03:21	03:19	03:19									-31,43	-115,42	35,938	25,72	
10055	11.03.2022	06:07	06:12	06:10	06:06	06:08	06:09		06:18	06:32				-31,43	-115,93	35,796	25,38	Stn 24
10056	11.03.2022	20:27	20:28	20:29	20:30									-31,43	-116,66	35,773	25,47	
10057	11.03.2022	23:28	23:29	23:30	23:31									-31,43	-117,43	35,532	25,20	
10058	12.03.2022	02:49	02:50	02:50	02:51									-31,43	-118,23	35,205	24,87	
10059	12.03.2022	06:09	06:10	06:10	06:11									-31,43	-118,94	35,183	24,82	Stn 25
10060	12.03.2022	16:26	16:24	16:25	16:26									-31,43	-119,77	35,611	25,17	
10061	12.03.2022	20:37	20:38	20:39	20:39									-31,43	-120,71	35,391	24,99	
10062	14.03.2022	06:49	06:51	06:52	06:53									-31,43	-125,68	35,434	24,85	
10063	14.03.2022	12:35	12:37	12:38	12:39									-31,43	-126,88	35,393	23,99	
10064	14.03.2022	16:36	16:36	16:36	16:36	16:41	16:42	16:33	16:29	15.03.2022 05:08	15.03.2022 05:21			-31,43	-127,89	35,418	24,36	Stn 28
10065	15.03.2022	07:24	07:26	07:27	07:25									31,43	-128,61	35,384	24,06	

10091	27.03.2022	17:51	17:53	17:54	17:52				17:49				-26,17	-164,45	34,955	26,16	
10092	27.03.2022	20:39	20:40	20:41	20:39								-26,17	-165,16	34,963	25,91	
10093	27.03.2022	23:23	23:23	23:24	23:25								-26,17	-165,87	34,891	26,22	
10094	28.03.2022	02:01	02:02	02:03	02:01								-26,17	-166,55	34,902	26,11	
10095	28.03.2022	04:56	04:58	04:58	04:57								-26,17	-167,31	34,830	26,72	
10096	28.03.2022	07:23	07:25	07:26	07:24						07:10-07:22		-26,17	-167,95	35,092	26,31	Stn 37
10097	28.03.2022	19:42	19:44	19:45	19:42								-26,17	-168,67	35,064	26,19	
10098	28.03.2022	22:36	22:37	22:38	22:36								-26,17	-169,40	35,020	26,11	
10099	29.03.2022	01:05	01:06	01:07	01:08								-26,17	-170,01	35,080	26,18	
10100	29.03.2022	04:03	04:05	04:04	04:03								-26,17	-170,75	35,102	25,91	
10101	29.03.2022	06:14	06:15	06:16	06:16								-26,17	-171,31	34,956	26,06	
10102	29.03.2022	08:38	08:39	08:40	08:41						Nd+Hf iso		-26,17	-171,92	34,991	26,11	Stn 38
10103	29.03.2022	20:41	20:42	20:43	20:41								-26,17	-172,63	35,073	25,95	
10104	29.03.2022	23:13	23:14	23:15	23:13								-26,17	-173,23	34,984	26,46	
10105	30.03.2022	02:33	02:34	02:35	02:33								-26,17	-174,01	34,865	26,39	
10106	30.03.2022	06:00	06:01	06:02	06:00								-26,17	-174,79	34,963	26,28	
10107	30.03.2022	08:32	08:33	08:34	08:32						08:30		-26,17	-175,35	35,061	26,25	Stn 39
10108	30.03.2022	22:17	22:18	22:19	22:19						22:21		-26,08	-175,91	35,154	26,16	
10109	31.03.2022	00:18	00:19	00:19	00:18						00:21		-26,02	-176,33	35,377	26,11	
10110	31.03.2022	02:24	02:25	02:26	02:24						02:28		-25,944	-176,766	35,098	26,32	
10111	31.03.2022	04:15	04:13	04:14	04:14	04:11	04:12	04:09	04:07		07:30-07:50	07:25	-25,88	-177,13	35,047	26,39	Stn 40
10112	31.03.2022	12:28	12:30	12:29	12:30						12:27		-25,84	-177,53	34,918	26,02	
10113	31.03.2022	15:32	15:35	15:34	15:33						15:37		-25,77	-178,21	35,348	25,99	
10114	31.03.2022	23:37	23:38	23:39	23:39						23:14-23:34		-25,72	-178,79	35,499	25,81	Stn 41

10115	01.04.2022	02:13	02:15	02:15	02:13						02:12		-25,72	-179,31	35,490	25,47	
10116	01.04.2022	06:19	06:20	06:21	06:19						06:23		-25,72	179,95	35,044	25,98	
10117	01.04.2022	09:16	09:17	09:18	09:16						09:15		-25,72	179,43	35,091	25,79	
10118	01.04.2022	11:27	11:28	11:29	11:30	11:31	11:32	11:26	11:23	11:35-11:44	11:45-12:05		-25,72	179,04	35,023	26,08	Stn 42
10119	02.04.2022	02:06	02:08	02:08	02:07						02:05		-25,72	178,42	35,071	25,81	
10120	02.04.2022	05:10	05:11	05:12	05:12						05:09		-25,72	177,78	35,407	25,57	
10121	02/04/2022	07:20	07:22	07:22	07:21						07:20		-25,72	177,34	35,381	25,59	
10122	02/04/2022	09:45	09:47	09:48	09:45						09:44		-25,72	176,87	35,336	25,49	
10123	02/04/2022	12:42	12:43	12:44	12:42						12:41		-25,72	176,29	35,265	25,74	
10124	03/04/2022	00:08	00:10	00:11	00:09						00:13-00:29		-25,72	175,47	35,192	25,77	Stn 43
10125	03/04/2022	03:15	03:16	03:17	03:14						03:13		-25,74	174,76	35,058	26,19	
10126	03/04/2022	05:34	05:35	05:36	05:34						05:38		-25,76	174,22	35,118	26,37	
10127	03/04/2022	08:12	08:13	08:14	08:11						08:10		-25,78	173,63	35,312	25,84	
10128	03/04/2022	10:52	10:55	10:54	10:53						10:52		-25,80	173,01	35,240	25,92	
10129	03/04/2022	12:53	12:54	12:55	12:56						12:52		-25,82	172,57	35,243	26,08	
10130	03/04/2022	15:12	15:13	15:14	15:15						14:55-15:03	15:05-15:10	-25,83	172,05	35,379	26,80	Stn 44

Table 12.24 In situ pump sample table

sample ID	ISP	Date UTC	Time UTC	Lat.	Long.	Depth [m]	Volume [L]	v e s i c u l a r	R a	Th 234	POC /PIC/ PON	P O P	B S i	ma jor ion s	m e t a l s	Cd isoto pes	Si iso top es	Ba iso top es	R E E	Ni iso top es	S e	p H	Hg iso top es	CN isoto pes	A W I	m i c r o s c o p y	m e t a b o l i t e s	s y n c h r o n i z a t i o n		
50001	PIS021	25.02.2022	00:30	-32.299	-71.599	20	122			x	x	x										x								
50002		25.02.2022	00:30	-32.299	-71.599	20	624	x					x	x	x	x	x												x	
50003	PIS020	25.02.2022	00:30	-32.299	-71.599	50	49			x	x	x											x							
50004		25.02.2022	00:30	-32.299	-71.599	50	331	x						x	x	x	x	x												x
50005	PIS009	25.02.2022	00:30	-32.299	-71.599	100	931		x	x	x	x											x							
50006	PIS010	25.02.2022	00:30	-32.299	-71.599	120	541	x						x	x	x														x
50007	AWI	25.02.2022	00:30	-32.299	-71.599	200	264			x	x	x											x							
50008		25.02.2022	00:30	-32.299	-71.599	200	112	x						x	x	x	x	x												x
50009	PIS007	25.02.2022	00:30	-32.299	-71.599	300	824		x	x	x	x											x							
50010	PIS011	25.02.2022	00:30	-32.299	-71.599	500	391	x	x					x	x	x														x
50011	Eddie	25.02.2022	00:30	-32.299	-71.599	700	63	x																						
50012	PIS012	25.02.2022	00:30	-32.299	-71.599	900	635	x	x					x	x	x														x
50013	PIS021	27.02.2022	02:00	-32.3	-76.36	20	350			x	x	x										x	x							
50014		27.02.2022	02:00	-32.3	-76.36	20	230	x						x	x	x	x	x	x	x										
50015	PIS020	27.02.2022	02:00	-32.3	-76.36	60	440			x	x	x										x	x							
50016		27.02.2022	02:00	-32.3	-76.36	60	228	x						x	x	x	x	x	x	x										
50017	PIS009	27.02.2022	02:00	-32.3	-76.36	100	1078		x	x	x	x										x	x							
50018	AWI-CTD	27.02.2022	02:00	-32.3	-76.36	150	516	x						x	x	x	x	x	x	x					x					x
50019	AWI	27.02.2022	02:00	-32.3	-76.36	200	9			x	x	x										x	x							

50045		06.03.2022	01:30	-32.3	-100	100	227	x			x	x	x	x	x	x	x	x			x	x	x					
50046	AWI- MiniC TD	06.03.2022	01:30	-32.3	-100	150	2198	x	x			x	x	x	x	x	x	x	x			x	x	x	x			
50047		06.03.2022	01:30	-32.3	-100	200	260			x	x	x									x	x						
50048	AWI	06.03.2022	01:30	-32.3	-100	200	418	x				x	x	x	x	x	x	x	x				x	x	x			
50049	PIS010	06.03.2022	01:30	-32.3	-100	300	1550		x	x	x	x									x	x						
50050	PIS007	06.03.2022	01:30	-32.3	-100	350	1138	x	x				x	x	x	x	x	x	x				x	x	x	x		
50051	AWI- CTD	06.03.2022	01:30	-32.3	-100	550	1139	x	x				x	x	x	x	x	x	x				x	x	x	x		
50052	Eddie	06.03.2022	01:30	-32.3	-100	700	3	x																				
50053	PIS011	06.03.2022	01:30	-32.3	-100	800	60	x	x				x	x	x	x	x	x	x					x	x	x		
50054	PIS012	06.03.2022	01:30	-32.3	-100	1100	1315	x	x				x	x	x	x	x	x	x					x	x	x		
50055		08.03.2022	05:30	-31.258	-107.599	20	773			x	x	x											x	x				
50056	PIS021	08.03.2022	05:30	-31.258	-107.599	20	423	x					x	x	x	x	x	x	x					x	x	x		
50057	PIS009	08.03.2022	05:30	-31.258	-107.599	100	2230		x	x	x	x											x	x				
50058		08.03.2022	05:30	-31.258	-107.599	150	850			x	x	x											x	x				
50059	PIS020	08.03.2022	05:30	-31.258	-107.599	150	436	x					x	x	x	x	x	x	x					x	x	x		
50060		08.03.2022	05:30	-31.258	-107.599	200	609			x	x	x											x	x				
50061	AWI	08.03.2022	05:30	-31.258	-107.599	200	144	x					x	x	x	x	x	x	x					x	x	x		
50062	PIS010	08.03.2022	05:30	-31.258	-107.599	300	1635		x	x	x	x											x	x				
50063	PIS007	08.03.2022	05:30	-31.258	-107.599	400	1300	x	x				x	x	x	x	x	x	x					x	x	x	x	
50064	AWI- MiniC TD	08.03.2022	05:30	-31.258	-107.599	600	986	x	x					x	x	x	x	x	x					x	x	x	x	
50065	Eddie	08.03.2022	05:30	-31.258	-107.599	700	115	x																				
50066	PIS011	08.03.2022	05:30	-31.258	-107.599	1100	1	x	x					x	x	x	x	x	x						x	x	x	
50067	PIS012	08.03.2022	05:30	-31.258	-107.599	1700	1294	x	x					x	x	x	x	x	x						x	x	x	
50068	AWI- CTD	08.03.2022	05:30	-31.258	-107.599	2300	2086	x	x					x	x	x	x	x	x						x	x	x	x
50069	PIS009	10.03.2022	01:30	-31.258	-111.594	20	153			x	x	x													x	x		

50070	PIS021	10.03.2022	01:30	-31.258	-111.594	150	865		x	x	x								x	x						
50071		10.03.2022	01:30	-31.258	-111.594	150	404	x				x	x	x	x	x	x	x			x	x	x			
50072	PIS010	10.03.2022	01:30	-31.258	-111.594	200	1446		x	x	x	x								x	x					
50073	AWI	10.03.2022	01:30	-31.258	-111.594	300	586			x	x	x								x	x					
50074		10.03.2022	01:30	-31.258	-111.594	300	82	x				x	x	x	x	x	x	x	x			x	x	x		
50075	PIS011	10.03.2022	01:30	-31.258	-111.594	600	-9	x	x			x	x	x	x	x	x	x	x			x	x	x		
50076	Eddie	10.03.2022	01:30	-31.258	-111.594	700	130	x																		
50077	PIS012	10.03.2022	01:30	-31.258	-111.594	1500	1024	x	x			x	x	x	x	x	x	x					x	x	x	
50078	PIS007	10.03.2022	01:30	-31.258	-111.594	2000	1167	x	x			x	x	x	x	x	x	x					x	x	x	
50079	PIS020	10.03.2022	01:30	-31.258	-111.594	2100	894			x	x	x									x	x				
50080		10.03.2022	01:30	-31.258	-111.594	2100	458	x				x	x	x	x	x	x	x					x	x	x	x
50081	AWI- MiniC TD	10.03.2022	01:30	-31.258	-111.594	2150	683	x	x			x	x	x	x	x	x	x					x	x	x	x
50082	AWI- CTD	10.03.2022	01:30	-31.258	-111.594	2300	1256	x	x			x	x	x	x	x	x	x					x	x	x	x
50083	PIS009	11.03.2022	09:15	-31.258	-116	20	1107			x	x	x											x	x		
50084	PIS021	11.03.2022	09:15	-31.258	-116	175	940			x	x	x											x	x		
50085		11.03.2022	09:15	-31.258	-116	175	364	x				x	x	x	x	x	x	x	x					x	x	x
50086	PIS010	11.03.2022	09:15	-31.258	-116	230	1504		x	x	x	x											x	x		
50087	AWI	11.03.2022	09:15	-31.258	-116	300	552			x	x	x											x	x		
50088		11.03.2022	09:15	-31.258	-116	300	132	x				x	x	x	x	x	x	x	x					x	x	x
50089	PIS011	11.03.2022	09:15	-31.258	-116	600	950	x	x			x	x	x	x	x	x	x					x	x	x	
50090	Eddie	11.03.2022	09:15	-31.258	-116	700	121	x																		
50091	PIS012	11.03.2022	09:15	-31.258	-116	1000	1128	x	x			x	x	x	x	x	x	x						x	x	x
50092	PIS007	11.03.2022	09:15	-31.258	-116	1350	1165	x	x			x	x	x	x	x	x	x						x	x	x
50093	AWI- MiniC TD	11.03.2022	09:15	-31.258	-116	2000	1181	x	x			x	x	x	x	x	x	x					x	x	x	x
50094	PIS020	11.03.2022	09:15	-31.258	-116	2150	943			x	x	x												x	x	

50095		11.03.2022	09:15	-31.258	-116	2150	227	x			x	x	x	x	x	x	x		x	x	x	x	
50096	AWI-CTD	11.03.2022	09:15	-31.258	-116	2300	1465	x	x			x	x	x	x	x	x		x	x	x	x	
50097	PIS009	15.03.2022	00:00	-31.258	-128	20	992			x	x	x								x	x		
50098	PIS021	15.03.2022	00:00	-31.258	-128	150	910			x	x	x								x	x		
50099		15.03.2022	00:00	-31.258	-128	150	321	x	x			x	x	x	x	x	x	x	x			x	x
50100	PIS010	15.03.2022	00:00	-31.258	-128	200	1503			x	x	x								x	x		
50101	AWI	15.03.2022	00:00	-31.258	-128	300	601			x	x	x								x	x		
50102		15.03.2022	00:00	-31.258	-128	300	127	x			x	x	x	x	x	x	x	x				x	x
50103	PIS011	15.03.2022	00:00	-31.258	-128	600	1113	x	x			x	x	x	x	x	x				x	x	
50104	Eddie	15.03.2022	00:00	-31.258	-128	700	116	x															
50105	PIS012	15.03.2022	00:00	-31.258	-128	1000	1326	x	x			x	x	x	x	x	x	x				x	x
50106	PIS007	15.03.2022	00:00	-31.258	-128	1500	1307	x	x			x	x	x	x	x	x					x	x
50107	AWI-MiniC TD	15.03.2022	00:00	-31.258	-128	2000	1094			x			x	x	x	x	x	x				x	x
50108	PIS020	15.03.2022	00:00	-31.258	-128	2150	964			x	x	x									x	x	
50109		15.03.2022	00:00	-31.258	-128	2150	307	x	x			x	x	x	x	x	x						x
50110	AWI-CTD	15.03.2022	00:00	-31.258	-128	2300	1360	x	x			x	x	x	x	x	x					x	x
50111	PIS009	18.03.2022	02:30	-21.258	-138	20	1086			x	x	x									x	x	x
50112	PIS020	18.03.2022	02:30	-31.258	-138	100	852			x	x	x									x	x	x
50113		18.03.2022	02:30	-31.258	-138	100	366	x				x	x	x	x	x	x	x					x
50114	PIS021	18.03.2022	02:30	-31.258	-138	150	856			x	x	x									x	x	x
50115		18.03.2022	02:30	-31.258	-138	150	428	x	x			x	x	x	x	x	x	x	x				x
50116	AWI	18.03.2022	02:30	-31.258	-138	200	214			x	x	x									x	x	x
50117		18.03.2022	02:30	-31.258	-138	200	41	x				x	x	x	x	x	x						x
50118	PIS010	18.03.2022	02:30	-31.258	-138	300	1478			x	x	x	x								x	x	x
50119	AWI-MiniC TD	18.03.2022	02:30	-31.258	-138	400	1703	x	x			x	x	x	x	x	x					x	x

50120	PIS011	18.03.2022	02:30	-31.258	-138	600	1021	x	x				x	x	x	x	x	x	x				x	x	x			
50121	Eddie	18.03.2022	02:30	-31.258	-138	700	129	x																				
50122	PIS012	18.03.2022	02:30	-31.258	-138	850	1151	x	x				x	x	x	x	x	x	x				x	x	x	x		
50123	PIS007	18.03.2022	02:30	-31.258	-138	1350	1266	x	x				x	x	x	x	x	x	x					x	x	x		
50124	AWI-CTD	18.03.2022	02:30	-31.258	-138	2300	2168	x	x				x	x	x	x	x	x	x				x	x	x	x		
50125	PIS009	24.03.2022	03:30	-26.102	-152	20	976			x	x	x											x	x	x			
50126	PIS020	24.03.2022	03:30	-26.102	-152	60	854			x	x	x											x	x	x			
50127		24.03.2022	03:30	-26.102	-152	60	325	x					x	x	x	x	x	x	x							x	x	x
50128	PIS010	24.03.2022	03:30	-26.102	-152	90	1037			x	x	x											x	x	x			
50129	PIS021	24.03.2022	03:30	-26.102	-152	120	825			x	x	x											x	x	x			
50130		24.03.2022	03:30	-26.102	-152	120	449	x	x					x	x	x	x	x	x	x	x						x	x
50131	PIS007	24.03.2022	03:30	-26.102	-152	140	1369			x	x	x											x	x	x			
50132	AWI-MiniCTD	24.03.2022	03:30	-26.102	-152	170	2			x	x	x											x	x	x			
50133	AWI	24.03.2022	03:30	-26.102	-152	200	631			x	x	x											x	x	x			
50134		24.03.2022	03:30	-26.102	-152	200	116	x						x	x	x	x	x	x	x							x	x
50135	PIS012	24.03.2022	03:30	-26.102	-152	250	1493			x	x	x	x										x	x	x			
50136	PIS011	24.03.2022	03:30	-26.102	-152	300	1409			x	x	x	x										x	x	x			
50137	AWI-CTD	24.03.2022	03:30	-26.102	-152	400	1829			x	x	x											x	x	x			
50138	Eddie	24.03.2022	03:30	-26.102	-152	700	122	x																				
50139	PIS009	27.03.2022	10:45	-26.102	-164	20	990			x	x	x											x	x	x			
50140	PIS020	27.03.2022	10:45	-26.102	-164	70	816			x	x	x											x	x	x			
50141		27.03.2022	10:45	-26.102	-164	70	383	x						x	x	x	x	x	x	x							x	x
50142	PIS021	27.03.2022	10:45	-26.102	-164	120	806			x	x	x											x	x	x			
50143		27.03.2022	10:45	-26.102	-164	120	300	x	x					x	x	x	x	x	x	x	x						x	x
50144	AWI	27.03.2022	10:45	-26.102	-164	200	627			x	x	x											x	x	x			
50145		27.03.2022	10:45	-26.102	-164	200	137	x						x	x	x	x	x	x	x							x	x

50146	PIS010	27.03.2022	10:45	-26.102	-164	300	1553	x	x	x	x									x	x	x											
50147	AWI-CTD	27.03.2022	10:45	-26.102	-164	400	1456	x	x			x	x	x	x	x	x	x							x	x	x	x					
50148	PIS012	27.03.2022	10:45	-26.102	-164	600	1112	x	x			x	x	x	x	x	x	x									x	x	x				
50149	Eddie	27.03.2022	10:45	-26.102	-164	700	114	x																									
50150	PIS011	27.03.2022	10:45	-26.102	-164	800	903	x	x			x	x	x	x	x	x	x									x	x	x	x			
50151	PIS007	27.03.2022	10:45	-26.102	-164	1500	1242	x	x			x	x	x	x	x	x	x											x	x	x		
50152	AWI-CTD	30.03.2022	11:50	-26.102	-175.238	5975	416	x	x					x	x	x	x	x	x	x									x	x	x	x	
50153	PIS020	31.03.2022	06:30	-25.525	-177.11	20	897			x	x	x																	x	x	x		
50154	PIS020	31.03.2022	06:30	-25.525	-177.11	20	221	x					x	x	x	x	x	x	x	x										x	x	x	
50155	PIS009	31.03.2022	06:30	-25.525	-177.11	50	973			x	x	x																	x	x	x		
50156	PIS021	31.03.2022	06:30	-25.525	-177.11	80	897			x	x	x																	x	x	x		
50157	PIS021	31.03.2022	06:30	-25.525	-177.11	80	285	x	x				x	x	x	x	x	x	x	x										x	x	x	
50158	AWI	31.03.2022	06:30	-25.525	-177.11	130	600			x	x	x																	x	x	x		
50159	AWI	31.03.2022	06:30	-25.525	-177.11	130	138	x					x	x	x	x	x	x	x	x	x									x	x	x	
50160	PIS012	31.03.2022	06:30	-25.525	-177.11	175	887	x	x				x	x	x	x	x	x	x	x										x	x	x	
50161	Eddie	31.03.2022	06:30	-25.525	-177.11	200	127	x																									
50162	PIS011	31.03.2022	06:30	-25.525	-177.11	250	1040	x	x				x	x	x	x	x	x	x	x										x	x	x	
50163	PIS010	31.03.2022	06:30	-25.525	-177.11	300	1482		x	x	x	x																	x	x	x		
50164	PIS007	31.03.2022	06:30	-25.525	-177.11	450	1152	x	x				x	x	x	x	x	x	x											x	x	x	
50165	PIS009	01.04.2022	18:30	-25.431	178.6	20	906			x	x	x																		x	x	x	
50166	AWI	01.04.2022	18:30	-25.431	178.6	60	802			x	x	x																		x	x	x	
50167	AWI	01.04.2022	18:30	-25.431	178.6	60	178	x					x	x	x	x	x	x	x	x											x	x	x
50168	PIS020	01.04.2022	18:30	-25.431	178.6	90	311			x	x	x																		x	x	x	
50169	PIS020	01.04.2022	18:30	-25.431	178.6	90	1374	x	x				x	x	x	x	x	x	x	x	x										x	x	x
50170	PIS021	01.04.2022	18:30	-25.431	178.6	200	858			x	x	x																		x	x	x	
50171	PIS021	01.04.2022	18:30	-25.431	178.6	200	427	x					x	x	x	x	x	x	x												x	x	x

50172	PIS010	01.04.2022	18:30	-25.431	178.6	300	1578	x	x	x	x							x	x	x							
50173	AWI-CTD	01.04.2022	18:30	-25.431	178.6	400	1441	x	x			x	x	x	x	x	x						x	x	x	x	
50174	PIS012	01.04.2022	18:30	-25.431	178.6	600	1021	x	x			x	x	x	x	x	x							x	x	x	x
50175	Eddie	01.04.2022	18:30	-25.431	178.6	700	148	x																			
50176	PIS011	01.04.2022	18:30	-25.431	178.6	1000	882	x	x			x	x	x	x	x	x							x	x	x	x
50177	PIS007	01.04.2022	18:30	-25.431	178.6	1650	1172	x	x			x	x	x	x	x	x								x	x	x

1360 1 7 70 70 7 4 94 9 94 91 88 8 88 6 7 65 30 2 8 7 9
 51 0 8 6 0 5 94 4 91 88 8 88 0 65 30 9 0 2 4